

GAZİANTEP UNIVERSITY GRADUATE SCHOOL OF
NATURAL & APPLIED SCIENCES

EFFECTS OF MINERAL ADMIXTURES ON THE FRESH AND
HARDENED PROPERTIES OF SELF COMPACTING
CONCRETES: BINARY, TERNARY AND QUATERNARY
SYSTEMS

Ph.D Thesis
IN
CIVIL ENGINEERING

BY
ERDOĞAN ÖZBAY
NOVEMBER 2007

Effects of Mineral Admixtures on the Fresh and Hardened Properties
of Self Compacting Concretes: Binary, Ternary, and Quaternary
Systems

PhD Thesis
in
Civil Engineering
University of Gaziantep

Supervisor
Asst. Prof. Dr. Mehmet GESOĞLU

by
Erdoğan ÖZBAY
November 2007

T.C.
GAZİANTEP UNIVERSITY
GRADUATE SCHOOL OF
NATURAL & APPLIED SCIENCES
CIVIL ENGINEERING

Name of the thesis: Effects of Mineral Admixtures on the Fresh and Hardened Properties of Self Compacting Concretes: Binary, Ternary, and Quaternary Systems
Name of student: Erdoğan ÖZBAY
Exam date:

Approval of the Graduate School of Natural and Applied Sciences

Prof. Dr. Sadettin ÖZYAZICI
Director

I certify that this thesis satisfies all the requirements as a thesis for the degree of Doctor of Philosophy

Assoc. Prof. Dr. Mustafa GÜNAL
Head of Department

This is to certify that we have read this thesis and that in our opinion it is fully adequate, in scope and quality, as a thesis for the degree of Doctor of Philosophy.

Asst. Prof. Dr. Mehmet GESOĞLU
Supervisor

Examining Committee Members

Signature

Prof. Dr. Mehmet Ali TAŞDEMİR

Prof. Dr. Turan ÖZTURAN

Prof. Dr. Mustafa ÖZAKÇA

Asst. Prof. Dr. Erhan GÜNEYİSİ

Asst. Prof. Dr. Mehmet GESOĞLU

*To my wife, daughter and son
Naile, Hatice Nihal and Osman*

ABSTRACT

EFFECTS OF MINERAL ADMIXTURES ON THE FRESH AND HARDENED PROPERTIES OF SELF COMPACTING CONCRETES: BINARY, TERNARY AND QUATERNARY SYSTEMS

ÖZBAY, Erdoğan

Ph.D Thesis in Civil Engineering

Supervisor: Asst. Prof. Dr. Mehmet GESOĞLU

November 2007, 275 pages

SCC is a new kind of high performance concrete with excellent deformability and segregation resistance. It can flow through and fill the gaps of reinforcement and corners of moulds without any need for vibration and compaction during the placing process. Use of SCC lowered the noise level on the construction site, diminished the effect on the environment, and increased productivity. Use of SCC, thus improved both the conditions for the labour on the work site and for the surroundings. In order to achieve a SCC of high fluidity and to prevent the segregation and bleeding during transportation and placing, the formulators have employed a high portland cement (PC) content and used superplasticizer, viscosity modifying admixtures and mineral admixtures.

In this study, an experimental program was conducted to investigate the effects of mineral admixtures used in binary (two components), ternary (three components), and quaternary (four components) cementitious blends on the mechanical, physical, and durability properties of self compacting concretes. In this frame work four mineral admixtures, namely fly ash, ground granulated blast furnace slag, silica fume, and metakaolin were employed. A total of 65 self compacting concrete mixtures were designed at 0.32 and 0.44 water/binder ratios. The fresh properties of the produced self compacting concretes were observed through slump flow diameter, slump flow time, V-funnel flow time, L-box height ratio, initial and final setting times, and viscosity. The concretes were also tested for the mechanical, physical, and durability properties. The hardened concretes were tested for the compressive strength, splitting tensile strength, and ultrasonic pulse velocity for the evaluation of

mechanical properties. Shrinkage accompanied by the water loss were also monitored. Moreover, the durability tests were conducted to investigate the resistance to chloride ion penetration, electrical resistivity, water absorption, sorptivity, and water permeability. Based on the test results, the fresh and hardened properties of self compacting concretes were predicted depending on the mixture constituents of SCCs using artificial neural network (ANN) and genetic programming (GEP) techniques. Using the explicit artificial neural networks based mathematical expressions single and multi objective optimization problems are formulated and solved to obtain the best possible values for ingredient of SCCs for single and several responses.

The test results revealed that it is possible to produce SCC with binary, ternary and quaternary blends of fly ash, ground granulated blast furnace slag, silica fume and metakaolin. The binary use of fly ash and ground granulated blast furnace improved the fresh properties but silica fume and metakaolin had adverse effect on the fresh properties. Mechanical properties of produced SCCs improved with ground granulated blast furnace slag, silica fume and metakaolin but decreased with FA. It was observed that use of mineral admixtures as binary, ternary and quaternary blends improved the durability properties of SCCs. In addition, ANN appeared to have a better prediction performance than GEP by having owing to the higher coefficient of correlation and the lower mean absolute percentage of error. However, the GEP suggested a much shorter and more user-friendly model than ANN.

Keywords: Self compacting concrete, mineral admixtures, artificial neural network, genetic programming, mixture optimization

ÖZET

MİNERAL KATKILARIN KENDİLİĞİNDEN YERLEŞEN BETONLARIN TAZE VE SERTLEŞMİŞ BETON ÖZELLİKLERİ ÜZERİNE ETKİLERİ: İKİLİ, ÜÇLÜ VE DÖRTLÜ SİSTEMLER

ÖZBAY, Erdoğan
Doktora Tezi, İnşaat Mühendisliği
Tez Yöneticisi: Yrd. Doç. Dr. Mehmet GESOĞLU
Kasım 2007, 275 sayfa

Kendiliğinden yerleşen beton (KYB) taze haldeki yüksek akıcılık ve yüksek ayrışma direncine sahip yeni bir yüksek performanslı beton türüdür. KYB'lar donatı aralarından vibrasyon ve sıkıştırma işlemine gerek olmadan geçebilerek kalıbı doldurabilme özelliğine sahiptirler. İnşaat alanında gürültü azalması, çevre ve çalışma koşullarında iyileşme, üretim kalitesi ve verimlilik artışı KYB kullanılması ile elde edilebilen faydalardan bazıları olarak sıralanabilir. KYB'lara bu özellikleri kazandıran yeni kuşak süperakışkanlaştırıcılar, viskozite düzenleyici katkıları ve mineral katkı malzemelerinin üretimde kullanılmasıdır.

Bu çalışmada, ikili, üçlü ve dörtlü mineral katkı kullanımının KYB'ın taze, mekanik ve durabilite özellikleri üzerindeki etkileri araştırılmıştır. Su/bağlayıcı oranı 0.32 ve 0.44 olan toplam 65 KYB üretiminde uçucu kül, öğütülmüş yüksek fırın curufu, silis dumanı ve metakaolin ikili, üçlü ve dörtlü olarak çimento ile yer değiştirilerek kullanılmıştır. KYB'ların taze özellikleri, yayılma süresi ve çapı, V-hunisi akma süresi, L-kutusu yükseklik oranı, priz başlangıç ve bitiş süreleri tayini ve viskozite üzerinden gözlemlenmiştir. Ayrıca, üretilen KYB numuneleri üzerinde basınç, yarmada çekme ve ultrasonik ses hızı deneyleri, serbest kuruma rötresi, hızlı klor geçirimsizliği, elektriksel özdirenç, su emme, kılcal su geçirimsizliği, ve basınçlı su geçirimsizliği deneyleri yapılmıştır.

Üretilmiş olan KYB'ların deney sonuçları karışım parametrelerine bağlı olarak yapay sinir ağları (ANN) ve genetik programlama (GEP) teknikleri yardımı ile tahmin edilmiştir. Elde edilen yapay sinir ağları temelli matematiksel fonksiyonlar kullanılarak beton karışım oranları tekli ve çoklu objektifli optimizasyon problemleri haline dönüştürülüp, hedef fonksiyonları optimum yapan karışım oranları

bulunmuştur.

Elde edilen sonuçlar ışığında, uçucu kül, öğütölmüş yüksek fırın cürufu, silis dumanı ve metakaolin'in çimento ile ikili, üçlü ve dörtlü kullanımları ile KYB'lar üretilebilmektedir. Uçucu kül ve öğütölmüş yüksek fırın cürufunun çimento ile ikili kullanımının KYB taze özelliklerini iyileştirdiği fakat silis dumanı ve metakaolinin ise taze beton özelliklerini olumsuz etkilediği görölmüştür. Kullanılan mineral katkıların ikili, üçlü ve dörtlü kullanımlarının üretilen KYB'ların durabilite özelliklerini iyileştirdiği fakat uçucu külün mekanik özellikleri özellikle 28. günde azalttığı gözlemlenmiştir. Ayrıca, KYB özelliklerinin iki çok iyi bilinen sezgisel yöntem yardımı ile (yapay sinir ağları ve genetik programlama) yüksek korelasyon katsayısı ve düşük ortalama mutlak hata yüzdesi ile tahmin edilebileceği görölmüştür. Yapay sinir ağları kullanılarak elde edilen formüller genetik programlama yöntemi ile elde edilenlere göre daha iyi istatistiksel verilere sahip olmasına rağmen genetik programlama yardımı ile elde edilen formüller daha kısa ve kullanımı kolay olduđu görölmüştür.

Anahtar Kelimeler: Kendiliğinden yerleşen beton, mineral kakılar, yapay sinir ağları, genetik programlama, karışım optimizasyonu

ACKNOWLEDGEMENT

I owe special thanks to my supervisor, Asst. Prof. Dr. Mehmet Gesođlu, for his help and endless encouragement throughout this study.

Deep appreciation and thanks are due to Prof. Dr. Turan Özturan and Asst. Prof. Dr. Erhan Güneyisi for serving on the committee and their valuable suggestions and comments.

I would like to thank Asst. Prof. Dr. Ahmet Öztaş, Süleyman Başaran, Talip Kahyaođlu, Erdoğan Kanca, and Hakan Özbebek for their contributions.

Thanks are also due to Mehmet Tolga Yanar, Mustafa Erkan Kocabađ, Vakıf Kiriş, Mustafa Şeker, Serkan Taşatan and Bekir Çeviksever for their assistance with laboratory work.

The supply of materials from ADANA cement factory, OYAK ready mixed concrete plant, OTS construction firm, OYSA cement factory, and BASF chemical company are gratefully acknowledged.

Finally, I would like to thank my wife, daughter and son (Naile, Hatice Nihal and Osman) for their continuous support and encouragement.

CONTENTS

ABSTRACT	iii
ÖZET	v
ACKNOWLEDGMENTS	vii
CONTENTS	viii
LIST OF FIGURES	xiv
LIST OF TABLES	xxv
LIST OF SYMBOLS	xxvii
CHAPTER 1: INTRODUCTION	1
1.1. General	1
1.2. Research Objectives	2
1.3 Organization of the Thesis	3
CHAPTER 2: LITERATURE REVIEW	5
2.1 General	5
2.2 Self Compacting Concrete (SCC)	5
2.2.1 Definitions	5
2.2.2 Workability requirements of fresh SCC	6
2.2.3 Rheology of SCC	7
2.3 Mineral Admixtures in Concrete Production	10
2.3.1 Mineral admixtures	10
2.3.1.1 Fly ash	10

2.3.1.2	Ground granulated blast furnace slag.....	11
2.3.1.3	Silica fume.....	13
2.3.1.4	Metakaolin.....	14
2.3.2	Effects of mineral admixtures on the fresh properties of concretes.....	16
2.3.2.1	Effects of fly ash on the fresh properties of concretes	16
2.3.2.2	Effects of ground granulated blast furnace slag on the fresh properties of concretes.....	18
2.3.2.3	Effects of silica fume on the fresh properties of concretes.....	19
2.3.2.4	Effects of metakaolin on the fresh properties of concretes.....	20
2.3.3	Effects of mineral admixtures on the hardened properties of concretes.....	20
2.3.3.1	Effects of fly ash on the hardened properties of concretes.....	20
2.3.3.2	Effects of ground granulated blast furnace slag on the hardened properties of concretes.....	22
2.3.3.3	Effects of silica fume on the hardened properties of concretes.....	23
2.3.3.4	Effects of metakaolin on the hardened properties of concretes.....	24
2.3.4	Effects of mineral admixtures on the durability properties of concretes.....	28
2.3.4.1	Effects of fly ash on the durability properties of concretes.....	28
2.3.4.2	Effects of ground granulated blast furnace slag on the durability properties of concretes.....	29

2.3.4.3	Effects of silica fume on the durability properties of concretes.....	30
2.3.4.4	Effects of metakaolin on the durability properties of concretes.....	31
CHAPTER 3:	EXPERIMENTAL PROGRAM AND METHODOLGY	32
3.1	Introduction	32
3.2	Materials.....	32
3.2.1	Cement.....	32
3.2.2	Mineral admixtures.....	33
3.2.2.1	Fly ash	33
3.2.2.2	Ground granulated blast furnace slag.....	33
3.2.2.3	Silica fume.....	33
3.2.2.4	Metakaolin.....	34
3.2.2	Aggregates.....	34
3.2.3	Superplasticizer	35
3.3	Concrete Mixtures	36
3.4	Concrete Casting, Test Specimens, and Curing.....	40
3.5	Tests for Fresh Properties.....	41
3.5.1	Slump flow	41
3.5.2	V-funnel flow time	42
3.5.3	L-box test.....	43
3.5.4	Setting time.....	44
3.5.5	Viscosity	45
3.6	Tests for Mechanical Properties	47
3.6.1	Compressive strength	47
3.6.2	Splitting tensile strength.....	47
3.6.3	Ultrasonic pulse velocity.....	48

3.7 Tests for Physical Properties	48
3.7.1 Free shrinkage and weight loss	48
3.8 Determination of the Durability Performance of Concrete	49
3.8.1 Rapid chloride permeability	49
3.8.2 Electrical resistivity	51
3.8.3 Water absorption	52
3.8.4 Sorptivity	52
3.8.5 Water Permeability	54
CHAPTER 4: TEST RESULTS AND EVALUATION	56
4.1 Fresh Concrete Properties	56
4.1.1 Slump flow diameter and slump flow time	56
4.1.2 V-funnel flow time	58
4.1.3 L-box height ratio, T_{200} and T_{400} times.....	60
4.1.4 Initial and final setting times	74
4.1.5 Viscosity	82
4.2. Mechanical Properties	97
4.2.1 Compressive strength	97
4.2.2 Ultrasonic pulse velocity (UPV)	100
4.2.3 Splitting tensile strength	102
4.3 Physical Properties	117
4.3.1 Drying shrinkage	117
4.3.2 Weight loss	120
4.4 Durability Related Properties	132
4.4.1 Rapid chloride permeability	132
4.4.2 Electrical resistivity	134
4.4.3 Water absorption	144

4.4.4 Sorptivity.....	146
4.4.5 Water permeability	148
4.5 Correlations between Properties of SCCs	161
4.5.1 Correlations between fresh properties of SCCs.....	161
4.5.2 Correlations between mechanical properties of SCCs	162
4.5.3 Correlation between chloride ion permeability and electrical resistivity	162
4.5.4 Correlations between permeation properties	163
4.5.5 Correlations between electrical and permeation properties.....	163
CHAPTER 5: PREDICTION OF SELF COMPACTING CONCRETE PROPERTIES BY SOFT COMPUTING TECHNIQUES	174
5.1 Soft Computing Techniques.....	174
5.2 An Overview of Artificial Neural Networks.....	174
5.2.1 General	174
5.2.2 Artificial neural networks.....	175
5.2.3 Artificial neural network principles.....	177
5.2.3.1 Feed forward neural networks	179
5.2.3.2 Back propagation algorithm	180
5.2.3.3 Supervised, unsupervised and reinforcement training	180
5.2.3.4 Training and testing artificial neural networks.....	181
5.2.4 Performance evaluation of ANN models	183
5.2.5 Review on ANN applications in construction materials area..	183
5.3 An Overview of Genetic Programming.....	186
5.4 Applications of Soft Computing Techniques on the Data Set.....	189
5.4.1 General	189
5.4.2 Construction of ANN models.....	190
5.4.3 Construction of GEP model	192

5.4.4 Proposed formulations and performance of the models	193
5.4.5 Comparisons of correlations obtained soft computing models	215
CHAPTER 6: OPTIMIZING CONCRETE MIXTURE PROPORTIONS	225
6.1 General	225
6.2 Optimization Based on Single Response.....	225
6.2.1 Cost calculation of self compacting concretes	225
6.2.2 Optimization model for cost minimization	226
6.2.3 Desirability function.....	228
6.2.4 Results of cost minimization optimization.....	230
6.3 Multi Objective Optimization Based on Several Responses	233
6.3.1 General	233
6.3.2 Multi objective optimization model	234
6.3.3 Results of multi objective optimization.....	235
CHAPTER 7: CONCLUSIONS.....	238
CHAPTER 8: FUTURE WORK	244
REFERENCES	245
APPENDIX A: ANN BASED EXPLICIT FORMULATIONS FOR SCCs PROPERTIES	255
APPENDIX B: GEP BASED EXPLICIT FIRMULATIONS FOR SCCs PROPERTIES	269

LIST OF FIGURES

Figure 2.1 Rheological behaviors of some viscous materials	9
Figure 2.2 Scanning electron microscope image of fly ash particles	11
Figure 2.3 Scanning electron microscope image of ground granulated blast furnace slag particles	12
Figure 2.4 TEM micrograph of silica fume.....	13
Figure 2.5 SEM micrograph of natural Metakaolin at higher magnification	16
Figure 2.6 Influence of silica fume replacement and water binder ratio on the compressive strength of concretes.....	23
Figure 2.7 Compressive strength changes with replacement ratio of MK and SF at various testing age	26
Figure 2.8 Splitting tensile strength variations with replacement ratio of MK and SF at varying testing age.....	27
Figure 2.9 Flexural strength variations with replacement ratio of MK and SF at various testing age	27
Figure 3.1 Aggregate grading curves	35
Figure 3.2 Photographic demonstration of measurement of slump flow diameter	42
Figure 3.3 Photographic view of V-funnel flow time measurement.....	43
Figure 3.4 Photographic view of L-box apparatus and testing procedure.....	44
Figure 3.5 Plot of penetration resistance values versus elapsed time and fit curve used to determine time of setting	45
Figure 3.6 Photographic view of viscosity test apparatus and measuring of viscosity	46
Figure 3.7 Time dependent viscosity behavior of SCC mortar	47
Figure 3.8 Drying shrinkage test set up.....	48
Figure 3.9 Experimental set-up for Rapid Chloride Permeability Test.....	50

Figure 3.10 Rapid chloride permeability test	51
Figure 3.11 Electrical resistivity measurement	52
Figure 3.12 Test set up for measurement of concrete sorptivity	53
Figure 3.13 Typical plot of rate of absorption versus time	54
Figure 3.14 Photographic view of water permeability test equipment.....	55
Figure 4.1 Binary effects of mineral admixtures on T50 slump flow time of SCCs at w/b ratio of 0.32	65
Figure 4.2 Ternary effects of mineral admixtures on T50 slump flow time of SCCs at w/b ratio of 0.32	65
Figure 4.3 Quaternary effects of mineral admixtures on T50 slump flow time of SCCs at w/b ratio of 0.32	66
Figure 4.4 Binary effects of mineral admixtures on T50 slump flow time of SCCs at w/b ratio of 0.44	66
Figure 4.5 Ternary and quaternary effects of mineral admixtures on T50 slump flow time of SCCs at w/b ratio of 0.44.....	67
Figure 4.6 Comparison of T50 slump flow time of SCCs at different w/b ratios	67
Figure 4.7 Binary effects of mineral admixtures on V-funnel flow time of SCCs at w/b ratio of 0.32	68
Figure 4.8 Ternary effects of mineral admixtures on V-funnel flow time of SCCs at w/b ratio of 0.32	68
Figure 4.9 Quaternary effects of mineral admixtures on V-funnel flow time of SCCs at w/b ratio of 0.32	69
Figure 4.10 Binary effects of mineral admixtures on V-funnel flow time of SCCs at w/b ratio of 0.44	69
Figure 4.11 Ternary and quaternary effects of mineral admixtures on T50 slump flow time of SCCs at w/b ratio of 0.44.....	70
Figure 4.12 Comparison of V-funnel flow time of SCCs at different w/b ratios.....	70
Figure 4.13 Binary effects of mineral admixtures on L box H2/H1 ratio of SCCs at w/b ratio of 0.32	71

Figure 4.14 Ternary effects of mineral admixtures on L box H2/H1 ratio of SCCs at w/b ratio of 0.32	71
Figure 4.15 Quaternary effects of mineral admixtures on L box H2/H1 ratio of SCCs at w/b ratio of 0.32	72
Figure 4.16 Binary effects of mineral admixtures on L box H2/H1 ratio of SCCs at w/b ratio of 0.44	72
Figure 4.17 Ternary and quaternary effects of mineral admixtures on L box H2/H1 ratio of SCCs at w/b ratio of 0.44.....	73
Figure 4.18 Comparison of L box H2/H1 ratio of SCCs at different w/b ratios	73
Figure 4.19 Binary effects of mineral admixtures on the initial and final setting times of SCCs at w/b ratio of 0.32	79
Figure 4.20 Ternary effects of mineral admixtures on the initial and final setting times of SCCs at w/b ratio of 0.32	79
Figure 4.21 Quaternary effects of mineral admixtures on the initial and final setting times of SCCs at w/b ratio of 0.32	80
Figure 4.22 Binary effects of mineral admixtures on the initial and final setting times of SCCs at w/b ratio of 0.44	80
Figure 4.23 Ternary and quaternary effects of mineral admixtures on the initial and final setting times of SCCs at w/b ratio of 0.44	81
Figure 4.24 Variation of initial setting times of SCCs with w/b ratios	81
Figure 4.25 Variation of final setting times of SCCs with w/b ratios	82
Figure 4.26 Viscosity of SCC with binary cementitious materials at different rotational speeds at w/b ratio of 0.32 a) T = 0; b) T = 20; c) T = 40.....	86
Figure 4.27 Viscosity of SCC with ternary (PC+FA+SF, PC+GGBFS+SF and PC+FA+GGBFS) cementitious materials at different rotational speeds at w/b ratio of 0.32 a) T = 0; b) T = 20; c) T = 40	87
Figure 4.28 Viscosity of SCC with ternary (PC+FA+MK and PC+GGBFS+MK) cementitious materials at different rotational speeds at w/b ratio of 0.32 a) T = 0; b) T = 20; c) T = 40	89

Figure 4.29 Viscosity of SCC with quaternary (PC+FA+SF+MK; PC+GGBFS+SF+MK; PC+FA+GGBFS+SF; PC+FA+GGBFS+MK) cementitious materials at different rotational speeds at w/b ratio of 0.32 a) T = 0; b) T = 20; c) T = 40	90
Figure 4.30 Viscosity of SCC with binary cementitious materials at different rotational speeds at w/b ratio of 0.44 a) T = 0; b) T = 20; c) T = 40.....	92
Figure 4.31 11 Viscosity of SCC with ternary (PC+FA+SF; PC+GGBFS+SF and PC+FA+GGBFS) cementitious materials at different rotational speeds at w/b ratio of 0.44 a) T = 0; b) T = 20; c) T = 40	93
Figure 4.32 Viscosity of SCC with quaternary (PC+FA+GGBFS+SF) cementitious materials at different rotational speeds at w/b ratio of 0.44 a) T = 0; b) T = 20; c) T = 40	95
Figure 4.33 Binary effects of mineral admixtures on compressive strength of SCCs at w/b ratio of 0.32	107
Figure 4.34 Ternary effects of mineral admixtures on compressive strength of SCCs at w/b ratio of 0.32	107
Figure 4.35 Quaternary effects of mineral admixtures on compressive strength of SCCs at w/b ratio of 0.32	108
Figure 4.36 Binary effects of mineral admixtures on compressive strength of SCCs at w/b ratio of 0.44	108
Figure 4.37 Ternary and quaternary effects of mineral admixtures on compressive strength of SCCs at w/b ratio of 0.44	109
Figure 4.38 Comparison of compressive strengths of SCCs at 28 days for different w/b ratios	109
Figure 4.39 Comparison of compressive strengths of SCCs at 28 days for different w/b ratios	110
Figure 4.40 Binary effects of mineral admixtures on UPV of SCCs at w/b ratio of 0.32	110
Figure 4.41 Ternary effects of mineral admixtures on UPV of SCCs at w/b ratio of 0.32	111

Figure 4.42 Quaternary effects of mineral admixtures on UPV of SCCs at w/b ratio of 0.32.....	111
Figure 4.43 Binary effects of mineral admixtures on UPV of SCCs at w/b ratio of 0.44.....	112
Figure 4.44 Ternary and quaternary effects of mineral admixtures on UPV of SCCs at w/b ratio of 0.44.....	112
Figure 4.45 Comparison of ultrasonic pulse velocity of SCCs at 28 days for different w/b ratios.....	113
Figure 4.46 Comparison of ultrasonic pulse velocity of SCCs at 28 days for different w/b ratios.....	113
Figure 4.47 Binary effects of mineral admixtures on the splitting tensile strength of SCCs at w/b ratio of 0.32.....	114
Figure 4.48 Ternary effects of mineral admixtures on the splitting tensile strength of SCCs at w/b ratio of 0.32.....	114
Figure 4.49 Quaternary effects of mineral admixtures on the splitting tensile strength of SCCs at w/b ratio of 0.32.....	115
Figure 4.50 Binary effects of mineral admixtures on the splitting tensile strength of SCCs at w/b ratio of 0.44.....	115
Figure 4.51 Ternary and quaternary effects of mineral admixtures on the splitting tensile strength of SCCs at w/b ratio of 0.44.....	116
Figure 4.52 Comparison of the splitting tensile strength of SCCs at different w/b ratios.....	116
Figure 4.53 Binary effects of mineral admixtures on the free shrinkage of SCCs at w/b ratio of 0.32.....	125
Figure 4.54 Ternary effects of mineral admixtures (PC+FA+SF; PC+GGBFS+SF; PC+FA+GGBFS) on the free shrinkage of SCCs at w/b ratio of 0.32.....	125
Figure 4.55 Ternary effects of mineral admixtures (PC+FA+MK; PC+GGBFS+MK; PC+SF+MK) on the free shrinkage of SCCs at w/b ratio of 0.32.....	126
Figure 4.56 Quaternary effects of mineral admixtures on the free shrinkage of SCCs at w/b ratio of 0.32.....	126

Figure 4.57 Binary effects of mineral admixtures on the free shrinkage of SCCs at w/b ratio of 0.44	127
Figure 4.58 Ternary effects of mineral admixtures on the free shrinkage of SCCs at w/b ratio of 0.44	127
Figure 4.59 Quaternary effects of mineral admixtures on the free shrinkage of SCCs at w/b ratio of 0.44	128
Figure 4.60 Binary effects of mineral admixtures on the weight loss of SCCs at w/b ratio of 0.32	128
Figure 4.61 Ternary effects of mineral admixtures (PC+FA+SF; PC+GGBFS+SF; PC+FA+GGBFS) on the weight loss of SCCs at w/b ratio of 0.32	129
Figure 4.62 Ternary effects of mineral admixtures (PC+FA+MK; PC+GGBFS+MK; PC+SF+MK) on the weight loss of SCCs at w/b ratio of 0.32	129
Figure 4.63 Quaternary effects of mineral admixtures on the weight loss of SCCs at w/b ratio of 0.32	130
Figure 4.64 Binary effects of mineral admixtures on the weight loss of SCCs at w/b ratio of 0.44	130
Figure 4.65 Ternary effects of mineral admixtures on the weight loss of SCCs at w/b ratio of 0.44	131
Figure 4.66 Quaternary effects of mineral admixtures on the weight loss of SCCs at w/b ratio of 0.44	131
Figure 4.67 Binary effects of mineral admixtures on the chloride ion permeability of SCCs at w/b ratio of 0.32	138
Figure 4.68 Ternary effects of mineral admixtures on the chloride ion permeability of SCCs at w/b ratio of 0.32	138
Figure 4.69 Quaternary effects of mineral admixtures on the chloride ion permeability of SCCs at w/b ratio of 0.32	139
Figure 4.70 Binary effects of mineral admixtures on the chloride ion permeability of SCCs at w/b ratio of 0.44	139
Figure 4.71 Ternary and quaternary effects of mineral admixtures on the chloride ion permeability of SCCs at w/b ratio of 0.44	140

Figure 4.72 Comparison of the chloride ion permeability of SCCs at different w/b ratios	140
Figure 4.73 Binary effects of mineral admixtures on electrical resistivity of SCCs at w/b ratio of 0.32	141
Figure 4.74 Ternary effects of mineral admixtures on electrical resistivity of SCCs at w/b ratio of 0.32	141
Figure 4.75 Quaternary effects of mineral admixtures on electrical resistivity of SCCs at w/b ratio of 0.32	142
Figure 4.76 Binary effects of mineral admixtures on electrical resistivity of SCCs at w/b ratio of 0.44	142
Figure 4.77 Ternary and quaternary effects of mineral admixtures on electrical resistivity of SCCs at w/b ratio of 0.44	143
Figure 4.78 Comparison of electrical resistivity of SCCs at 28 days for different w/b ratios	143
Figure 4.79 Comparison of electrical resistivity of SCCs at 28 days for different w/b ratios	144
Figure 4.80 Binary effects of mineral admixtures on water absorption of SCCs at w/b ratio of 0.32	152
Figure 4.81 Ternary effects of mineral admixtures on water absorption of SCCs at w/b ratio of 0.32	152
Figure 4.82 Quaternary effects of mineral admixtures on water absorption of SCCs at w/b ratio of 0.32	153
Figure 4.83 Binary effects of mineral admixtures on water absorption of SCCs at w/b ratio of 0.44	153
Figure 4.84 Ternary and quaternary effects of mineral admixtures on water absorption of SCCs at w/b ratio of 0.44	154
Figure 4.85 Comparison of the water absorption of SCCs at different w/b ratios ...	154
Figure 4.86 Binary effects of mineral admixtures on water sorptivity of SCCs at w/b ratio of 0.32	155

Figure 4.87 Ternary effects of mineral admixtures on water sorptivity of SCCs at w/b ratio of 0.32	155
Figure 4.88 Quaternary effects of mineral admixtures on water sorptivity of SCCs at w/b ratio of 0.32	156
Figure 4.89 Binary effects of mineral admixtures on water sorptivity of SCCs at w/b ratio of 0.44	156
Figure 4.90 Ternary and quaternary effects of mineral admixtures on water sorptivity of SCCs at w/b ratio of 0.44	157
Figure 4.91 Comparison of the water sorptivity of SCCs at different w/b ratios.....	157
Figure 4.92 Binary effects of mineral admixtures on water permeability of SCCs at w/b ratio of 0.32	158
Figure 4.93 Ternary effects of mineral admixtures on water permeability of SCCs at w/b ratio of 0.32	158
Figure 4.94 Quaternary effects of mineral admixtures on water permeability of SCCs at w/b ratio of 0.32	159
Figure 4.95 Binary effects of mineral admixtures on water permeability of SCCs at w/b ratio of 0.44	159
Figure 4.96 Ternary and quaternary effects of mineral admixtures on water permeability of SCCs at w/b ratio of 0.44.....	160
Figure 4.97 Comparison of the water permeability of SCCs at different w/b ratios	160
Figure 4.98 Correlation between T50 slump flow time and V-funnel flow time.....	165
Figure 4.99 Correlation between T50 slump flow time and viscosity at 5 rpm	166
Figure 4.100 Correlation between V-funnel flow time and viscosity at 5 rpm.....	166
Figure 4.101 Correlation between compressive and splitting tensile strengths at 90 days.....	167
Figure 4.102 Correlation between compressive strength and ultrasonic pulse velocity at 90 days.....	167
Figure 4.103 Correlation between ultrasonic pulse velocity and splitting tensile strength at 90 days.....	168

Figure 4.104 Correlation between electrical resistivity and chloride ion permeability .	168
Figure 4.105 Correlation between water absorption and water permeability	169
Figure 4.106 Correlation between water absorption and water sorptivity	169
Figure 4.107 Correlation between water sorptivity and water permeability	170
Figure 4.108 Correlation between chloride ion permeability and water absorption	170
Figure 4.109 Correlation between chloride ion permeability and water permeability ..	171
Figure 4.110 Correlation between chloride ion permeability and water sorptivity..	171
Figure 4.111 Correlation between electrical resistivity and water permeability.....	172
Figure 4.112 Correlation between electrical resistivity and water absorption	172
Figure 4.113 Correlation between electrical resistivity and water sorptivity.....	173
Figure 5.1 A simplified model of a biological neuron	177
Figure 5.2 Basic elements of an artificial neuron.....	177
Figure 5.3 Multilayered artificial neural network	179
Figure 5.4 Schematic presentation of weight correction in BPNN	180
Figure 5.5 Five major preparatory steps for the basic versions of genetic programming	187
Figure 5.6 A typical example of the GEP expression tree	189
Figure 5.7 Proposed ANN architecture for prediction of slump flow diameter, compressive strength, splitting tensile strength, chloride ion permeability, water absorption, water permeability, and electrical resistivity of SCC	197
Figure 5.8 Proposed ANN architecture for prediction of T50 slump flow time, V-funnel flow time, L-box H2/H1 ratio, initial setting time, final setting time, ultrasonic pulse velocity, free shrinkage and water sorptivity of SCC	198
Figure 5.9 Performance of the formulation of slump flow diameter of SCC a) train set b) test set	200
Figure 5.10 Performance of the formulation of T50 slump flow time of SCC a) train set b) test set	201

Figure 5.11 Performance of the formulation of V-funnel flow time of SCC a) train set b) test set.....	202
Figure 5.12 Performance of the formulation of L-box height ratio (H2/H1) of SCC a) train set b) test set.....	203
Figure 5.13 Performance of the formulation of initial setting time of SCC a) train set b) test set.....	204
Figure 5.14 Performance of the formulation of final setting time of SCC a) train set b) test set.....	205
Figure 5.15 Performance of the formulation of compressive strength of SCC a) train set b) test set.....	206
Figure 5.16 Performance of the formulation of UPV of SCC a) train set b) test set	207
Figure 5.17 Performance of the formulation of splitting tensile strength of SCC a) train set b) test set.....	208
Figure 5.18 Performance of the formulation of free shrinkage of SCC a) train set b) test set.....	209
Figure 5.19 Performance of the formulation of chloride ion permeability of SCC a) train set b) test set.....	210
Figure 5.20 Performance of the formulation of electrical resistivity of SCC a) train set b) test set.....	211
Figure 5.21 Performance of the formulation of water absorption of SCC a) train set b) test set.....	212
Figure 5.22 Performance of the formulation of water sorptivity of SCC a) train set b) test set.....	213
Figure 5.23 Performance of the formulation of water permeability of SCC a) train set b) test set.....	214
Figure 5.24 T ₅₀ slump flow time and V-funnel flow time tests based comparisons of prediction performance of soft computing techniques.....	218
Figure 5.25 Compressive strength and velocity through concrete tests based comparisons of prediction performance of soft computing techniques.....	218

Figure 5.26 Velocity through concrete and splitting tensile strength tests based comparisons of prediction performance of soft computing techniques.....	219
Figure 5.27 Electrical resistivity and chloride ion permeability tests based comparisons of prediction performance of soft computing techniques.....	219
Figure 5.28 Water absorption and water sorptivity tests based comparisons of prediction performance of soft computing techniques	220
Figure 5.29 Water absorption and water permeability tests based comparisons of prediction performance of soft computing techniques	220
Figure 5.30 Water sorptivity and water permeability tests based comparisons of prediction performance of soft computing techniques	221
Figure 5.31 Chloride ion permeability and water absorption tests based comparisons of prediction performance of soft computing techniques.....	221
Figure 5.32 Chloride ion permeability and water sorptivity tests based comparisons of prediction performance of soft computing techniques.....	222
Figure 5.33 Chloride ion permeability and water permeability tests based comparisons of prediction performance of soft computing techniques.....	222
Figure 5.34 Electrical resistivity and water absorption tests based comparisons of prediction performance of soft computing techniques	223
Figure 5.35 Electrical resistivity and water sorptivity tests based comparisons of prediction performance of soft computing techniques	223
Figure 5.36 Electrical resistivity and water permeability tests based comparisons of prediction performance of soft computing techniques	224
Figure 6.1 Graphically demonstration of changing of desirability function with SF and MK.....	231
Figure 6.2 Graphically demonstration of changing of overall desirability function with SF and MK	237

LIST OF TABLES

Table 2.1 Alloy types and their silica fume contents	14
Table 2.2 Slag activity index	22
Table 3.1 Chemical composition and physical properties of cement and mineral admixtures	33
Table 3.2 Sieve analysis and physical properties of the fine and coarse aggregates..	34
Table 3.3 Properties of superplasticizer	35
Table 3.4 Concrete mixture proportioning at a w/b ratio of 0.32	37
Table 3.5 Concrete mixture proportioning at a w/b ratio of 0.44	39
Table 3.6 Interpretation of results obtained using RCPT test	50
Table 4.1 Slump flow, L-box and V-funnel properties of SCCs at w/b of 0.32	63
Table 4.2 Slump flow, L-box and V-funnel properties of SCCs at w/b of 0.44	64
Table 4.3 Initial and final setting times of SCCs at w/b ratio of 0.32	77
Table 4.4 Initial and final setting times of SCCs at w/b ratio of 0.44	78
Table 4.5 The equation constants and regression coefficients of the best fit curves for binary mineral admixtures at w/b ratio of 0.32	95
Table 4.6 The equation constants and regression coefficients of the best fit curves for ternary mineral admixtures at w/b ratio of 0.32	96
Table 4.7 The equation constants and regression coefficients of the best fit curves for quaternary mineral admixtures at w/b ratio of 0.32	96
Table 4.8 The equation constants and regression coefficients of the best fit curves at w/b ratio of 0.44	97
Table 4.9 Mechanical properties of SCCs at 0.32 w/b ratio.....	105
Table 4.10 Mechanical properties of SCCs at 0.44 w/b ratio.....	106

Table 4.11 Free shrinkage and weight loss performance of the SCCs at w/b ratio of 0.32	123
Table 4.12 Free shrinkage and weight loss performance of the SCCs at w/b ratio of 0.44	124
Table 4.13 Chloride ion permeability of SCCs at w/b ratio of 0.32.....	136
Table 4.14 Chloride ion permeability of SCCs at w/b ratio of 0.44.....	137
Table 4.15 Results of water absorption, sorptivity and water permeability tests at w/b ratio of 0.32	150
Table 4.16 Results of water absorption, sorptivity and water permeability tests at w/b ratio of 0.44	151
Table 5.1 Normalization coefficient and data range of parameters for ANN models ...	197
Table 5.2 Statistical performance of the proposed ANN and GEP formulations for prediction SCCs properties.....	199
Table 6.1 Unit prices of raw materials	226
Table 6.2 Design variables and responses constraints in the single objective optimization.....	228
Table 6.3 Optimum mix proportions for cost minimization	231
Table 6.4 Predicted response values of the SCC properties according to ten optimal mixtures	232
Table 6.5 Design variables and responses constraints in the multi objective optimization.....	235
Table 6.6 Optimum mix proportions for multi objective optimization.....	236
Table 6.7 Predicted response values of the SCC properties according to four optimal mixtures	236

LIST OF SYMBOLS/ABBREVIATIONS

ϕ	Concrete porosity
S	Degree of saturation
ρ	Electrical resistivity of the concrete
ρ_w	Electrical resistivity of the pore solution
m'	Mean values of measured values
p'	Mean values of predicted values
γ'	Shear strain rate
τ	Shear stress
μ	Viscosity
τ_0	Yield stress
dV / dy	Shear rate
D	Overall desirability
d_i	Desirability function
MAE	Mean absolute error
MAPE	Mean absolute percentage error
m_i	Measured values for i^{th} experiment
MSE	Mean square error
p_i	Predicted value for i^{th} experiment
R	Correlation coefficient
UP	Unit price
W_1	Oven-dry weights

W_2	Saturated surface dry weights
WA	Water absorption
w_{ij}	Weight coefficient between i^{th} and j^{th} neurons
γ	Rotational speed in revolutions per minute
ACI	American Concrete Institute
ANN	Artificial Neural Network
ASTM	American Society for Testing and Materials
CANMET	Canada Center for Mineral and Energy Technology
CSF	Condensed Silica Fume
DIN	Deutsches Institut für Normung
EFNARC	European Federation of National Trade Association
ET	Expression Tree
FA	Fly Ash
GEP	Genetic Expression Programming
GGBFS	Ground Granulated Blast Furnace Slag
GP	Genetic Programming
HPC	High Performance Concrete
LM	Levenberg Marquardt
MK	Metakaolin
MOO	Multi Objective Optimization
PC	Portland Cement
RCPT	Rapid Chloride Permeability Test
SAI	Slag-Activity Index
SCC	Self Compacting Concrete
SEM	Scanning Electron Microscope
SF	Silica Fume

SP	Superplasticizer
TEM	Thermal Electron Microscope
TS EN	Turkish Standard European Norm
UPV	Ultrasonic Pulse Velocity

1. INTRODUCTION

1.1. General

Since self-compacting concrete (SCC) was introduced to the construction industry in the early 1990s, much of the extensive research and development work has of necessity been concerned with the achievement and assessment of fresh and hardened properties (Domone, 2007). SCC is a new kind of high performance concrete with excellent deformability and segregation resistance. It can flow through and fill the gaps of reinforcement and corners of moulds without any need for vibration and compaction during the placing process (Okamura, 1997; Okamura et al., 1993). Use of SCC lowered the noise level on the construction site, diminished the effect on the environment, and increased productivity. Use of SCC, thus improved both the conditions for the labour on the work site and for the surroundings (Persson, 2001).

The common practice to produce SCC is to limit the coarse aggregate content associated with its maximum size and to use the lower water-binder ratios together with appropriate superplasticizers (Okamura and Ozawa, 1995). In order to achieve a SCC of high fluidity and to prevent the segregation and bleeding during transportation and placing, the formulators have employed a high portland cement (PC) content and used superplasticizer and viscosity modifying admixtures (Sari et al., 1999; Sakata et al., 1996; Lachemi et al. 2004; Saric-Coric et al., 2003). However, the cost of such concretes were remarkably higher associated with the use of high volume of PC and chemical admixtures. In some cases, the savings in labour cost might offset increased cost. However, the use of mineral admixtures such as fly ash (FA) and ground granulated blast furnace slag (GGBFS) reduced the dosage of superplasticizer and improved the workability of concretes but they retarded the setting time and lowered the early strength. Using of silica fume (SF) and metakaolin (MK), on the other hand, increased superplasticizer demand and affected the workability negatively. These negative effects may be remedied by the combined use of the mineral admixtures.

Using mineral admixtures especially in SCC necessitates further attention. On incorporation of such materials, certain properties of the concretes may be enhanced whereas others may worsen relative to the plain portland cement concrete. Previous investigations show that the uses of FA, GGBFS, SF, and MK in concrete production improve the durability of concretes. SF and MK increase substantially early concrete strength but imparts sharp fall in workability to fresh concrete (FIP Commission, 1988). While FA decreases early strength, retards setting time but improves workability (Cabrera, 1986). Park et al (2005) investigated the influence of the cementitious materials containing fine particles on the rheology of the pastes. The mineral admixtures used were finely GGBFS, FA, and SF. Cementitious pastes were designed as one component (PC), two-components (PC-GGBFS, PC-FA, and PC-SF), and three-components (PC-GGBFS-SF and PC-FA-SF) systems. It was found for the two-component system the yield stress and viscosity decreased with replacing PC with GGBFS and FA. In the case of PC-SF system, however, the yield stress and viscosity steeply increased with increasing SF. For both of the three-component systems the rheological properties of the cementitious pastes improved compared with the PC-SF binary systems.

1.2. Research Objectives

The objectives of this thesis can be listed as follows:

- Investigating the effects of mineral admixtures used in binary (two components), ternary (three components), and quaternary (four components) cementitious blends on the fresh, mechanical, physical, and durability properties of self compacting concretes. In this context four mineral admixtures, namely fly ash, ground granulated blast furnace slag, silica fume, and metakaolin were employed.
- Based on the test results, the fresh and hardened properties of self compacting concretes were predicted depending on the mixture constituents of SCCs using neural network and genetic programming which handle complex nonlinear relationships between various inputs and outputs. Moreover, the cost of each mixture was determined per cubic-meter of concrete.

- Using the explicit mathematical expressions developed in the prior task single and multi objective optimization problems are formulated in order to obtain the best possible values for ingredients of SCCs for single and several responses.

Within the scope of the experimental test program, a total of 65 SCC mixtures were prepared with two different water binder ratios (0.32 and 0.44) and two different total binder contents (550 kg/m^3 and 450 kg/m^3). Fresh properties of SCCs were observed through slump flow time and flow diameter, V-funnel flow time, L-box height ratio, initial and final setting time, and viscosity. The time dependent viscosity of each mixture was also determined by using Brookfield rheometer equipment. Hardened properties were evaluated in terms of compressive strength, splitting tensile strength, ultrasonic pulse velocity, and drying shrinkage. Moreover, the SCCs were tested for water absorption, water sorptivity, water permeability, chloride ion permeability test, and electrical resistivity to account for the influence of combined use of the mineral admixtures on the mentioned durability properties.

1.3 Organization of the Thesis

This thesis consists of seven chapters. Chapter 2 presents a literature review and presents a general background information about SCC. Workability requirements of SCC and its rheological behavior were explained. Moreover, in this section mineral admixtures and their effects on the fresh, mechanical, and durability properties of SCCs were also discussed.

Chapter 3 covers the experimental program conducted throughout this study. Properties of cement, aggregates, mineral and chemical admixtures used in the concrete production as well as the tests on fresh and hardened properties of SCCs are included.

Chapter 4 provides the test results of testing program conducted in task 3. Furthermore, how the binary, ternary and quaternary use of mineral admixtures affect the fresh, mechanical, and durability properties of SCCs are explained in this chapter.

Furthermore, the possible relationships between the properties of concretes were investigated and presented.

Chapter 5 presents the general information and literature review about artificial neural networks (ANNs) and genetic programming (GEP). Fresh, hardened, and durability properties of SCC were estimated using these soft computing techniques. Moreover, ANN and GEP based explicit formulations were derived for the predicted SCC properties and statistical performances of the proposed formulations were compared.

Chapter 6 first presents the background of optimization theory, and then using the explicit ANN based formulations achieved in chapter 5 single and multi objective optimization problems are formulated in order to obtain the best possible values for ingredient of the SCC for single and several responses.

Chapter 7 gives a summary of thesis and lists the results of this research. Possible further studies complementing this thesis are also included in chapter 7.

2. LITERATURE REVIEW

2.1 General

The following literature review focuses on the definition and properties of self compacting concretes. Brief information about the structure, formation and properties of mineral admixtures, namely, fly ash (FA), ground granulated blast furnace slag (GGBFS), silica fume (SF), and metakaolin (MK) are presented. Moreover, the effects of mineral admixtures on the fresh, hardened, and durability properties of SCCs are discussed.

2.2 Self Compacting Concrete (SCC)

2.2.1 Definitions

Increased productivity and improved working environment have had high priority in the development of concrete construction over the last decade. Development of a material not needing vibration for compaction i.e. self compacting concrete (SCC) has successfully met the challenge and is now increasingly being used in routine practice (RILEM TC report, 2006). European Federation of National Trade Association (EFNARC) defined the SCC as “concrete that is able to flow under its own weight and completely fill the formwork, even in the presence of dense reinforcement, without need of any vibration, whilst maintaining homogeneity” (EFNARC, 2002). According to Okamura, SCC is a new kind of high performance concrete (HPC) with excellent deformability and segregation resistance that can flow through and fill the gaps of reinforcement and corners of moulds without any need for vibration and compaction during the placing process (Okamura, 1999).

From many other researches and the experimental work of this study, the following definition can be adopted for SCC: concrete that is able to flow under its own weight up to leveling, completely fill the formwork even in the presence of dense reinforcement, airs out, compacts and consolidates without the need of any vibration, whilst maintaining homogeneity due to high resistance to segregation.

2.2.2 Workability requirements of fresh SCC

Fresh properties of SCC are crucial to its ability to be placed satisfactorily so the functional requirements on a fresh SCC are different from those on a conventional fresh concrete. Filling of formwork with a liquid suspension requires workability performance which is recommended by ERNARC (2002) and RILEM (2006) technical committee to be described as follows:

- Filling ability is the ability to complete filling of formwork and encapsulation of reinforcement and inserts. It must be substantial to horizontal and vertical flow of the concrete within the formwork with maintained homogeneity.
- Passing ability is the ability of passing of obstacles such as narrow sections of the formwork, closely spaced reinforcement etc. without blocking caused by interlocking of aggregate particles.
- Resistance to segregation is the ability of maintaining the homogeneity throughout mixing, and during transportation and casting. The dynamic stability refers to the resistance to segregation during placement. While the static stability refers to resistance to bleeding, segregation and surface settlement after casting.

According to RILEM technical committee report (2006), in addition to the above mentioned three important fresh properties, the following criteria must be satisfied by SCCs:

Precision and accuracy: It is more essential to keep target workability for SCC as the casting is fully relying on the material properties as no tools normally will be available for manual material transport and compaction.

Pumping ability: SCC is generally easier to pump. Depending on the specific rheological properties of the fresh concrete the pumping pressure versus the feeding rate has to be optimised.

Finishing ability: SCC normally has less bleeding tendency. In many cases the finishing will be made on a coarser and stickier surface. Appropriate materials on the finishing tools must be used.

If the expected workability requirements have been achieved from the produced concretes, the following most important advantages can be obtained (Okamura, 1999):

- Faster construction
- Reduction in site manpower
- Better surface finishes
- Easier placing
- Improved durability
- Greater freedom in design
- Thinner concrete sections
- Reduced noise levels, absence of vibration
- Safer working environment

2.2.3 Rheology of SCC

Rheology is the study of material flow, or deformation, under stress. The fresh state characteristics of cementitious materials can be described using rheological parameters. For cementitious materials, rheological parameters help in describing the ease with which it can be used in the fresh state, including workability, placeability, compactability, finishability, flowability, pumpability, and extrudability. Different applications require different rheological characteristics. By understanding the rheology of basic cementitious materials, mix designs can be tailored to the desired applications (Kuder et al., 2007). Concrete that is not properly consolidated may have defects, such as honeycombs, air voids, and aggregate segregation. Such an important performance attribute has triggered the design of numerous test methods (Ferraris, 1999).

Generally, for fluids the flow behavior is classified into two: Newtonian and non-Newtonian (Şahmaran, 2006). For a well ordered flow (laminar) whereby fluid particles move in straight, parallel lines (parallel flow) Newton states that the shear stress on an interface tangent to the direction of flow is proportional to the distance rate of change of velocity, wherein the differentiation is taken in a direction normal to the interface (Shames, 1992). Mathematically this is stated as

$$\tau \propto \frac{\partial V}{\partial n} \quad (2.1)$$

Inserting the coefficient of proportionality into Newton's viscosity law leads to the results

$$\tau = \mu \frac{\partial V}{\partial n} \quad (2.2)$$

where μ is called the coefficient of viscosity and the unit of which being the poise corresponding to 1 g/cm*s.

Newtonian fluid in this context is a viscous material. Non-Newtonian fluids are also viscous materials wherein the shear stress is related to the shear rate, dV/dy , in a more complicated way. The power law may be used to describe the behavior of a viscous material. This can be formulized as follows:

$$\tau = k \left(\frac{dV}{dy} \right)^n \quad (2.3)$$

For a Newtonian fluid, $k = \mu$, and $n = 1$. The other values of n , however, lead to a non-Newtonian fluid. A non-Newtonian fluid whose behaviour is described by equation 2.3 with $n < 1$ is called a pseudoplastic. This name obtains because with increasing shear rate, $\left(\frac{dV}{dy} \right)$, there is curiously a decrease in effective viscosity. That is, on increasing shear rate the fluid is "thinning". This stress, shear-rate curve is given in Figure 2.1. Many non-Newtonian slurries are pseudoplastic. If, on the other hand, $n > 1$, the fluid is called dilatant. This time, the fluid "thickens" with increasing shear rate (Shames, 1992).

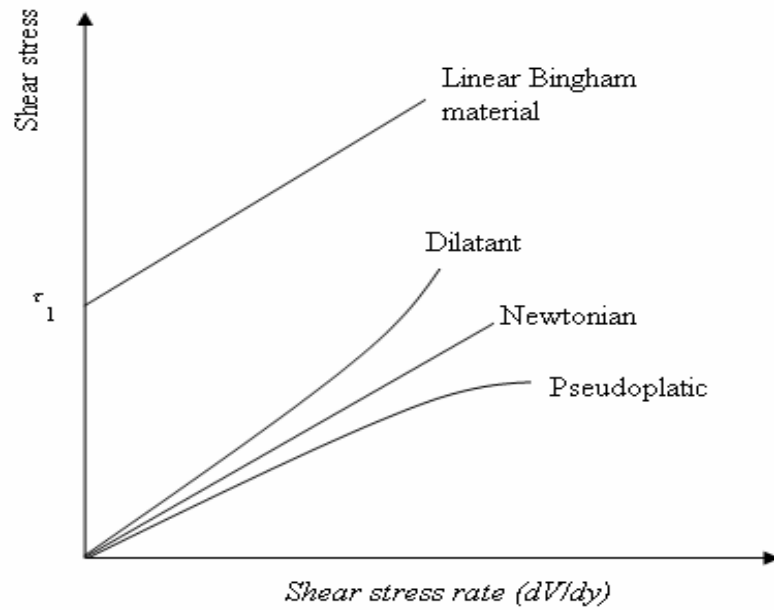


Figure 2.1 Rheological behaviour of some viscous materials (Shames, 1992)

Paste, mortar, and concrete are often considered as non-Newtonian fluids (Ferraris, 1999a). The rheological behaviour of a fluid such as cement paste, mortar or concrete is most often characterized by at least two parameters, τ_0 and μ , as defined by Bingham equation (Tattersall, 1991)

$$\tau = \tau_0 + \mu\dot{\gamma} \quad (2.4)$$

where τ is the shear stress applied to the material (in Pa), τ_0 is the yield stress (in Pa), μ is the plastic viscosity (in Pa*s), and $\dot{\gamma}$ is the shear strain rate (also is called the strain gradient) (in s^{-1}). The yield stress and plastic viscosity are the Bingham parameters that characterize the flow properties of materials. For self compacting concrete, a third parameter may be necessary to correctly represent the shear rate-shear stress relationship (Ferraris, 1999).

The rheology of fresh concrete is most often described by the Bingham model in which the flow curve has an intercept on the stress axis, indicating a minimum stress which is required to start the flow as seen in Figure 2.1. According to this model, fresh concrete must overcome a limiting stress (yield stress, τ_0) before it can flow. Once the fresh concrete starts to flow, shear stress will increase linearly with an

increase in strain rate as defined by plastic viscosity as a measure of the ease of flow. Therefore, in order to fully describe the rheological properties of fresh concrete by Bingham model, two parameters, namely, plastic viscosity and the yield stress are necessary (Ozawa et al., 1989; Şahmaran, 2006).

2.3 Mineral Admixtures Used in Concrete Production

2.3.1 Mineral admixtures

The most often used mineral admixture in the concrete industry is pozzolan. According to American Concrete Institute (ACI), a pozzolan is defined as “siliceous or siliceous and aluminous materials which in themselves possesses little or no cementitious value but will, in finely divided form and the presence of moisture, chemically react with calcium hydroxide at ordinary temperatures to form compounds possessing cementitious properties”. ACI 231 defines the chemical reaction between the siliceous and/or siliceous-alumina components in the pozzolan, calcium hydroxide and water as pozzolanic reaction.

There are two types of pozzolan, namely natural pozzolan and man-made pozzolan. Natural pozzolans are of volcanic origin (these were used by the early Romans and Greeks) such as trass, certain pumicites, perlite, and kaoline. Man-made pozzolans include industrial by-products such as fly ash, blast furnace slag, and silica fume (Güneyisi, 2004).

2.3.1.1 Fly ash

Fly ash is a by-product of the combustion of coal in thermal power plants, which is capable of reacting with $\text{Ca}(\text{OH})_2$ at room temperature. The pozzolanic activity of fly ash depends on the presence of SiO_2 and Al_2O_3 in the amorphous form (Baker, 1984; Gesoğlu, 2004; Naik and Singh, 1997). The use of fly ash in concrete technology dates back 1930s (Şengül, 2005). It is estimated that about 450 million tons of fly ash is produced worldwide annually, but only 6% of the total available is used as pozzolan in blended cements or in concrete mixtures (Baker, 1984). In Turkey, there

are twelve active coal-burning power plants with annual fly ash production of about 15 millions tons.

According to ASTM C 618 (2002) fly ash is categorized in two classes: Class F and Class C. The classification is mainly based on if the fly ash in question carries only pozzolanic (Class F) or pozzolanic and cementitious (Class C) properties. The former is normally generated due to combustion of anthracite or bituminous coal whereas the latter is produced by means of burning of lignite or sub-bituminous coal. From a physical point of view, fly ash can also be very different from one another. They can appear in shapes such as spherical, rounded, irregular and angular. The particle size distribution of fly ash obtained by scanning electron microscope is provided in Figure 2.2

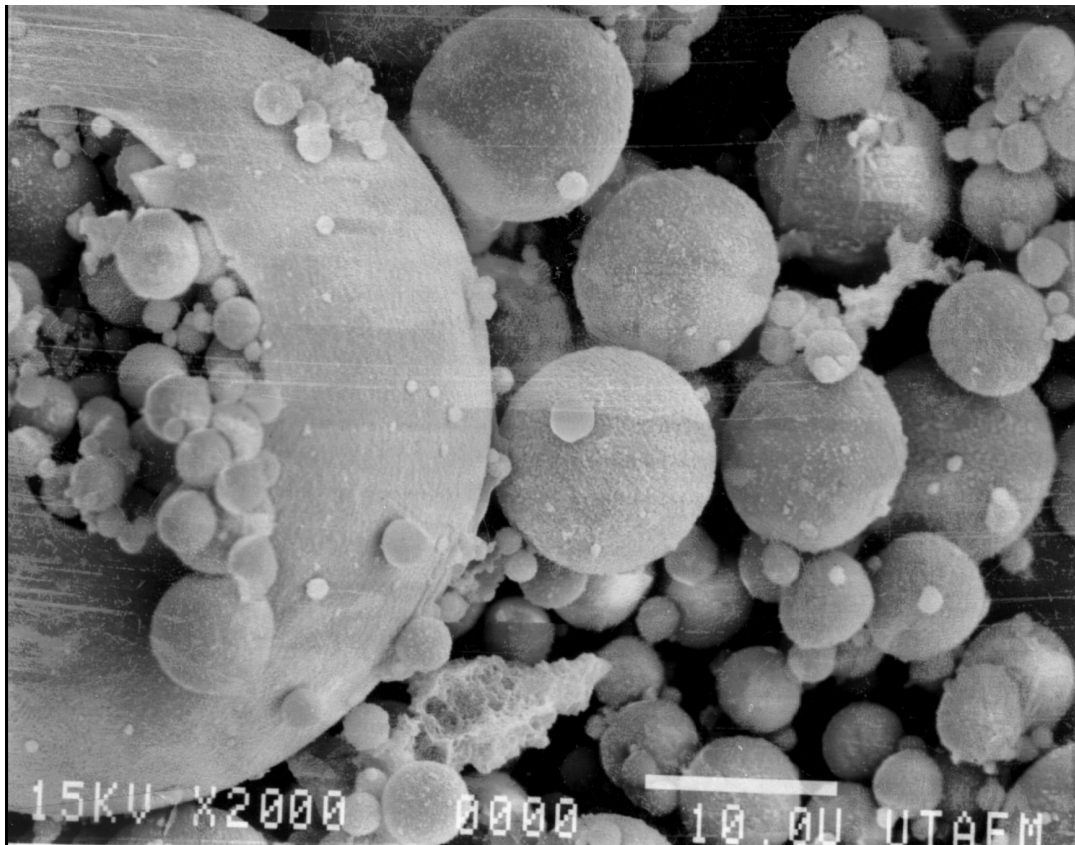


Figure 2.2 Scanning electron microscope image of fly ash particles (ACI 232.2 R-96, 1996)

2.3.1.2 Ground granulated blast furnace slag

Slags are residues from metallurgical processes, either from production of metals from ore or refinement of impure metals. They are derived from lime-based

inorganic fluxes used to extract impurities from metals which solidify on cooling. The slags used in concrete come from the blast furnace production of iron from ore. The iron ore is fed into the furnace with coke and limestone. The slag is formed at a temperature of 1300-1600 °C as a liquid layer floating on the top of liquid iron. It is then collected and cooled (Lee, 1974). The speed of cooling affects the properties of the slag. If allowed to cool slowly, it crystallizes to give a material having virtually no cementing materials. If cooled sufficiently rapidly to below 800 °C, it forms a glass which is latent hydraulic cement. This substance is then ground into a very fine powder with a minimum of 80 percent less than 45 microns in size. This is the cementitious material called ground granulated blast furnace slag (GGBFS). GGBFS has been used for many years as a supplementary cementitious material in portland cement concrete, either as a mineral admixture or as a component of blended cement. Blast furnace slag particles have mostly rough, sharp edged shapes as shown in Figure 2.3.

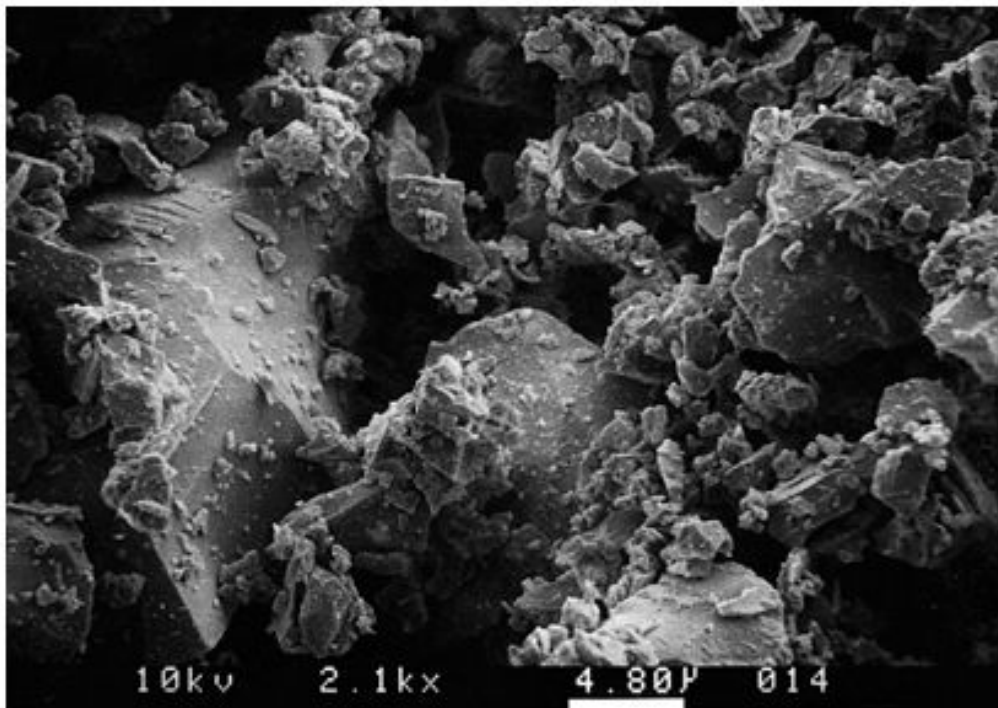


Figure 2.3 Scanning electron microscope image of ground granulated blast furnace slag particles (Lee, 1974)

2.3.1.3 Silica fume

Silica fume is a by-product resulting from the reduction of high-purity quartz with coal or coke and wood chips in an electric arc furnace during the production of silicon metal or ferrosilicon alloys. The silica fume, which condenses from the gases escaping from the furnaces, has a very high content of amorphous silicon dioxide and consists of very fine spherical particles (Figure 2.4).

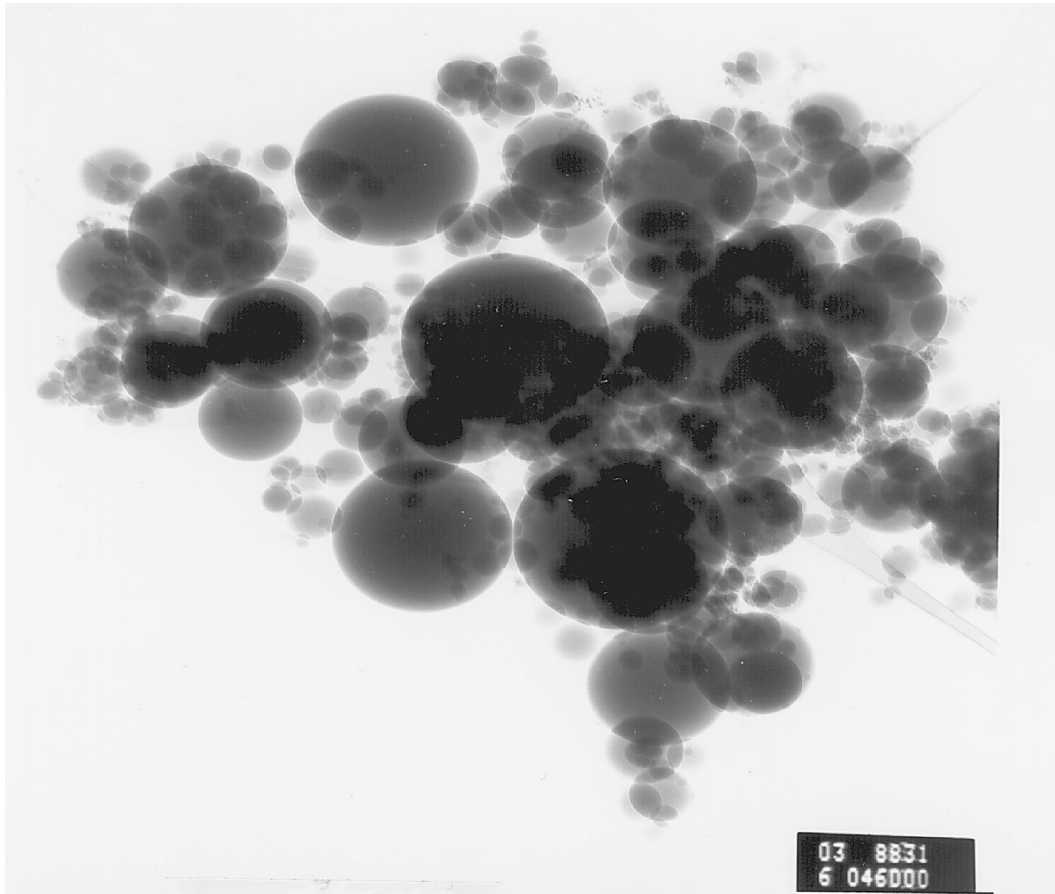


Figure 2.4 TEM micrograph of silica fume (ACI 234 R-96, 1996)

Ferrosilicon alloys are produced with nominal silicon contents of 61 to 98 percent. When the silicon content reaches 98 percent, the product is called silicon metal rather than ferrosilicon. As the silicon content increases in the alloy, the SiO_2 content will increase in the silica fume (see Table 2.1). The majority of published data and field use of silica fume have been from production of alloys of 75 percent ferrosilicon or higher. Limited applications have been made using silica fume from production of 50 percent ferrosilicon alloys (ACI 234 R-96, 1996).

Table 2.1 Alloy types and their silica fume contents (ACI 234 R-96, 1996)

Alloy type	SiO ₂ content of silica fume
50 percent ferrosilicon	61 to 84 percent
75 percent ferrosilicon	84 to 91 percent
silicon metal (98 percent)	87 to 98 percent

Most silica fumes range from light to dark grey in colour. Because SiO₂ is colourless, the colour is determined by the non-silica components, which typically include carbon and iron oxide. In general, the higher the carbon content, the darker the colour of the silica fumes. The carbon content of silica fume is affected by many factors relating to the manufacturing process such as: wood chip composition, wood chip use versus coal use, furnace temperature, furnace exhaust temperature, and the type of product (metal alloy) being produced. The degree of compaction may also affect the colour.

The average diameter of silica fume particles are 0.1 μm, and their specific surface area is about 20000 m²/kg, as compared to 250 to 450 m²/kg for an ordinary portland cement or a fly ash. Silica fume contains 85 to 95% SiO₂ depending on the type of silicon alloy which is produced. Its chemical composition is generally very constant because of the high purity of the two main raw materials used in the process (quartz and coal). Its carbon content is generally less than 2 % (Delage and Aitcin, 1983)

2.3.1.4 Metakaolin

The raw material input in the manufacture of metakaolin is kaolin clay. Kaolin is a fine, white, clay mineral that has been traditionally used in the manufacture of porcelain. It is thought that the term kaolin is derived from the Chinese Kaoling, which translates loosely to white hill and has been related to the name of a mountain in China. Kaolinite is the mineralogical term that is applicable to kaolin clays. Kaolinite is defined as a common mineral, hydrated aluminum disilicate, Al₂Si₂O₅(OH)₄, being the most common constituent of kaolin. Kaolin is a mineral typical of continental weathering where solutions percolate and are purified over

time. Kaolinite cannot develop in sedimentary basins where solutions accumulate and are enriched. Kaolin is one of the more highly prized of the industrial mineral clays. Kaolin's traditional markets in ceramics over the past centuries have yielded to the now dominant consumption by the paper industry where it is extensively used as a filler, opacifier, and as an important input to high-end coatings. Additional, smaller markets for kaolin are in the refractory, rubber, paint, plastic, chemical, pharmaceutical, and ceramic industries (www.metakaolin.com, 2007).

Metakaolin is a thermally activated alumino-silicate material obtained by calcining kaolin clay within the temperature range 650–800 °C (Poon et al. 2006). It contains typically 50–55% SiO₂ and 40–45% Al₂O₃ and is highly reactive. An important difference between MK and natural pozzolans or other types of artificial pozzolans is that MK is a primary product, while SF and FA are secondary products or by-products.

The key in producing metakaolin for use as a supplementary cementing material, or pozzolan is to achieve as near to complete dehydroxilization as possible without over heating. Successful processing results in a disordered, amorphous state, which is highly pozzolanic. Thermal exposure beyond a defined point will result in sintering and the formation of mullite, which is dead burnt and not reactive. In other words, kaolinite, to be optimally altered to a metakaolin state, requires that it is thoroughly roasted but never burnt (Kriven et al, 1994). Scanning electron microscope image of natural Metakaolin is given in Figure 2.5.

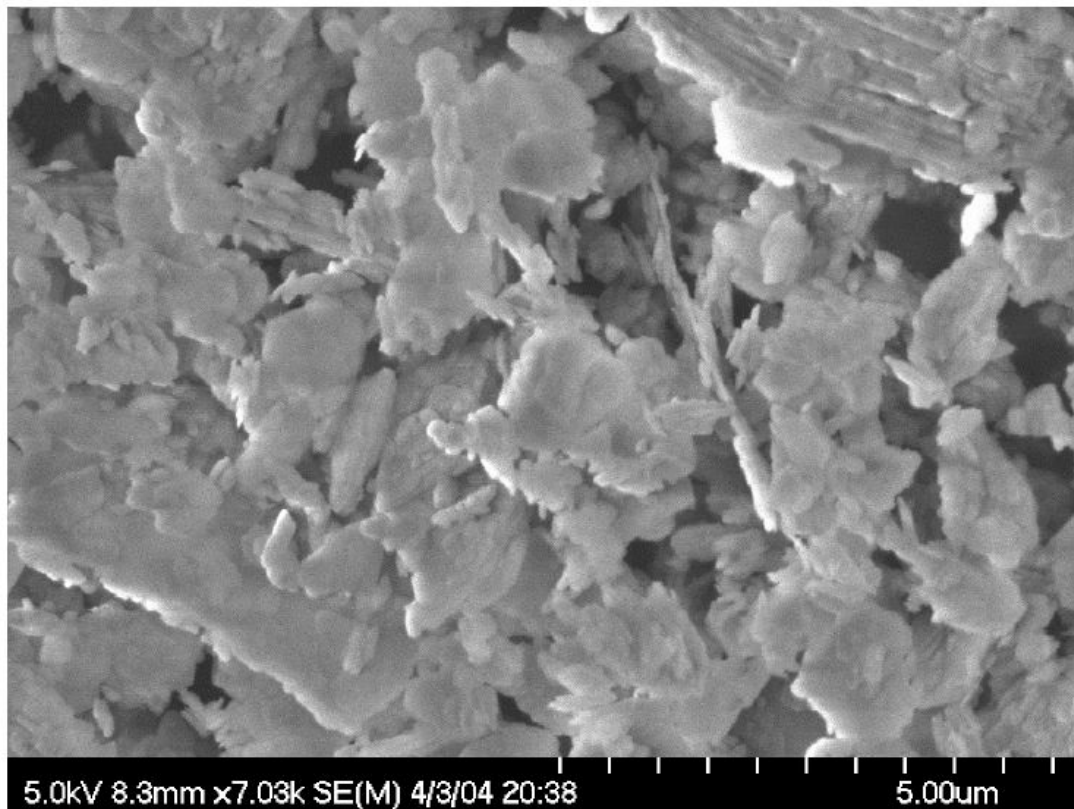


Figure 2.5 SEM micrograph of natural Metakaolin at higher magnification (Kriven, 1994)

2.3.2 Effects of mineral admixtures on the fresh properties of concretes

2.3.2.1 Effects of fly ash on the fresh properties of concretes

The absolute volume of cement plus fly ash normally exceeds that of cement in similar concrete mixtures not containing fly ash. This is because the fly ash normally is of lower density and the mass of fly ash used is usually equal to or greater than the reduced mass of cement. While it depends on the proportions used, this increase in paste volume produces a concrete with improved plasticity and better cohesiveness. In addition, the increase in the volume of fines from fly ash can compensate for deficient aggregate fines. Fly ash changes the flow behaviour of the cement paste; in general spherical shape of fly ash particles normally results in a reduction in the water demand in the concrete for a given workability (ACI 232.2 R-96, 1996).

Bouzoubaa and Lachemi (2001) produced self compacting concrete (SCC) with a cement replacement of 40%, 50%, and 60% by Class F fly ash. They demonstrated that incorporating fly ash improved the slump flow diameter and decreased the V-

funnel flow time of SCCs. Besides, the temperature rise of the SCC was 5 to 10 °C lower than that of the control concrete and the setting times of SCCs were 3 to 4 hours longer than those of the control concrete.

It was found in the study of Şahmaran (2006) that fly ash increased the setting time of the mortars, due to a spherical geometry and a coarse particle size, causing a reduction in the surface area to adsorb free water. Smooth surface characteristics and spherical shape of the FA is also important to improve the workability characteristics of SCC mixtures.

Sonebi (2004) reported that the incorporation of pulverized fuel ash and limestone powder lessened the requirement of superplasticizer necessary to obtain the desired slump. The use of these materials also improved the rheological properties and reduced the risk of cracking of concrete due to the heat of hydration, thus led to more durable concrete. According to ACI 232.2R-96 (1996) report, the use of fly ash may extend the time of setting of concrete if the portland cement content is reduced.

Sekino and Narita (2003) conducted a study to propose the mix design method for SCCs containing high volume fly ash, and to evaluate the effects of replacing cement by fly ash on the strength and durability of the SCCs. They concluded that SCC at 50% replacement level of FA had excellent workability and filling ability at the site of construction.

Xie et al (2002) studied the preparation technology of high-strength self-compacting concrete (SCC) containing ultra-pulverized fly ash and superplasticizer. They found out that the effect of ultra-pulverized fly ash on fresh concrete is to improve the viscosity of fresh concrete, and the effect being the same as that of a viscosity agent. It does not decrease the flowability of fresh concrete. Kim et al. (1996) studied the properties of super flowing concrete containing fly ash and reported that the replacement of cement by 30% fly ash resulted in excellent workability and flowability. Miura et al. (1993) evaluated the influence of supplementary cementitious materials on workability and concluded that the replacement of cement by 30% fly ash can significantly improve rheological properties.

2.3.2.2 Effects of ground granulated blast furnace slag on the fresh properties of concretes

Wood (1981) reported that the workability and placeability of concrete containing ground granulated blast furnace slag (GGBFS) yielded improved characteristics when compared with the concrete without GGBFS. This result was attributed to the surface characteristics of the GGBFS, which created smooth slip planes in the paste. The author also theorized that, due to the smooth, dense surfaces of the GGBFS particles, little if any water was absorbed by the GGBFS during initial mixing, unlike portland cement. Cementitious matrix containing GGBFS had greater workability due to the increased paste content and increased cohesiveness of the paste. Pastes containing GGBFS exhibited different rheological properties compared to paste of portland cements alone. The results indicated a better particle dispersion and higher fluidity of the pastes and mortars, both with and without water-reducing admixtures (ACI 233 R-95, 1995).

Usually, an increase in setting time can be expected when GGBFS is used as a partially replacement of the portland cement in concrete mixtures. The degree to which the setting time is affected is dependent on the initial temperature of the concrete, the proportion of the blend used, the water-cementitious materials ratio, and the characteristics of the portland cement. Although significant retardation has been observed at low temperatures, the additions of conventional accelerators, such as calcium chloride or other accelerating admixtures, can greatly reduce or eliminate this effect. Since the amount of portland cement in a mixture usually determines setting characteristics, changing the GGBFS proportions may be considered in cold weather. At higher temperatures, the slower rate of setting is desirable in most cases, but care may need to be taken to minimize plastic shrinkage cracking (ACI 233 R-95, 1995).

GGBFS provides reactive fines with a low heat of hydration. A high proportion of GGBFS may affect stability of SCC resulting in reduced robustness with problems of consistence control while slower setting can also increase the risk of segregation (EFNARC, 2002).

2.3.2.3 Effects of silica fume on the fresh properties of concretes

The water demand of concrete increases with increasing the amounts of silica fume used due primarily to its high surface area (Scali et al., 1987; Caretta and Malhotra, 1983). Fresh concrete containing silica fume is more cohesive and less prone to segregation than concrete without silica fume. As the silica-fume content increases, the concrete may appear to become sticky. Concrete containing silica fume shows significantly reduced bleeding. This effect is caused primarily by the high surface area of the silica fume to be wetted; there is very little free water left in the mixture for bleeding. Additionally, the silica fume reduces bleeding by physically blocking the pores in the fresh concrete (ACI 234 R-96, 1996).

Silica-fume concrete usually includes chemical admixtures that may affect the time of setting of the concrete. Previous experiences indicate that the setting time is not significantly affected by the use of silica fume alone. Practical control of the setting time may be achieved by using appropriate chemical admixtures. In the literature, there is a general agreement on the retardation of initial and final setting times of the concretes containing FA and GGBFS. The behaviour seen in the SF concretes was different from those with FA and GGBFS in that the addition of SF generally reduced the initial and final setting times of the concretes, especially at 10 and 15% replacement levels. No general agreement could be found in the literature considering the effect of SF content on the setting times of concretes (Gesoglu and Özbay, 2007). Some researchers (Brooks et al., 2000; Alshamsi et al., 1993; Khedr and Abou-Zeid, 1994) stated that SF has retarding effect while some others reported its accelerating effect on the setting times. According to Pistilli et al. (1984) and De Almeida and Goncalves (1990), for a lower water/binder ratio concrete containing a superplasticizer, the effect of SF was to reduce the setting times when compared to those of control concrete containing the same amount of superplasticizer.

Park et al. (2005) investigated the influence of the cementitious materials containing fine particles on the rheology of the pastes. The mineral admixtures used were finely GGBFS, FA, and SF. Cementitious pastes were designed as one component Portland cement (PC), two-components (PC-GGBFS, PC-FA, and PC-SF), and three-components (PC-GGBFS-SF and PC-FA-SF) systems. It was found for the two-component system that yield stress and viscosity decreased with replacing PC with

GGBFS and FA. In the case of PC-SF system, however, yield stress and viscosity steeply increased with increasing SF. For both of the three-component systems the rheological properties of the cementitious pastes improved compared with the PC-SF binary systems.

2.3.2.4 Effects of metakaolin on the fresh properties of concretes

It is well known that Metakaolin (MK) adversely affects the workability of concretes (Sabir et al. 2001). Bai et al (2002) reported that there was a systematic decrease in both slump and compacting factor and a systematic increase in Vebe time as the portland cement was partially replaced by MK with a level of 0 to 15%.

Effects of MK on the setting time and consistency of mortars were determined by Batis et al. (2005). The MK blended cements demand significantly more water than relatively pure cement owing to the high fineness of MK. The increase in the MK content causes a significant increase of the water demand compared with other blended cements. The initial and final setting times of metakaolin cements is higher than the setting time of pure cement.

2.3.3 Effects of mineral admixtures on the hardened properties of concretes

2.3.3.1 Effects of fly ash on the hardened properties of concretes

Fly ash concretes generally have lower early strength due to the slow pozzolanic reaction of fly ash. This strength reduction depends on the content and properties of the fly ash used. In the 1980s, CANMET designed the so-called high-volume fly ash (HVFA) concrete in which 55–60% of the portland cement is replaced by Class F fly ash and such concrete eventually demonstrated excellent mechanical and durability properties (Canada Energy Mines and Resources, 1986; Bilodeau and Malhotra, 2000; Malhotra, 1986).

Yazıcı (2007) performed a study to find out the effects of high volume FA replacement ratio on the properties of SCCs. In that study, cement was replaced by a Class C FA in various proportions from 30 to 60%. Similar tests were carried out

with the incorporation of 10% SF to the same mixtures. The results showed that the compressive strength decreased with the increasing FA content at all ages. The compressive strength of control (0% FA) and 60% FA mixtures were 61.8 MPa and 28.4 MPa, respectively at 28 days. All mixes showed strength gain beyond 28 days and the control mixture reached to 72.5 MPa at 90 days while this value was 38 MPa for 60% FA content. However, it was possible to produce a SCC with a compressive strength value of 50 MPa with 30–40% FA replacement. 10% SF addition to the system positively affected the compressive strength and contributed to the production of SCC mixtures that develop high-mechanical properties incorporating high-volume of FA. At 30% and 40% FA replacement levels, compressive strength values even exceeded the compressive strength of the control specimens at 28 days.

Saraswathy et al. (2003) prepared concrete specimens with 10%, 20%, 30% and 40% of activated fly ash replacement levels and evaluated their compressive strength at 7, 14, 28 and 90 days and the results were compared with that the ordinary portland cement concrete (without fly ash). They also measured electrical resistivity and ultrasonic pulse velocity of the concretes to understand the quality of concrete. In that study, it was noted that, curing time increased the compressive strength of concrete, irrespective of amount of fly ash replaced. A decrease in compressive strength i.e. 1.5 times was observed as the percentage of fly ash replacement increased from 10 to 40%. Saraswathy et al. (2003) also found that the electrical resistance of activated fly ash system showed less resistivity values than ordinary portland cement at replacement levels of 20% and above. This behaviour was observed due to the fact that, in activated fly ash the compatibility with hydrated cement phases and the remaining mineral phases act as more porous in the concrete formulation. With this result, the decrease in resistivity was observed. In addition, activated fly ash contains impurities like unburnt carbon, sulphur etc., increases the electrical conductivity and consequently decreases the resistivity values. Ultrasonic pulse velocity values observed for ordinary portland cement is found to be 4.35 km/s, whereas that for activated fly ash system ranged between 4.36 and 4.00 km/s.

2.3.3.2 Effects of ground granulated blast furnace slag on the hardened properties of concretes

ACI 233 R-95 (1995) provides for three strength grades of GGBFS, depending on their respective mortar strengths when blended with an equal mass of portland cement. The classifications are grades 120, 100, and 80, based on the slag-activity index expressed as in equation 2.5

$$SAI = \text{slag - activity index (\%)} = \left(\frac{SP}{P} * 100 \right) \quad (2.5)$$

where SP is the average compressive strength of slag-reference cement mortar cubes (psi), and P is the average compressive strength of reference cement mortar cubes (psi). Classification is given in Table 2.2

Table 2.2 Slag activity index (ACI 233 R-95, 1995)

Grade	Slag-activity index, minimum percent	
	Average of the last five consecutive samples	Any individual sample
	7-day index	
80	-	-
100	75	70
120	95	90
	28-day index	
80	75	70
100	95	90
120	115	110

Compressive and flexural strength-gain characteristics of concrete containing GGBFS can vary over a wide range. When compared to portland cement concrete, use of grade 120 slag typically results in reduced strength at early ages (1 to 3 days) and increased strength at later ages (7 days and beyond) .Use of grade 100 results in lower strengths at early ages (1 to 21 days), but equal or greater strength at later ages. Grade 80 leads to lower strength at all ages. The extent to which GGBFS affect the strength is dependent on the slag activity index of the particular GGBFS and the ratio in which it is used in the mixture (ACI 233 R-95, 1995).

The proportions of GGBFS and portland cement influence the development of strength of the resulting concrete. For the highest medium-term strength, the proportions are about 1:1, that is, a 50% content of GGBFS in the cementitious

material, the early strength is inevitably lower than with the same content of cementitious materials consisting of portland cement only. The incorporation of GGBFS in concrete does not alter significantly the usual relations between compressive strength and flexural strength or between the compressive strength and modulus of elasticity (Neville, 1996).

2.3.3.3 Effects of silica fume on the hardened properties of concretes

Since silica fume improves the bond between the paste and aggregate, the influence of the quality of the aggregate on the mechanical properties of concrete becomes more important in silica-fume concrete.

Bhanja and Sengupta (2005) carried out an extensive experimental study over the water–binder ratios ranging from 0.26 to 0.42 and silica fume–binder ratios from 0.0 to 0.3. They were determined, compressive, flexural and split-tensile strengths at 28 days. The compressive, as well as the tensile strengths increased with silica fume incorporation, and the results indicated that the optimum content is not constant but depends on the water–cementitious material (w/cm) ratio of the mixture as seen in Figure 2.6. When compared to splitting tensile strength, flexural strength has exhibited greater improvements.

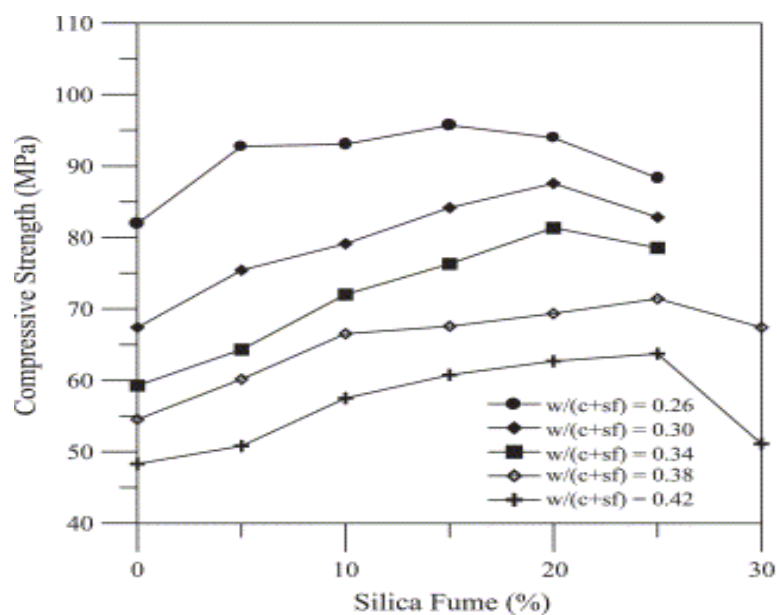


Figure 2.6 Influence of silica fume replacement and water binder ratio on the compressive strength of concretes (Bhanja and Sengupta, 2005)

According to ACI committee report (ACI 234 R-96, 1996) the static elastic modulus of silica fume concretes is apparently similar to that of portland cement concrete of similar strength. Helland et al (1983) concluded that the stress-strain behaviour of silica-fume concrete was similar to that of portland-cement concrete. Sellevold and Nilsen (1987) found that the dynamic modulus of elasticity increases with increasing silica-fume content in pastes.

Mazloom et al. (2004) demonstrated that the compressive strength development of the concrete mixtures containing silica fume was negligible after the age of 90 days; however, there were 26% and 14% strength increase in the control concrete after one year compared to its 28 and 90 days strengths, respectively. At the age of 28 days, the strength of concrete containing 15% silica fume was about 21% higher than that of the control concrete. Therefore, the inclusion of silica fume in concrete mixture, mainly affects short-term strength of concrete. The difference in strength development in ordinary portland cement concrete and silica fume concrete can be attributed (Wild et al., 1995) to the rapid formation of an inhibiting layer of the reaction products preventing further reaction of SF with calcium hydroxide beyond 90 days. In the case of the control concrete, hydration is at a less advanced stage and strength still shows significant improvement.

2.3.3.4 Effects of metakaolin on the hardened properties of concretes

In metakaolin blended cement concretes, metakaolin contributes to the strength of concrete not only at early ages mainly by the filling effect, but also at later ages due to the fast pozzolanic reaction (Poon et al., 2006).

Naveen et al. (2006) presented the results of experimental studies wherein fly ash, metakaolin and their blends were used as fillers in SCC. The results showed that SCC can be produced with cement content, as low as 200 kg/m³ of concrete together with rest of the powder coming from fly ash. High strength SCC can be obtained through incorporation of metakaolin.

The use of MK is reported to increase the concrete strength especially during the early ages of hydration (Zhang and Malhotra, 1995). After 14 days of curing the contribution that MK provides to concrete strength is reduced (Wild et al., 1996).

The increase in compressive strength of MK concrete is thought to be due to the filling effect where MK particles fill the space between cement particles, acceleration of cement hydration and pozzolanic reaction of MK. This effect is similar to that of silica fume. Although the pore volume slightly increases in pastes containing MK, the pore structure of paste, however, is found to be refined (Khatib and Wild, 1996). The improvement in pore structure of the paste is increased when the amount of MK increases up to at least 20% as partial substitution of PC (Khatib and Hibbert, 2005). The incorporation of up to at least 30% MK increases the sulphate resistance of mortar (Khatib and Wild, 1998). The portlandite content in MK paste and mortar is reduced due to the reaction between PC hydration products and MK (Wild and Khatib, 1997).

In order to evaluate and compare the mechanical properties of the concrete having metakaolin, Kim et al. (2007) conducted compressive, splitting tensile and flexural strength tests on the concrete specimens using various replacements of silica fume and metakaolin. The compressive strengths obtained at 1, 3, 7, 28, 56, and 91 days of the above mentioned study are given in Figure 2.7. This demonstrated that the level of compressive strength developed according to the replacement ratio of the binder by MK and SF, from 5% to 20%. A replacement ratio of 15% was seen to improve the development of compressive strength, but such effect appears to reduce for 20%. In other words, the most remarkable strengths were developed for replacement ratios from 10 to 15%, with poor improvement effect for a replacement ratio of 15% compared to 20%.

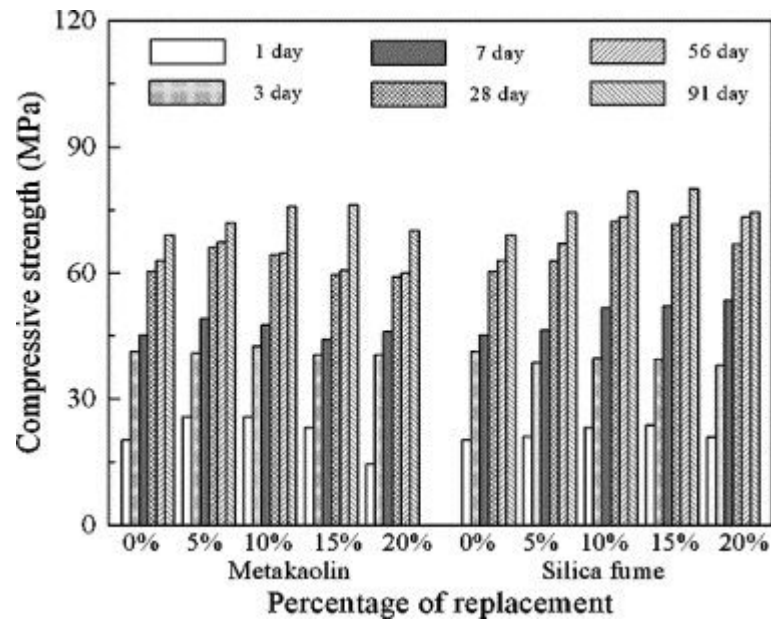


Figure 2.7 Compressive strength changes with replacement ratio of MK and SF at various testing age (Kim et al., 2007)

Figure 2.8 presents the tensile strengths measured for tests performed at 1, 3, 7, 28, 56, and 91 days. It was observed that the level of splitting tensile strength developed dependent mainly on the replacement ratio of the binder by MK and SF, from 5% to 20%. For a replacement ratio ranging between 10% and 15%, it was observed that the strength enhanced as the replacement ratio increased, while there was strength reduction at 20%. It was also detected that the values of splitting tensile strength reached about 6% of the compressive strength.

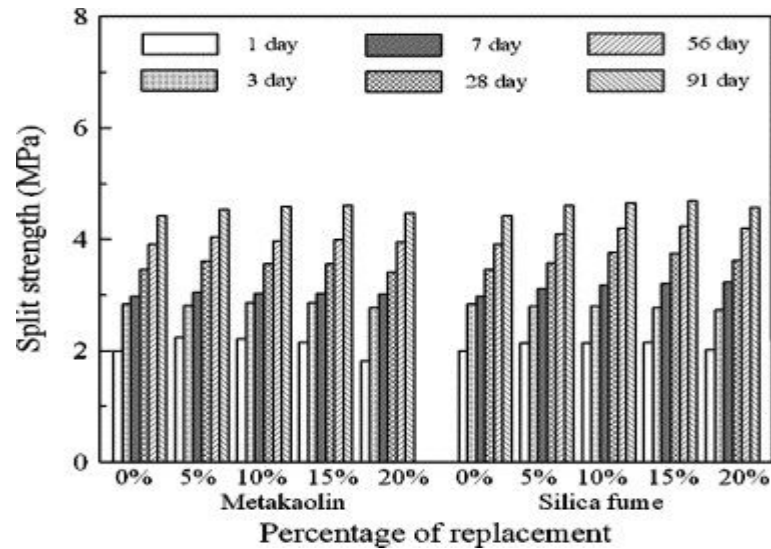


Figure 2.8 Splitting tensile strength variations with replacement ratio of MK and SF at varying testing age (Kim et al., 2007)

The flexural strengths measured at 1, 3, 7, 28, 56 and 91 days are plotted in Figure 2.9 to verify the level of flexural strength developed depending on the binder replacement ratios. Test results revealed that the strength increases with increasing the replacement ratio of the binder employed. It can be verified that the values of the flexural strength reach about 10% of the compressive strength.

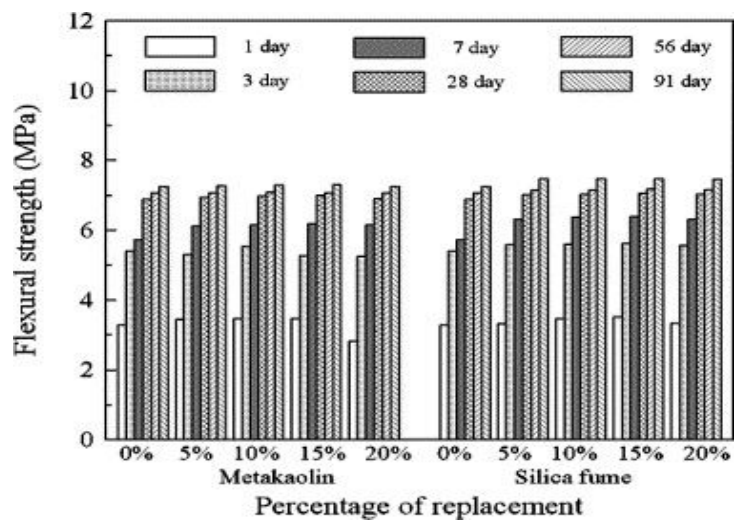


Figure 2.9 Flexural strength variations with replacement ratio of MK and SF at various testing age (Kim et al., 2007)

2.3.4 Effects of mineral admixtures on the durability properties of concretes

2.3.4.1 Effects of fly ash on the durability properties of concretes

Deterioration of concrete depends on the penetration of aggressive substances into concrete via microcracks and interconnected pore system. Permeability of fly ash concretes at early ages can be significantly higher when compared to that of portland cement concrete. At later ages, however, fly ash concretes can have much lower permeability depending on the content and characteristics of the fly ash used (Taşdemir, 2003).

Bilodeau et al. (1994) presented the results of investigations to determine the various durability aspects of high-volume fly ash concretes using eight fly ashes and two portland cements obtained from US sources. Briefly, in high-volume fly ash concrete, the water and cement content were kept low at about 115 and 155 kg/m³ of concrete, respectively, and the proportion of fly ash in the total cementitious materials content ranged from 55 to 60%. The durability aspects investigated included resistance to the repeated cycles of freezing and thawing, deicing salt-scaling resistance, resistance to the chloride-ion penetration, and determination of water permeability coefficient. Based upon the test results, it was concluded that regardless of the type of fly ash and the cement used, the air-entrained high-volume fly ash concrete exhibited excellent durability characteristics in the tests investigated. The only exception was the deicing salt-scaling test in which the performance of the concretes investigated was less than satisfactory.

McCarthy and Dhir (2005) performed a study to examine the use of high levels of low-lime fly ash (high volume FA) as a cement component in concrete. Durability tests covering water absorption, water permeability, carbonation rates and chloride diffusion were carried out on the produced concretes. At the end of the experimental study, it was observed that water absorption, water permeability, and chloride diffusion tests indicated enhanced performance with high FA levels, while for carbonation rates similar performance to PC concrete was generally noted, although this may be slightly poorer at low design strength.

Malhotra (2000) prepared a report on the resistance of concrete to the chloride ion penetration measured according to the ASTM C 1202 on 10 year old concretes so as

to indicate the long term performance of the concretes with pozzolans. The charge passed through the concrete mixtures investigated in this study was less than 1000 coulombs at 10 years indicating very low chloride-ion penetrability. For the high volume fly ash concrete, the charge passed was 0, giving a chloride ion penetrability rating of these concretes as negligible. It is extremely rare to achieve values as low as this in portland cement concrete (Şengül, 2005).

Scaling of concrete exposed to deicing salts occurs when immature or non air-entrained concrete pavements are exposed to large quantities of deicing salts in a freezing and thawing environment. Concrete pavements containing fly ash that are exposed to deicing salts should be air entrained and allowed to reach a specified strength or maturity. There is some laboratory research that indicates concrete containing 40 percent fly ash, as a percentage of the total mass of cementitious material, may be more susceptible to scaling (ACI 232.2 R-96, 1996).

2.3.4.2 Effects of ground granulated blast furnace slag on the durability properties of concretes

The beneficial effects of GGBFS arise from the denser microstructure of hydrated cement paste, more of the pore space being filled with C-S-H than in portland cement only paste. As a result of improved pore structure of hydrated paste of a portland cement-GGBFS blend, and also because of low content of calcium hydroxide, the resistance to the sulphate attack is improved. Tests on concrete containing GGBFS have confirmed good resistance to penetration by chloride ions e.g. when the GGBFS content is at least 60% by mass of the cementitious materials and the water/cement ratio is 0.50, the diffusion coefficient of the concrete exposed to chloride ions is at least ten times smaller than when the cementitious materials consists entirely of portland cement (Neville, 1996).

The electrical resistivity of concrete is an important component of reinforcing steel corrosion cells, as high resistivity of the concrete reduces corrosion currents, and thus slowing the rate of corrosion. Gesoğlu and Özbay (2007) investigated the effects of GGBFS on the electrical resistivity of the self compacting concretes. In that study GGBFS replaced portland cement at 20%, 40% and 60% levels. Test results showed

that the lowest electrical resistivity was obtained at normal portland cement concrete with 12.8 kohm-cm and there was a gradual increase in the electrical resistivity of SCC with increasing GGBFS content.

Although some laboratory tests with slag blended cement indicate less resistance to deicing salts, many researchers have found, in field exposure, little difference when compared to concrete not containing slag (ACI 233 R-95, 1995). Similar results were reported using blends of 50 percent GGBFS and 50 percent portland cement, by Hogan and Meusel (1981). Most research indicates that scaling is usually found when the concrete has a high water-cementitious materials ratio associated with high amount of GGBFS (ACI 233 R-95, 1995).

2.3.4.3 Effects of silica fume on the durability properties of concretes

Alexander and Magee (1999) examined the durability performance of various condensed silica fume (CSF) concretes in comparison to portland cement (PC) and PC/GGBFS controls. Oxygen permeability index, water sorptivity, chloride conductivity tests were performed on the produced concrete samples and the test results indicated that durability performance was significantly improved when using CSF in all tests.

Pigeon et al. (1986) investigated the freeze-thaw durability of concrete with and without silica fume in accordance with the requirements of ASTM Test Method for Resistance of Concrete to Rapid Freezing and Thawing (C 666 Procedure A). The water-cement ratio of all mixes was 0.5, and the silica-cement ratio of the silica fume mixes being 0.1. The test results showed that the critical value of the air-void spacing factor in these ASTM C 666 tests is significantly lower for the silica fume concretes. Such concretes therefore appeared to be more susceptible to internal cracking caused by rapid freeze-thaw cycles in water, even though the use of silica fume decreased the surface scaling of the test specimens. This confirms that scaling and internal cracking are two different forms of frost damage caused by rapid freeze-thaw cycles in water.

The sulphate resistance of concrete containing silica fume is good, partly because of lower permeability, and partly in consequence of a lower content of calcium

hydroxide and of alumina, which has become incorporated in C-S-H. Tests on mortar have shown also the beneficial effect of silica fume upon resistance to solutions magnesium, sodium, and calcium chlorides (Neville, 1996).

2.3.4.4 Effects of metakaolin on the durability properties of concretes

There is a strong evidence that metakaolin greatly influence the pore structure in the paste and the mortars and produces substantial pore refinement. This leads to significant modification to the water transport properties and diffusion rates of harmful ions (Sabir et al., 2001). It has been reported that MK reduces the volume of capillary pores of sizes (0.05-10 μ m) normally associated with increased permeability. Rate of water absorption of mortar is halved by replacing 20% of the cement by MK (ECC International Document Product, 1996). Coleman and Page (1997) have shown that cement paste blended with 10% or 20% MK exhibited higher capacities than PC pastes, to chloride ions introduced by contamination of the mix water, thus reducing Cl⁻ concentration in pore solution.

Kostuch et al. (1993) showed that expansion in concrete due to alkali silica reaction is completely eliminated by replacing the standard portland cement used by 15% MK. Pera et al. (1998) examined the influence of MK on the resistance of concrete to solutions of lactic acid and ammonium sulphate simulating and aggressive agricultural environment. The result of this research showed that the presence of 10% MK limited the damage caused by exposure to lactic acid.

3. EXPERIMENTAL PROGRAM AND METHODOLOGY

3.1 Introduction

In this study an experimental program was conducted to investigate the effects of mineral admixtures in binary (two components), ternary (three components), and quaternary (four components) cementitious blends on the fresh and hardened properties of self compacting concretes. For this purpose four mineral admixtures, namely fly ash (FA), ground granulated blast furnace slag (GGBFS), silica fume (SF) and metakaolin (MK) were used in the production of self compacting concretes. The fresh properties of the self compacting concretes produced were observed through slump flow diameter, slump flow time, V-funnel flow time, L-box height ratio, initial and final setting times, and viscosity. The concretes were also tested for the mechanical, physical, and durability properties. The hardened concretes were tested for the compressive strength, splitting tensile strength, and ultrasonic pulse velocity at 28 and 90 days for the evaluation of mechanical properties. Shrinkage accompanied by the water loss were also monitored for a drying period of 50 days. Moreover, the durability tests were conducted to investigate the resistance to chloride ion penetration, electrical resistivity, water absorption, sorptivity, and water permeability at the age of 90 days.

3.2 Materials

3.2.1 Cement

The cement used in all SCC mixtures was a normal portland cement of CEM I 42.5 R (PC) which corresponds to ASTM Type I grade. It had a specific gravity of 3.15 g/cm³ and Blaine fineness of 3260 cm²/g. Data showing the physical and chemical analysis reported by the cement manufacturer are given in Table 3.1.

Table 3.1 Chemical composition and physical properties of cement and mineral admixtures

Chemical analysis [%]	Portland cement	SF	FA	GGBFS	MK
CaO	62.58	0.45	4.24	34.12	0.78
SiO ₂	20.25	90.36	56.2	36.41	52.68
Al ₂ O ₃	5.31	0.71	20.17	10.39	36.34
Fe ₂ O ₃	4.04	1.31	6.69	0.69	2.14
MgO	2.82	-	1.92	10.26	0.16
SO ₃	2.73	0.41	0.49	-	-
K ₂ O	0.92	1.52	1.89	0.97	0.62
Na ₂ O	0.22	0.45	0.58	0.35	0.26
Loss of ignition	3.02	3.11	1.78	1.64	0.98
Physical Properties					
Specific gravity	3.15	2.2	2.25	2.79	2.50
Blaine Fineness [m ² /kg]	3260	21080	287	418	12000

3.2.2 Mineral admixtures

3.2.2.1 Fly ash

The fly ash (FA) used in this research was a class F type according to ASTM C 618 (2002) and obtained from Yumurtalik-Sugozy thermal power plant in the form of commercial grade. It had a specific gravity of 2.25 g/cm³ and the Blaine fineness of 287 m²/kg. The chemical analysis of FA is shown in Table 3.1.

3.2.2.2 Ground granulated blast furnace slag

A ground granulated blast furnace slag (GGBFS) was obtained from Iskenderun cement production factory. It had a specific gravity of 2.79 g/cm³ and Blaine fineness of 418 m²/kg. The chemical composition of GGBFS is also given in Table 3.1.

3.2.2.3 Silica fume

A commercial grade silica fume (SF) obtained from Norway was utilized in this study. It had a specific gravity of 2.2 g/cm³ and the specific surface area (Nitrogen BET Surface Area) of 21080 m²/kg. In Table 3.1, both the chemical analysis and physical properties of SF is provided.

3.2.2.4 Metakaolin

The metakaolin (MK) used in this study is a white powder with a Hunter L whiteness value of greater than 90 (on a scale from “0-black” to “100-maximum whiteness”). It was obtained from USA and, the specific gravity and specific surface area reported by the manufacturer to be 2.50 g/cm³ and 12000 m²/kg, respectively. Data showing the physical and chemical analysis of MK provided by the manufacturer are given in Table 3.1.

3.2.2 Aggregates

The coarse aggregate used was river gravel with a nominal maximum size of 16 mm. As fine aggregate, a mixture of natural river sand and crushed limestone was used with a maximum size of 5 mm. The coarse aggregate had a specific gravity of 2.72 and its water absorption was 0.45%. The specific gravity and water absorptions of natural river sand and crushed limestone were 2.66 and 2.45 g/cm³, and 0.55% and 0.92%, respectively. The particle size gradation obtained through the sieve analysis and physical properties of the fine and coarse aggregates are presented in Table 3.2. Grading curves of fine and coarse aggregates associated with that of the control mixture are presented in Figure 3.1.

Table 3.2 Sieve analysis and physical properties of the fine and coarse aggregates

Sieve size [mm]	Fine aggregate		Coarse aggregate
	River sand	Crushed sand	
16	100	100	100
8	100	100	31.5
4	86.6	95.4	1.0
2	56.7	63.3	0.5
1	37.7	39.1	0.5
0.5	25.7	28.4	0.5
0.25	6.7	16.4	0.4
Fineness modulus	2.87	2.57	5.66
Specific gravity	2.66	2.45	2.72
Absorption [%]	0.55	0.92	0.45

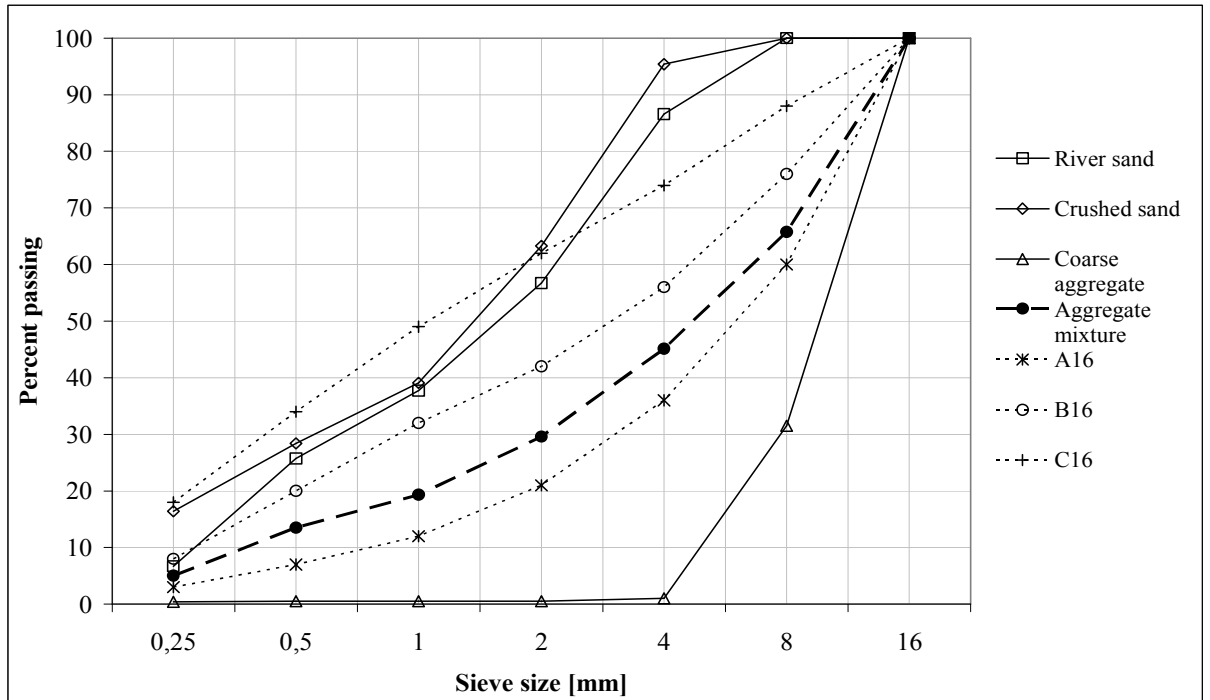


Figure 3.1 Aggregate grading curves

3.2.3 Superplasticizer

A polycarboxylic-ether type superplasticizer (SP) with a specific gravity of 1.07 and pH of 5.7 was used in all mixtures. The properties of superplasticizer are given in Table 3.3 as reported by the local supplier.

Table 3.3 Properties of superplasticizer

Properties	Superplasticizer
Name	Glenium 51
Color tone	Dark brown
State	Liquid
Specific gravity (kg/l)	1.07
Chemical description	Modified polycarboxylic type polymer
Recommended dosage	%1-2 (% binder content)

3.3 Concrete Mixtures

A total of 65 SCC mixtures were designed at 0.32 and 0.44 water/binder ratios (w/b). In the design of the first group concretes, enumerated from M1 to M43 given in Table 3.4, the w/b ratio was 0.32 and the total cementitious materials content was 550 kg/m^3 . In the production of such concretes the mineral admixtures used were FA, GGBFS, SF and MK. The mixture M1 in Table 3.4 was designated as the control mixture which included only ordinary portland cement as the binder while the remaining mixtures (M2 to M43) incorporated binary (PC+FA, PC+GGBFS, PC+SF, PC+MK), ternary (PC+FA+GGBFS, PC+FA+SF, PC+GGBFS+SF, PC+FA+MK, PC+GGBFS+MK, PC+SF+MK), and quaternary (PC+FA+GGBFS+SF, PC+FA+GGBFS+MK, PC+FA+SF+MK, PC+GGBFS+SF+MK) cementitious blends in which a proportion of portland cement was replaced with the mineral admixtures. The replacement ratios for both FA and GGBFS were 20, 40, and 60% while those of SF and MK were 5, 10, and 15 % by weight of the total binder. In the design of the concretes within the second group (M44 to M65 in Table 3.5) however, a w/b ratio of 0.44 associated with a cement content of 450 kg/m^3 was employed. The mineral admixtures used in producing the concretes in this were FA, GGBFS, and SF. The M44 mixture in Table 3.5 was designed to be the control mixture including only ordinary portland cement as the binder while the remaining mixtures (M45 to M65) incorporated binary (PC+FA, PC+GGBFS, PC+SF), ternary (PC+FA+GGBFS, PC+FA+SF, PC+GGBFS+SF), and quaternary (PC+FA+GGBFS+SF) cementitious blends in which the mineral additives replaced a proportion of portland cement. The similar replacement ratios were used for the mineral admixtures as in the case of the 0.32 w/b ratio. The mixture M40 (22.5FA22.5GGBFS15SF), for example, includes 22.5% FA, 22.5% GGBFS and 15% SF. When preparing ternary and quaternary mixtures, FA and GGBFS, and MK and SF were considered as the similar type cementitious materials so that they were used in equal amounts in the mixtures which contained both of them.

Table 3.4 Concrete mixture proportioning at a w/b ratio of 0.32

Mix No	Mix Description	W/B	Water [kg/m ³]	PC [kg/m ³]	FA [kg/m ³]	GGBFS [kg/m ³]	SF [kg/m ³]	MK [kg/m ³]	Natural sand [kg/m ³]	Crushed sand [kg/m ³]	Coarse aggregate [kg/m ³]	SP [kg/m ³]
M1	0.32W/B Control-PC	0.32	176	550	0	0	0	0	522	206	935	8.43
M2	0.32W/B20FA	0.32	176	440	110	0	0	0	512	202	917	7.43
M3	0.32W/B40FA	0.32	176	330	220	0	0	0	502	198	899	7.43
M4	0.32W/B60FA	0.32	176	220	330	0	0	0	492	194	881	6.67
M5	0.32W/B20GGBFS	0.32	176	440	0	110	0	0	520	205	931	10.43
M6	0.32W/B40GGBFS	0.32	176	330	0	220	0	0	518	204	928	10.00
M7	0.32W/B60GGBFS	0.32	176	220	0	330	0	0	516	204	924	8.89
M8	0.32W/B5SF	0.32	176	522.5	0	0	27.5	0	519	205	930	9.56
M9	0.32W/B10SF	0.32	176	495	0	0	55	0	516	204	925	10.67
M10	0.32W/B15SF	0.32	176	467.5	0	0	82.5	0	513	203	920	12.00
M11	0.32W/B5MK	0.32	176	522.5	0	0	0	27.5	520	205	932	11.00
M12	0.32W/B10MK	0.32	176	495	0	0	0	55	519	205	929	11.00
M13	0.32W/B15MK	0.32	176	467.5	0	0	0	82.5	517	204	927	11.00
M14	0.32W/B15FA5SF	0.32	176	440	82.5	0	27.5	0	511	202	916	8.22
M15	0.32W/B30FA10SF	0.32	176	330	165	0	55	0	501	198	898	9.11
M16	0.32W/B45FA15SF	0.32	176	220	247.5	0	82.5	0	491	194	880	8.89
M17	0.32W/B15FA5MK	0.32	176	440	82.5	0	0	27.5	513	202	919	8.00
M18	0.32W/B30FA10MK	0.32	176	330	165	0	0	55	504	199	903	6.00
M19	0.32W/B45FA15MK	0.32	176	220	247.5	0	0	82.5	495	195	887	6.80
M20	0.32W/B15GGBFS5SF	0.32	176	440	0	82.5	27.5	0	517	204	927	9.78
M21	0.32W/B30GGBFS10SF	0.32	176	330	0	165	55	0	513	203	920	10.78
M22	0.32W/B45GGBFS15SF	0.32	176	220	0	247.5	82.5	0	509	201	912	10.22
M23	0.32W/B15GGBFS5MK	0.32	176	440	0	82.5	0	27.5	519	205	929	8.00
M24	0.32W/B30GGBFS10MK	0.32	176	330	0	165	0	55	516	204	924	8.00

Table 3.4 Contnd

Mix No	Mix Description	W/B	Water [kg/m ³]	PC [kg/m ³]	FA [kg/m ³]	GGBFS [kg/m ³]	SF [kg/m ³]	MK [kg/m ³]	Natural sand [kg/m ³]	Crushed sand [kg/m ³]	Coarse aggregate [kg/m ³]	SP [kg/m ³]
M25	0.32W/B45GGBFS15MK	0.32	176	220	0	247.5	0	82.5	513	202	919	8.00
M26	0.32W/B10FA10GGBFS	0.32	176	440	55	55	0	0	516	204	924	8.00
M27	0.32W/B20FA20GGBFS	0.32	176	330	110	110	0	0	510	201	913	7.50
M28	0.32W/B30FA30GGBFS	0.32	176	220	165	165	0	0	504	199	903	4.44
M29	0.32W/B2.5SF2.5MK	0.32	176	522.5	0	0	13.75	13.75	519	205	931	9.00
M30	0.32W/B5SF5MK	0.32	176	495	0	0	27.5	27.5	517	204	927	9.70
M31	0.32W/B7.5SF7.5MK	0.32	176	467.5	0	0	41.25	41.25	515	203	923	10.78
M32	0.32W/B15FA2.5SF2.5MK	0.32	176	440	82.5	0	13.75	13.75	512	202	917	7.50
M33	0.32W/B30FA5SF5MK	0.32	176	330	165	0	27.5	27.5	502	198	900	7.50
M34	0.32W/B45FA7.5SF7.5MK	0.32	176	220	247.5	0	41.25	41.25	493	195	883	6.50
M35	0.32W/B15GGBFS2.5SF2.5MK	0.32	176	440	0	82.5	13.75	13.75	518	204	928	7.00
M36	0.32W/B30GGBFS5SF5MK	0.32	176	330	0	165	27.5	27.5	514	203	922	7.25
M37	0.32W/B45GGBFS7.5SF7.5MK	0.32	176	220	0	247.5	41.25	41.25	511	202	915	7.55
M38	0.32W/B7.5FA7.5GGBFS5SF	0.32	176	440	41.25	41.25	27.5	0	514	203	922	6.40
M39	0.32W/B15FA15GGBFS10SF	0.32	176	330	82.5	82.5	55	0	507	200	909	6.48
M40	0.32W/B22.5FA22.5GGBFS15SF	0.32	176	220	123.75	123.75	82.5	0	500	197	896	8.00
M41	0.32W/B7.5FA7.5GGBFS5MK	0.32	176	440	41.25	41.25	0	27.5	516	204	924	8.00
M42	0.32W/B15FA15GGBFS10MK	0.32	176	330	82.5	82.5	0	55	510	201	913	7.00
M43	0.32W/B22.5FA22.5GGBFS15MK	0.32	176	220	123.75	123.75	0	82.5	504	199	903	7.00

Table 3.5 Concrete mixture proportioning at a w/b ratio of 0.44

Mix No	Mix Description	W/B	Water [kg/m ³]	PC [kg/m ³]	FA [kg/m ³]	GGBFS [kg/m ³]	SF [kg/m ³]	MK [kg/m ³]	Natural sand [kg/m ³]	Crushed sand [kg/m ³]	Coarse aggregate [kg/m ³]	SP [kg/m ³]
M44	0.44W/B Control-PC	0.44	198	450	0	0	0	0	592	234	868	3.5
M45	0.44W/B20FA	0.44	198	360	90	0	0	0	583	230	855	3.2
M46	0.44W/B40FA	0.44	198	270	180	0	0	0	574	227	842	2.96
M47	0.44W/B60FA	0.44	198	180	270	0	0	0	565	223	829	3
M48	0.44W/B20GGBFS	0.44	198	360	0	90	0	0	590	233	866	3.7
M49	0.44W/B40GGBFS	0.44	198	270	0	180	0	0	589	232	863	3.44
M50	0.44W/B60GGBFS	0.44	198	180	0	270	0	0	587	232	860	2.8
M51	0.44W/B5SF	0.44	198	427.5	0	0	22.5	0	590	233	865	4.88
M52	0.44W/B10SF	0.44	198	405	0	0	45	0	587	232	861	5.2
M53	0.44W/B15SF	0.44	198	382.5	0	0	67.5	0	585	231	858	7.76
M54	0.44W/B15FA5SF	0.44	198	360	67.5	0	22.5	0	583	230	855	4.24
M55	0.44W/B30FA10SF	0.44	198	270	135	0	45	0	574	227	841	4.52
M56	0.44W/B45FA15SF	0.44	198	180	202.5	0	67.5	0	565	223	828	4.824
M57	0.44W/B15GGBFS5SF	0.44	198	360	0	67.5	22.5	0	588	232	863	4
M58	0.44W/B30GGBFS10SF	0.44	198	270	0	135	45	0	585	231	857	4.56
M59	0.44W/B45GGBFS15SF	0.44	198	180	0	202.5	67.5	0	581	229	852	5.76
M60	0.44W/B10FA10GGBFS	0.44	198	360	45	45	0	0	587	232	860	3.2
M61	0.44W/B20FA20GGBFS	0.44	198	270	90	90	0	0	581	230	852	3.2
M62	0.44W/B30FA30GGBFS	0.44	198	180	135	135	0	0	576	227	845	2.8
M63	0.44W/B7.5FA7.5GGBFS5SF	0.44	198	360	33.75	33.75	22.5	0	586	231	859	4.2
M64	0.44W/B15FA15GGBFS10SF	0.44	198	270	67.5	67.5	45	0	579	229	849	4.24
M65	0.44W/B22.5FA22.5GGBFS15SF	0.44	198	180	101.25	101.25	67.5	0	573	226	840	5.04

3.4 Concrete Casting, Test Specimens, and Curing

In the production of SCCs, the mixing sequence and duration are so important that a special procedure proposed by Khayat et al. (2000) was employed to supply the same homogeneity and uniformity in all mixtures. The batching sequence consisted of homogenizing the fine and coarse aggregates for 30 sec in a rotary planetary mixer, then adding about half of the mixing water into the mixer and continuing to mix for one more minute. Thereafter, the aggregates were left to absorb the water in the mixer for one minute. After the cement and mineral admixtures were added, the mixing was resumed for another minute. Finally, the SP with remaining water was introduced, and the concrete was mixed for 3 min and then left for 2 min to rest. Eventually, the concrete was mixed for additional two minutes to complete the mixing sequence. The concretes were designed to give a slump flow of 70 ± 3 cm which was achieved by using the superplasticizer at varying amounts. For this, trial batches were produced for each mixture till the desired slump flow was obtained.

After the mixing procedure had been completed, tests were conducted on the fresh concrete to determine slump flow time and diameter, V-funnel flow time, L-Box height ratio, initial and final setting times, and viscosity. Segregation and bleeding were also visually checked during the slump flow test. The compressive strength, splitting tensile strength, ultrasonic pulse velocity, drying shrinkage, weight loss, rapid chloride permeability, electrical resistivity, water absorption, sorptivity and water permeability properties of SCCs were also determined in the hardened state. All of the specimens were cast full without any compaction and vibration.

Specimens cast from a typical mixture consisted mainly of the following:

- Six 150 mm cubes for the compressive strength evaluation at 28 and 90 days, which also provided UPV measurement prior to compression test.
- Two 150 mm cubes for water permeability test
- Two 100x200 mm cylinders for rapid chloride permeability
- Two 150x300 mm cylinders for splitting tensile strength determination
- Two 100x200 mm cylinders for electrical resistivity measurement

- Four 70x70x280 mm prisms to monitor free shrinkage and weight loss

Additionally, one 100x100x100 mm cube mortar was sieved from the fresh concrete for the measurement of the initial and final setting times of SCCs. Furthermore, a 0.5 liter beaker mortar was obtained by sieving the SCC for viscosity determination of SCCs.

Immediately after casting, free shrinkage test specimens were cured for 24 hr at 20 °C and 100% relative humidity and then demoulded. After the gage length was formed on each specimen by gluing the pins on the face of the specimen, its initial weight was recorded to monitor the weight loss during drying period. Then, the specimens were exposed to drying in a humidity cabinet at 23 ± 2 °C and $50 \pm 5\%$ relative humidity for about 50 days. All the other specimens were covered with a plastic sheet and left in the casting room for 24 hr. Then, they were demoulded and water cured up to 28 days. The specimens that would be tested at 90 days were further kept in a curing room at 23 ± 2 °C and $65 \pm 5\%$ relative humidity till the testing age.

3.5 Tests for Fresh Properties

3.5.1 Slump flow

The slump flow test specified by the Japan society of civil engineers evaluates the capacity of concrete to flow under its own weight without any restraint, except from the friction of surface and test based on the slump cone test, used for traditional concrete. To measure the slump flow, an ordinary slump flow cone is filled with SCC without any compaction and leveled. The cone is lifted and average diameter of the resulting concrete spread is measured as seen Figure 3.2. A slump flow value ranging from 650 mm to 800 mm for a concrete to be compacted according to EFNARC (2002). In this study, slump flow diameter of all the mixtures was kept constant at about 70 ± 3 cm. In the slump flow test, the time (T_{50}) was also measured which determines the time taken for the concrete to reach the 500 mm spread circle. A lower time indicates greater flowability. EFNARC suggests a T_{50} of 2 to 5 sec for a SCC.

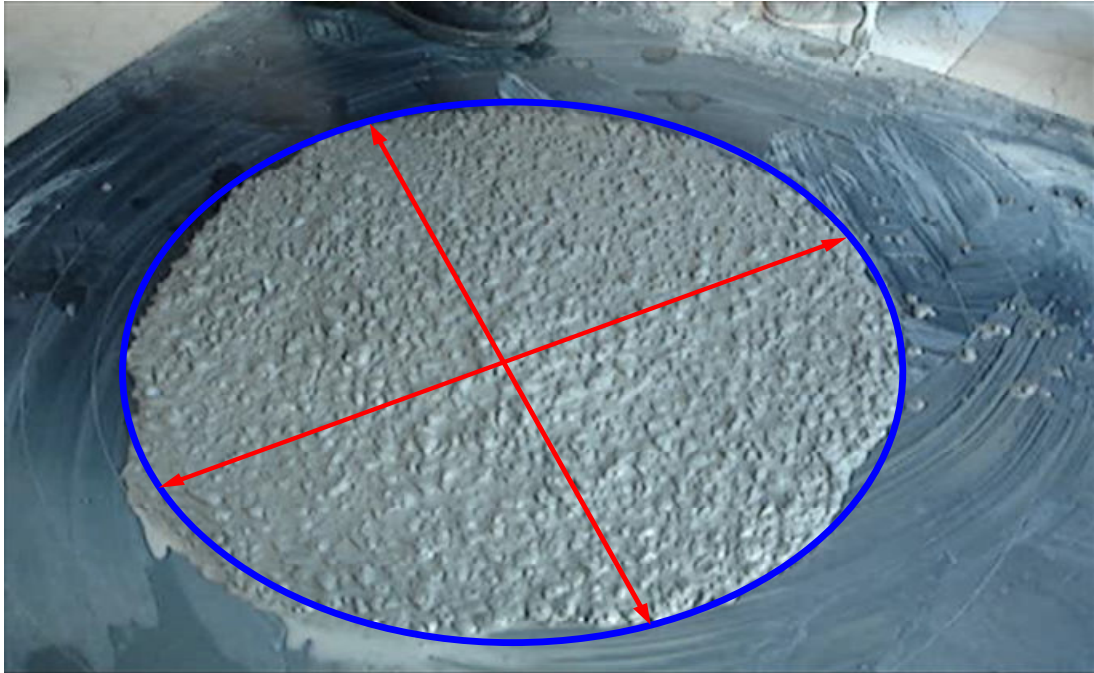


Figure 3.2 Photographic demonstration of measurement of slump flow diameter

3.5.2 V-funnel flow time

In evaluating the flowability and the viscosity of the mixtures the V-Funnel test was conducted (Figure 3.3). The flow time is determined using a simple procedure in which the funnel is completely filled with fresh concrete, and the flow time is measured as the time between the opening of the orifice and the complete emptying of the funnel. Good flowable and stable concrete would consume short time to flow out. According to Khayat et al. (1997), a funnel test flow time (t_{v-f}) less than 6 sec is recommended for a concrete to qualify for self compacting. According to EFNARC, t_{v-f} ranging from 6 to 12 sec is considered adequate for a SCC.



Figure 3.3 Photographic view of V-funnel flow time measurement

3.5.3 L-box test

The L-box apparatus consists of a rectangular-section box in the shape of an 'L', with a vertical and horizontal section, separated by a moveable gate, in front of which vertical lengths of reinforcement bar are fitted (Figure 3.4). The vertical section is filled with concrete, and then the gate is lifted to let the concrete flow into the horizontal section. When the flow has stopped, the height of the concrete at the end of the horizontal section is expressed as a proportion of that remaining in the vertical section. It indicates the slope of the concrete when at rest. This is an indication of passing ability, or the degree to which the passage of concrete through the bars is restricted. The horizontal section of the box can be marked at 200mm and 400mm from the gate and the times taken to reach these points measured. These are known as the T_{200} and T_{400} times and are an indication for the filling ability. L-box test assesses filling and passing ability of SCCs, and serious lack of stability (segregation) can be detected visually. Segregation may also be detected by subsequently sawing and inspecting sections of the concrete in the horizontal section. Typical acceptance values according to EFNARC are in the range of 0.8 to 1.0. If the

concrete flows as freely as water, at rest it will be horizontal, so H_2/H_1 reaches 1. Therefore, the closer this test value so called ‘the blocking ratio’ is to unity, the better the flow of the concrete.



Figure 3.4 Photographic view of L-box apparatus and testing procedure

3.5.4 Setting time

Initial and final setting times of the self compacting concrete mixtures were determined by means of a setting time apparatus conforming the ASTM C/C 403M-99. The test was performed on mortar which was obtained by sieving freshly mixed concrete through a 5 mm sieve. Then, the mortar was placed in a 100 mm cube container and stored in a controlled environment of 20 ± 2 °C and $65\pm 5\%$ relative

humidity throughout the test duration. At regular time intervals, the force required for a needle to penetrate 25 mm in to the mortar was measured. From a plot of penetration resistivity versus elapsed time, the initial and final setting times were determined as shown in Figure 3.5. The former and the latter are defined as the times at which the penetration resistance reaches values of 3.5 and 27.6 MPa, respectively.

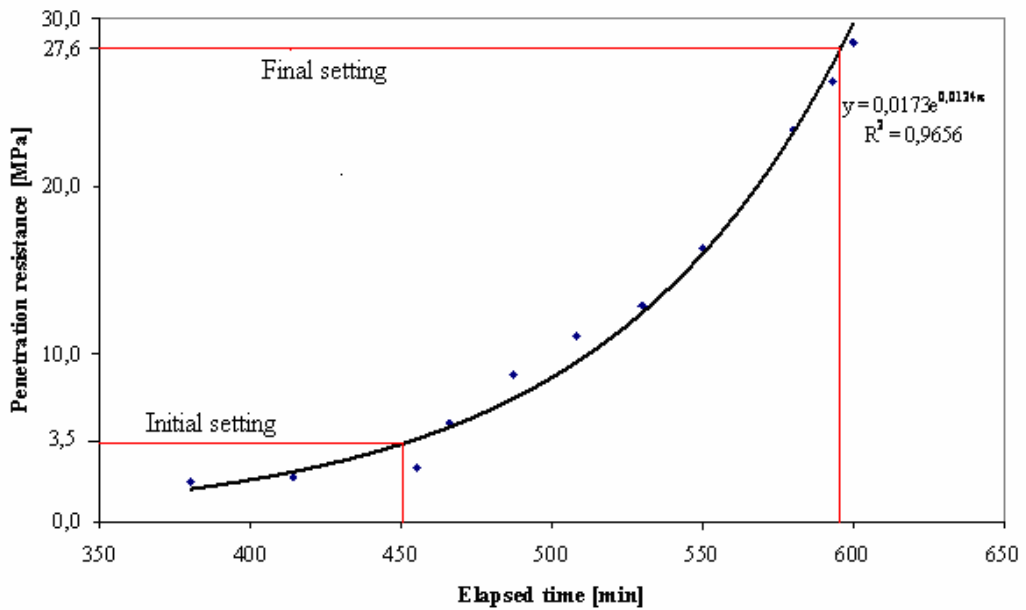


Figure 3.5 Plot of penetration resistance values versus elapsed time and fit curve used to determine time of setting

3.5.5 Viscosity

Viscosity was measured on the mortar phase of the SCC. For this, a part of fresh concrete for each mixture was wet sieved on a vibrating sieve through a mesh size of 5 mm as in the case the setting time measurement. The separated matrix mortar was then taken as the sample for determination of viscosity (Shi et al., 2004). Viscosity measurements were performed using a Brookfield DV-E model viscometer as seen in Figure 3.6. It is a rotational viscometer with a smooth-walled concentric cylinder. Viscosity of the concretes was measured at different rotational speeds as seen in Figure 3.7. Moreover, the time dependent viscosity of the concretes were determined so as to prevent the inaccurate yield stress and unusual viscosity readings at low stress levels resulting from the wall slip (Felekoğlu et al., 2006). The measurements

were realized at the seven rotational speeds (1, 2.5, 5, 10, 20, 50, and 100 rpm) at 0, 20 and 40 minutes after mixing.



Figure 3.6 Photographic view of viscosity test apparatus and measuring of viscosity

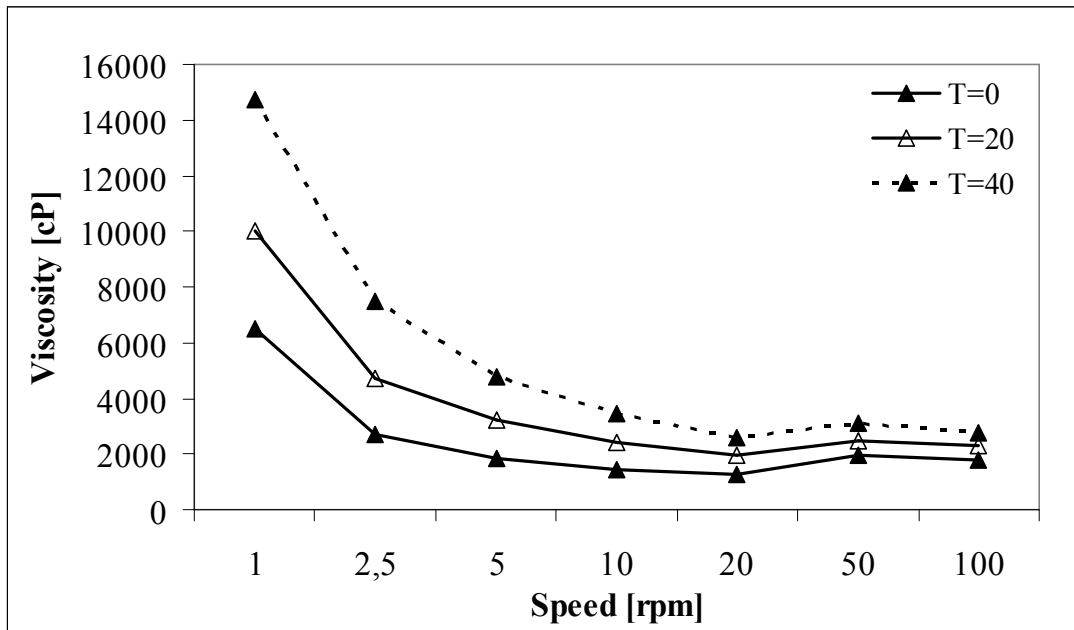


Figure 3.7 Time dependent viscosity behavior of SCC mortar

3.6 Tests for Mechanical Properties

3.6.1 Compressive strength

For compressive strength measurement of SCCs, 150x150 mm cubes were tested according to ASTM C 39 by means of a 3000 kN capacity testing machine. The test was conducted on three 150x150x150 mm cubes for each mixture at the ages of 28 and 90 days. The compressive strength was computed from average of three cylinders at each testing age.

3.6.2 Splitting tensile strength

Splitting tensile strength of the SCCs was measured on 150x300 mm cylinder specimens at the 90 days as recommended by ASTM C 496. The splitting tensile strength reported herein was as the average of three cylinders.

3.6.3 Ultrasonic pulse velocity

Prior to compression test, UPV test was conducted at 28 days and 90 days as recommended by ASTM C 597.

3.7 Tests for Physical Properties

3.7.1 Free shrinkage and weight Loss

For monitoring the drying shrinkage and weight loss of the SCCs, four 70x70x280 mm prisms were used as per ASTM C 157. Immediately after demoulding the concrete specimens, the gage length was formed by gluing pins on the surface as shown in Figure 3.8. The initial gage length and the specimen weight were measured and consecutive readings were taken at certain time intervals. Specimens were maintained in a LEEC humidity cabinet at 23 °C and 50% relative humidity for about 50 days. The length change was measured by means of a dial gage extensometer with 200 mm gage length which had a capability of measuring 0.002 strain.

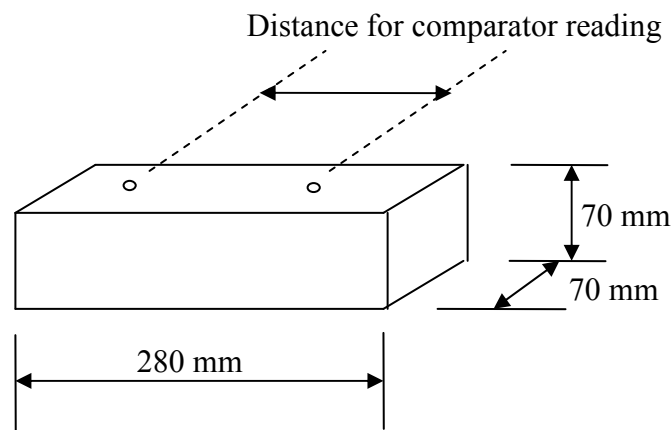


Figure 3.8 Drying shrinkage test set up

3.8 Determination of the Durability Performance of Concrete

3.8.1 Rapid chloride permeability

An experimental setup meeting the ASTM C 1202 recommendations was used to determine the rapid chloride permeability of SCCs as shown in Figure 3.9. The chloride ion permeability of the concretes was measured at the age of 90 days; two specimens being tested simultaneously for each mixture. For this, two 50 mm thick disc samples were cut from the mid-section of each cylinder. Then, the discs were allowed to surface dry in air. In order to prevent evaporation of water from the saturated specimen, a rapid setting coating was applied onto the lateral surface of the specimens prior to a vacuum-saturation procedure for 2 hrs. Finally, the specimens were immersed in water in the curing room at 20 °C and 50 % relative humidity for 18 ± 2 hrs.

Following this conditioning procedure, the disc specimens were transferred to a test cell in which one face of the specimen was in contact with 0.30 N NaOH solution and the other was with 3% NaCl solution (Figures 3.9 and 3.10). A direct voltage of 60.0 ± 0.1 V was applied across the faces. Due to this applied voltage the chloride ions in the NaCl solution, being negatively charged, were attracted by the opposite positive electrode (+) and they penetrate through the pores of saturated concrete. The data was measured at every 30 minutes to record the current passing through the specimens over a 6 hour period. Terminating the test after 6 hours, current (in amperes) versus time (in seconds) were plotted for each concrete and the area underneath the curve was integrated to obtain the charge passed (in coulombs). AASHTO T277 classifies the chloride permeability in concrete into five classes from 'High' to 'Negligible' on the basis of on the basis of total coulomb value as given in Table 3.6.

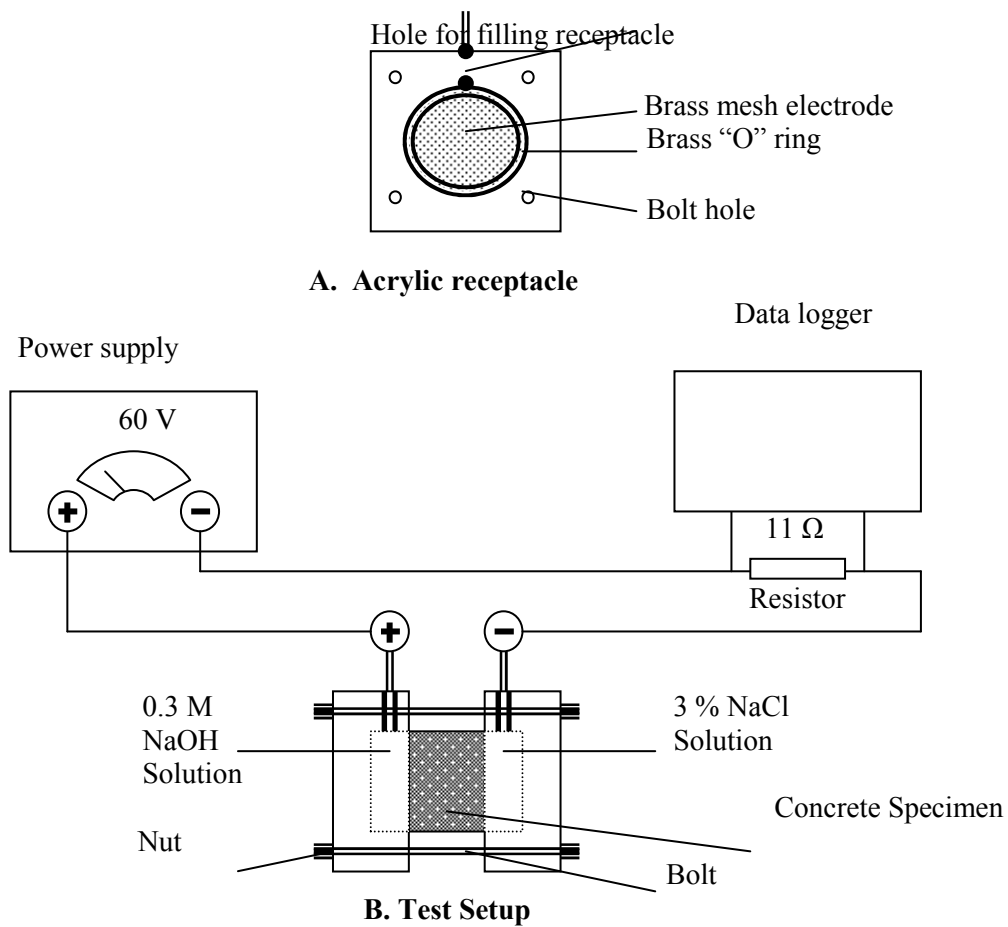


Figure 3.9 Experimental set-up for Rapid Chloride Permeability Test

Table 3.6 Interpretation of results obtained using RCPT test

Charge Passed [Coulombs]	Chloride Permeability	Typical of -
>4.000	High	High w/c ratio (< 0.6) conventional portland cement concrete
2.000 – 4.000	Moderate	Moderate w/c ratio (0.4 – 0.5) conventional portland cement concrete
1.000 – 2.000	Low	Low w/c ratio (< 0.4) conventional portland cement concrete
100 – 1.000	Very Low	Latex-modified concrete, Internally sealed concrete
< 100	Negligible	Polymer-impregnated concrete, Polymer concrete



Figure 3.10 Rapid chloride permeability test

3.8.2 Electrical resistivity

Commercially available non-destructive testing RM-8000 model resistivity meter was used for evaluating the resistivity of SCCs. The test was performed on $\text{Ø}100 \times 200$ mm cylinder specimens at age of 28 and 90 days. For this purpose, the two electrodes of the resistivity meter were placed in holes drilled to a depth of 8 mm in concrete and filled with conductive gel as seen in Figure 3.11. The spacing between electrodes was 50 mm for the present study. During the test, a small alternative current was applied between probes and the resultant potential difference measured across the probes. The resistivity R of concrete, for a semi-infinite geometry, was then determined. Two measurements were taken on the side face of each cylinder, and the average of four reading on the three specimens was reported.



Figure 3.11 Electrical resistivity measurement

3.8.3 Water absorption

Water absorption was determined using the bottom 75mm sections of 100x200 mm cylinder specimens cast for RCPT. Thus, two disc samples cut from two Ø100x200 mm cylinders were tested for each concrete mixture at the age of 90 days. As per ASTM C 642, the specimens were initially oven dried at 105 ± 5 °C for 72 hrs to reach constant mass to obtain the oven-dry weights (W_1). Then, they were immersed in water for 72 hrs and the saturated surface dry weights (W_2) of the specimens were measured. Eventually, the water absorption (WA) of each concrete was calculated through Eqn 3.1.

$$WA (\%) = \left(\frac{W_2 - W_1}{W_1} \right) * 100 \quad (3.1)$$

3.8.4 Sorptivity

The sorptivity test measures the rate at which water is drawn into the pores of concrete. For this, three test specimens having a dimension of Ø100x60 mm cut from

Ø100x200 mm cylinders were employed. The specimens were dried in an oven at about 100 °C until constant mass and then allowed to cool to the ambient temperature in a sealed container. Afterwards, the sides of the specimens were coated by paraffin, the sorptivity test was carried out by placing the specimens on glass rods in a tray such that their bottom surface up to a height of 3 mm is in contact with water. This procedure was considered to allow free water movement through the bottom surface. The total surface area of water within the tray should not be less than 10 times that of the specimen cross-sectional area (Razak et al., 2004). The specimens were removed from the tray and weighed at different time intervals up to 1 hour to evaluate mass gain. The volume of water absorbed was calculated by dividing the mass gained by the nominal surface area of the specimen and by the density of water. Test set up was given in Figure 3.12. These values were plotted against the square root of time. The slope of the line of the best fit was defined as the sorptivity coefficient of concrete as seen Figure 3.13. For each mixture, three specimens were tested and the average them was reported herein.

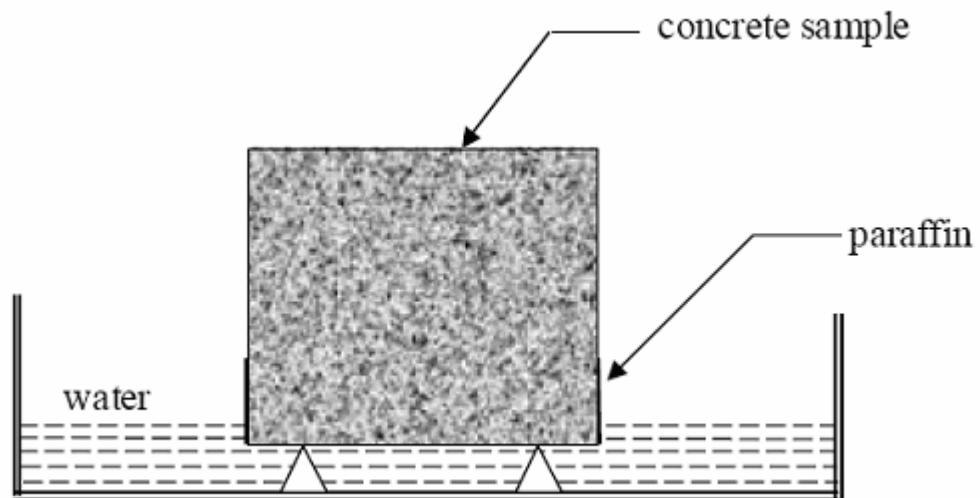


Figure 3.12 Test set up for measurement of concrete sorptivity

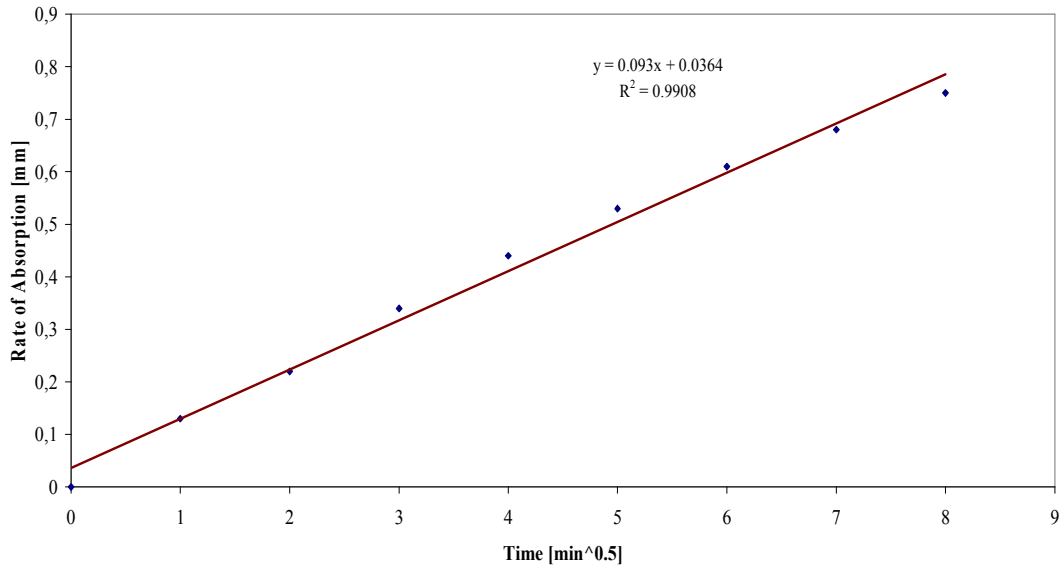


Figure 3.13 Typical plot of rate of absorption versus time

3.8.5 Water Permeability

TS EN 12390-8 was followed in determining the water permeability of SCCs. For this, a 500 ± 50 KPa downward pressure was applied on the specimens for 72 hrs. Drinkable water was used for the test. At the end of 72 hrs period, the test specimens were split in the middle and the greatest penetration depth of water was measured in mm. In order to characterize the concrete resistant to the chemical attack, water does not penetrate to a depth of more than 50 mm in concrete likely to come in contact with slightly aggressive media and not more than 30mm if concrete is likely to come in contact with aggressive media. A photograph of the water permeability test equipment was given in Figure 3.14.



Figure 3.14 Photographic view of water permeability test equipment

4. TEST RESULTS AND EVALUATION

4.1 Fresh Concrete Properties

4.1.1 Slump flow diameter and slump flow time

In this study, all of the concrete mixtures were designed to give a slump flow diameter of 70 ± 3 cm which was realized by using superplasticizer at varying amounts. Therefore, as seen in Table 4.1 and 4.2 the slump flow diameter of the concretes ranged from 67 to 73 cm, conforming EFNARC recommendations because the lower and upper acceptance limit of slump flow diameter according to EFNARC was 65 and 80 cm, respectively. Slump flow times (T_{50}) of all produced concretes were less than 7 sec. Table 4.1 and Figure 4.1 showed that concretes with binary blends of FA, GGBFS and SF had generally lower slump flow time (T_{50}) than the control concrete at low w/b (w/b = 0.32) ratio concretes. However, the concretes containing MK had similar T_{50} duration with the control concrete at low w/b ratio. Binary blends of FA, GGBFS, and SF reduced the slump flow time of the concretes when compared to that of the control concrete at low w/b ratio. There was a gradual decrease in the slump flow time of concrete with increasing replacement level of FA and GGBBS. Contrary to GGBFS and FA, there was a gradual increase with increasing of SF and MK contents. Increasing the MK content from 5 to 15% prolonged the slump flow time from 5 to 7 sec as seen in Figure 4.1. Therefore, the mixtures namely M12 and M13 violated the EFNARC limitation. In addition M35 and M42 did not fulfill the upper limit of EFNARC for slump flow time.

The effects of using mineral admixtures with ternary and quaternary systems on the T_{50} duration are presented in Figures 4.2 and 4.3, respectively. It was observed in Figures 4.2 and 4.3 that the ternary and quaternary systems improved the flow characteristics of the MK concretes in that T_{50} durations were significantly reduced by the combined use of FA, GGBFS, and MK. The concretes with SF binary systems had a slump flow of as high as 5 sec which decreased to 2 sec for most of the

concretes with the ternary binder system at low w/b ratio. In the quaternary use of PC, FA, SF, and MK (M32 to M34), lower T_{50} time was acquired when compared to quaternary use of PC, GGBFS, SF, and MK concretes.

As seen in Figure 4.2 and Table 4.1, in the case of using ternary blends of PC, SF, and MK (M29 to M31), the T_{50} slump flow time was measured to be 4 sec and it did not change with the increase in SF and MK contents from 2.5 to 7.5% in the mixtures with ternary blends. The quaternary use of PC, FA, SF, and MK in the production of SCC eliminated the increasing effect of binary use of PC and MK on the T_{50} duration.

The slump flow time of concretes with 0.44 w/b ratio are given in Table 4.2 and plotted in Figure 4.4 and 4.5 for binary, ternary, and quaternary mixtures, respectively. At high w/b ratio concretes (w/b = 0.44) (M44 to M65), slump flow time was generally measured to be lower than 5 sec for all of the concretes meeting the upper limit of EFNARC. As seen in Table 4.2 and Figures 4.4 and 4.5, however, the control mixture (M44) as well as the mixture containing 60% FA (M47) had a slump flow time of as low as 1 sec while the lower limit of EFNARC for that property being 2 sec. The reason for this behavior seems the lack of cohesion of these mixtures which in turn being remedied by the combined use of the mineral admixtures. The highest slump flow time was observed at the binary blends of 5% SF and 95% portland cement (M51).

The binary use of FA, GGBFS, and SF with portland cement increased the slump flow time of SCC when compared to that of the control mixture at high w/b ratio except for M47. Increasing the replacement ratio of GGBFS did not alter the slump flow time. Indeed, T_{50} time was 3 sec for all mixtures with binary blends of PC and GGBFS. Table 4.2 clearly demonstrated that when the slump flow of the concretes is taken into account, using the ternary and quaternary blends of the mineral admixtures provided better performance than the binary blends.

Figure 4.6 depicts the effect of water binder ratio on the T_{50} slump flow time of concretes. As seen from the figure in the control and binary blends of PC and FA concretes, the T_{50} slump flow time showed a decreasing trend with increasing the w/b ratio. A similar trend was also observed in the quaternary blends of PC, FA,

GGBFS, and SF. In the ternary blends of PC, FA, and GGBFS, an increase was monitored in the slump flow time of SCCs with the rise in w/b ratio. In the binary blends of PC+GGBFS and PC+SF and ternary blends of PC+FA+SF and PC+GGBFS+SF concretes, no meaningful relation was detected with the changing of w/b ratio.

4.1.2 V-funnel flow time

The flowability and viscosity of SCCs was evaluated by means of V-funnel flow time. According to EFNARC (2002), the concrete having a V-funnel flow time within 6 to 12 sec may be highly resistant to possible segregation. The variation of V-funnel flow time of the produced SCCs is given in Tables 4.1 and 4.2 and Figures 4.7 to 4.12. The time measured via the V-funnel flow was in the range of 6.3–37 sec depending mainly on the concrete composition. It was observed in Tables 4.1 and 4.2 that apart from the control one (M1), some of the other concretes at low w/b ratio (M2, M4, M6, M7, M8, M10, M11-M13, M17, M18, M20, M23, M24, M27, M29-M31, M35-M38, M41-M43), and some at high w/b ratio (M49 and M51) did not fulfil the EFNARC recommendation for V funnel flow time. Similar findings have been reported in the literature such that the upper limit of V-funnel flow time extended to as high as 46 sec (Felekoğlu et al., 2006).

As was the case in T_{50} slump flow time, the control and the concrete with binary blends of PC+FA had shorter V-funnel flow time with increasing w/b ratio as seen in Figure 4.12. A similar trend was also monitored in the concretes with the binary blends of PC+GGBFS, ternary blends of PC+FA+SF, and quaternary blends of PC+FA+GGBFS+SF. A fluctuation of V-funnel flow time was also observed in the concretes having binary (PC+SF) and ternary (PC+FA+GGBFS and PC+GGBFS+SF) blends as seen in Figure 4.12.

Figures 4.7 and 4.10 show the variation in the V-funnel flow time of the concretes made with binary blends of cementitious materials for 0.32 and 0.44 w/b ratios, respectively. It was observed that increasing the replacement ratio of FA from 20 to 60% resulted in a gradual reduction in the V-funnel flow time of concretes for both w/b ratios. Unlike FA, increasing GGBFS content slightly prolonged the flow time,

especially at high w/b ratio. Incorporating of SF in the binary blends, however, provided comparable behavior to that of the reference concrete at low w/b ratio, but significantly increased the flow time at high w/b ratio.

In the case of using the ternary blend of PC+FA+SF, however, there was an increase in the V funnel flow time of the concretes with increasing the content of mineral admixtures used at low w/b ratio but a decrease was observed at high w/b ratio (Figures 4.8 and 4.11, respectively). A steady decrease was observed in the concretes with ternary blends of PC+GGBFS+SF at low w/b ratio as the replacement level of mineral admixtures increased.

The behavior of MK concretes was much different such that incorporating MK increased the cohesion of the concretes which in turn prolonged the V-funnel flow time as seen in Figure 4.7. According to Figures 4.8 and 4.9, the ternary and quaternary use of FA and MK, however, remarkably diminished this negative effect of MK. Indeed, the concrete with 45% FA and 15% MK had a V-funnel flow time of 8 sec while those of the control concrete and the concrete with 15% MK only were 14 and 22 sec, respectively. Interestingly, it was seen in Figure 4.8 that the combined use of SF and MK slightly decreased the V-funnel flow time of the mixtures (M29-M31), especially at higher replacement levels of about 7.5% for the former and 7.5% for the latter. With increasing SF and MK contents in the ternary use of PC+SF+MK blends from 2.5% to 7.5%, the V-funnel flow time decreased from 37 sec to 20 sec. The quaternary use of both PC+FA+SF+MK and PC+GGBFS+SF+MK blends also diminished the negative effect of incorporating SF and/or MK on the V-funnel flow time. For example, V funnel flow times of the concretes with the ternary blends of PC+SF+MK were 37, 36 and, 20 sec, respectively, depending on the replacement level of SF and MK. However, these values lessened to 11, 9, 8 and 24, 21, 13 sec for the concretes made with the quaternary blends of PC+FA+SF+MK and PC+GGBFS+SF+MK, respectively.

At high w/b ratio concretes (M44 to M65) the time measured via the V-funnel was in the range of 3.2 to 14 sec depending mainly on the mineral admixture used. The lowest V-funnel flow time of 3.2 sec was measured for the control concrete while the mixture with 40% GGBFS had flow time of 14 sec. Incorporating SF or GGBFS in the binary system generally made the concretes more cohesive so that these concretes

had higher flow times as seen in Figure 4.10. However, using FA beyond a replacement level of 20% decreased the cohesion which in turn resulted in much lower V-funnel flow time of the concretes. Therefore, the reducing effect of FA and the increasing effect of GGBFS and/or SF were combined in the ternary and quaternary blends to impart much better performance in terms of V-funnel flow time. Interestingly, it was observed in Table 4.2 that all of the concretes incorporating any of the ternary cementitious blends generally satisfied the EFNARC limitations.

4.1.3 L-box height ratio, T_{200} and T_{400} times

Passing ability of the self compacting concretes was measured by means of the L-box test. The test provided H_2/H_1 ratio as a measure of the flowability among reinforcing bars. The variation in the L-box height ratio (H_2/H_1) is presented in Tables 4.1 and 4.2 and Figures 4.13 to 4.18. All mixtures but M1, M30, M44, M45, M48-M51 and M56 satisfied the EFNARC limitation given for the L-box height ratio. H_2/H_1 ratio value ranged from 0.704 to 0.976 depending mainly on the mineral admixture used in concrete and w/b ratio. The ratio of H_2/H_1 was in the range of 0.8 to 1.0 for all mixtures except for M30 containing one or more of the supplementary cementitious materials at low w/b ratio (Figures 4.13 to 4.15), thus generally satisfying the EFNARC recommendation for the passing ability in terms of L-box test.

It was observed in Figure 4.13 that increasing the replacement level of GGBFS from 20 to 60% in the binary blends increased the H_2/H_1 ratio for the low w/b ratio concretes. A similar pattern was observed in the concretes with PC+FA blends in that the effect of adding FA was generally to increase this ratio, irrespective of the replacement level. PC+SF and PC+MK concretes also exhibited similar trend so that the ratio of H_2/H_1 reached relatively higher values than that of the reference concrete. The effect of the replacement level for these mineral admixtures was quite lower. The L-box height ratio of the concretes containing ternary blends of cementitious materials exhibited a pattern much similar to that seen in the case of the concretes with binary blends. As clearly seen in Figure 4.14, the concretes with the ternary blends of cementing materials had higher H_2/H_1 ratio indicating a better performance in terms of passing ability than the reference concrete. Figure 4.15 demonstrates

variation in the L-box height ratio of the concretes with the quaternary blends. There was a consistent trend that all of the concretes such cementitious blends fulfilled the EFNARC limitation.

At high w/b ratio concretes (M44-M65), the L-box test showed that apart from the control mixture (M44), the mixtures namely, M45 and from M48 to M51 each of which having binary blends of cementitious materials, and M56 containing 45% FA and 15% SF did not satisfy the lower limit of EFNARC. In performing the L box test the authors did not observe any blockage or segregation, thus the reason of the low H_2/H_1 value might be the lack of cohesion in these mixtures. It was clearly observed, however, in Table 4.2 that all of the concretes made with ternary and quaternary blends of supplementary cementitious materials had H_2/H_1 ratios of 0.82 to 0.93 meeting the EFNARC limitations. Therefore, the combined use of the mineral admixtures in ternary and quaternary blends remarkably improved the filling and passing ability of the SCCs.

As clearly seen in Figures 4.16 and 4.17 that binary (PC+FA, PC+GGBFS, PC+SF) and ternary use of (PC+FA+GGBFS) mineral admixtures in the production of SCCs at high w/b ratio increased the H_2/H_1 ratio with the increase in replacement level of mineral admixtures incorporated. It may be noted that, however, the combined use of the GGBFS and SF led to a reduction at high replacement levels. As well observed in both Table 4.2 and Figure 4.17, the H_2/H_1 ratio of the binary PC+GGBFS and binary PC+SF concretes ranged from 0.704 to 0.732 and from 0.732 to 0.918, respectively. The combined use of PC, GGBFS and SF in ternary blends provided these values within 0.929 to 0.824. The concretes with the combined use of PC+FA+SF, however, had H_2/H_1 ratio of as low as 0.79 which being about the lower limit of EFNARC. Therefore, test results suggested that at high w/b ratio the concretes with the ternary blends of PC, GGBFS, and SF outperformed the others.

T_{200} and T_{400} times to be taken for the mixture to reach a distance of 200 and 400 mm along the horizontal section from the sliding door of the L-box were also given in Tables 4.1-4.2. These results gave some indication about the easy flow of the concrete mixtures with the mineral admixtures compared to the control mixture. The T_{400} time of the control concrete was about 17 sec which lessened to as low as 6, 7.5, 13, and 13 sec as the FA, GGBFS, SF, and MK had partially replaced the PC.

Moreover, the combined use of mineral admixtures in ternary and quaternary blends further reduced these values depending mainly on the type and the amount of the mineral admixtures used.

Table 4.1 Slump flow, L-box and V-funnel properties of SCCs at w/b of 0.32

Mix No	Mix Description	Slump flow			L-box		V-funnel flow time
		T ₅₀ [sec]	D [cm]	T ₂₀₀ [sec]	T ₄₀₀ [sec]	H ₂ /H ₁	[sec]
M1	Control-PC	6	67	7	17	0.788	14
M2	20FA	4	73	5	7	0.929	17
M3	40FA	2.21	73	3	6	0.963	7
M4	60FA	2.2	73	3	7	0.904	14
M5	20GGBFS	3.2	70	3	7.5	0.882	11
M6	40GGBFS	3.3	70	5	15	0.938	15
M7	60GGBFS	1.2	73	3	13	0.951	13
M8	5SF	3	69.5	7	14	0.878	13.3
M9	10SF	4.3	67.5	5	13	0.875	9.5
M10	15SF	5	68.5	6	18	0.863	12.1
M11	5MK	5	72.5	5	13	0.904	18
M12	10MK	6	73	7	20	0.890	18
M13	15MK	7	69	3	8	0.901	22
M14	15FA5SF	2	70.5	6	18	0.927	7.1
M15	30FA10SF	2.2	73	1.2	4	0.938	7.3
M16	45FA15SF	2.2	73	1.2	3.2	0.963	8.2
M17	15FA5MK	4	73	4.6	10.4	0.915	15.4
M18	30FA10MK	4.4	71	4	7.7	0.915	13.4
M19	45FA15MK	2.5	69.5	2	4	0.915	8
M20	15GGBFS5SF	2.33	73	1.47	3.8	0.939	13.6
M21	30GGBFS10SF	3.25	71	2.39	5.83	0.951	9.3
M22	45GGBFS15SF	4	72.5	4	6	0.938	8
M23	15GGBFS5MK	3	73	2	5	0.975	15
M24	30GGBFS10MK	4	72.5	6	16	0.829	20
M25	45GGBFS15MK	4	70.5	3	6	0.904	13.2
M26	10FA10GGBFS	2	73	2	4.1	0.963	8.1
M27	20FA20GGBFS	2	73	4	8.2	0.938	12.2
M28	30FA30GGBFS	2	73	4	9	0.976	6.3
M29	2.5SF2.5MK	4	72.5	6	20	0.877	37
M30	5SF5MK	4	68.5	8	23	0.729	36
M31	7.5SF7.5MK	4	70	4	12	0.913	20
M32	15FA2.5SF2.5MK	4	70	3	7	0.951	11
M33	30FA5SF5MK	2	73	3	8	0.904	9
M34	45FA7.5SF7.5MK	2.5	70.5	2	5	0.880	8
M35	15GGBFS2.5SF2.5MK	6	70	5	14	0.975	24
M36	30GGBFS5SF5MK	3	70	6	18	0.890	21
M37	45GGBFS7.5SF7.5MK	5	67	7	19	0.854	13
M38	7.5FA7.5GGBFS5SF	5	67	3	6.4	0.833	13.1
M39	15FA15GGBFS10SF	4	67	2.3	6.4	0.875	8.3
M40	22.5FA22.5GGBFS15SF	3	70	3	6.2	0.875	9.3
M41	7.5FA7.5GGBFS5MK	3	73	3	9	0.928	15
M42	15FA15GGBFS10MK	6	70	2.5	7	0.917	18
M43	22.5FA22.5GGBFS15MK	2.5	73	3.5	8	0.902	17

Table 4.2 Slump flow, L-box and V-funnel properties of SCCs at w/b of 0.44

Mix No	Mix Description	Slump flow			L-box		V-funnel flow time	
		T ₅₀ [sec]	D [cm]	T ₂₀₀ [sec]	T ₄₀₀ [sec]	H ₂ /H ₁	[sec]	
M44	Control-PC 2	1	67	1	3	0.706	3.2	
M45	20FA	2	67.5	1	2	0.706	10.4	
M46	40FA	2	73	0.7	1.4	0.800	6.0	
M47	60FA	1	72	*	*	0.950	4.0	
M48	20GGBFS	3	67	*	*	0.704	10.0	
M49	40GGBFS	3	71	1	3	0.706	14.0	
M50	60GGBFS	3	70.5	1	3	0.732	12.0	
M51	5SF	5	66	1	2	0.732	10.0	
M52	10SF	4	68	2	4	0.824	10.0	
M53	15SF	4	69.5	3	7	0.918	10.0	
M54	15FA5SF	3	69	3	7	0.844	6.0	
M55	30FA10SF	2	69.5	1	2	0.892	4.0	
M56	45FA15SF	3	72	1	2	0.791	4.0	
M57	15GGBFS5SF	4	68	1	3.1	0.929	8.0	
M58	30GGBFS10SF	3	71.5	1.4	2.8	0.824	5.2	
M59	45GGBFS15SF	3.8	70.5	1	2.8	0.824	11.2	
M60	10FA10GGBFS	3	70.5	5	8.6	0.854	9.9	
M61	20FA20GGBFS	2.2	69	0.6	1.2	0.859	6.6	
M62	30FA30GGBFS	3	73	0.5	1	0.904	6.2	
M63	7.5FA7.5GGBFS5SF	3.4	67.5	1.8	2.85	0.871	6.0	
M64	15FA15GGBFS10SF	2.8	67.5	1.9	3.9	0.851	4.9	
M65	22.5FA22.5GGBFS15SF	2.8	70	0.8	1.9	0.869	4.2	
Acceptance criteria of SCC suggested by ERNARC								
	Minimum		2	65	-	-	0.8	6
	Maximum		5	80	-	-	1.0	12

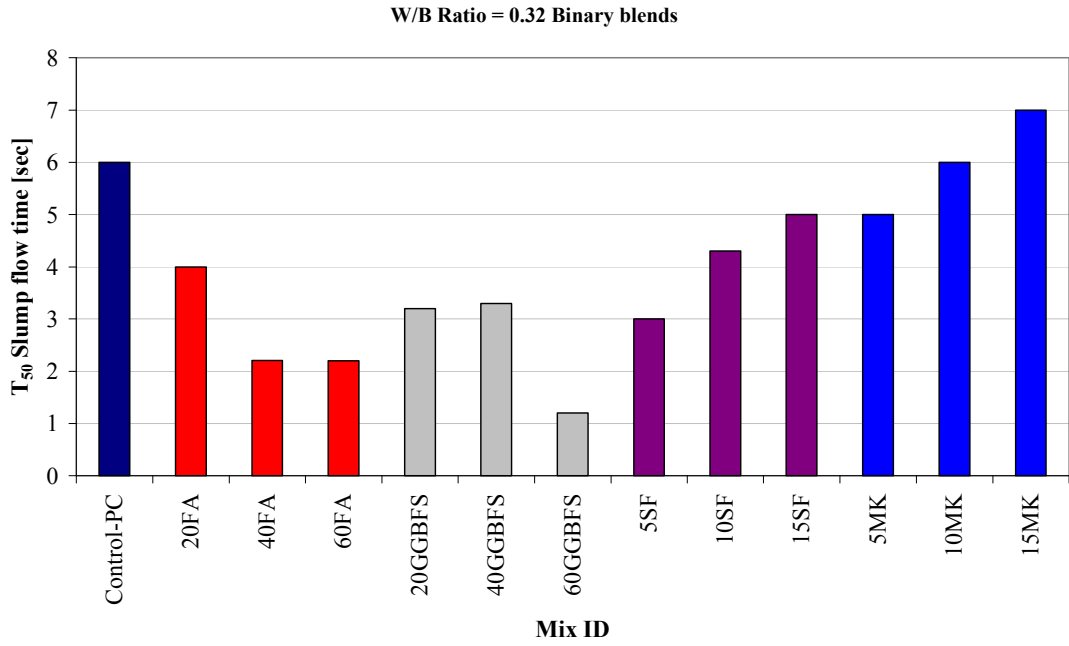


Figure 4.1 Binary effects of mineral admixtures on T₅₀ slump flow time of SCCs at w/b ratio of 0.32

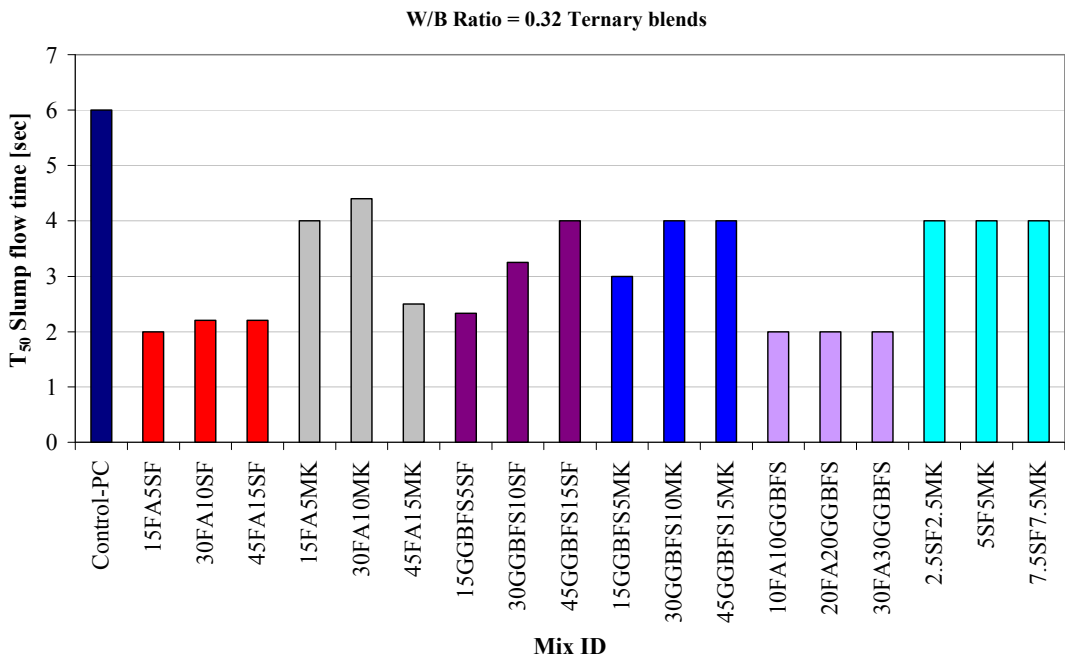


Figure 4.2 Ternary effects of mineral admixtures on T₅₀ slump flow time of SCCs at w/b ratio of 0.32

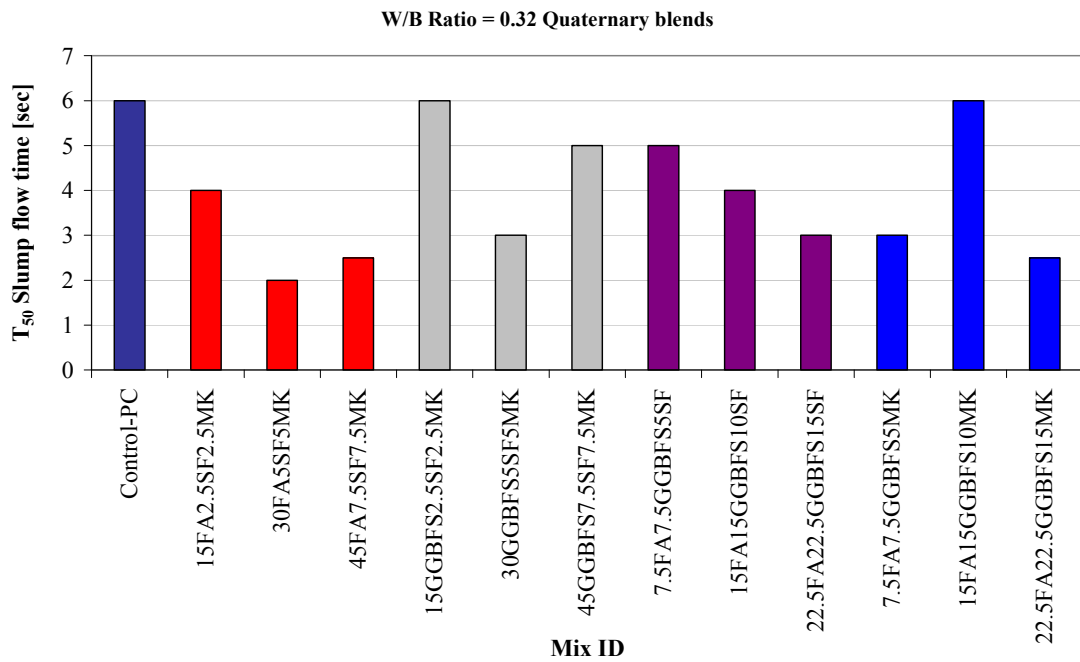


Figure 4.3 Quaternary effects of mineral admixtures on T₅₀ slump flow time of SCCs at w/b ratio of 0.32

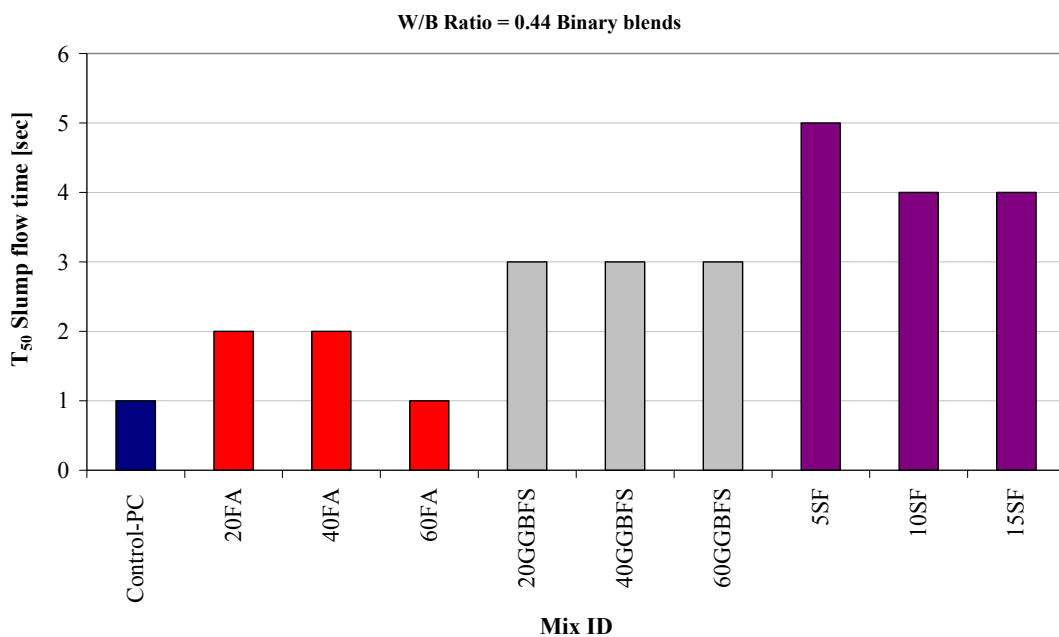


Figure 4.4 Binary effects of mineral admixtures on T₅₀ slump flow time of SCCs at w/b ratio of 0.44

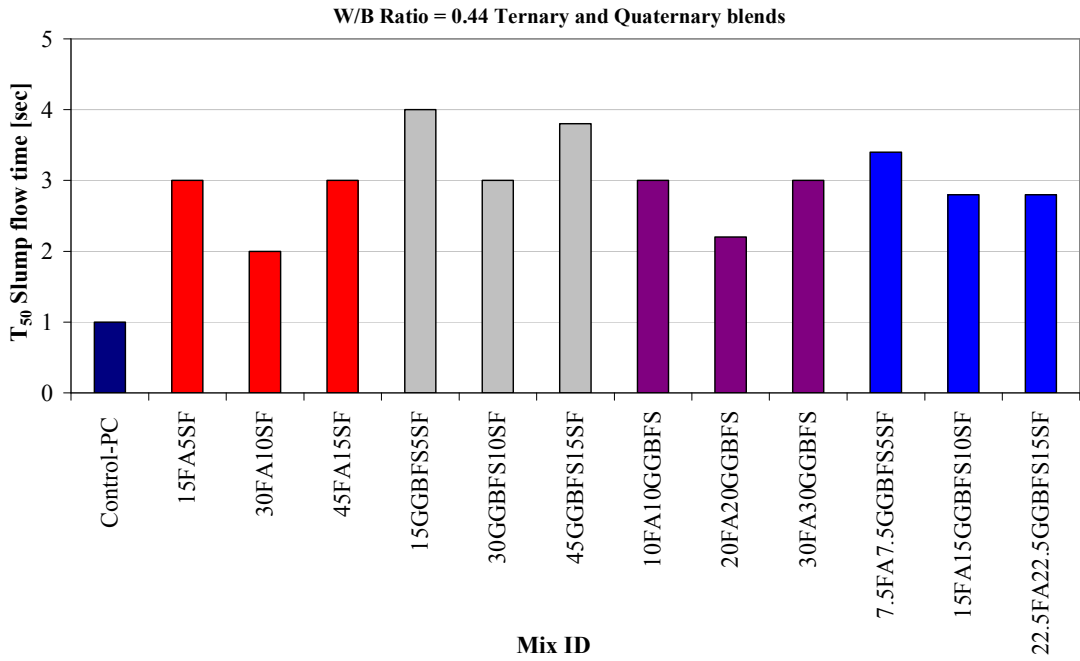


Figure 4.5 Ternary and quaternary effects of mineral admixtures on T₅₀ slump flow time of SCCs at w/b ratio of 0.44

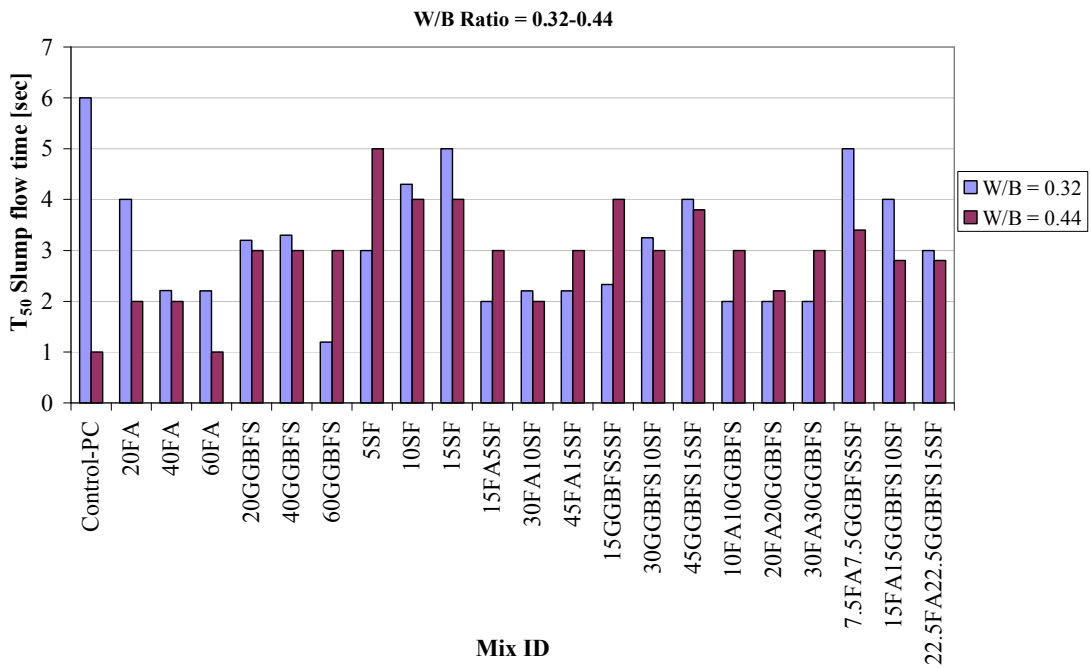


Figure 4.6 Comparison of T₅₀ slump flow time of SCCs at different w/b ratios

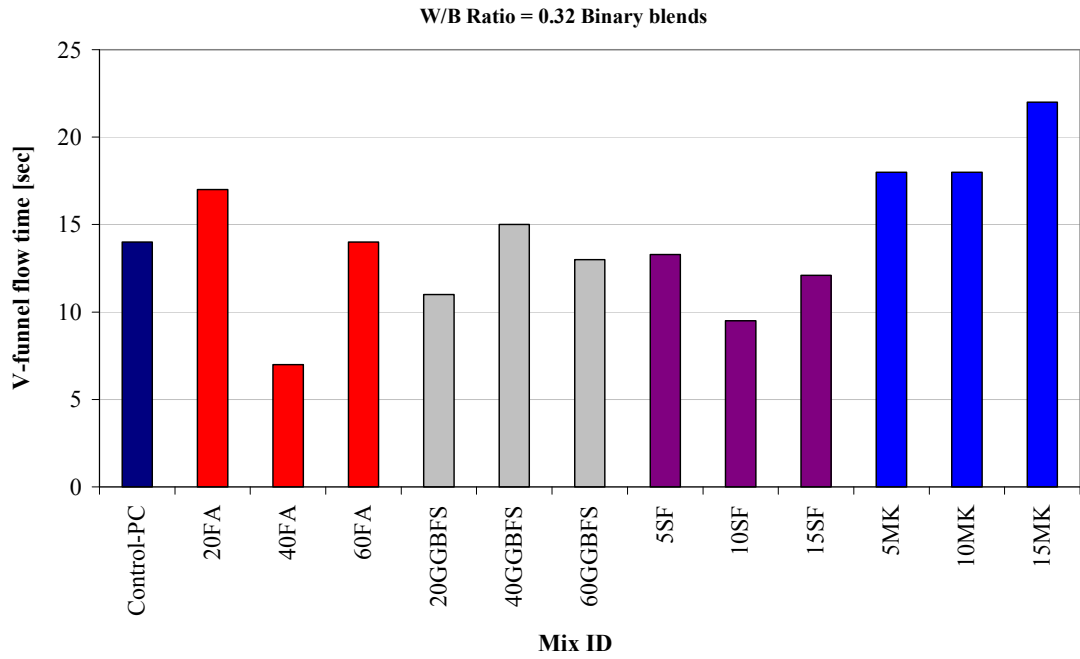


Figure 4.7 Binary effects of mineral admixtures on V-funnel flow time of SCCs at w/b ratio of 0.32

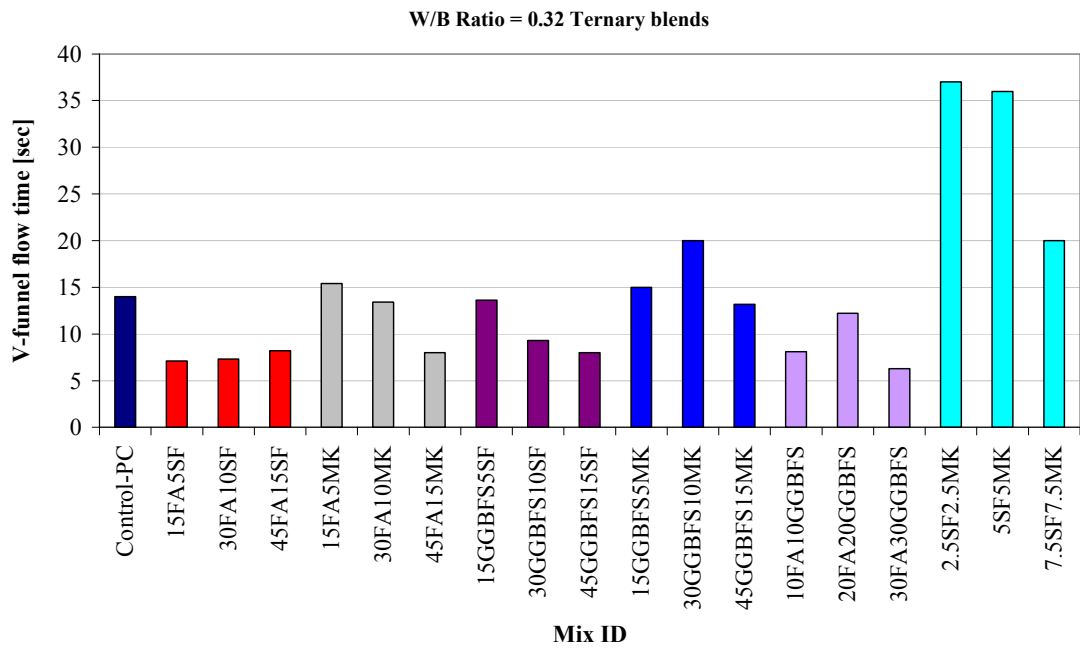


Figure 4.8 Ternary effects of mineral admixtures on V-funnel flow time of SCCs at w/b ratio of 0.32

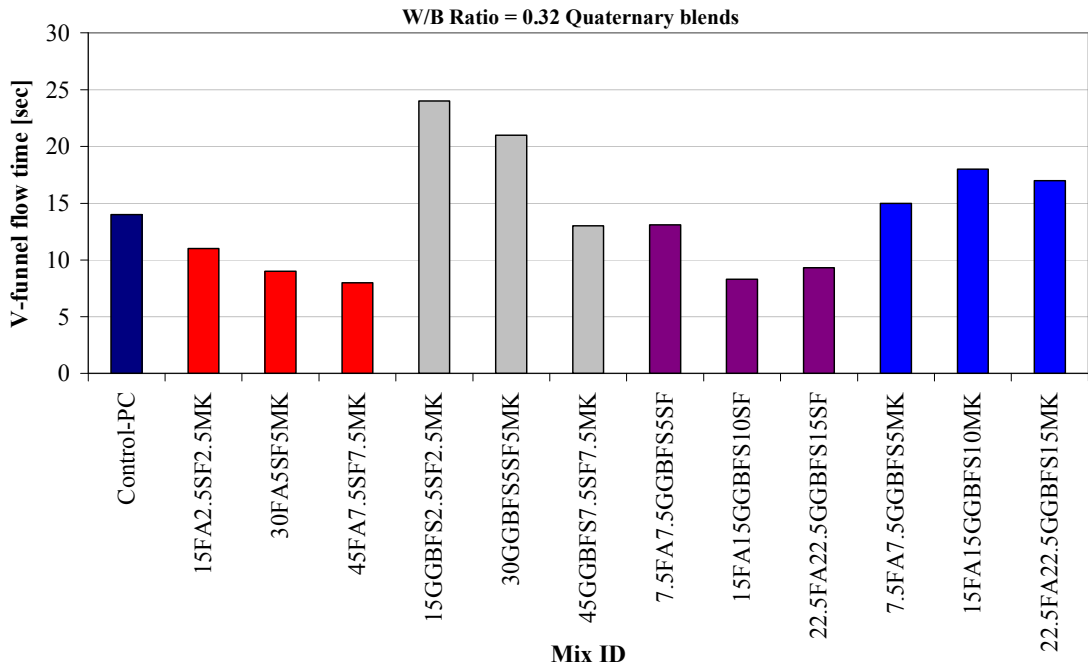


Figure 4.9 Quaternary effects of mineral admixtures on V-funnel flow time of SCCs at w/b ratio of 0.32

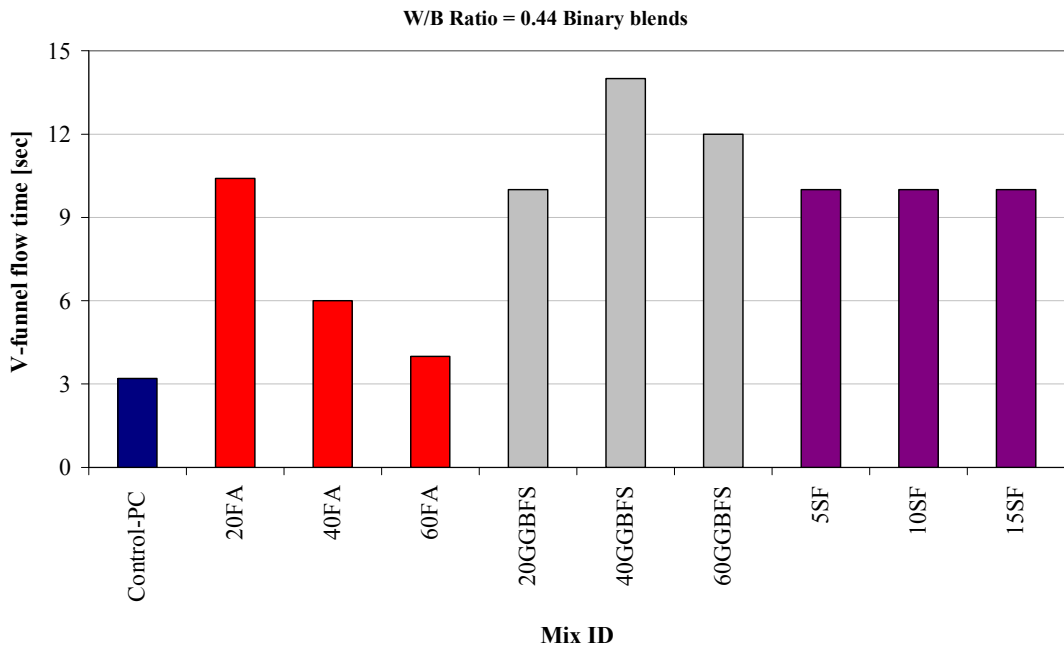


Figure 4.10 Binary effects of mineral admixtures on V-funnel flow time of SCCs at w/b ratio of 0.44

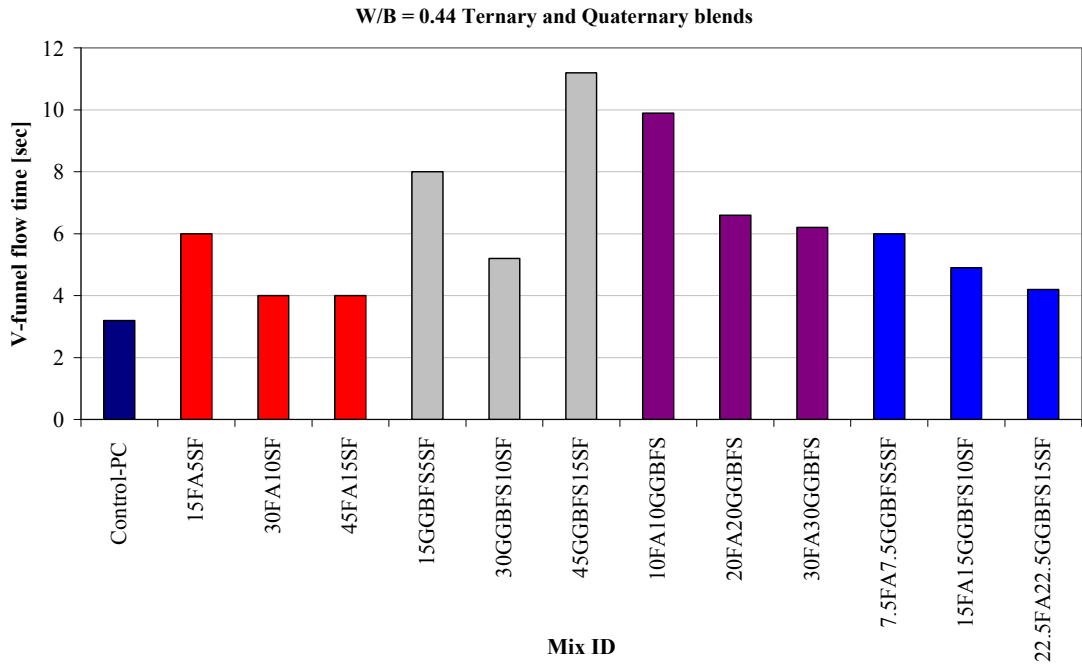


Figure 4.11 Ternary and quaternary effects of mineral admixtures on T_{50} slump flow time of SCCs at w/b ratio of 0.44

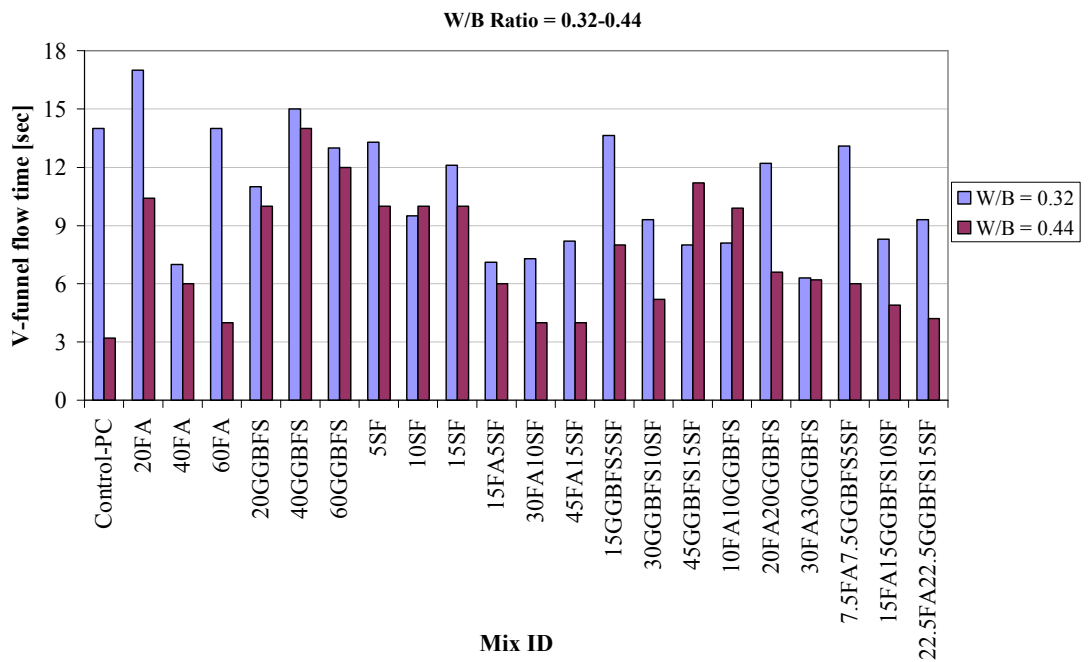


Figure 4.12 Comparison of V-funnel flow time of SCCs at different w/b ratios

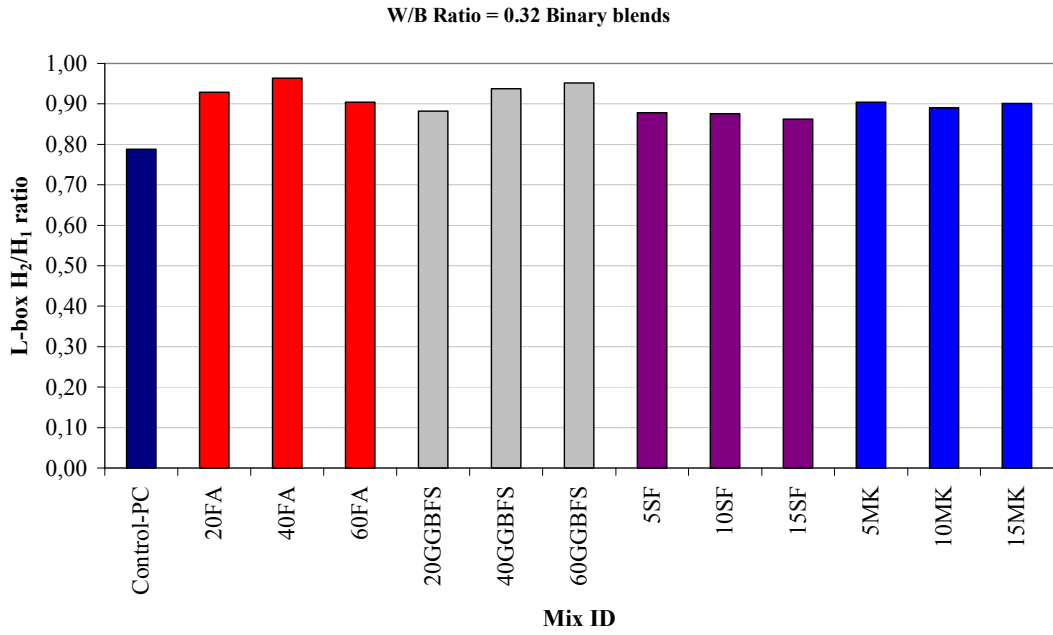


Figure 4.13 Binary effects of mineral admixtures on L box H_2/H_1 ratio of SCCs at w/b ratio of 0.32

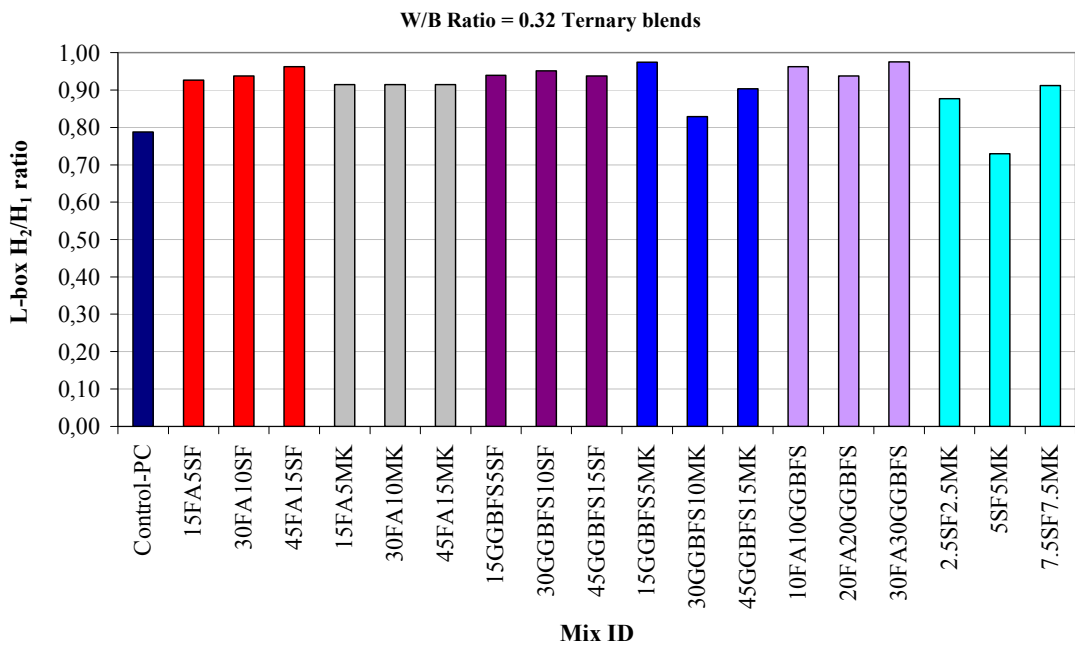


Figure 4.14 Ternary effects of mineral admixtures on L box H_2/H_1 ratio of SCCs at w/b ratio of 0.32

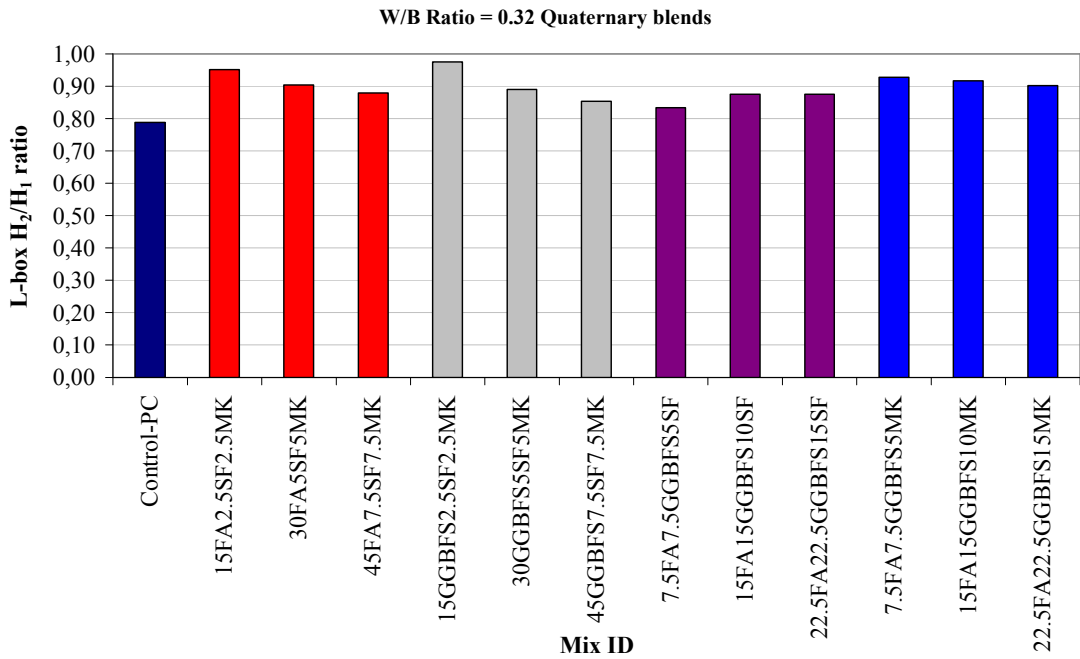


Figure 4.15 Quaternary effects of mineral admixtures on L box H_2/H_1 ratio of SCCs at w/b ratio of 0.32

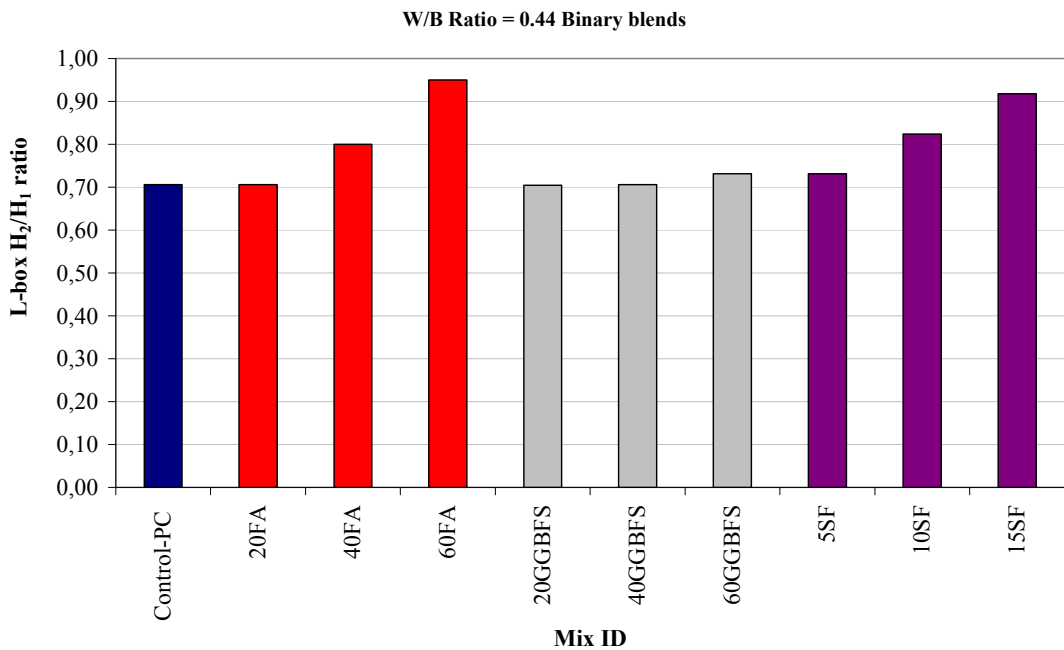


Figure 4.16 Binary effects of mineral admixtures on L box H_2/H_1 ratio of SCCs at w/b ratio of 0.44

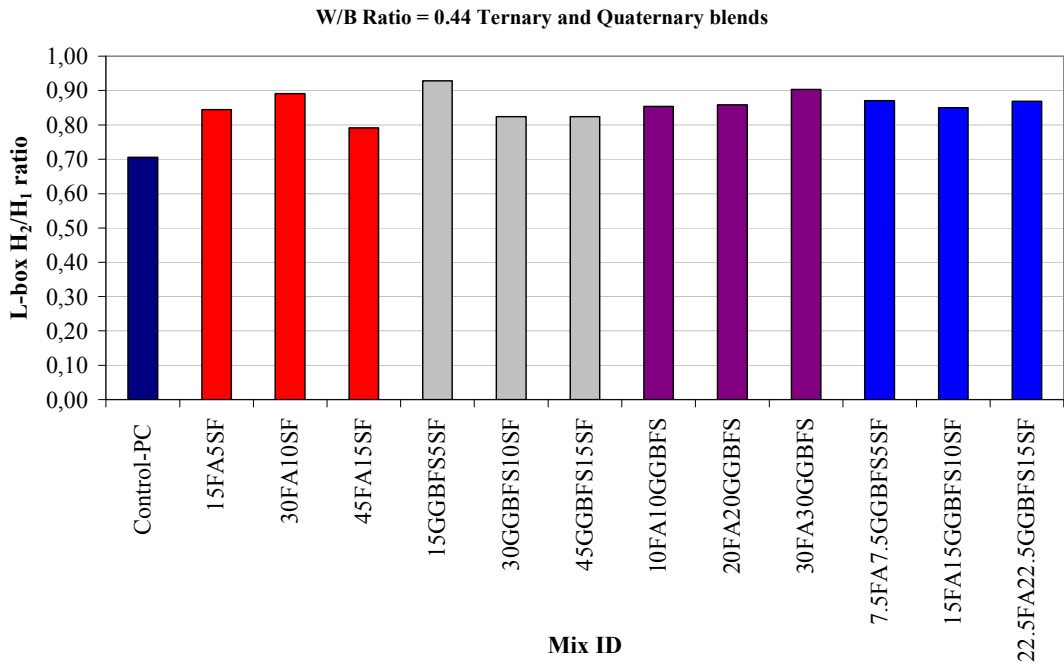


Figure 4.17 Ternary and quaternary effects of mineral admixtures on L box H_2/H_1 ratio of SCCs at w/b ratio of 0.44

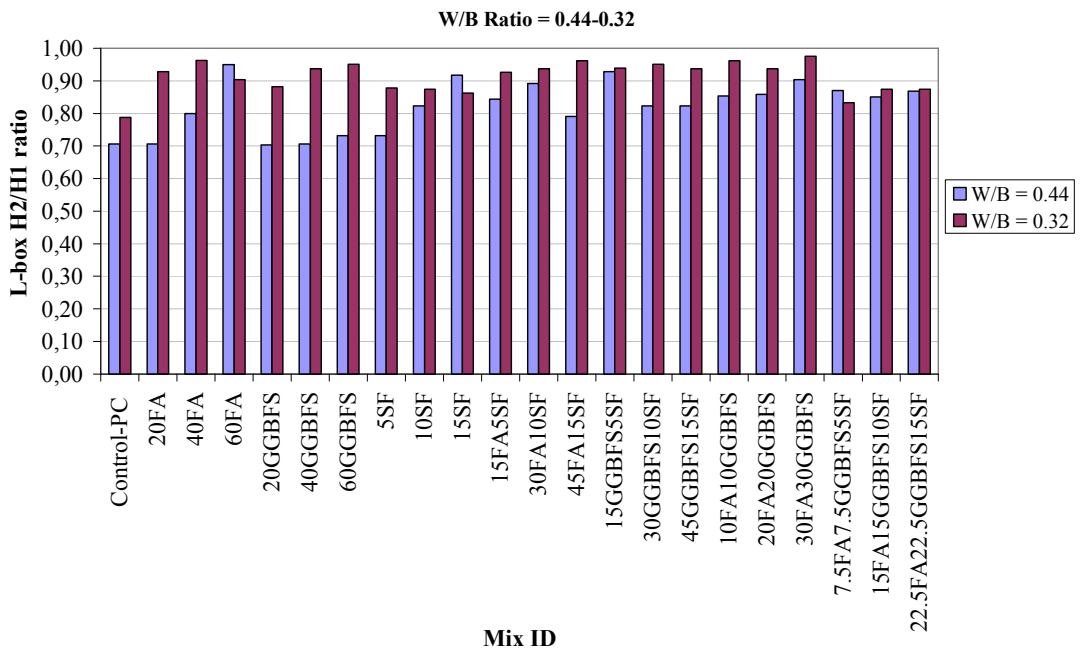


Figure 4.18 Comparison of L box H_2/H_1 ratio of SCCs at different w/b ratios

4.1.4 Initial and final setting times

Previous research indicates that setting times of the concretes are influenced by the ambient temperature, water-binder ratio, total binder content, source and type of admixtures as well as the composition of the cement used (Brooks et al., 2000; Alshamsi et al., 1993; Eren et al., 1995; Naik and Singh, 1997). In this study, ambient temperature, type of admixture, and chemical composition of cement were kept constant all throughout the experimental part but two different water binder ratios and two cement dosages with four mineral admixtures were employed to explore the effects of these parameters on the setting times of SCCs. Initial and final setting times of the concrete mixtures at low and high w/b ratio are presented in Tables 4.3 and 4.4, respectively. The variation in setting times of the concretes with respect to the mixture composition and w/b ratio are presented in Figures 4.19 to 4.25.

It was observed in Tables 4.3 and 4.4, Figures 4.19 and 4.22 that the binary use of FA and PC significantly prolonged both the initial and final setting times of the SCCs for both water-binder ratios. Moreover, the effect of increasing the replacement level of FA was to increase further the setting times of the concretes, especially in the case of low w/b concretes. Similarly, binary use of GGBFS and PC retarded the setting times at low w/b ratio. There was an extension in the initial setting times in comparison to the reference PC concrete (M44) at high w/b as seen in Figure 4.22. The effect of SF was to reduce both initial and final setting times of the SCCs especially when used at 10 and 15% replacement levels at low w/b ratio. However, the effect displayed an increasing trend in the final set of the concretes at high w/b ratio as seen in Figure 4.22. The setting times of MK concretes at low w/b (M11 to M13) slightly increased with increasing MK content from 5 to 10% (Figure 4.19). When the amount of MK, however, further increased to 15%, there was a marginal reduction in both initial and final setting times in comparison to those of the concrete having 5 or 10% MK content. The reason for this may be due to the greater water demand at the higher MK content which could have produced a binder phase that is much denser and could speed up setting. In this case, the effect of higher water demand would have to offset the effect of lower cement content and higher effective superplasticizer dosage (Brooks et al., 2000).

When the influence of using ternary blends of PC, SF, FA or GGBFS were evaluated, Figure 4.20 revealed that the inclusion of SF remarkably diminished the delay in the setting times of the concretes compared to that containing only PC plus FA or GGBFS at low w/b. For example, the concrete having 20% FA had initial and final setting times of 500 and 557 min, respectively while these values were 375 and 440 min for the concrete containing 15% FA and 5% SF. A similar behavior was observed in the case of the concretes with SF and GGBFS in that the addition of SF reduced the setting times of the concretes. The combined use of the FA and GGBFS in the concretes also slightly reduced both the initial and final setting times of the concretes when compared to those with the binary blends of FA or GGBFS. Indeed, the concrete having a 10% FA and 10% GGBFS had the initial and final setting times of 481 and 538 min, respectively while the former and the latter were 500 and 557 min for the companion concrete with PC and FA only. As it is seen in Figure 4.23, the ternary use of PC, SF, and FA in high w/b ratio concretes (M54 to M56) enhanced the retardation in the initial and final setting times when compared to concretes containing only PC plus FA (M45 to M47) or SF (M51 to M53). For the concretes with ternary blends of PC, GGBFS, and SF (M57 to M59), initial and final setting times increased when compared to those with the binary blends of PC and GGBFS (M48 to M50), as well. This finding indicates that incorporating SF at low w/b ratio concretes governed the reduction in the setting time of the concretes. In the case of high w/b ratio concretes, however, FA or GGBFS generally dominated the extension in the setting times.

The combined use of the PC, MK, FA, and/or GGBFS in the ternary as well as the quaternary blends provided remarkable reductions in the setting times of the concretes when compared to those containing only FA or GGBFS, as well (Figure 4.21). Indeed, the concrete containing 45% FA and 15% MK had IS and FS times of 457 and 598 min, respectively while the former and the latter were 925 and 1020 min, respectively, for the concrete containing 60% FA only. A similar behavior was observed in the case of the concretes having MK and GGBFS in that the addition of MK reduced the setting times of the concretes, especially when used at 15% replacement level at which MK began to decrease the setting time. The ternary use of PC, SF, and MK provided higher initial and final setting times when compared to the concrete with the binary blends of PC, SF or MK. The quaternary use of PC, FA,

GGBFS, and SF (M63 to M65), however, caused a slight decrease when compared to that of the concrete with binary blends of PC and FA (M45 to M47) while led to a retardation according to the binary use of PC and GGBFS (M48 to M50) and PC and SF (M51 to M53) concretes.

The effect of w/b ratio on the initial and final setting times of the concretes are demonstrated in Figures 4.24 and 4.25, respectively. It was observed that the concretes with low w/b ratio had generally greater setting times, irrespective of the mineral admixture. This effect was more pronounced in the concretes made with the binary blends of PC+FA and PC+GGBFS, especially at high replacement levels. But the combined use of the mineral admixtures, particularly in the quaternary blends, remarkably diminished the difference the effect of w/b ratio.

Table 4.3 Initial and final setting times of SCCs at w/b ratio of 0.32

Mix ID	Mix Description	Initial set [min]	Final set [min]
M1	Control-PC	332	449
M2	20FA	500	557
M3	40FA	653	740
M4	60FA	925	1020
M5	20GGBFS	436	595
M6	40GGBFS	465	700
M7	60GGBFS	913	1021
M8	5SF	357	426
M9	10SF	300	380
M10	15SF	307	380
M11	5MK	397	498
M12	10MK	410	512
M13	15MK	362	454
M14	15FA5SF	375	440
M15	30FA10SF	457	515
M16	45FA15SF	490	560
M17	15FA5MK	525	617
M18	30FA10MK	485	579
M19	45FA15MK	457	598
M20	15GGBFS5SF	390	450
M21	30GGBFS10SF	436	473
M22	45GGBFS15SF	394	467
M23	15GGBFS5MK	491	610
M24	30GGBFS10MK	367	468
M25	45GGBFS15MK	460	588
M26	10FA10GGBFS	481	538
M27	20FA20GGBFS	567	640
M28	30FA30GGBFS	350	417
M29	2.5SF2.5MK	435	558
M30	5SF5MK	413	466
M31	7.5SF7.5MK	399	495
M32	15FA2.5SF2.5MK	513	620
M33	30FA5SF5MK	626	751
M34	45FA7.5SF7.5MK	648	840
M35	15GGBFS2.5SF2.5MK	883	1074
M36	30GGBFS5SF5MK	380	445
M37	45GGBFS7.5SF7.5MK	331	422
M38	7.5FA7.5GGBFS5SF	242	293
M39	15FA15GGBFS10SF	260	295
M40	22.5FA22.5GGBFS15SF	324	417
M41	7.5FA7.5GGBFS5MK	680	811
M42	15FA15GGBFS10MK	662	799
M43	22.5FA22.5GGBFS15MK	457	599

Table 4.4 Initial and final setting times of SCCs at w/b ratio of 0.44

Mix ID	Mix Description	Initial set [min]	Final set [min]
M44	Control-PC	278	306
M45	20FA	312	361
M46	40FA	318	363
M47	60FA	372	442
M48	20GGBFS	220	268
M49	40GGBFS	245	316
M50	60GGBFS	236	315
M51	5SF	263	342
M52	10SF	270	330
M53	15SF	300	366
M54	15FA5SF	360	433
M55	30FA10SF	329	420
M56	45FA15SF	326	410
M57	15GGBFS5SF	267	337
M58	30GGBFS10SF	242	309
M59	45GGBFS15SF	261	325
M60	10FA10GGBFS	313	376
M61	20FA20GGBFS	310	424
M62	30FA30GGBFS	323	415
M63	7.5FA7.5GGBFS5SF	281	350
M64	15FA15GGBFS10SF	315	395
M65	22.5FA22.5GGBFS15SF	297	395

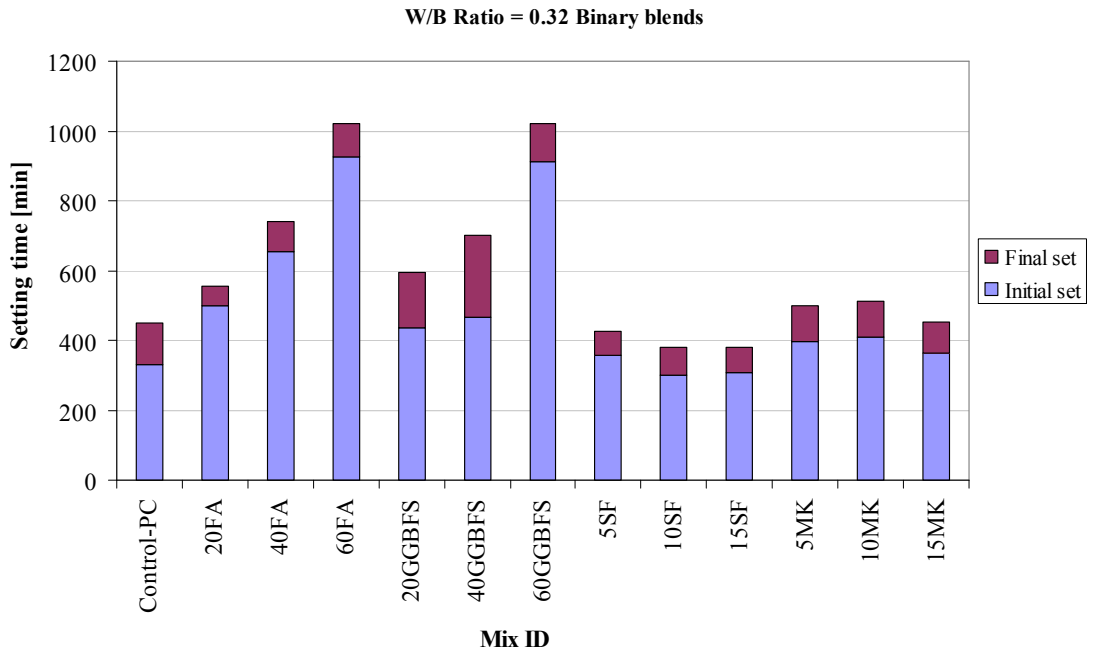


Figure 4.19 Binary effects of mineral admixtures on the initial and final setting times of SCCs at w/b ratio of 0.32

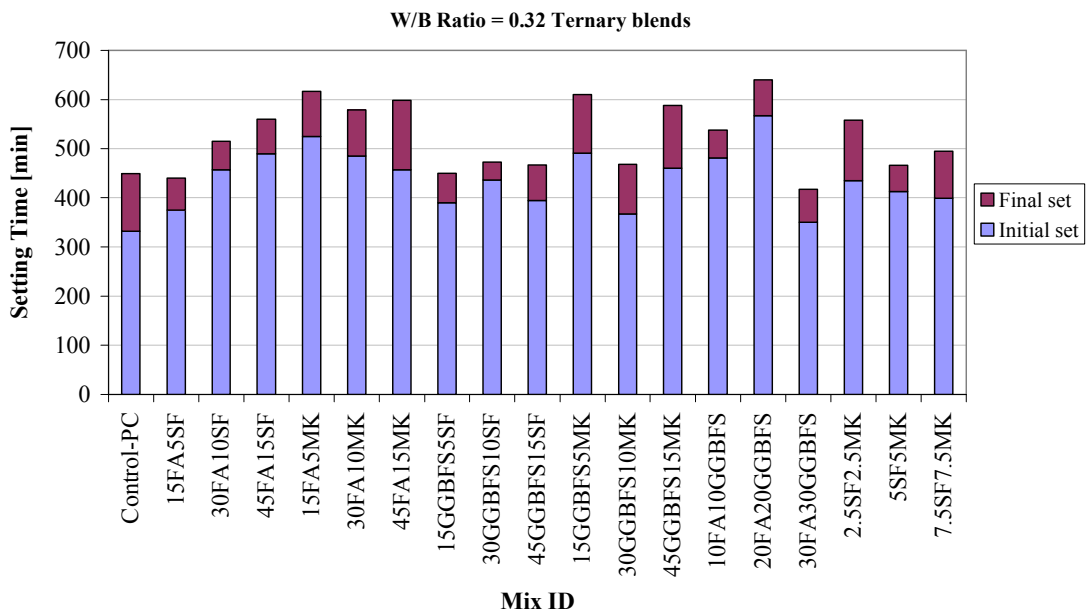


Figure 4.20 Ternary effects of mineral admixtures on the initial and final setting times of SCCs at w/b ratio of 0.32

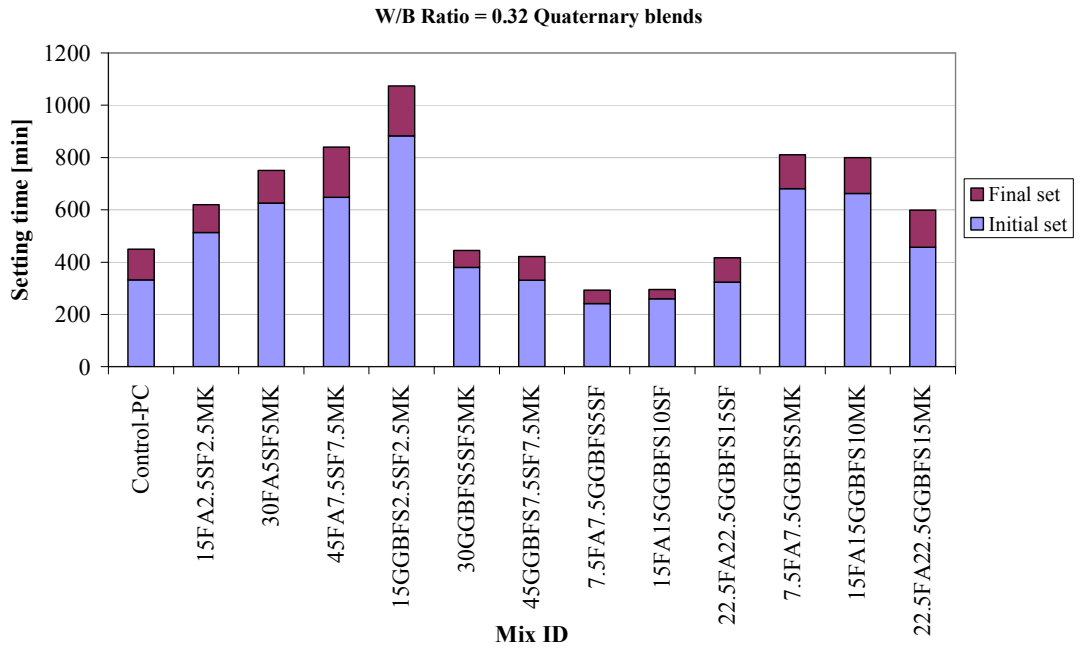


Figure 4.21 Quaternary effects of mineral admixtures on the initial and final setting times of SCCs at w/b ratio of 0.32

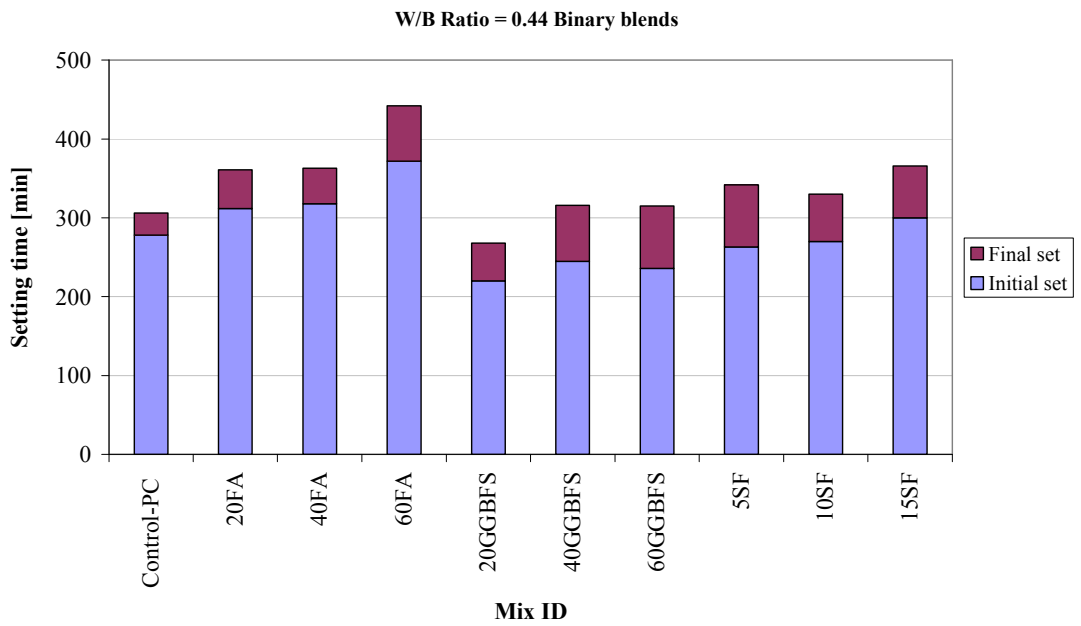


Figure 4.22 Binary effects of mineral admixtures on the initial and final setting times of SCCs at w/b ratio of 0.44

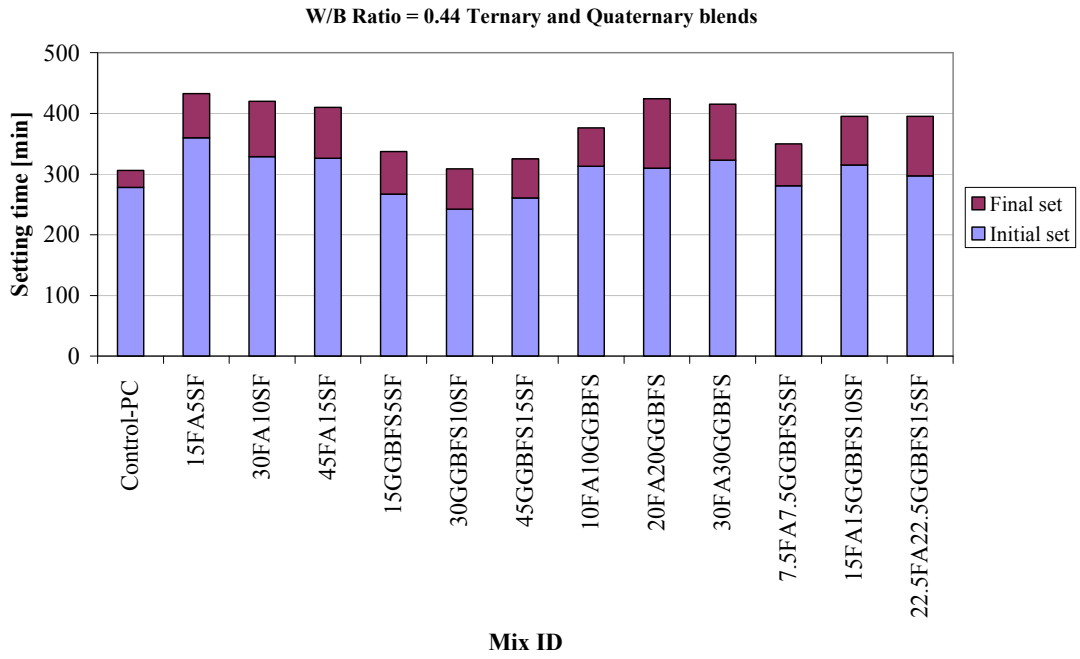


Figure 4.23 Ternary and quaternary effects of mineral admixtures on the initial and final setting times of SCCs at w/b ratio of 0.44

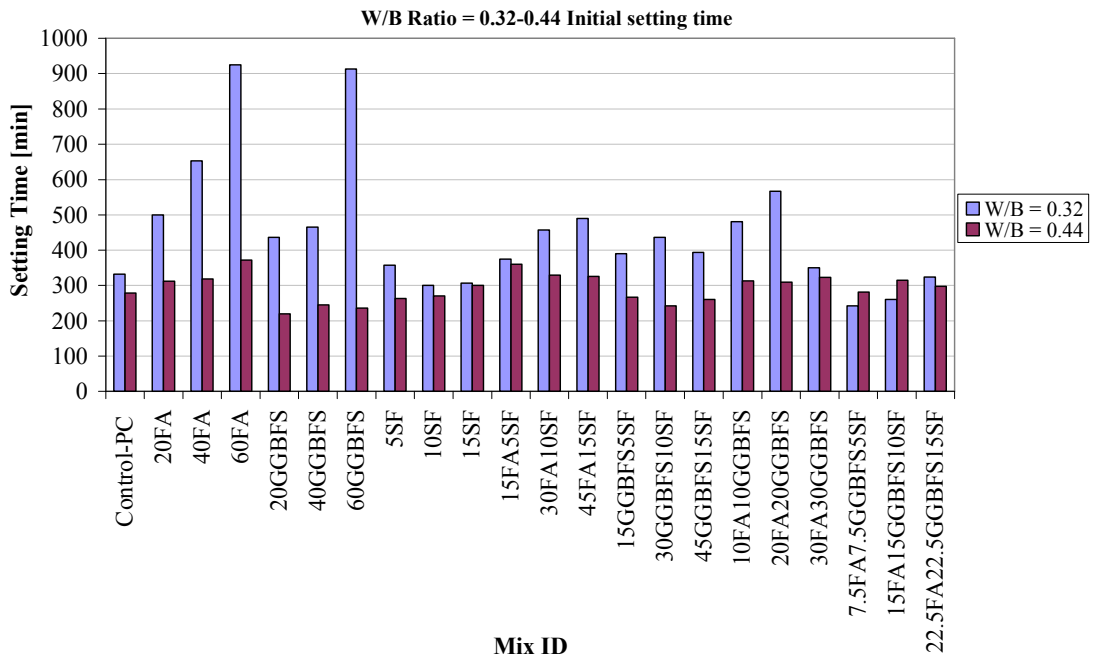


Figure 4.24 Variation of initial setting times of SCCs with w/b ratios

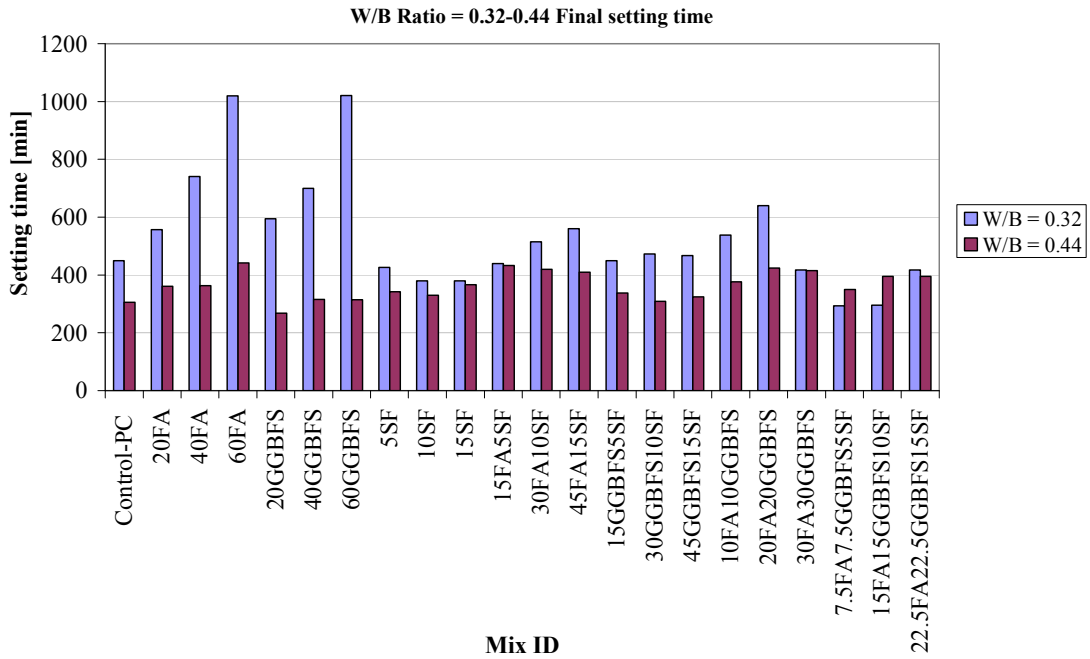


Figure 4.25 Variation of final setting times of SCCs with w/b ratios

4.1.5 Viscosity

The rotational speed (rpm) and viscosity (cP) of the concrete mixtures were drawn, which yielded similar tendency, irrespective of measuring time. As reported in Felekoglu et al (2006), the equation of $\mu = a\gamma^b$ well fitted the measurements, where μ is the viscosity in centipoise, and γ is the rotational speed in revolutions per minute. The constants a and b were calculated using the best fit equations. The correlation coefficients and the values of constants a and b for all concrete mixtures are given in Tables 4.5 to 4.8. The time dependent variations in the viscosity of all the produced concretes are plotted in Figures 4.26 to 4.32 for both water binder ratios.

As seen in the Figure 4.26a, b and c, the replacement of cement with FA or GGBFS decreased the values of viscosity, irrespective of time of measurement at low w/b ratio concretes. However, the silica fume and metakaolin concretes had consistently higher viscosity values than that of the control concrete. A similar result was also reported by Ferraris (1999). In her study, the mixtures with fly ash represented the best rheological improvement while SF represented the worst. It was shown that the replacement of cement by FA and GGBFS resulted in a reduction in a water demand and the superplasticizer dosage to maintain the same workability with the control

mixture. In contrast, the replacement of cement by SF and MK increased the superplasticizer demand to maintain the desired slump flow diameter, thus resulted in a more viscous behavior. As seen in Figure 4.26, the higher the MK content, the concretes displayed more viscous behavior. At low w/b ratio concretes, when the binary effects of the mineral admixtures on the viscosity of SCCs were ranked, it was listed in the order of SF, MK and FA or GGBFS. There were no significant difference in the viscosity of FA and GGBFS blended concretes.

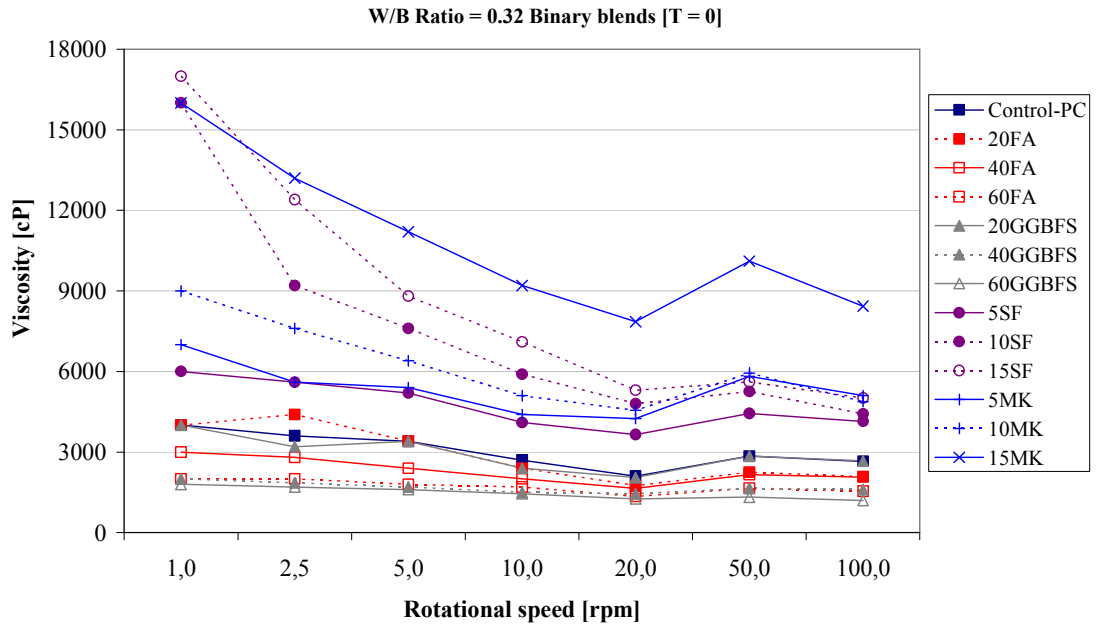
The time dependent development of viscosity of SCC with ternary (PC+FA+SF and PC+GGBFS+SF) cementitious materials at different rotational speeds are demonstrated in Figure 4.27. It was observed that the high rotational speed reduced the viscosity of all of the concrete mixtures. This indicated that the SCCs of high workability can be obtained through mixing by high shear rate blenders. Moreover, all of the concretes exhibited more viscous behavior with time. Sun et al. (2006) reported a similar behavior in that viscosity became nonlinear and increased with time. When the ternary effect of cementitious materials were evaluated (PC+FA+SF and PC+GGBFS+SF), the effect of SF was to increase the viscosity of SCCs in comparison to that of the control concrete. Because the effects of using FA and GGBFS were to decrease the viscosity of the concretes, it can also be postulated from the test results that among the mineral admixtures used that the SF dominated the viscous behavior of the concretes that have the ternary blends. The same trend was also observed in behavior of the concretes with the quaternary blends of PC, FA, GGBFS and SF. However, in the case of the ternary use of PC, FA and GGBFS the viscosity decreased with respect to control concrete.

When the viscosity of the concretes with ternary blends (PC+FA+MK and PC+GGBFS+MK) was evaluated, it was observed in Figure 4.28 that the combined use of mineral admixtures reduced the viscosity of the concretes at all measuring times although the concretes containing 10% or higher MK had consistently higher viscosity than the control mixture at low w/b ratio concretes. The mixture containing 15% MK had a viscosity of as high as 11200 cP at 5 rpm (Figure 4.26a) while that of the mixture containing 45% FA and 15% MK was 5400 cP (Figure 4.28a) indicating a reduction of approximately 50%. A similar behavior was also seen in the concretes with quaternary blends (Figure 4.29) in that the use of FA and GGBFS with MK

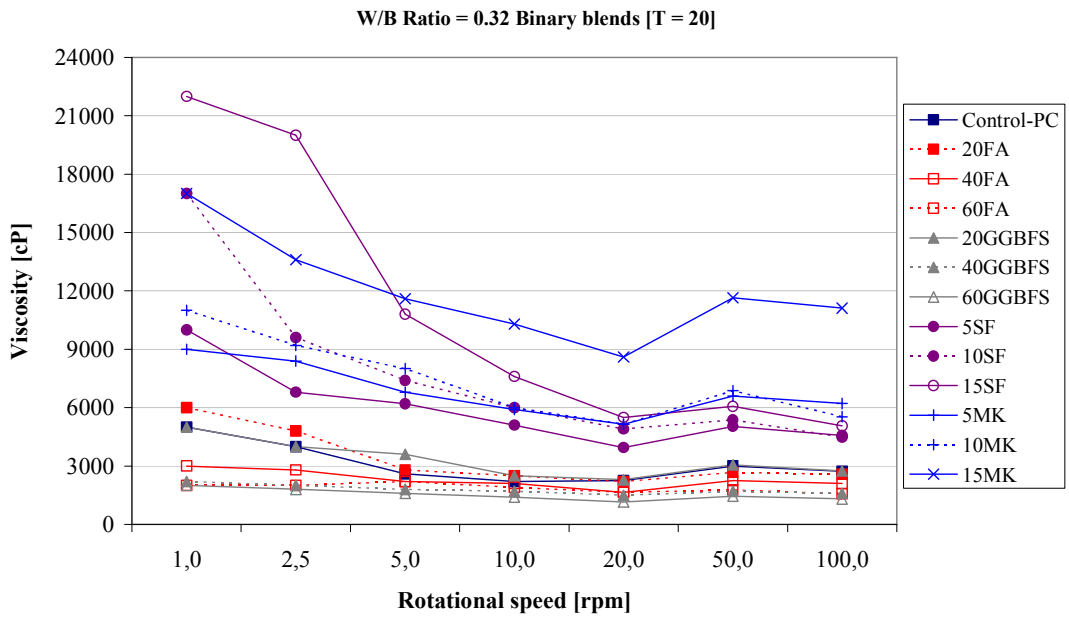
provided a marked reduction in the viscosity of the concretes in comparison to that of the concrete made only with binary blends of MK.

The binary effects of mineral admixtures at high w/b ratio concretes were depicted in Figure 4.30. Increasing the viscosity testing time from 0 to 40 min increased the viscosity of SCCs for all mineral admixtures. At testing time of $t=0$, the lowest viscosity was observed in the concretes with 60% FA or GGBFS but at testing time 20 and 40 min, the lowest viscosity was measured in the concretes with 40% GGBFS or 60% FA . The highest viscosity was also measured at SF blended SCCs irrespective of time of measurement.

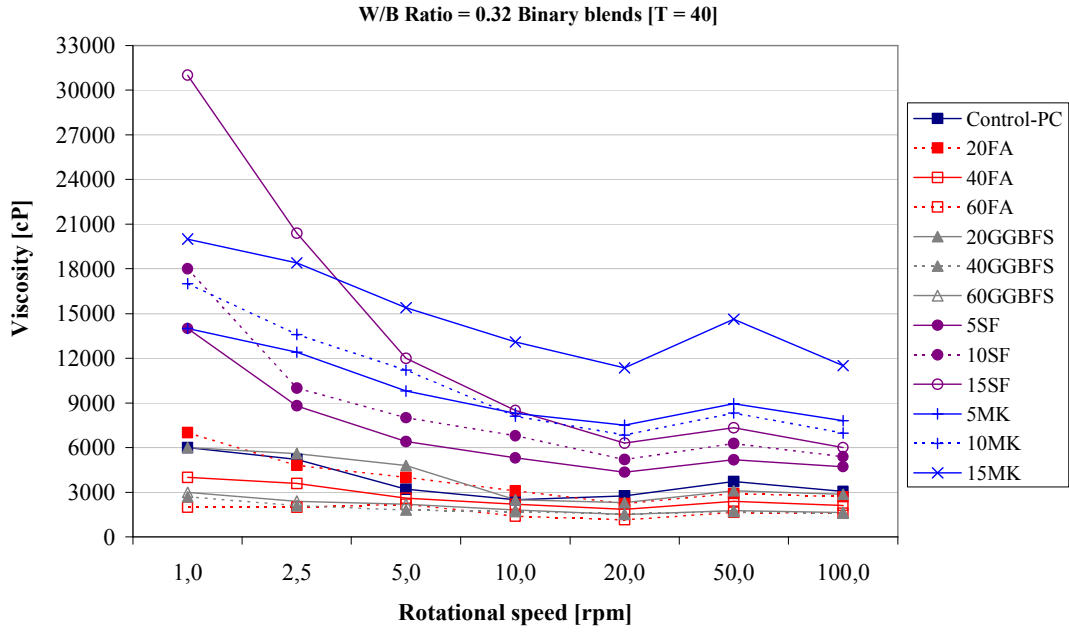
At high w/b ratio concretes, generally, the best fit equations with the higher correlation coefficient was obtained when compared to low w/b ratio concretes. As can be seen in Table 4.8, all of the concretes at all viscosity testing time have correlation coefficients as high as 0.97. As can also be seen in Figures 4.31 and 4.32, the ternary (PC+FA+SF and PC+GGBFS+SF) and quaternary (PC+FA+GGBFS+SF) use of mineral admixtures abolished the negative effect of silica fume. Moreover, the concretes with SF in addition to FA had better performance in terms viscosity. For example, the mixture with 60% FA (M47) had so low cohesion that it could not fulfill the EFNARC limitations for both the slump flow and V-funnel flow times as seen in Table 4.2. Addition of SF, in this case, even remedied this adverse effect of using high volume FA in the SCCs at high w/b ratio. It was also seen in Figure 4.31 that combined use of FA and GGBFS with PC in the ternary blends did not significantly impress the viscosity when compared to the binary blends of PC+FA and PC+GGBFS. When comparing the viscosity of self compacting concretes according to water binder ratios, increasing the water binder ratio from 0.32 to 0.44, generally, decreased the viscosity.



a)

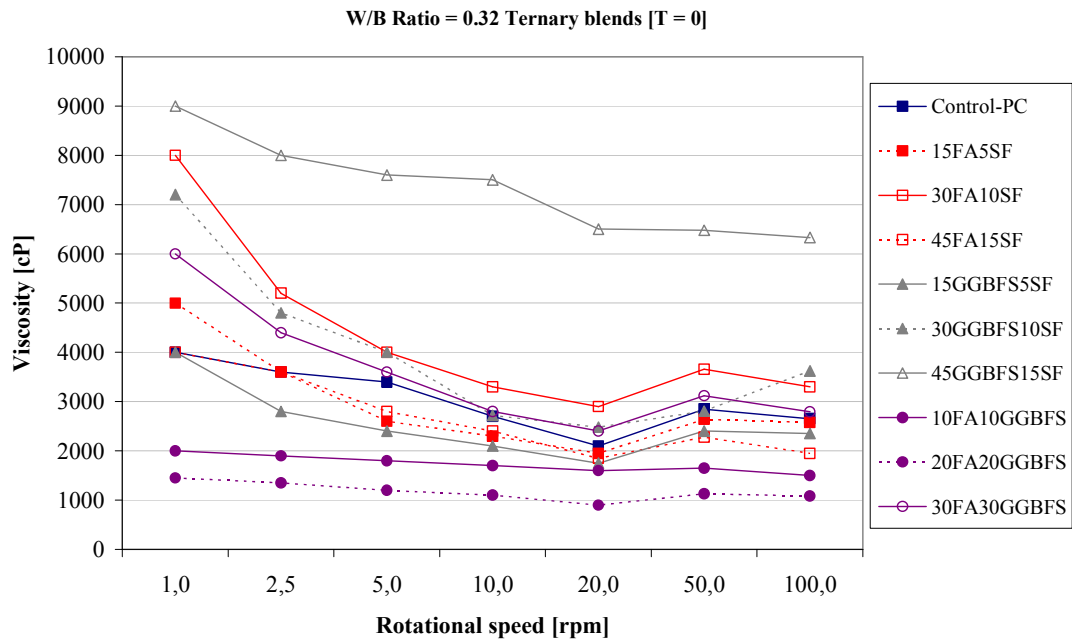


b)



c)

Figure 4.26 Viscosity of SCC with binary cementitious materials at different rotational speeds at w/b ratio of 0.32 a) T = 0; b) T = 20; c) T = 40



a)

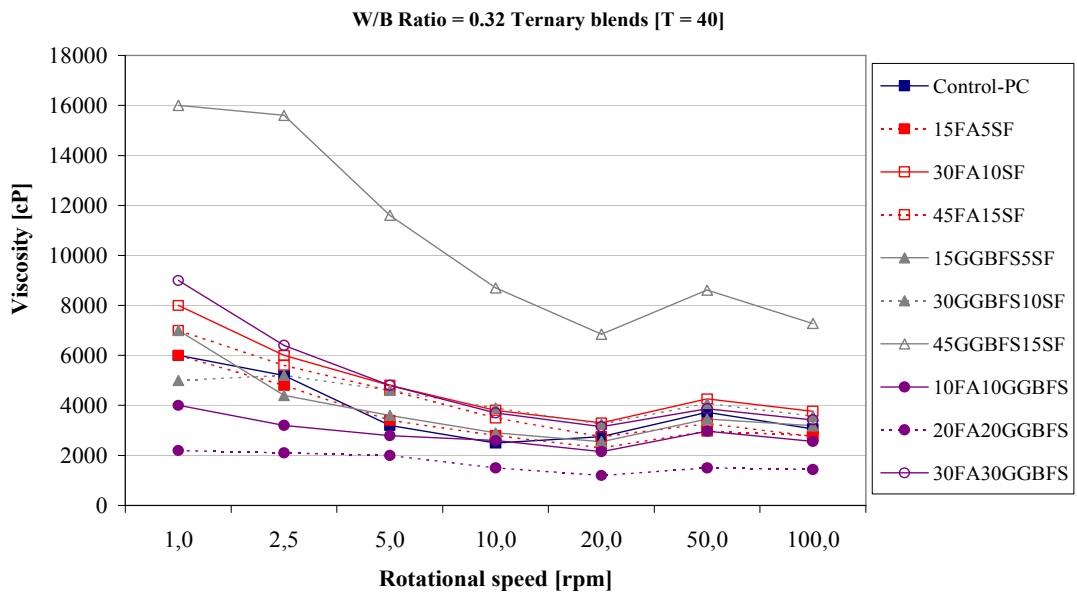
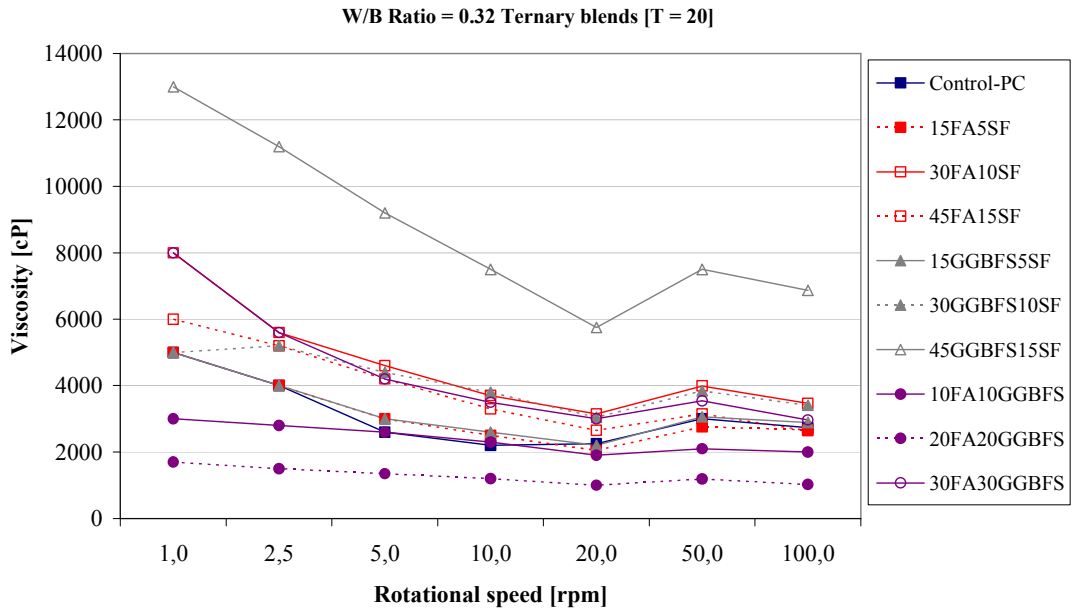
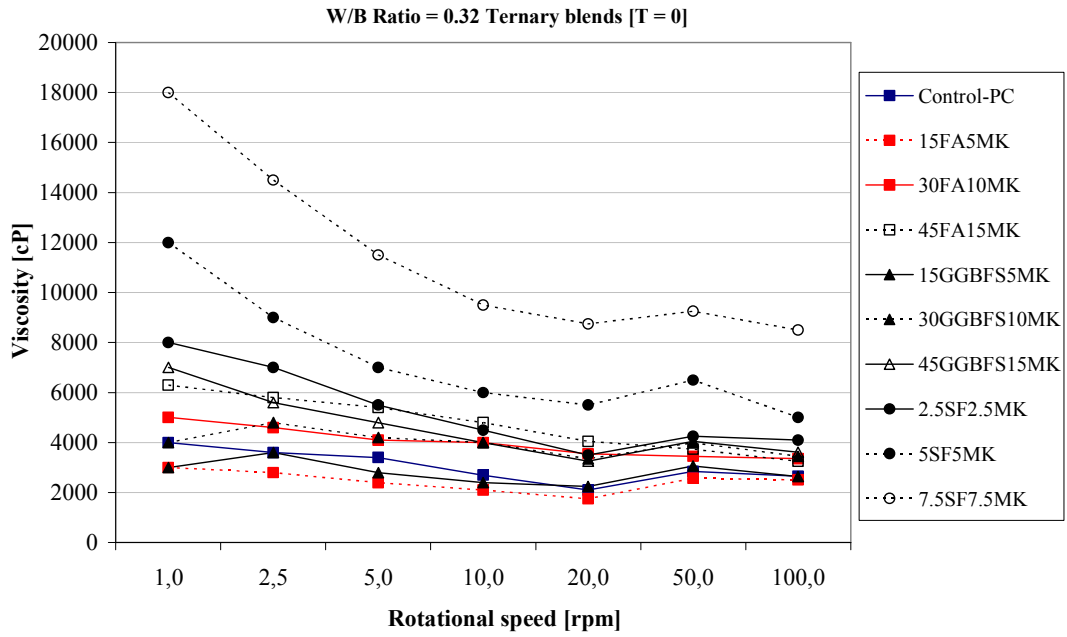
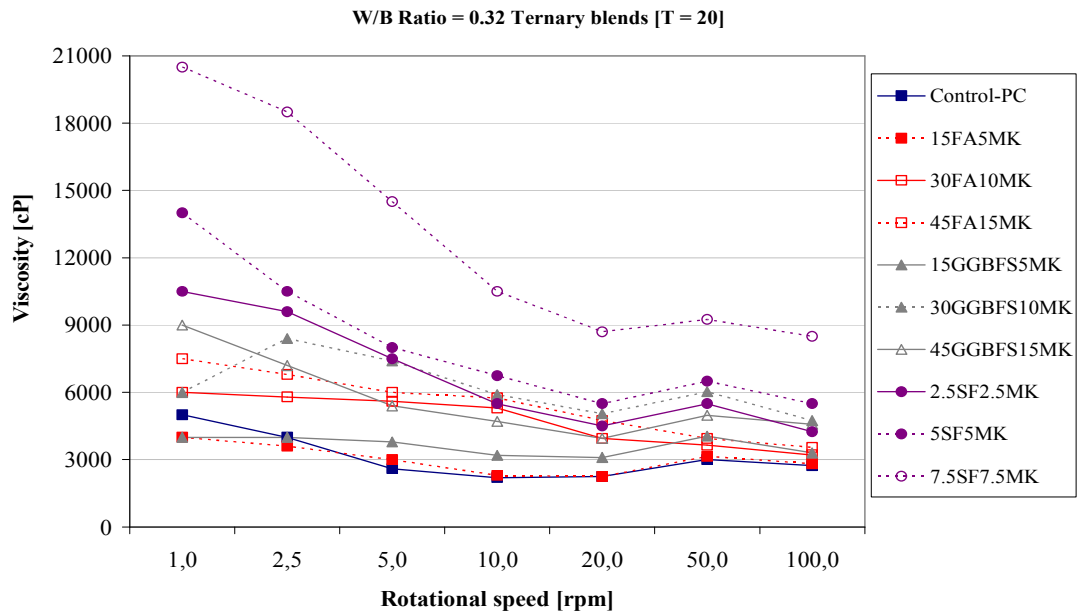


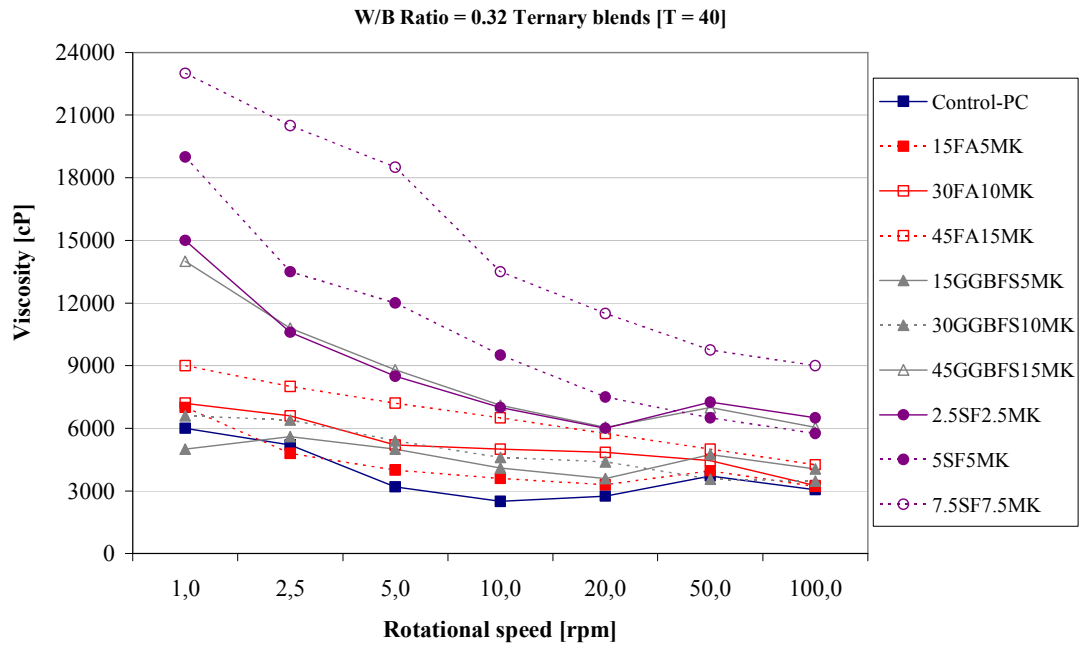
Figure 4.27 Viscosity of SCC with ternary (PC+FA+SF, PC+GGBFS+SF and PC+FA+GGBFS) cementitious materials at different rotational speeds at w/b ratio of 0.32 a) T = 0; b) T = 20; c) T = 40



a)

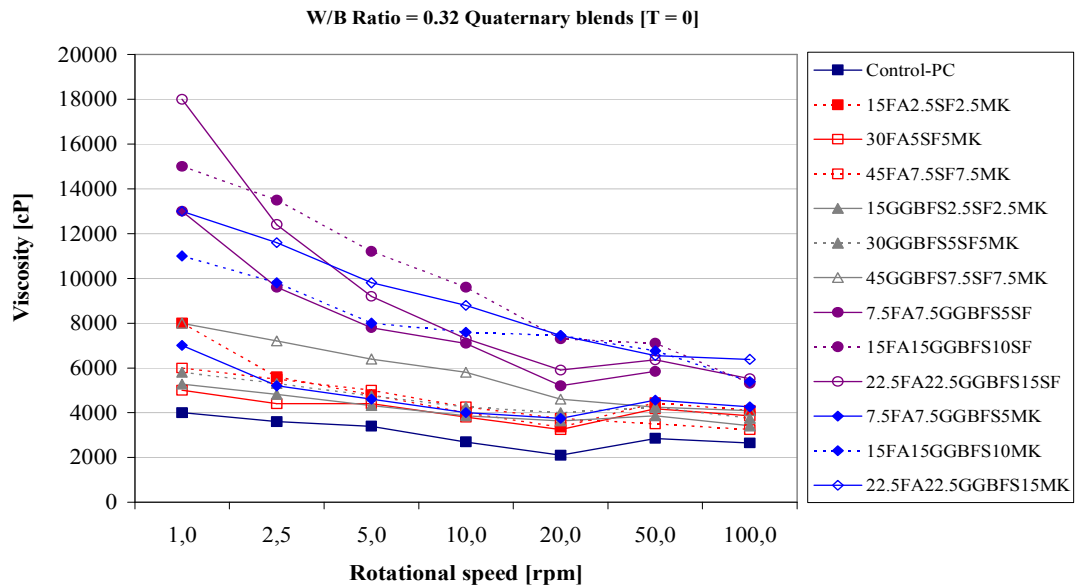


b)



c)

Figure 4.28 Viscosity of SCC with ternary (PC+FA+MK and PC+GGBFS+MK) cementitious materials at different rotational speeds at w/b ratio of 0.32 a) T = 0; b) T = 20; c) T = 40



a)

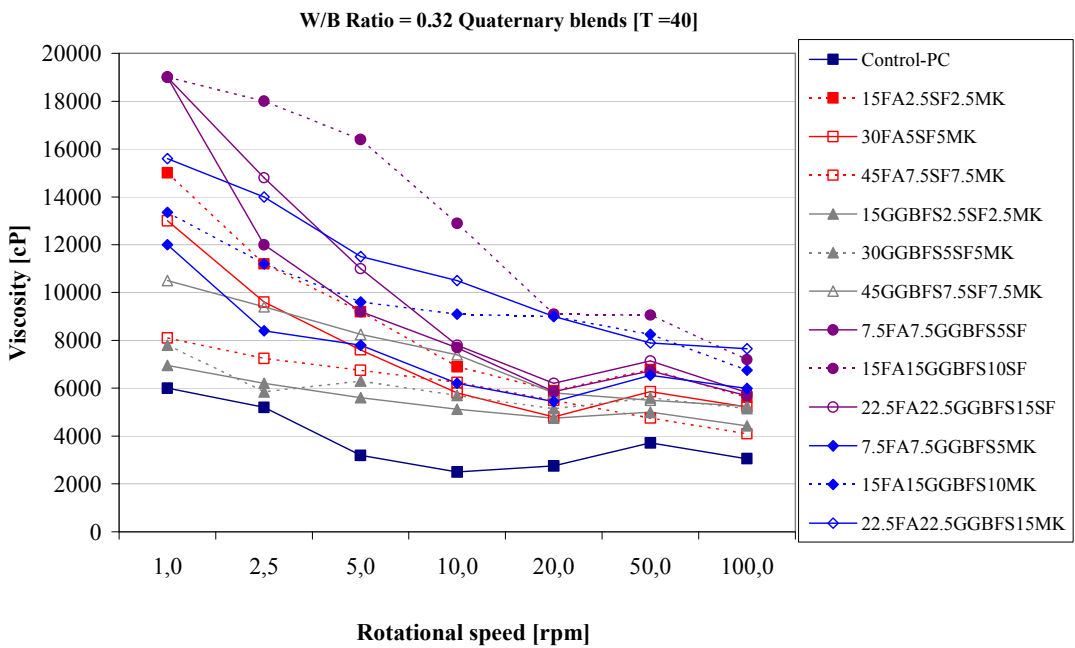
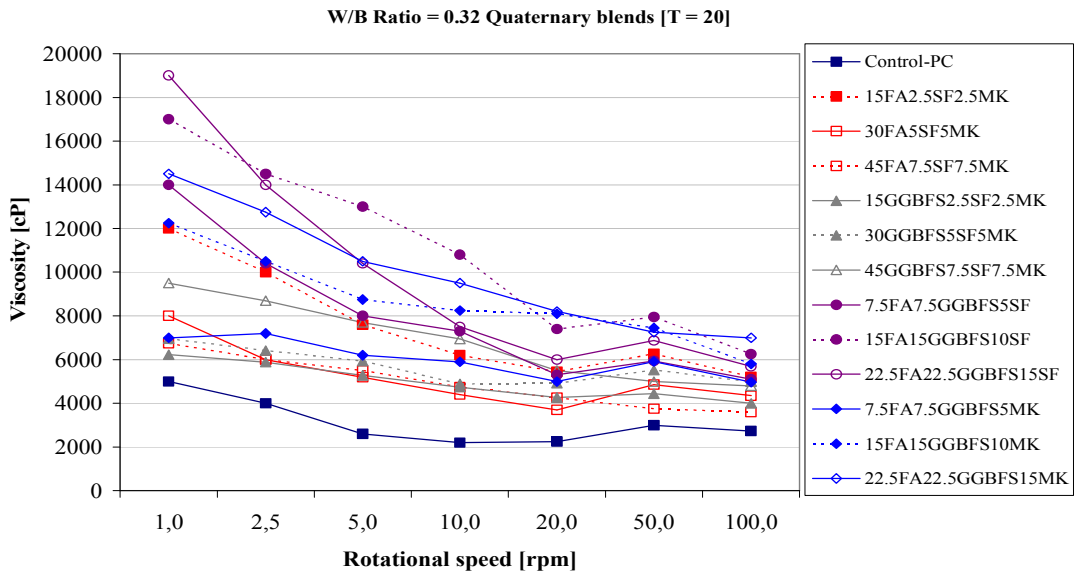
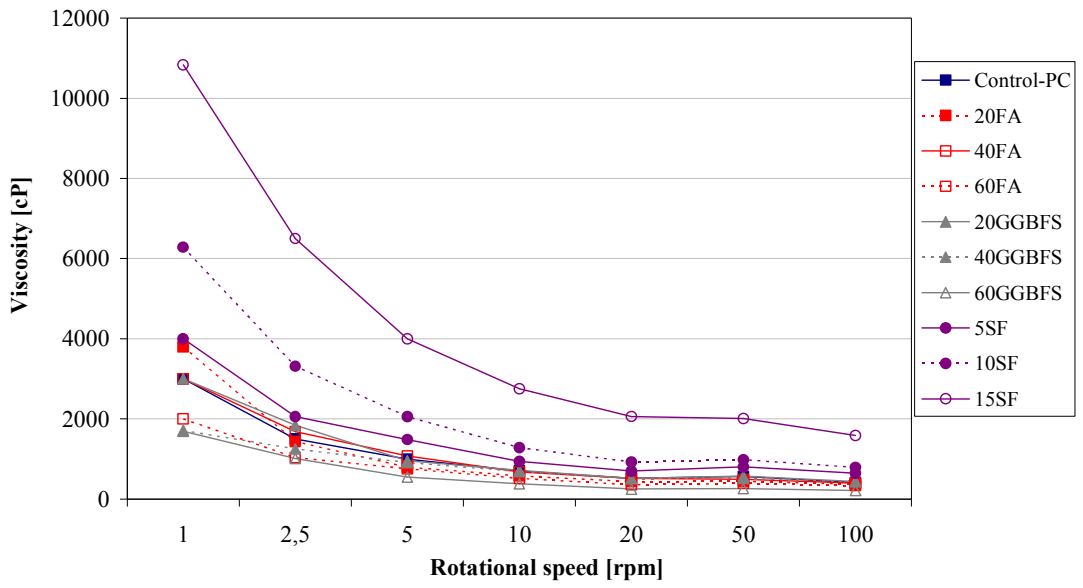


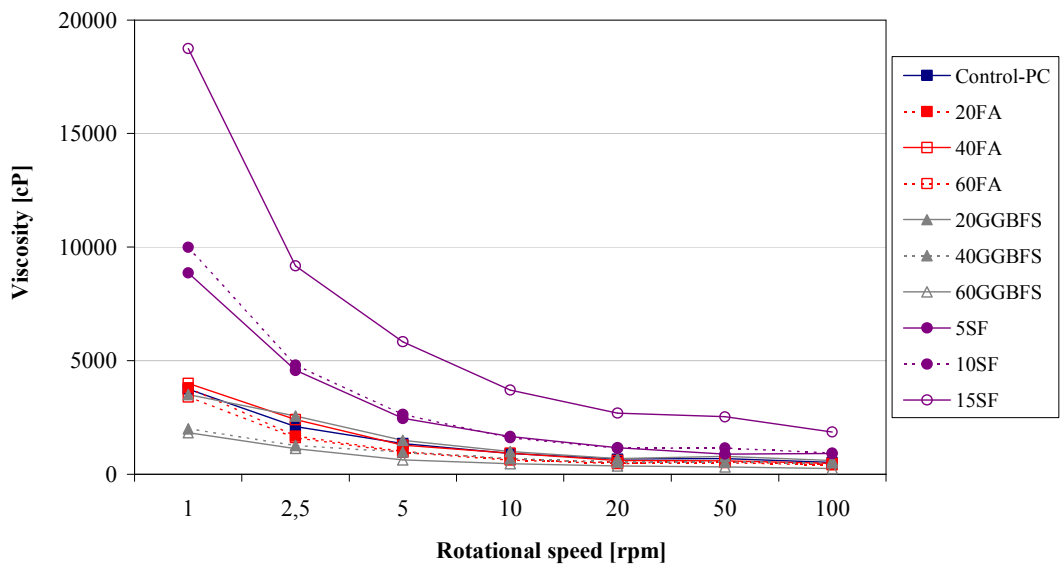
Figure 4.29 Viscosity of SCC with quaternary (PC+FA+SF+MK; PC+GGBFS+SF+MK; PC+FA+GGBFS+SF; PC+FA+GGBFS+MK) cementitious materials at different rotational speeds at w/b ratio of 0.32 a) T = 0; b) T = 20; c) T = 40

W/B Ratio = 0.44 Binary blends [T = 0]

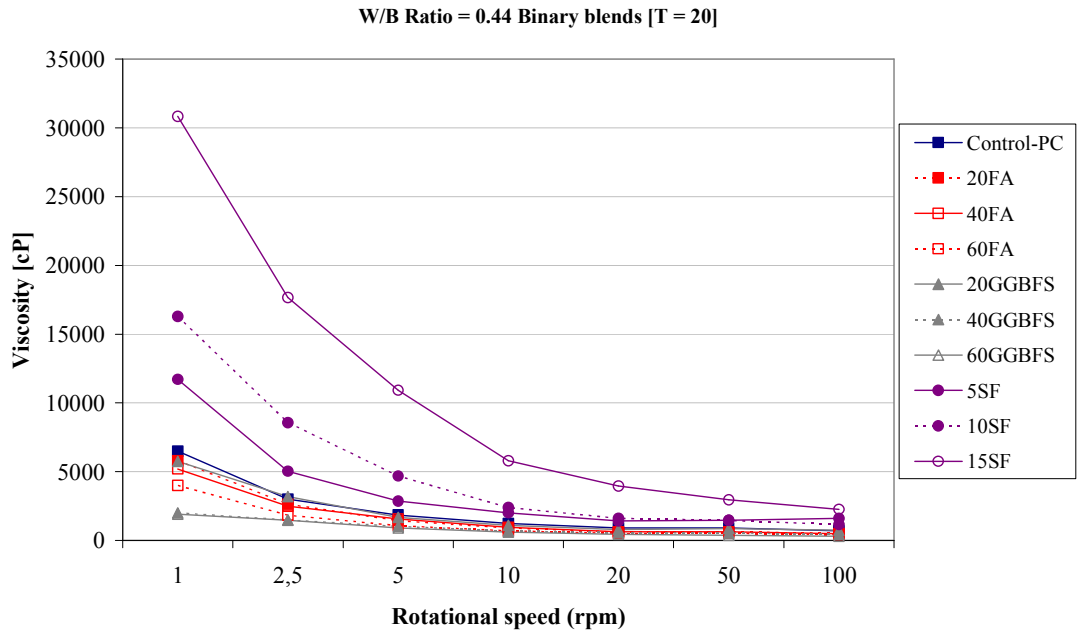


a)

W/B Ratio = 0.44 Binary blends [T = 20]

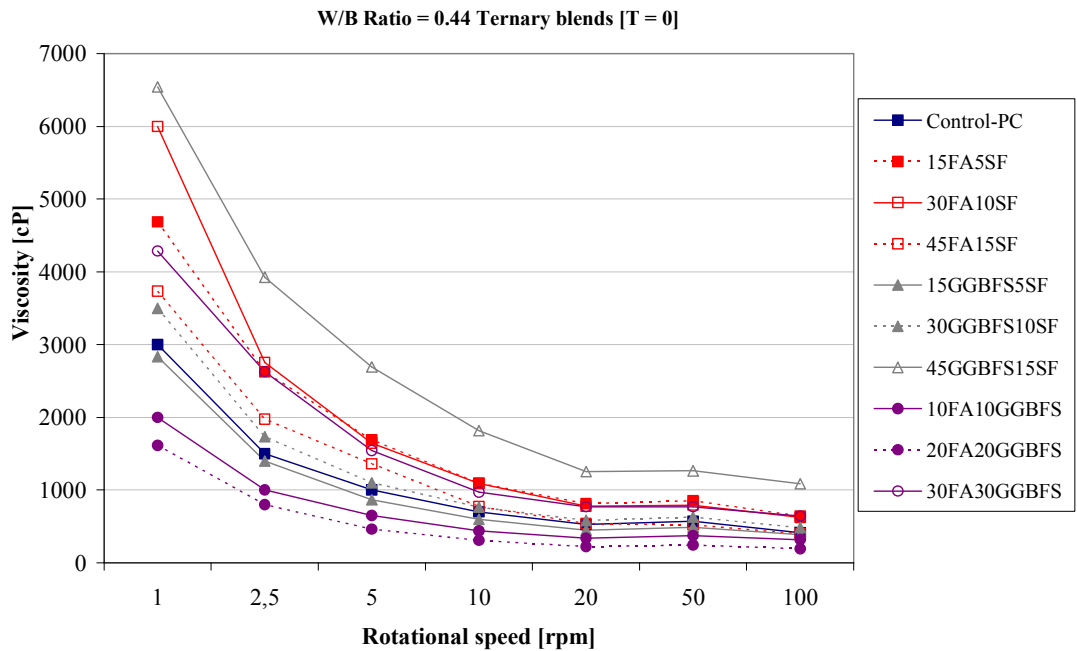


b)

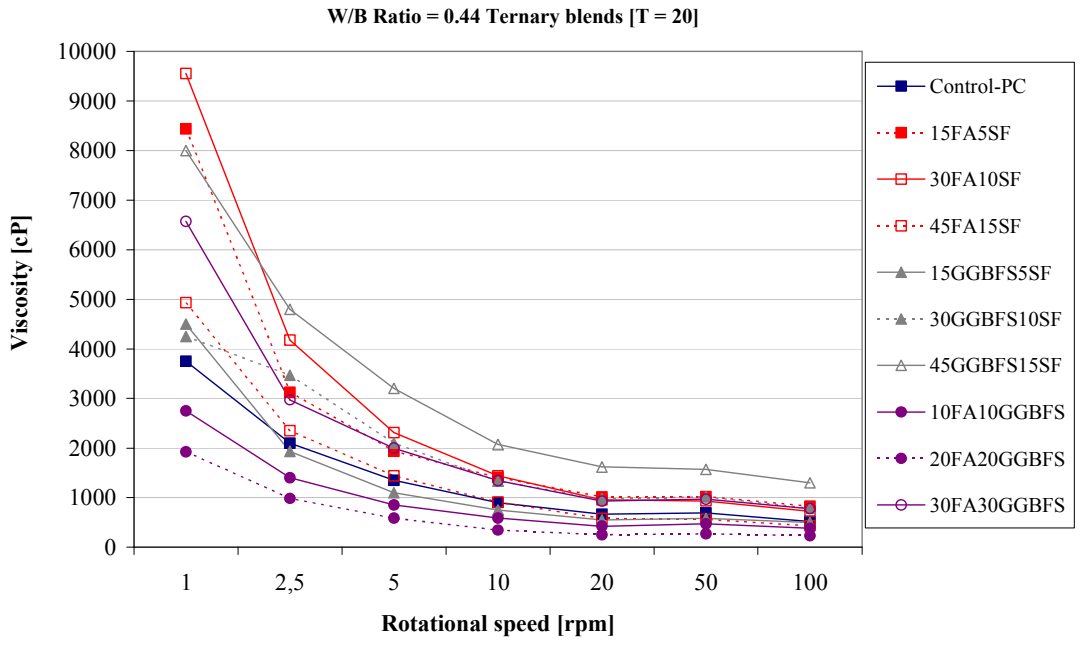


c)

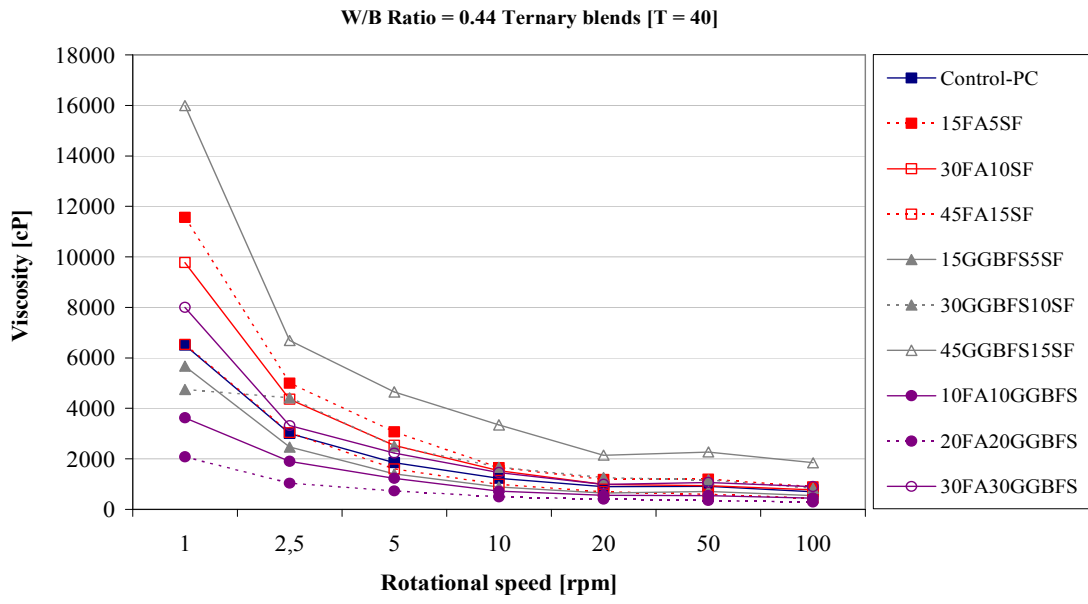
Figure 4.30 Viscosity of SCC with binary cementitious materials at different rotational speeds at w/b of 0.44 a) T = 0; b) T = 20; c) T = 40



a)

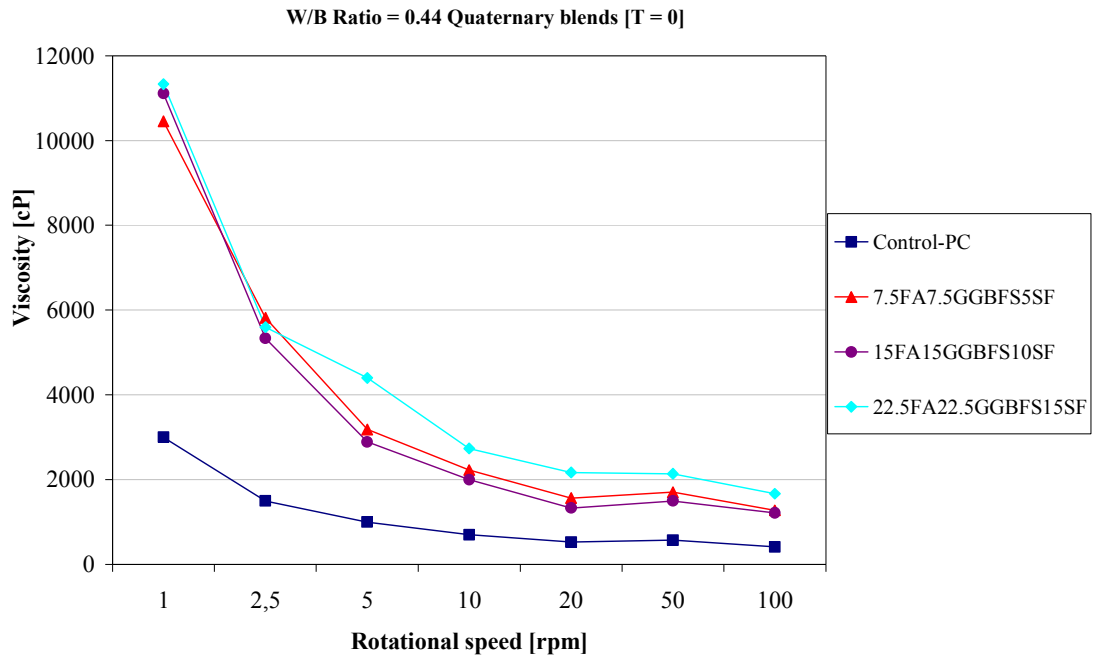


b)

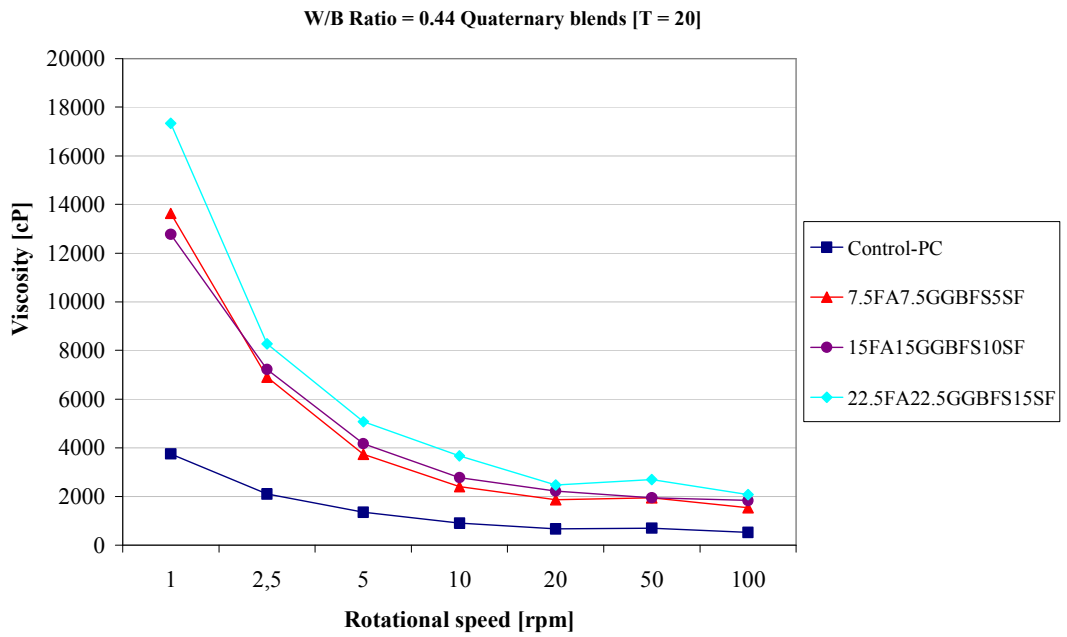


c)

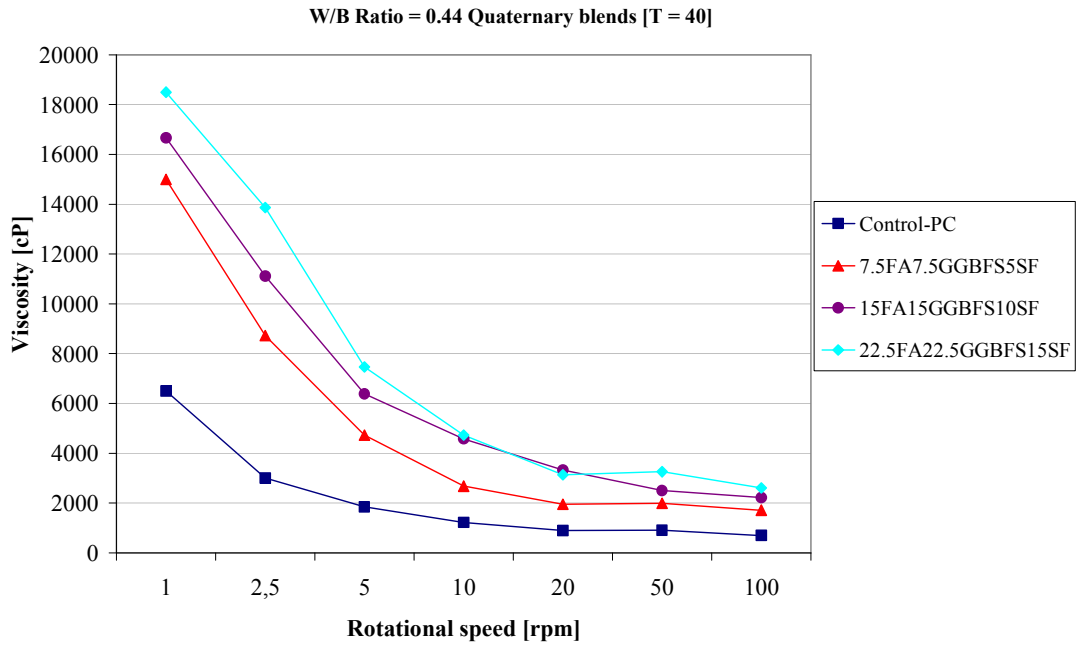
Figure 4.31 Viscosity of SCCs with ternary (PC+FA+SF; PC+GGBFS+SF and PC+FA+GGBFS) cementitious materials at different rotational speeds at w/b of 0.44 a) T = 0; b) T = 20; c) T = 40



a)



b)



c)

Figure 4.32 Viscosity of SCC with quaternary (PC+FA+GGBFS+SF) cementitious materials at different rotational speeds at w/b of 0.44 a) T = 0; b) T = 20; c) T = 40

Table 4.5 The equation constants and regression coefficients of the best fit curves for binary mineral admixtures at w/b ratio of 0.32

Mix No	Mix ID	T = 0			T = 20			T = 40		
		a	b	R ²	a	b	R ²	a	b	R ²
M1	Control-PC	4103	-0.26	0.67	4580	-0.35	0.63	5712	-0.38	0.63
M2	20FA	4708	-0.44	0.74	5797	-0.50	0.83	6872	-0.54	0.90
M3	40FA	3052	-0.25	0.68	2991	-0.23	0.63	4079	-0.37	0.81
M4	60FA	2089	-0.17	0.65	2154	-0.12	0.49	2141	-0.20	0.36
M5	20GGBFS	3895	-0.25	0.58	4905	-0.35	0.75	6583	-0.49	0.71
M6	40GGBFS	1974	-0.14	0.69	2200	-0.18	0.85	2567	-0.27	0.91
M7	60GGBFS	1898	-0.22	0.89	2030	-0.25	0.78	2596	-0.33	0.89
M8	5SF	6176	-0.23	0.74	9502	-0.42	0.88	13066	-0.58	0.93
M9	10SF	15246	-0.65	0.98	15981	-0.67	0.97	16433	-0.01	0.94
M10	15SF	17918	-0.67	0.97	26293	-0.85	0.92	32500	-0.90	0.96
M11	5MK	8991	-0.33	0.81	11197	-0.37	0.82	17561	-0.49	0.91
M12	10MK	6473	-0.16	0.44	9017	-0.24	0.69	14191	-0.32	0.87
M13	15MK	15976	-0.34	0.85	16000	-0.25	0.66	20654	-0.28	0.79

Table 4.6 The equation constants and regression coefficients of the best fit curves for ternary mineral admixtures at w/b ratio of 0.32

Mix No	Mix ID	T = 0			T = 20			T = 40		
		a	b	R ²	a	b	R ²	a	b	R ²
M14	15FA5SF	4540	-0.39	0.73	4824	-0.39	0.77	5912	-0.45	0.85
M15	30FA10SF	7282	-0.47	0.86	7601	-0.44	0.89	7702	-0.42	0.85
M16	45FA15SF	4245	-0.40	0.88	6416	-0.45	0.91	7379	-0.51	0.93
M17	15FA5MK	2904	-0.15	0.33	3871	-0.22	0.50	6458	-0.37	0.87
M18	30FA10MK	11741	-0.41	0.84	12219	-0.44	0.77	23840	-0.67	0.93
M19	45FA15MK	6973	-0.33	0.87	8376	-0.37	0.86	9882	-0.36	0.89
M20	15GGBFS5SF	3586	-0.31	0.67	4710	-0.33	0.69	6176	-0.43	0.77
M21	30GGBFS10SF	6604	-0.48	0.75	5404	-0.24	0.70	5373	-0.21	0.66
M22	45GGBFS15SF	9134	-0.19	0.94	13379	-0.38	0.83	17846	-0.47	0.84
M23	15GGBFS5MK	3205	-0.11	0.24	4052	-0.09	0.30	5410	-0.14	0.41
M24	30GGBFS10MK	4454	-0.10	0.32	7393	-0.16	0.24	16478	-0.49	0.93
M25	45GGBFS15MK	6978	-0.37	0.88	8765	-0.39	0.85	14091	-0.45	0.94
M26	10FA10GGBFS	2051	-0.14	0.92	3147	-0.24	0.86	3776	-0.23	0.66
M27	20FA20GGBFS	1459	-0.19	0.68	1740	-0.27	0.87	2353	-0.28	0.71
M28	30FA30GGBFS	5753	-0.43	0.85	7746	-0.52	0.94	8761	-0.53	0.91
M29	2.5SF2.5MK	8337	-0.41	0.87	11636	-0.49	0.88	14310	-0.45	0.91
M30	5SF5MK	11721	-0.45	0.92	14006	-0.49	0.95	20572	-0.62	0.96
M31	7.5SF7.5MK	18124	-0.41	0.94	22799	-0.52	0.92	26680	-0.52	0.90

Table 4.7 The equation constants and regression coefficients of the best fit curves for quaternary mineral admixtures at w/b ratio of 0.32

Mix No	Mix ID	T = 0			T = 20			T = 40		
		a	b	R ²	a	b	R ²	a	b	R ²
M32	15FA2.5SF2.5MK	7391	-0.37	0.80	12377	-0.44	0.93	15304	-0.52	0.95
M33	30FA5SF5MK	4921	-0.15	0.57	7580	-0.33	0.81	12934	-0.51	0.92
M34	45FA7.5SF7.5MK	6521	-0.33	0.92	7273	-0.33	0.92	8856	-0.33	0.92
M35	15GGBFS2.5SF2.5MK	5400	-0.22	0.94	6545	-0.24	0.93	7075	-0.22	0.96
M36	30GGBFS5SF5MK	5940	-0.22	0.94	6996	-0.18	0.78	7402	-0.19	0.81
M37	45GGBFS7.5SF7.5MK	8769	-0.37	0.91	10548	-0.38	0.90	11501	-0.38	0.92
M38	7.5FA7.5GGBFS5SF	13292	-0.50	0.96	14367	-0.53	0.96	18524	-0.63	0.97
M39	15FA15GGBFS10SF	17424	-0.52	0.88	19393	-0.52	0.88	22957	-0.51	0.83
M40	22.5FA22.5GGBFS15SF	18209	-0.63	0.97	19987	-0.65	0.96	20498	-0.65	0.95
M41	7.5FA7.5GGBFS5MK	6440	-0.26	0.76	7439	-0.18	0.72	11334	-0.37	0.88
M42	15FA15GGBFS10MK	11609	-0.32	0.90	12777	-0.33	0.90	13650	-0.31	0.93
M43	22.5FA22.5GGBFS15MK	14156	-0.39	0.94	15611	-0.40	0.96	16936	-0.39	0.95

Table 4.8 The equation constants and regression coefficients of the best fit curves at w/b ratio of 0.44

Mix no	Mix ID	T = 0			T = 20			T = 40		
		a	b	R ²	a	b	R ²	a	b	R ²
M44	Control-PC 2	11898	-1.01	0.99	15814	-1.03	0.99	25939	-1.16	0.99
M45	20FA	17032	-1.20	0.98	18079	-1.14	0.98	29570	-1.30	0.99
M46	40FA	16053	-1.07	0.99	22278	-1.15	0.98	27564	-1.24	0.99
M47	60FA	9979.1	-0.95	0.98	16640	-1.13	0.98	19882	-1.19	0.99
M48	20GGBFS	15731	-1.02	0.97	28706	-1.20	0.98	35829	-1.25	0.97
M49	40GGBFS	6575.7	-0.73	0.97	7209	-0.76	0.98	7814	-0.80	0.97
M50	60GGBFS	26130	-1.11	0.98	28490	-1.05	0.99	33116	-0.99	0.95
M51	5SF	13854	-0.96	0.97	33521	-1.26	0.99	37386	-1.12	0.95
M52	10SF	22851	-1.11	0.98	36268	-1.27	0.99	66858	-1.44	0.98
M53	15SF	36268	-1.27	0.99	47584	-1.19	0.99	92881	-1.39	0.97
M54	15FA5SF	15829	-1.04	0.98	24446	-1.19	0.99	38349	-1.34	0.99
M55	30FA10SF	26971	-1.19	0.99	44585	-1.36	0.99	46510	-1.36	0.99
M56	45FA15SF	31027	-1.18	0.98	39809	-1.28	0.99	53554	-1.41	0.99
M57	15GGBFS5SF	16614	-1.04	0.98	25439	-1.17	0.98	33021	-1.23	0.98
M58	30GGBFS10SF	20556	-1.02	0.99	45676	-1.19	0.99	53784	-1.19	0.99
M59	45GGBFS15SF	19410	-0.97	0.98	23498	-0.97	0.99	42258	-1.12	0.99
M60	10FA10GGBFS	15373	-0.98	0.98	21764	-1.05	0.98	30429	-1.12	0.98
M61	20FA20GGBFS	20947	-1.12	0.98	25674	-1.16	0.98	27366	-1.02	1.00
M62	30FA30GGBFS	16087	-1.03	0.98	22661	-1.11	0.99	26670	-1.15	0.98
M63	7.5FA7.5GGBFS5SF	24130	-1.11	0.98	30331	-1.16	0.98	36295	-1.21	0.97
M64	15FA15GGBFS10SF	19905	-1.18	0.98	24032	-1.07	0.99	35321	-1.09	0.98
M65	22.5FA22.5GGBFS15SF	17093	-0.98	0.99	25780	-1.10	0.99	47047	-1.32	0.99

4.2. Mechanical Properties

4.2.1 Compressive strength

The summary of the test results relevant to the compressive strength of the concretes having different mixture compositions at low and high w/b ratios are given in Tables 4.9 and 4.10, respectively. The overall compressive strength ranged from 30.3 to 98.6 and from 42.5 to 113.1 MPa at 28 and 90 days, respectively. The variation in the compressive strength of these low w/b ratio concretes with binary blends (M1 through M13) is shown in Figure 4.33. It was observed from the figure that there was a marked reduction in the compressive strength of the concretes with increasing FA

content while the concretes having GGBFS had comparable strength values to that of the control concrete, irrespective of the replacement level. The SF and MK concretes, on the other hand, had consistently higher compressive strength than the control concrete. As Figure 4.33 clearly shows that MK is the most effective mineral admixture on the compressive strength of SCC for both testing ages. Poon et al. (2006), Gesoglu et al. (2007), Mermerdaş (2006) and Güneyisi and Gesoglu (2007) stated that MK contributes to the strength of concrete not only at 28 days mainly by filling effect but also at later ages due to the fast pozzolanic reaction. As it is seen in Tables 4.9 and 4.10, the compressive strength of the mineral admixture blended concretes increased with time. With respect to 28 day compressive strength of the concretes, the highest increment was achieved for the mixtures M4 and M47 both of which having 60% FA at low and high w/b ratios, respectively. The lowest, on the other hand, belonged to the mixtures M41 and M53 at low and high w/b ratios, respectively. The former contained a quaternary blend of 7.5FA7.5GGBFS5MK while the latter had only binary blends of 15% SF. Test results suggested that it was the FA governing the reduction in the strength of the concretes when used at higher amounts. It is a known fact that FA generally has negative effects on the concrete strength, particularly at early ages. However, FA concretes may have better strength performance at long term when they are prepared at lower water to binder ratios (Babu and Rao, 1994).

Influence of using mineral admixtures within ternary blends on the compressive strength of SCCs at low w/b ratio is exhibited in Figure 4.34. In the case of ternary use of PC+FA+SF and PC+FA+MK, the compressive strength slightly decreased with the replacement ratio but the rate of reduction was much less compared to the case in the binary use of PC+FA. The ternary use of PC+FA+GGBFS also caused a reduction in the compressive strength when compared to the control concrete for both testing ages. However, the ternary use of PC+GGBFS+SF and PC+GGBFS+MK provided a marked positive effect on the compressive strength, especially the effect being more pronounced at 90 days. For example, the reference concrete had a 90-day compressive strength of about 91 MPa. The ternary use of PC+GGBFS+SF and PC+GGBFS+MK led to an improvement of about 11 and 15%. In the ternary use of PC+FA+GGBFS, on the other hand, the strength values displayed a reduction as compared to that of the control concrete, but nevertheless,

relatively higher compressive strengths were achieved according to the binary use PC+FA for both testing ages. As seen in Table 4.9 that the compressive strength of the concrete with 40%FA at 90 days was measured to be 77.9 MPa which slightly increased to 82.8 MPa for the concrete containing 20FA20GGBFS, but the situation was converse in the binary use of PC+GGBFS. The ternary use of PC+SF+MK consistently increased the compressive strength of SCCs when compared to that of the control concrete. The compressive strength of such concretes ranged from 92 to 94 and from 100 to 107 MPa at 28 and 90 days, respectively.

Figure 4.35 demonstrates the effect of quaternary use of mineral admixtures on the compressive strength of SCCs at low w/b ratio. It was observed that there was an increase in the compressive strength of SCCs up to a binder replacement level of 40%. However, beyond that threshold the strength began to lessen as FA governed the reduction in the strength values. Of all 43 concretes produced with 0.32 w/b ratio, the highest compressive strength of about 113 MPa was acquired in the concrete having the quaternary blends of 15GGBFS2.5SF2.5MK. When compared to ternary use of PC+MK+SF, the quaternary use of PC+FA+SF+MK decreased the compressive strength of SCCs for both testing ages.

Compressive strength test results of high w/b ratio concretes were given in Table 4.10. Figures 4.36 and 4.37 show the variation in that property of the concretes incorporating binary, and ternary and quaternary blends, respectively. The compressive strengths of these SCCs were in the range of 30.3 to 71.1 and 42.5 to 78.0 MPa for 28 and 90 days, respectively. Regarding the effect of FA, the concretes in this group exhibited a similar pattern to that seen in the case of low w/b ratio. Therefore, the existence of FA generally lowered the compressive strength of concretes. For instance, it was observed in Figure 4.36 that replacing PC with 60% FA caused a reduction in the compressive strength of about 40% for both testing ages. Moreover, there was a gradual decrease in the compressive strength of the concretes having ternary and/or quaternary blends including FA (Figure 4.37). Therefore, the test results suggested that it was the FA among the mineral admixtures used that governed the reduction in the compressive strength of the SCCs. However, this adverse effect of FA seemed to be remedied by the combined use of the mineral admixtures. The concretes with GGBFS and/or SF, on the other hand, had generally

comparable strength values to that of the control concrete. In this group of concrete, no significant change occurred in the ternary and quaternary use of mineral admixtures when compared to binary blends of mineral admixtures. Interestingly, the concrete incorporating 10% FA and 10% GGBFS achieved the highest compressive strength of this group mixture at 90 days.

The influence of w/b ratio and testing age on the compressive strength of SCCs are demonstrated in Figures 4.38 and 4.39, respectively. As expected, the compressive strength of SCCs decreased with increasing w/b ratio. As mentioned earlier, the compressive strength of concrete increased with time for both w/b ratios. This improvement in compressive strength with the testing age was higher at the high w/b ratio. Approximately, 23% and 17% mean increments in the compressive strength were observed at high and low water-binder ratio, respectively.

4.2.2 Ultrasonic pulse velocity (UPV)

The ultrasonic pulse velocities of the concretes of different mixtures are given in Tables 4.9 and 4.10 and graphically shown in Figures 4.40 to 4.46. The overall pulse velocity ranged from 4644 to 5172 m/sec and 4800 to 5303 m/sec for the low w/b ratio concretes at 28 and 90 days, respectively. However, the high w/b ratio concretes had pulse velocities varying from 4738 to 4999 m/sec and 4760 to 5050 m/sec at 28 and 90 days, respectively. Whitehurst (1951) classified the concretes as excellent, good, doubtful, poor, and very poor for the UPV values of 4500 m/sec and above, 3500–4500, 3000–3500, 2000–3000, and 2,000 m/sec and below, respectively. The concretes produced in this study had UPV values of greater than 4500 m/sec for both w/b ratios so that the rating of the concretes was found to be excellent.

The variation in pulse velocity of SCCs with the binary blends of mineral admixtures at low w/b ratio is demonstrated in Figure 4.40 with respect to the mineral admixtures content and testing ages. The binary use of FA in the SCC caused a reduction in UPV at low w/b ratio at 28 days. The amount of reduction increased with increasing the replacement level of FA. However, at 90 days, the comparable UPV were obtained in the control concretes as well as those with 20% and 40 % FA. In case of the concretes containing the binary blends of PC+GGBFS, there was a

gradual reduction according to the control concrete at 28 days, but a remarkable enhancement in the 90 days. Binary use of PC+SF led to a lower UPV value at the 5% SF replacement whereas the UPV values exceeded that of the control at 28 days as the SF content had been used at 10 or 15%. At 90 days, however, all replacement levels of SF resulted in higher UPV values than that of control concrete. Similarly, binary blends of PC+MK concretes had higher UPV values than that of control concrete at all replacement levels of MK for both testing ages. However, the gradual increase in the MK content from 5% to 15% in the binary blends of PC+MK, decreased the UPV values gradually at the 90 days. The highest UPV value in all produced SCCs was achieved at 5% MK content (M11) at the 90 days.

Variation of the UPV values of SCCs with the ternary blends of mineral admixtures at low w/b ratio was demonstrated in Figure 4.41. The figure revealed that the ternary use of PC+FA+SF did not provide a significant further improvement upon the UPV value of the concrete with the binary blends of PC+FA. Moreover, there was a gradual decrease in the UPV values of this group concrete with the increasing of replacement level of mineral admixtures for both testing ages. A similar trend was observed in case of the ternary blends of PC+GGBFS+MK, PC+FA+GGBFS, and PC+SF+MK concretes, as well. Figure 4.42 demonstrated that the variation in the UPV values of the low w/b ratio concretes with the quaternary blends was much similar to that observed in the case of the ternary-blended-concretes in that the UPV values were much comparable to that of the control as well as those of the binary concretes. Indeed, 90-day UPV of the concrete with 20% GGBFS was about 5120 m/sec while the concrete with 15% GGBFS+2.5%SF+2.5%MK had a UPV of 4936 m/sec.

The variation of UPV values at high w/b ratio concretes were given in Table 4.10 and Figures 4.43 and 4.44. According to the Figure 4.43, the highest UPV of 5050 m/sec was acquired at 20% GGBFS replacement level. Interestingly, the binary use of PC+GGBFS had relatively higher UPV values than those of the concrete made with PC+SF blends, especially at 90 days. As was the case in the low w/b ratio concretes, there was a gradual increase in the UPV values of PC+FA concretes at high w/b ratio at 90 days.

In Figure 4.44, UPV values of the concretes with the ternary and quaternary blends of mineral admixtures at high w/b ratio are compared. There was a remarkable decrease in the UPV values of PC+FA+SF blended mixtures according to the control concrete at 28 and 90 days. However, the quaternary use of PC+FA+GGBFS+SF raised the UPV value progressively with respect to the control concrete. Approximately the same UPV values were observed in the ternary (PC+FA+GGBFS) and quaternary (PC+FA+GGBFS+SF) use of mineral admixtures, irrespective of the testing age.

Figures 4.45 and 4.46 represent the effects of w/b ratio and testing age on the pulse velocity of the SCCs. The pulse velocity generally increased with a drop in w/b ratio, irrespective of the testing age. Furthermore, as expected, all the concrete specimens exhibited an increase in their pulse velocities with age. However, the amount of increment was found to very low.

4.2.3 Splitting tensile strength

The indirect tensile strength of the SCCs measured by splitting test at 90 days are given in Tables 4.9 and 4.10 and graphically depicted in Figures 4.47 to 4.52. The variation in splitting tensile strength with the binary blends of cementitious materials at low w/b ratio is shown in Figure 4.47. As for compressive strength, the splitting tensile strength of SCCs exhibited a gradual decrease with the increase in the replacement level of FA from 20 to 60% in the concrete with binary blends. The control concrete had splitting tensile strength of 5.8 MPa reducing to 4.7 MPa as the 60% FA had replaced the PC. However, quite similar strength values were measured at all replacement levels of GGBFS, the value being around 5.7 MPa. Furthermore, this value was much close to the splitting tensile strength of the control concrete at low w/b ratio. Incorporating MK or SF, on the other hand, gave rise to an increase in the strength values. The splitting tensile strengths of the concretes with the former and the latter ranged from 6.1 to 6.6 MPa, and from 5.8 to 6.3 MPa, respectively. Figure 4.48 indicates the splitting tensile strength test results of SCCs produced with the ternary blends of mineral admixtures at low w/b ratio. Unlike the case in compressive strength, the negative effect of FA on the splitting tensile strength did

not diminish substantially when the ternary blends of PC, FA and SF had been employed. Even though, a gradual decrease was observed for the ternary use of PC, FA and MK, there was a steady increase in the ternary use of PC, GGBFS and SF. The ternary use of PC, SF and MK gave the highest splitting tensile strength values at low w/b ratio. Of all 43 concretes produced at low w/b ratio, the highest splitting tensile strength of 6.7 MPa was measured in the quaternary mixture of 15GGBFS2.5SF2.5MK as shown in Figure 4.49. According to the ternary use of PC, SF and MK, there was a slight decrease in the strength of the concretes with the quaternary use of PC, FA, SF and MK at low w/b ratio resulting from the strength decreasing effect of FA. Moreover, with increasing the amount mineral admixtures employed a decreasing trend was observed in the splitting tensile strength of SCCs made with the quaternary use of PC+GGBFS+SF+MK and PC+FA+GGBFS+MK blends.

As for low w/b ratio concretes, the splitting tensile strength of binary blends of PC and FA exhibited a gradual decrease with the increasing of FA replacement level from 20% to 60% at high w/b ratio as shown in Figure 4.50. Moreover, the splitting tensile strength values of these concretes (M45-M47) appeared to be less than that of the control concrete (M44). This can be the result of weaker bond between the matrix and aggregates which in turn being attributed to the anhydrate FA particles that are present in the matrix, acting as fillers that are present because of the lack of a CH compound (Şahmaran, 2006). Unlike FA, GGBFS replacement, especially up to 40%, improved the splitting tensile strength of the concretes with respect to the control concrete. In the case of SF replacement, the strength value of the concrete with 5% SF was initially lower than that of the control concrete, whereas at 10 and 15% SF contents higher strength values were achieved.

Figure 4.51 presents the splitting tensile strength test results of the concretes with the ternary and quaternary use of cementitious materials at high w/b ratio. As it is clearly seen in Figure 4.51, the combined use of FA and SF did not significantly diminish the negative effect of FA on the splitting tensile strength of SCCs. There was a gradual reduction in the strength of the concretes incorporating the ternary blends of PC, FA and SF. The same trend was also observed in concretes having the ternary (PC+FA+GGBFS) and quaternary PC+FA+GGBFS+SF blends. However, the rate of

reduction in the splitting tensile strength of the concretes was measured to be higher when the quaternary blends of PC+FA+GGBFS+SF had been used. This strength loss in the concretes with the ternary and quaternary blends may be attributed to the inclusion of again FA which always aggravated the mechanical properties.

Figure 4.52 represents the effects of w/b on the splitting tensile strength of the concretes. As for compressive strength and pulse velocity, the results showed that splitting tensile strength generally increased with a drop in w/b ratio.

Table 4.9 Mechanical properties of SCCs at w/b ratio of 0.32

Mix ID	Mix Description	Compressive Strength [MPa]		UPV [m/sec]		Splitting Tensile Strength [MPa]
		28 days	90 Days	28 Days	90 Days	90 Days
M1	Control-PC1	80.9	91.1	5016	5068	5.8
M2	20FA	69.8	84.4	5042	5068	5.6
M3	40FA	60.9	77.9	4936	5068	5.2
M4	60FA	47.5	64.8	4902	4902	4.7
M5	20GGBFS	75.1	86.8	4959	5120	5.7
M6	40GGBFS	80.1	92.6	4985	5209	5.8
M7	60GGBFS	78.1	89.2	4902	5146	5.7
M8	5SF	80.4	91.8	4901	5119	5.8
M9	10SF	85.7	99.2	5027	5119	6.3
M10	15SF	84.4	96.7	5052	5119	6.0
M11	5MK	96.3	103.5	5051	5303	6.3
M12	10MK	91.4	100.1	5025	5276	6.1
M13	15MK	98.6	111.1	5119	4967	6.6
M14	15FA5SF	79.2	86.3	4983	5068	5.7
M15	30FA10SF	67.2	80.1	4983	4984	5.3
M16	45FA15SF	60.0	68.3	4959	4926	4.8
M17	15FA5MK	81.0	95.0	5042	5294	6.0
M18	30FA10MK	84.2	91.2	4959	5206	5.8
M19	45FA15MK	67.5	81.3	4862	4862	5.4
M20	15GGBFS5SF	79.6	96.1	4878	5236	6.0
M21	30GGBFS10SF	87.6	95.0	5093	5068	6.0
M22	45GGBFS15SF	84.5	100.9	4901	5017	6.2
M23	15GGBFS5MK	89.7	106.2	5017	5267	6.5
M24	30GGBFS10MK	81.2	103.7	5034	5285	6.4
M25	45GGBFS15MK	83.1	94.5	4926	4926	5.9
M26	10FA10GGBFS	77.0	94.9	4950	5146	6.1
M27	20FA20GGBFS	62.3	82.8	4926	5068	5.5
M28	30FA30GGBFS	69.4	79.2	4926	5094	5.3
M29	2.5SF2.5MK	93.9	100.7	4934	5051	6.3
M30	5SF5MK	92.6	107.2	4902	4992	6.5
M31	7.5SF7.5MK	94.4	107.3	4902	4951	6.5
M32	15FA2.5SF2.5MK	78.5	93.7	4926	4975	5.9
M33	30FA5SF5MK	74.1	91.1	4870	5025	5.8
M34	45FA7.5SF7.5MK	60.7	77.7	4839	4800	5.2
M35	15GGBFS2.5SF2.5MK	90.6	113.1	4950	4936	6.7
M36	30GGBFS5SF5MK	88.5	98.2	4886	4975	6.1
M37	45GGBFS7.5SF7.5MK	74.1	88.7	4644	4894	5.7
M38	7.5FA7.5GGBFS5SF	78.6	88.4	4950	5131	5.6
M39	15FA15GGBFS10SF	72.7	88.9	4983	5000	5.7
M40	22.5FA22.5GGBFS15SF	64.3	79.0	4879	5046	5.2
M41	7.5FA7.5GGBFS5MK	91.2	97.9	5172	5008	6.1
M42	15FA15GGBFS10MK	85.4	95.7	4870	5059	6.1
M43	22.5FA22.5GGBFS15MK	76.5	87.0	4815	4910	5.6

Table 4.10 Mechanical properties of SCCs at w/b ratio of 0.44

Mix ID	Mix Description	Compressive Strength [MPa]		UPV [m/sec]		Splitting Tensile Strength [MPa]
		28 days	90 Days	28 Days	90 Days	90 Days
M44	Control-PC 2	61.5	73.6	4902	4902	5.0
M45	20FA	52.1	68.0	4947	4975	4.7
M46	40FA	44.7	60.3	4979	4879	4.4
M47	60FA	30.3	42.5	4825	4850	3.5
M48	20GGBFS	59.0	72.6	4979	5050	4.9
M49	40GGBFS	58.0	74.9	4944	5000	5.0
M50	60GGBFS	56.2	65.7	4955	4950	4.7
M51	5SF	60.7	71.2	4858	4910	4.8
M52	10SF	58.5	76.1	4919	4950	5.1
M53	15SF	71.1	74.8	4959	4950	5.0
M54	15FA5SF	61.5	67.2	4851	4900	4.7
M55	30FA10SF	46.9	57.6	4811	4850	4.5
M56	45FA15SF	37.4	44.8	4738	4760	3.7
M57	15GGBFS5SF	60.1	68.0	4910	4900	4.8
M58	30GGBFS10SF	58.3	68.2	4999	5000	4.7
M59	45GGBFS15SF	57.6	70.7	4921	4950	4.8
M60	10FA10GGBFS	62.4	78.0	4953	4950	5.2
M61	20FA20GGBFS	53.6	69.2	4966	4950	4.7
M62	30FA30GGBFS	45.9	60.6	4933	4950	4.3
M63	7.5FA7.5GGBFS5SF	60.6	76.0	4917	4933	5.1
M64	15FA15GGBFS10SF	54.7	66.8	4905	4945	4.6
M65	22.5FA22.5GGBFS15SF	44.2	55.2	4959	4975	4.0

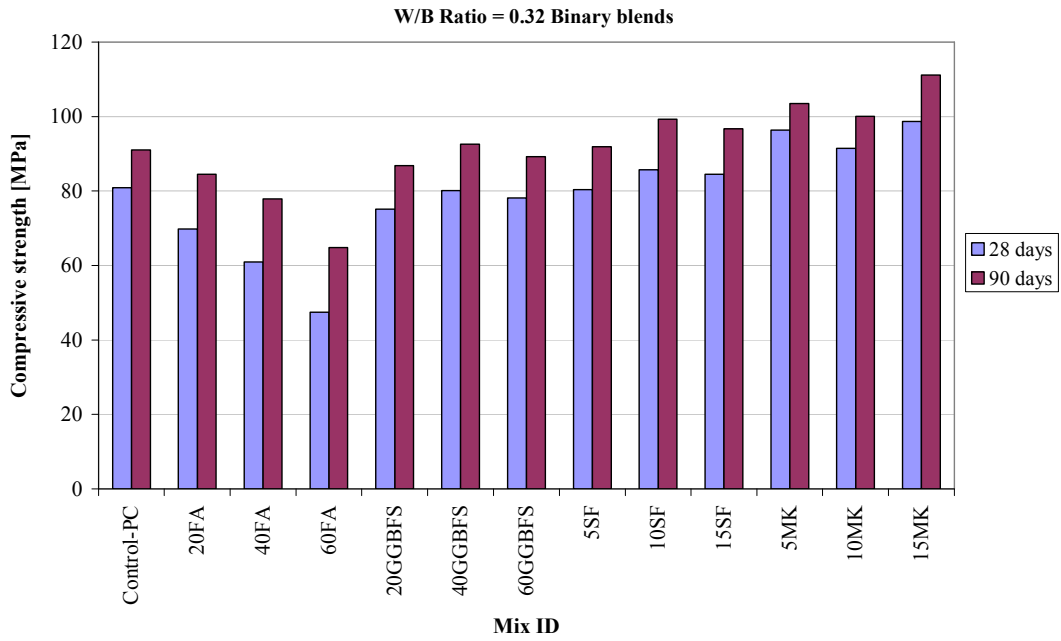


Figure 4.33 Binary effects of mineral admixtures on compressive strength of SCCs at w/b ratio of 0.32

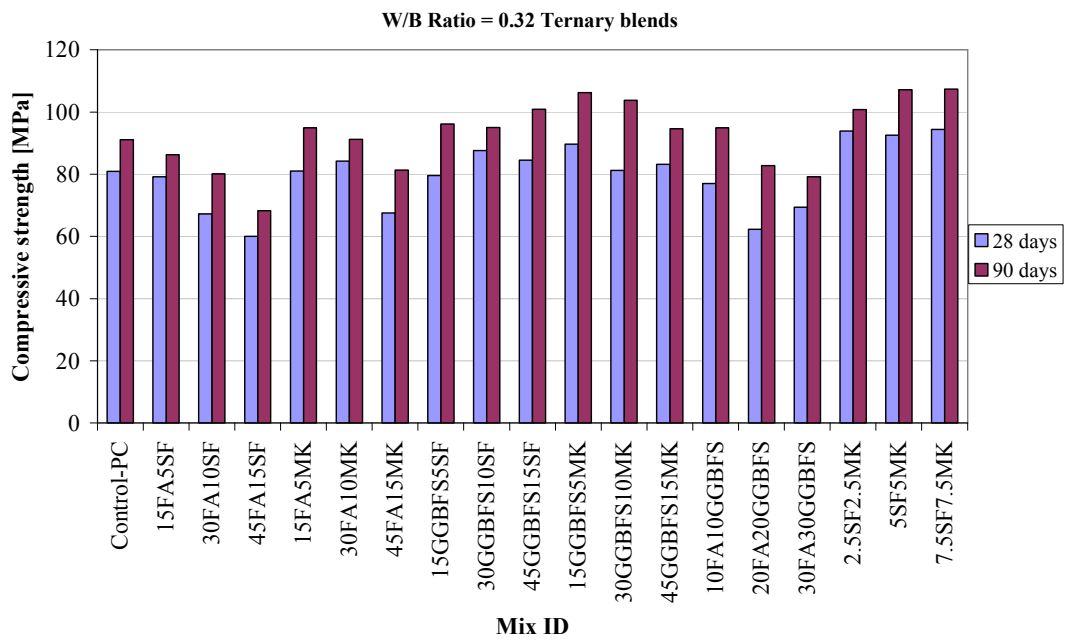


Figure 4.34 Ternary effects of mineral admixtures on compressive strength of SCCs at w/b ratio of 0.32

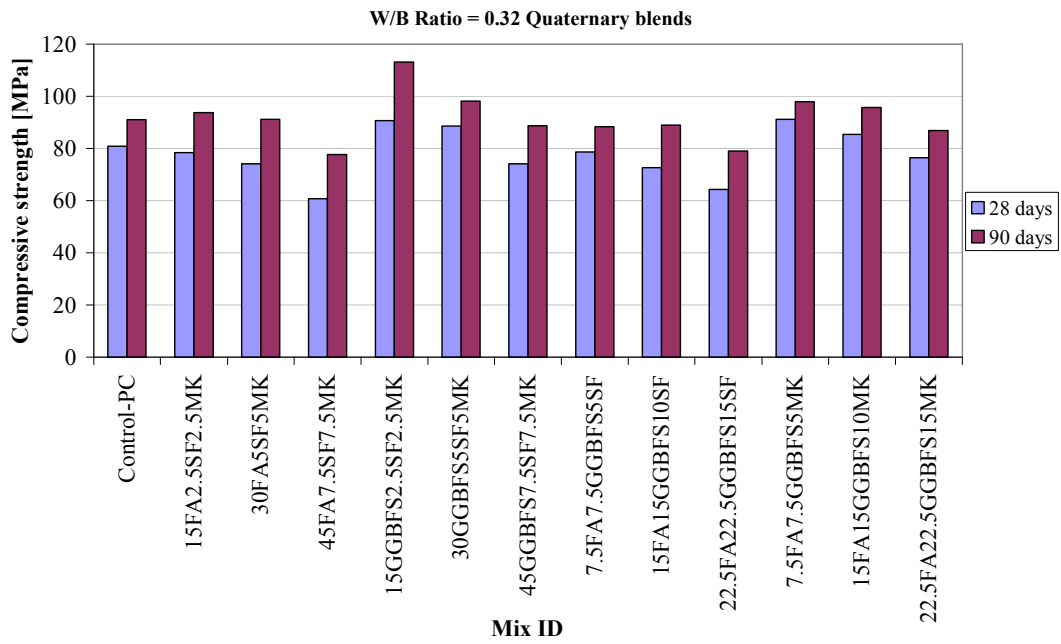


Figure 4.35 Quaternary effects of mineral admixtures on compressive strength of SCCs at w/b ratio of 0.32

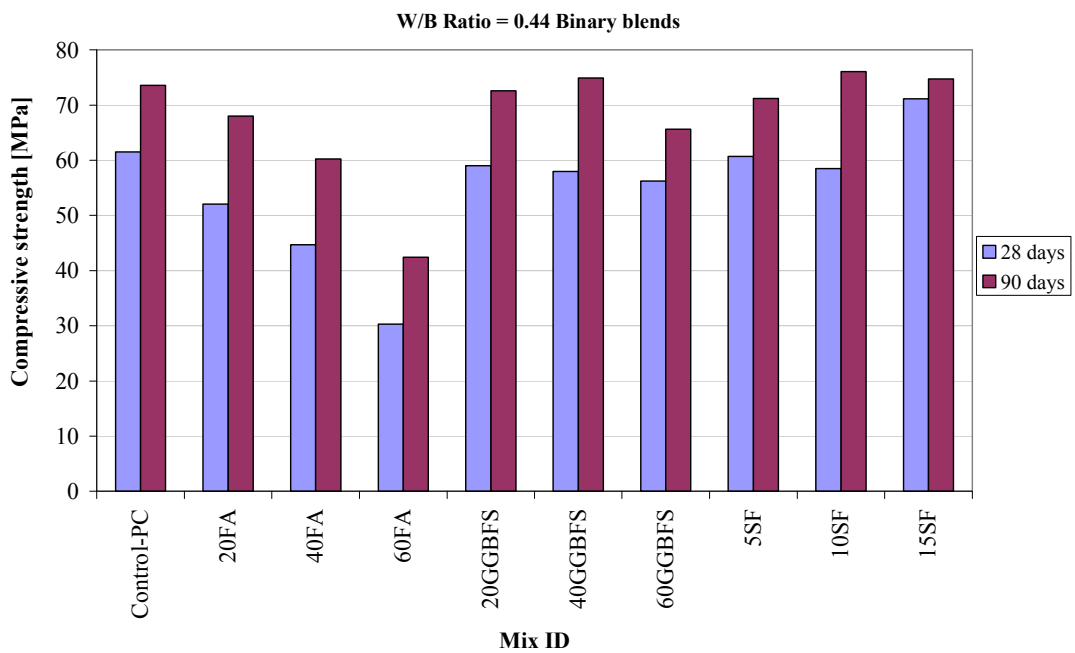


Figure 4.36 Binary effects of mineral admixtures on compressive strength of SCCs at w/b ratio of 0.44

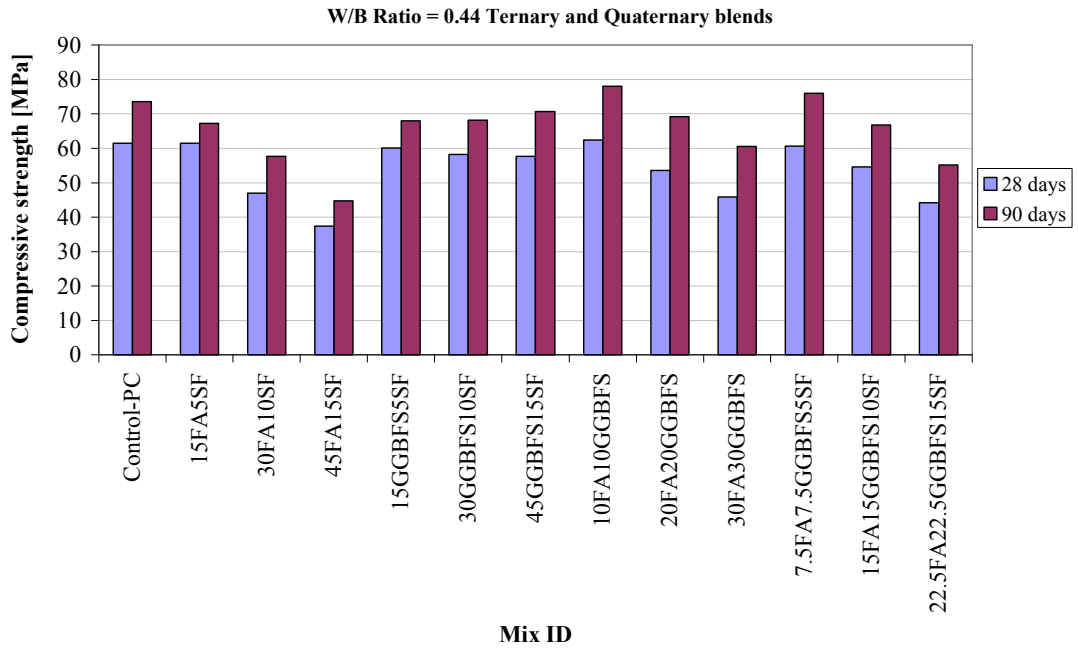


Figure 4.37 Ternary and quaternary effects of mineral admixtures on compressive strength of SCCs at w/b ratio of 0.44

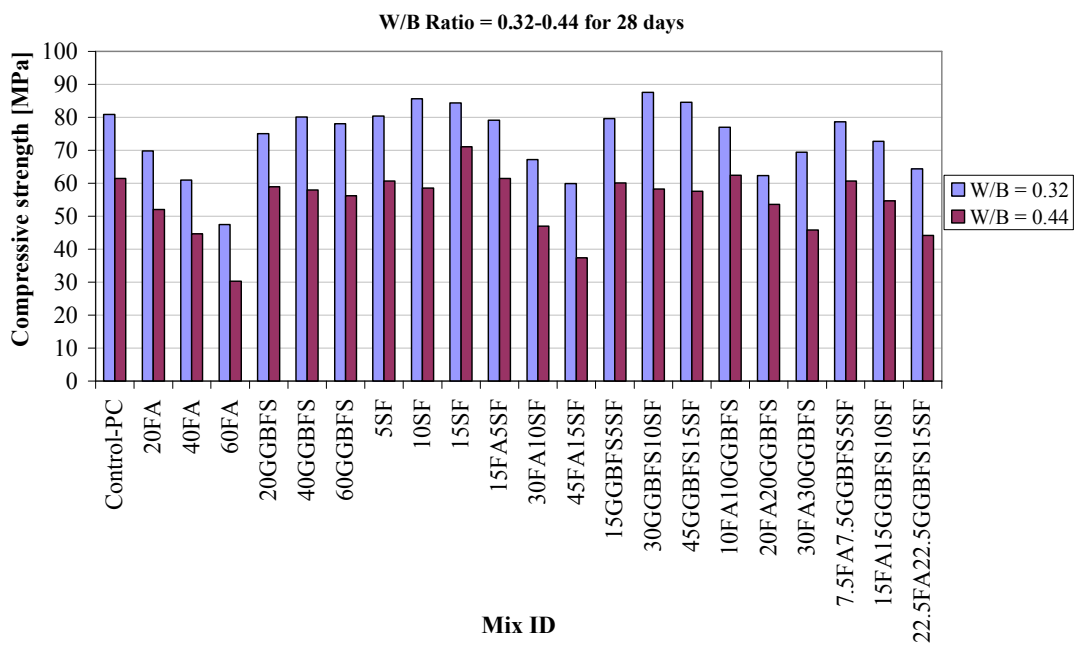


Figure 4.38 Comparison of compressive strengths of SCCs at 28 days for different w/b ratios

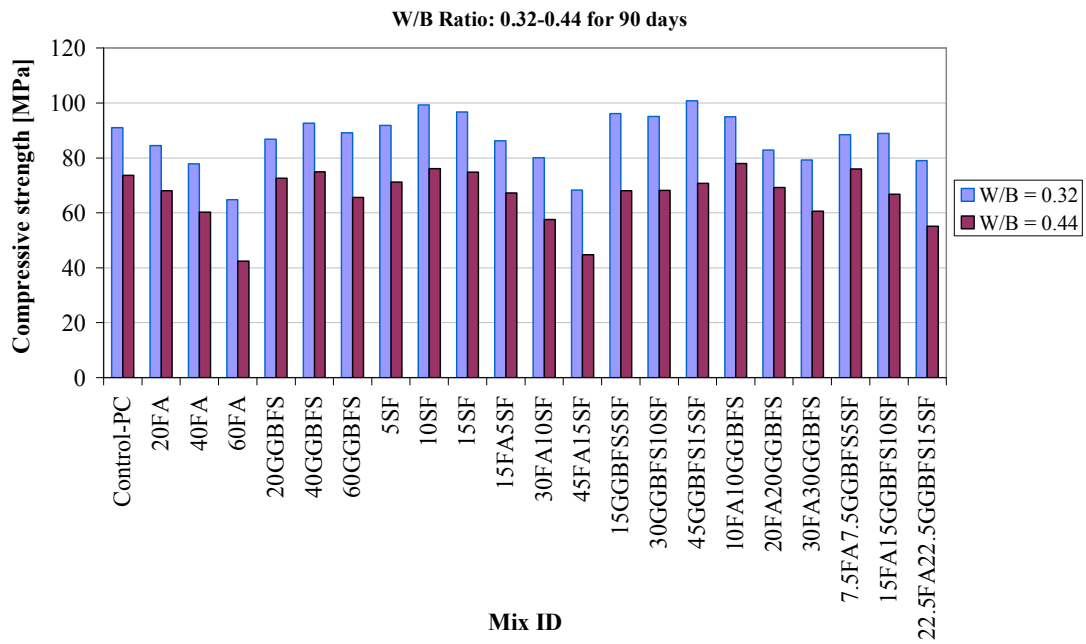


Figure 4.39 Comparison of compressive strengths of SCCs at 28 days for different w/b ratios

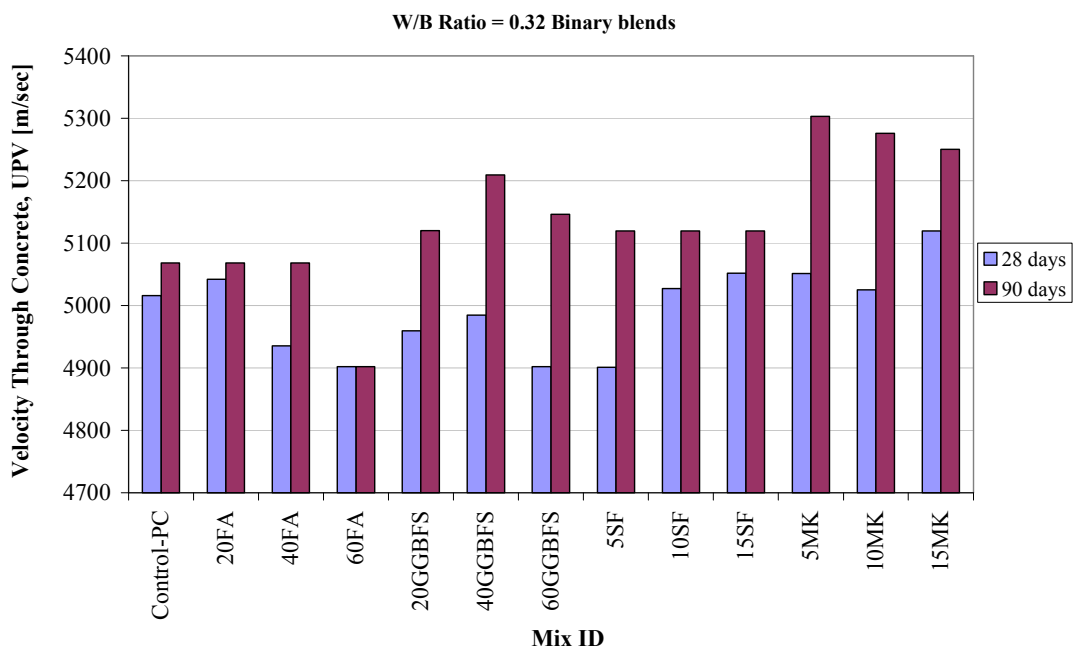


Figure 4.40 Binary effects of mineral admixtures on UPV of SCCs at w/b ratio of 0.32

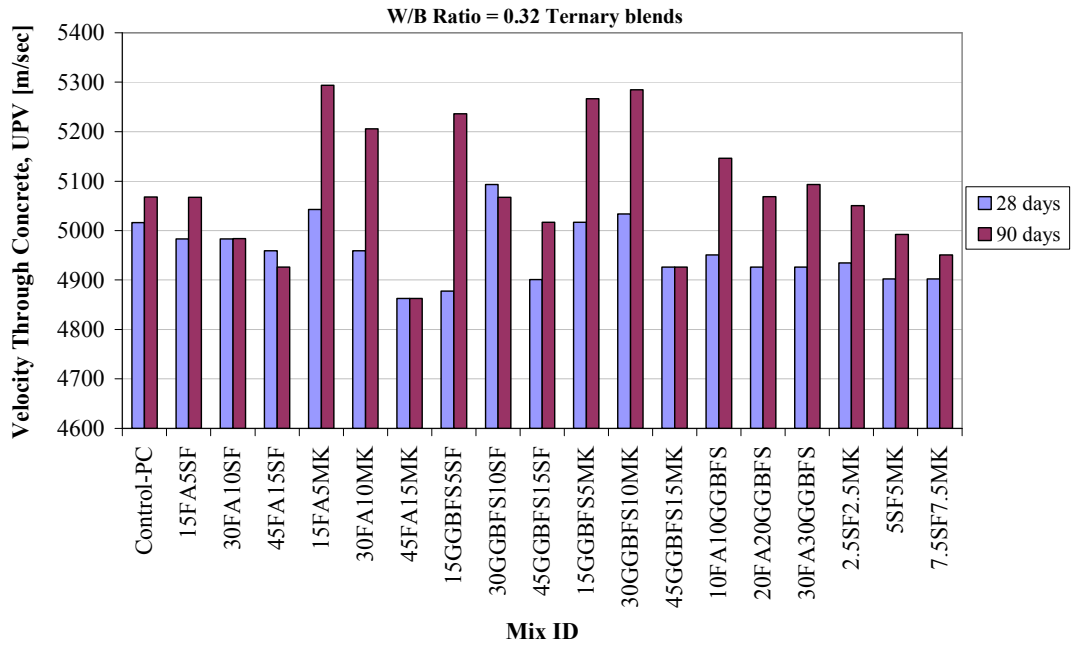


Figure 4.41 Ternary effects of mineral admixtures on UPV of SCCs at w/b ratio of 0.32

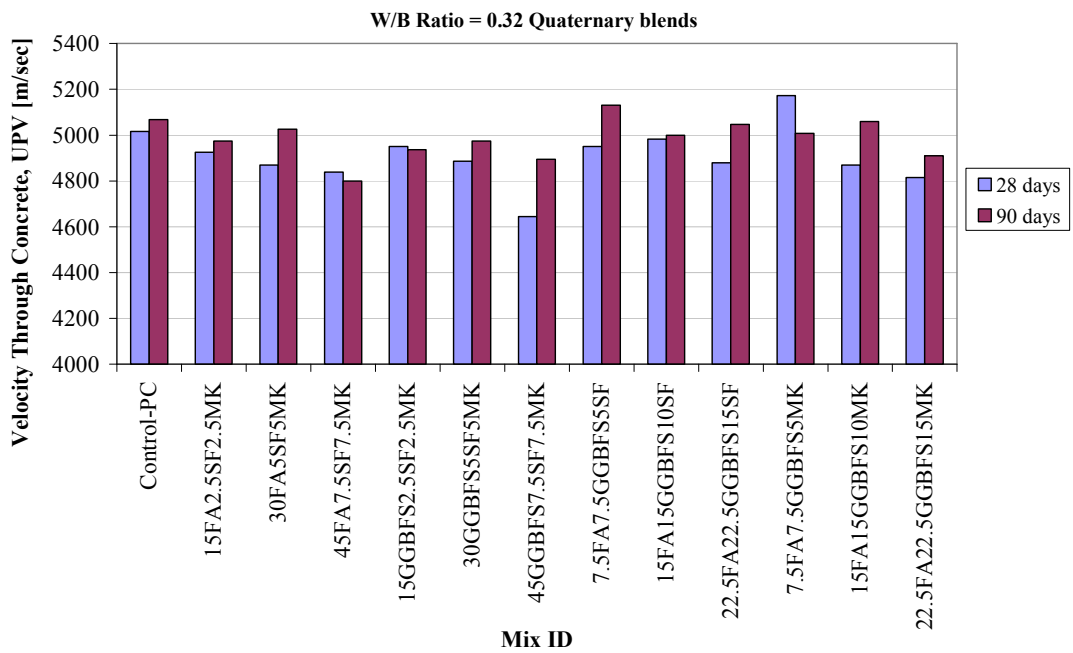


Figure 4.42 Quaternary effects of mineral admixtures on UPV of SCCs at w/b ratio of 0.32

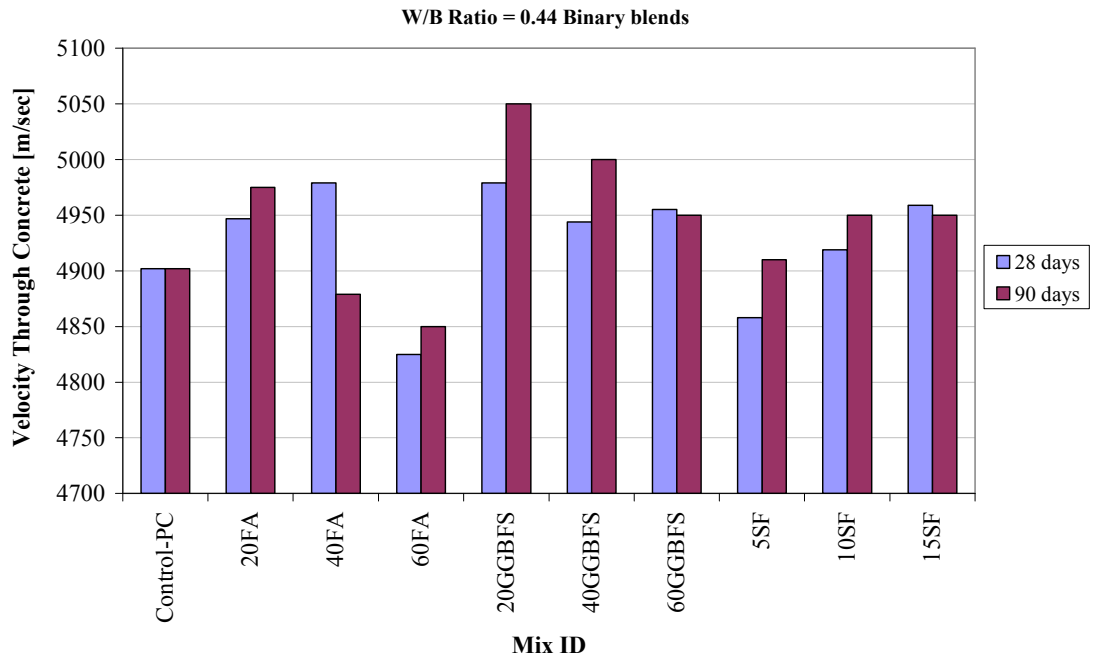


Figure 4.43 Binary effects of mineral admixtures on UPV of SCCs at w/b ratio of 0.44

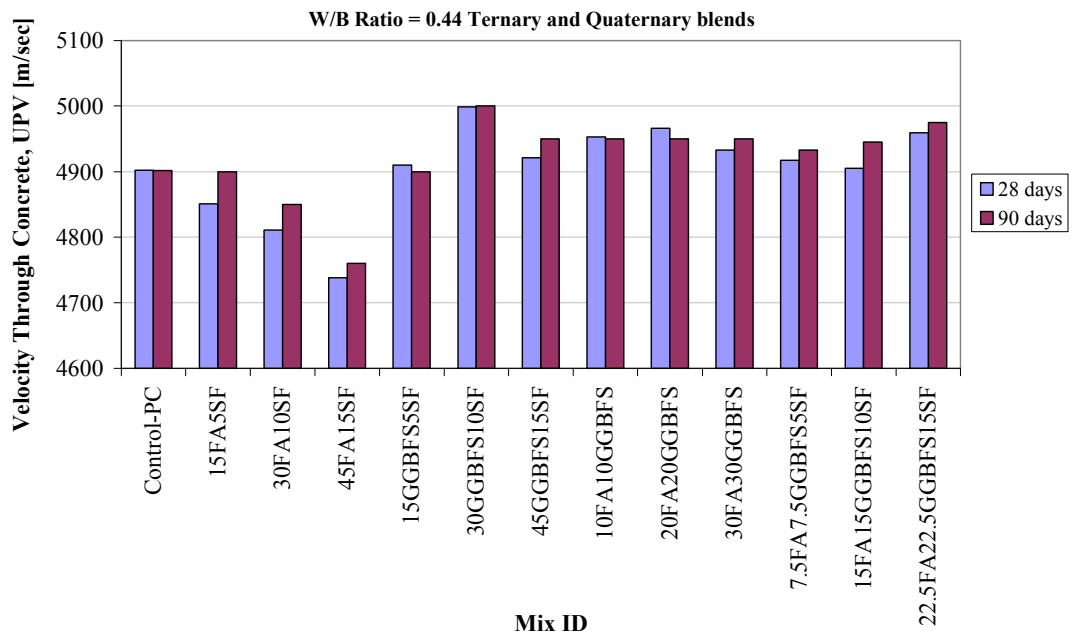


Figure 4.44 Ternary and quaternary effects of mineral admixtures on UPV of SCCs at w/b ratio of 0.44

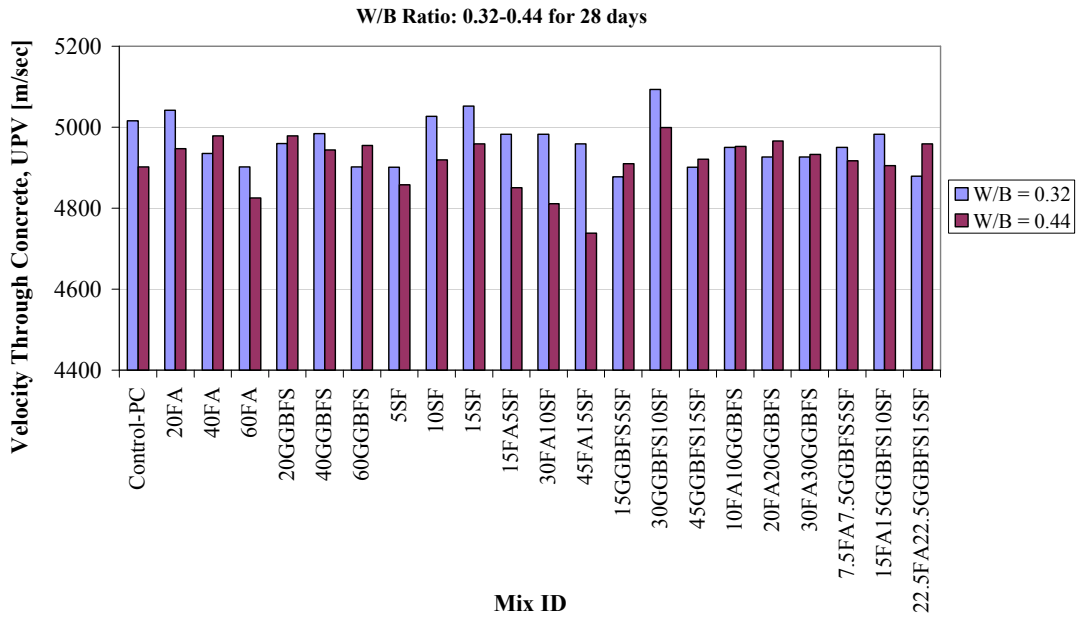


Figure 4.45 Comparison of ultrasonic pulse velocity of SCCs at 28 days for different w/b ratios

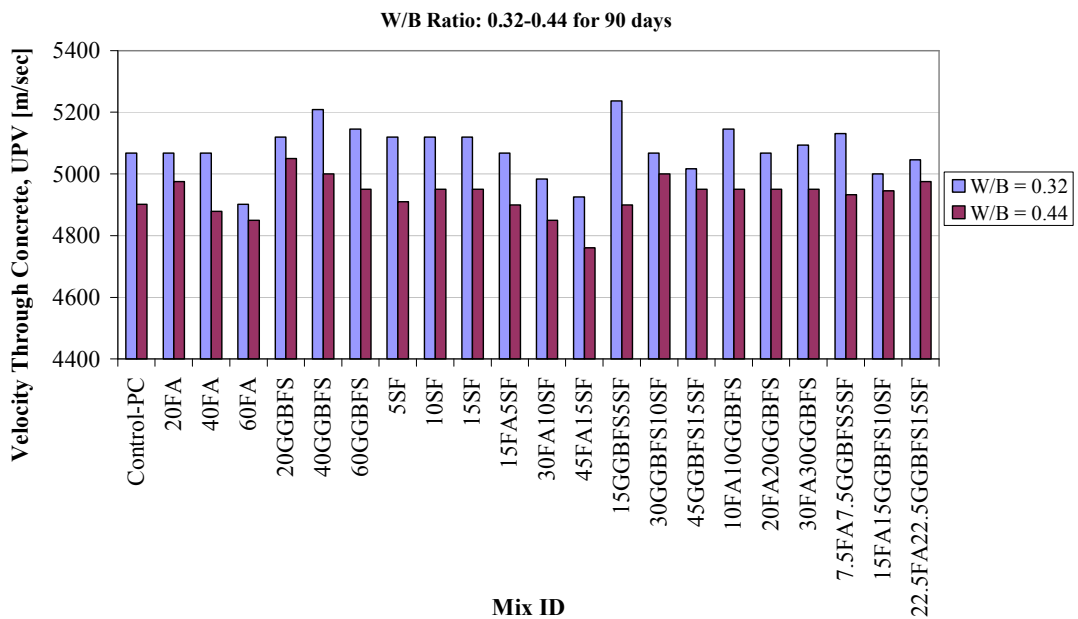


Figure 4.46 Comparison of ultrasonic pulse velocity of SCCs at 28 days for different w/b ratios

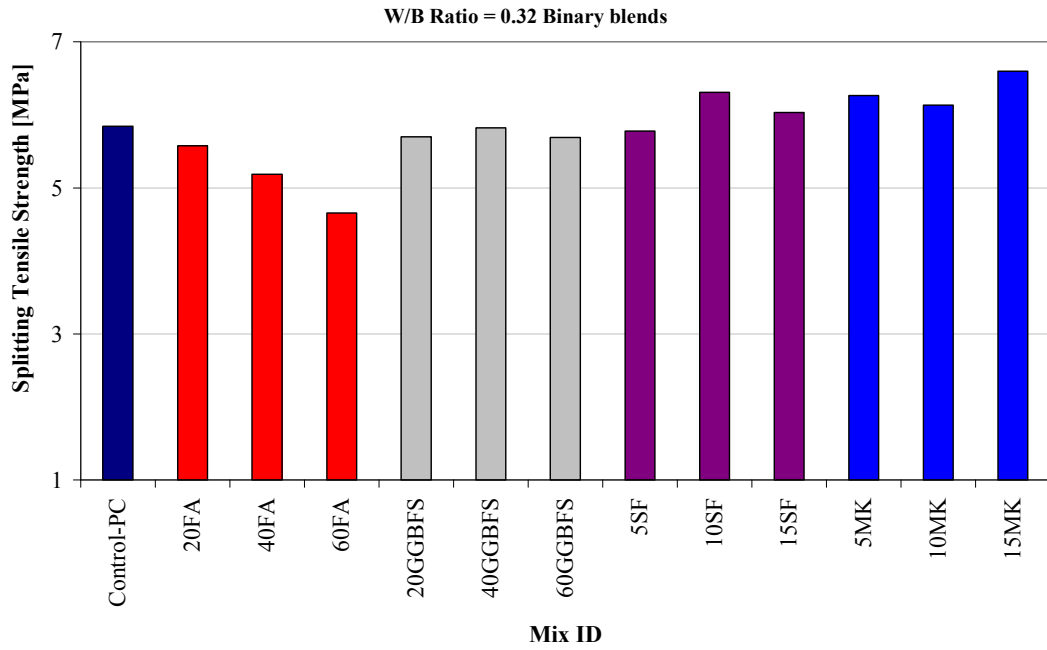


Figure 4.47 Binary effects of mineral admixtures on the splitting tensile strength of SCCs at w/b ratio of 0.32

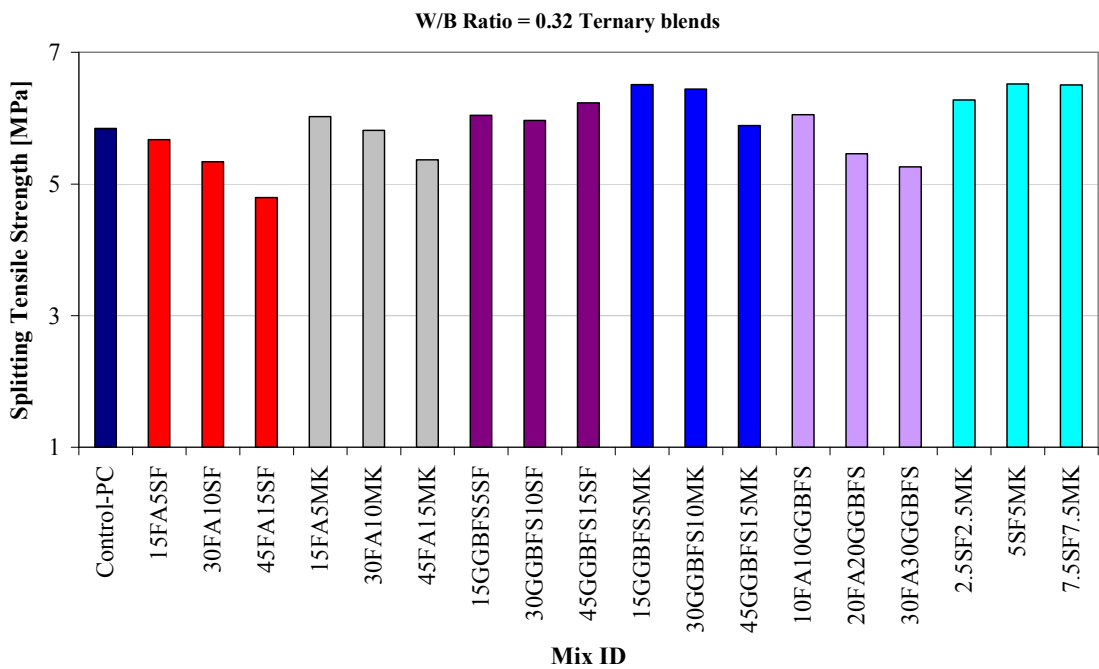


Figure 4.48 Ternary effects of mineral admixtures on the splitting tensile strength of SCCs at w/b ratio of 0.32

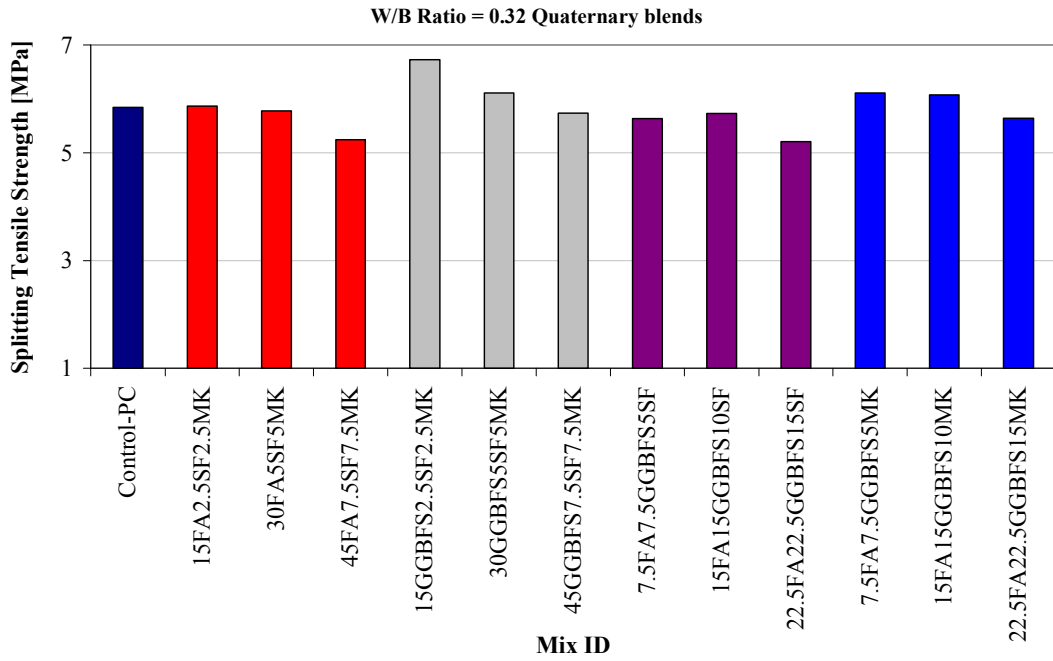


Figure 4.49 Quaternary effects of mineral admixtures on the splitting tensile strength of SCCs at w/b ratio of 0.32

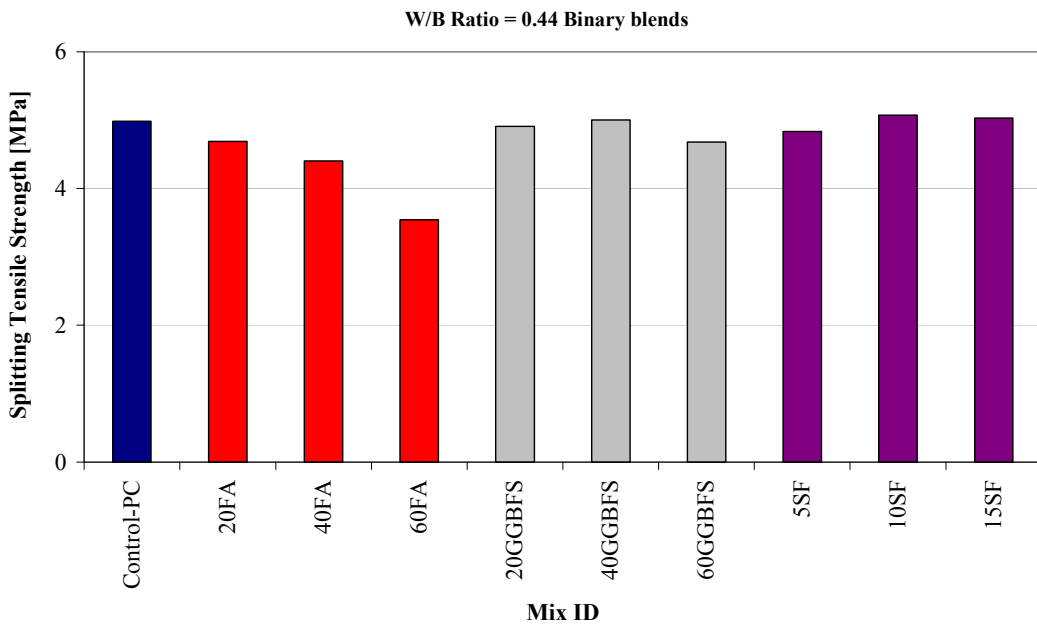


Figure 4.50 Binary effects of mineral admixtures on the splitting tensile strength of SCCs at w/b ratio of 0.44

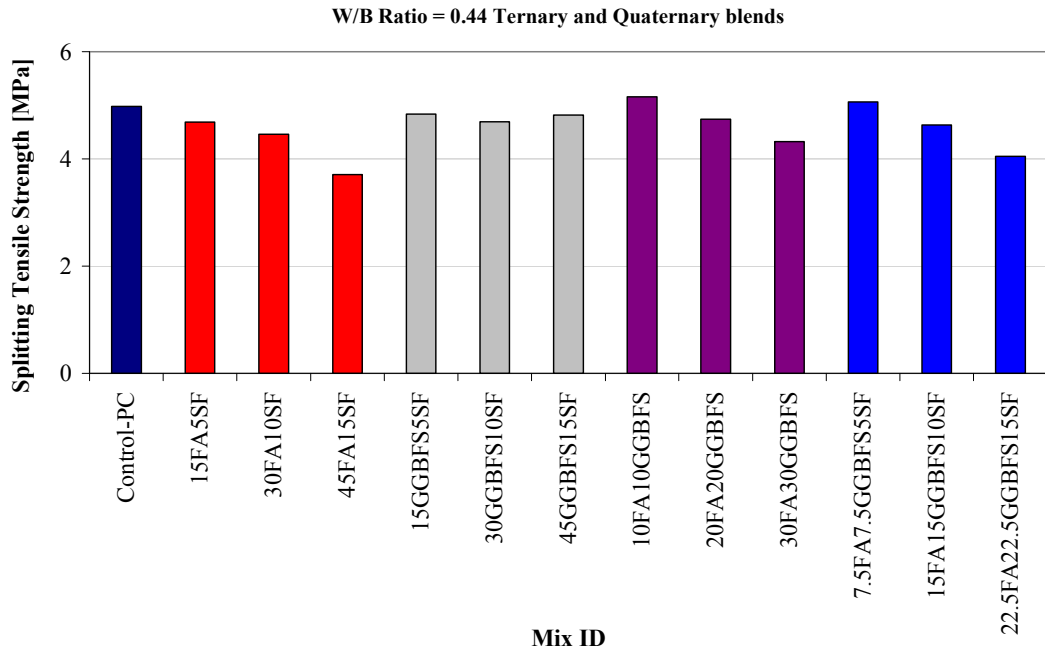


Figure 4.51 Ternary and quaternary effects of mineral admixtures on the splitting tensile strength of SCCs at w/b ratio of 0.44

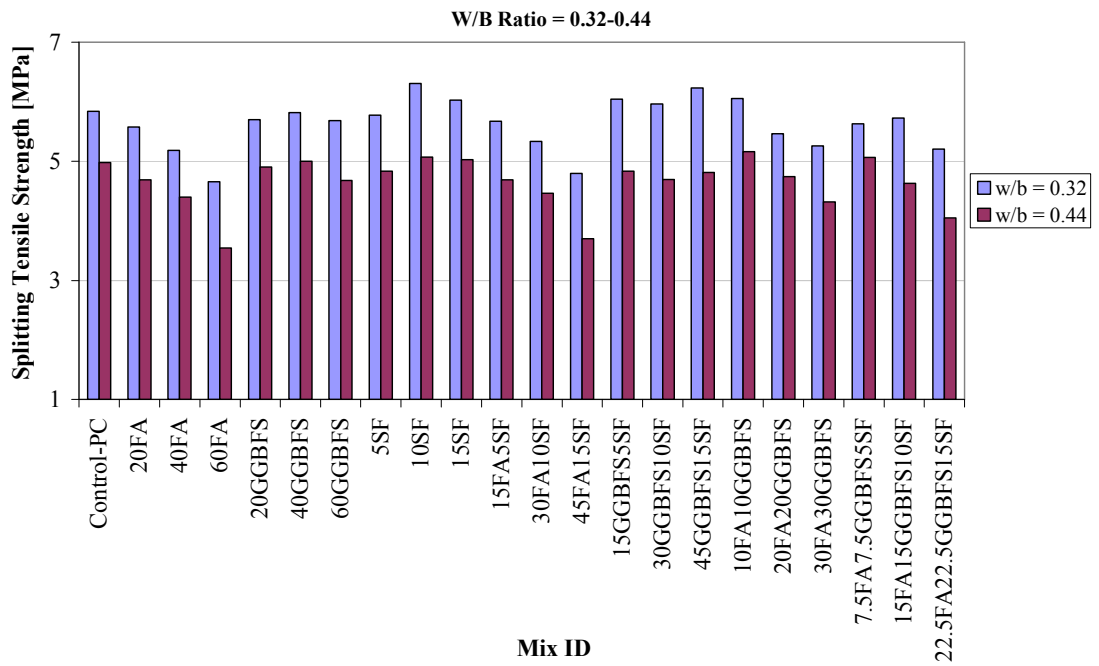


Figure 4.52 Comparison of the splitting tensile strength of SCCs at different w/b ratios

4.3 Physical Properties

4.3.1 Drying shrinkage

Drying shrinkage can be defined as the volumetric change due to the drying of concrete. This change in volume of the concrete is not equal to the volume of water lost. The loss of free water occurs first; this causes little to no shrinkage. As the drying of the concrete continues, the adsorbed water is removed. This adsorbed water is held by hydrostatic tension in the small capillaries (<50 nm). The loss of this water produces tensile stresses, which cause the concrete to shrink. The shrinkage due to this water loss is significantly larger than that associated with the loss of free water (Neville, 1996). The addition of mineral and chemical admixtures can have an effect on the shrinkage of concrete. Pozzolans, such as fly ash and microsilica, and slag cement are specified for the prevention of alkali silicate reaction and low-permeable concrete. The addition of pozzolans and slag cement generally increases the pore refinement of the concrete. This creates smaller pores and drying shrinkage is directly associated with the water held in the smaller pores (Mokarema et al., 2005). Drying shrinkage tests alone can not offer sufficient information on the behavior of concrete structures since virtually all concretes are restrained in some way either by reinforcement or by the structure. However, measurement of the shrinkage upon drying can provide necessary information on how the drying shrinkage stresses develop (Shah et al., 1992; Wiegrink et al., 1996).

The strain developments versus time of drying shrinkage for different concretes demoulded 24 hr after casting are presented in Figures 4.53 through 4.59. Also, the final values of the shrinkage strains are given in Tables 4.11 and 4.12 for the concretes with low and high w/b ratio, respectively. It is seen in Figures 4.53 to 4.59, the shrinkage strains were somewhat comparable at very early ages of the drying period. However, the shrinkage strains differed for various concretes at later ages.

It is evident in Figure 4.53 that the effects of replacing the PC by FA, GGBFS or MK were to reduce the free shrinkage of SCCs remarkably at low w/b ratio. When the shrinkage strains measured at 50 days were considered, the shrinkage of the concrete with binary use of PC+MK exhibited the highest reduction in comparison to the control concrete. It was pointed out that the higher the replacement level of FA,

GGBFS, and MK, the higher reduction in shrinkage. For example, the drying shrinkage of the concretes with 5 and 15% MK were 22 and 26% lower than that of the control concrete. It was reported in the study of Brooks and Megat-Johari (2001) that the total shrinkage measured from 24 hr was reduced by the use of MK while drying shrinkage was significantly less for the MK concretes than for the control concrete. They reported that the influence of MK was to reduce the drying shrinkage of ordinary portland cement concrete by about 50%. In the case of FA and GGBFS included concretes, similarly, the former and the latter had lower the shrinkage strains by about 14 and 26%, and 5 and 14% at the replacement levels of 20 and 60%, respectively. The test results presented herein agreed the findings of the studies conducted by US Bureau of Reclamation (1984) and Symons and Fleming (1980). They found that increase in fly ash content resulted in slightly less drying shrinkage. Moreover, drying shrinkage of concrete is a function of the fractional volume of paste, water content, type and content of cement, the type of aggregate. In the cases wherein the addition of fly ash and ground granulated blast furnace slag increase the paste volume so that drying shrinkage may be decreased slightly. Chen et al. (2007) performed a study in order to investigate the influence of fly ash on shrinkage of concrete. They used the fly ash as partial replacement at 35%, 40% and 45% in the mass of total cementitious materials. The results of study showed that the high volume fly ash remarkably reduced the drying shrinkage of concretes, especially at the later ages. Furthermore, the test results agreed with the findings of the study conducted by Jainyong and Yan (2001) for the effect of the ultrafine mineral admixtures on the shrinkage and creep of concretes. In the study of Jainyong and Yan (2001), they showed that ultrafine ground granulated blast-furnace slag can substantially promote hydration of cement and increase the amount of AFt crystal hydrates and C-S-H gel hydrates in cement paste, which offers a hardened concrete with a stronger structure and higher resistance to deformation caused by applied forces. Moreover, this binder may fill small pores and voids harmful to the structure of concrete. That might be the mechanism of reducing effect of ultrafine mineral admixtures (i.e. GGBS and SF) on creep and drying shrinkage of concrete. However, the binary use of SF with PC increased the shrinkage of SCCs. The information in the literature about the influence of SF on the drying shrinkage is found to be somewhat contradictory. As the binary use of PC+SF was considered, there was a gradual increase in shrinkage of SCC with the increasing of replacement level.

Jainyong and Yan (2001) and Al-Khaja (1994) reported its increasing effect while Wiegrink et al. (1996) and Gesoglu (2004) revealed that the SF had increasing effect on the drying shrinkage.

The influence of the ternary use of mineral admixtures on the free shrinkage of the SCCs having w/b ratio of 0.32 was demonstrated in Figure 4.54. As it is clearly seen in the figure all of the mixtures in ternary use of the mineral admixtures have low drying shrinkage values when compared to the control concrete. The negative effect of SF on the shrinkage of SCCs was relatively eliminated with the ternary use of mineral admixtures. The concretes with the ternary blends of PC+FA+SF and PC+GGBFS+SF had lower shrinkage strains than that of the control concrete. Furthermore, the higher the replacement levels of FA and GGBFS in the ternary use of PC+FA+SF and PC+GGBFS+SF concretes, the higher the reduction in free shrinkage.

Figure 4.55 shows the effects of ternary use of PC+FA+MK, PC+GGBFS+MK and PC+SF+MK on the free shrinkage of SCCs. The lowest shrinkage of 300 microstrain was measured for M19 (45%FA15%MK). As known from the binary use of mineral admixtures, FA, GGBFS, and MK had the decreasing effect on the free shrinkage. As seen in Figure 4.55, combined use of PC+FA+MK, PC+GGBFS+MK and PC+SF+MK also decreased free shrinkage of SCCs. As was expected, increasing the replacement level of mineral admixtures decreased the shrinkage of SCCs gradually. In the ternary use of PC+SF+MK, MK eliminated the negative effect of SF on shrinkage as in the case of using FA or GGBFS. According to the control concrete, there was a small increase in the shrinkage for the mixture of %2.5SF%2.5MK. However, increasing the replacement level of MK from %2.5 to %7.5 the shrinkage even decreased below that of the control concrete.

The negative effect of SF on the free shrinkage of SCCs was completely eliminated in the quaternary use of mineral admixtures as shown in Figure 4.56. In the quaternary use of PC+FA+SF+MK, PC+GGBFS+SF+MK, PC+FA+GGBFS+SF, PC+FA+GGBFS+MK, a considerable reduction was observed. The mixtures containing 22.5FA22.5GGBFS15SF and 22.5FA22.5GGBFS15MK had lower shrinkage strains by about 8 and 34%, respectively, than the control concrete.

Furthermore, it was pointed out that the higher the amount of the mineral admixture used, the less shrinkage strains were measured.

The shrinkage of binary, ternary and quaternary use of FA, GGBFS and SF at high w/b ratio were depicted in Figures 4.57 through 4.59. As seen in the figures the shrinkage values yielded approximately comparable values at the very early ages of drying period. However, a clear distinction was observed for different concretes after about ten days. It was clearly observed in Figure 4.57 that the concretes with binary blends of FA or GGBFS had lower shrinkage strains than that of the control concrete. This beneficial effect appeared to be more pronounced with increasing replacement level of mineral admixtures. The concrete having 60% FA had the lowest shrinkage strain. When used at 10% and 15% replacement levels, however, SF enhanced the shrinkage strain of the concretes. The remedy to diminish the adverse effect of SF on the shrinkage may be the use of this mineral within ternary and/or quaternary blends. Indeed, Figures 4.58 and 4.59 clearly exhibited that the control concrete had the highest shrinkage strain. The combined use of the mineral admixtures fairly reduced the negative influence of SF.

4.3.2 Weight loss

The weight loss of the SCCs was measured on the same specimens as the free shrinkage test and the maximum values of the weight loss are given in Tables 4.11 and 4.12 for the concretes with 0.32 and 0.44 w/b ratios, respectively. Moreover, Figures 4.60 to 4.66 present the rate of the water loss during the drying period for various concrete mixtures. As in free shrinkage, the weight loss for the different concretes was comparable within the first three to seven days of the drying, but distinctive water loss could be measured particularly on seven days onwards. As seen in Tables 4.11 and 4.12 and Figures 4.60 and 4.64, increasing the replacement level of FA and GGBFS in the binary use of PC+FA and PC+GGBFS from 20 to 60% increased the weight loss of SCCs gradually. Furthermore, these concretes had higher weight loss than that of control concretes. When the weight loss of the concretes with the binary blends of PC+SF or PC+MK were considered, the effect of replacement level on the water loss of these concretes was significantly lower. In the case of 0.32

w/b ratio, for instance, the weight loss measured at the end of the drying were about 50 and 35 g in the SF and MK blended cement concretes, respectively. Interestingly, all concretes but those with MK had higher water loss than the control concrete. The MK blended concrete, however, exhibited less water loss by about %22 than the reference. As seen in Figure 4.64, a similar behavior was also observed in the binary SF concretes in that the inclusion of SF generally led to lower water loss such concretes than the plain control concrete. In the binary use of PC and SF at high water binder ratio concretes, the weight loss of SCCs increased gradually up to 10% SF replacement but then the weight loss decreased. The weight loss of 15%SF replacement mixture was less than the 5% SF replacement mixture. Moreover, the 15% SF replacement mixture had the lowest weight loss in the high w/b ratio concretes. This behaviour seen in both SF and MK concretes may be because there is less evaporable water available in the mixes as hydration and pozzolanic reactions used up significant amount of free water. Overall, the foregoing trends lead to confirm that the MK concretes have a lower porosity and finer pore structure which encourages loss of water by self-desiccation rather than by diffusion to the outside environment (Wiegrink et al., 1996; Brooks and Megat-Johari, 2001).

As seen in Figure 4.61 that all mixtures in the ternary use of PC+FA+SF, PC+GGBFS+SF, and PC+FA+GGBFS exhibited higher weight loss than the control concrete. Moreover, increasing the replacement level of mineral admixtures increased the water loss of SCCs. In Figure 4.62, the effects using ternary blends of PC+FA+MK, PC+GGBFS+MK, and PC+SF+MK on the weight loss of SCCs were depicted. In case of concrete with the ternary blends of PC+FA+MK and PC+GGBFS+MK, higher weight loss was measured according to the control concrete, whereas the combined use of PC+SF+MK resulted in less weight. In the quaternary use of mineral admixtures, all of the mixtures but M41 appeared to have higher weight loss than the control concrete at low w/b ratio (Figure 4.63). It may be postulated that the weight loss of the concretes with ternary or quaternary blends were generally dominated by FA, GGBFS on both of them.

As it seen in Figure 4.65 and 4.66, a remarkable increase in weight loss was seen with increasing the replacement level of the mineral admixtures employed. This effect seemed to be more pronounced for FA and GGBFS. For a given replacement

level of 20%, all the concretes had lower weight loss than the control concrete. However, beyond that point weight loss began to exceed that of the control concrete.

Table 4.11 Free shrinkage and weight loss of the SCCs at w/b ratio of 0.32

Mix ID	Mix Description	Maximum Free Shrinkage [microstrain]	Maximum Weight Loss [gr]
M1	Control-PC1	474	45.0
M2	20FA	407	66.4
M3	40FA	364	89.0
M4	60FA	357	124.4
M5	20GGBFS	452	70.3
M6	40GGBFS	420	84.8
M7	60GGBFS	410	91.9
M8	5SF	442	52.8
M9	10SF	513	48.8
M10	15SF	533	50.1
M11	5MK	366	34.5
M12	10MK	352	35.3
M13	15MK	350	37.7
M14	15FA5SF	440	71.0
M15	30FA10SF	444	91.4
M16	45FA15SF	452	113.0
M17	15FA5MK	446	72.3
M18	30FA10MK	346	47.3
M19	45FA15MK	300	98.6
M20	15GGBFS5SF	435	62.3
M21	30GGBFS10SF	475	74.6
M22	45GGBFS15SF	414	82.0
M23	15GGBFS5MK	400	43.1
M24	30GGBFS10MK	330	59.9
M25	45GGBFS15MK	374	83.1
M26	10FA10GGBFS	431	65.0
M27	20FA20GGBFS	399	92.0
M28	30FA30GGBFS	337	110.6
M29	2.5SF2.5MK	481	38.8
M30	5SF5MK	410	29.0
M31	7.5SF7.5MK	386	33.2
M32	15FA2.5SF2.5MK	379	46.3
M33	30FA5SF5MK	340	66.9
M34	45FA7.5SF7.5MK	330	102.3
M35	15GGBFS2.5SF2.5MK	398	48.3
M36	30GGBFS5SF5MK	373	46.1
M37	45GGBFS7.5SF7.5MK	340	72.6
M38	7.5FA7.5GGBFS5SF	414	60.9
M39	15FA15GGBFS10SF	410	52.4
M40	22.5FA22.5GGBFS15SF	437	91.5
M41	7.5FA7.5GGBFS5MK	344	41.0
M42	15FA15GGBFS10MK	327	59.3
M43	22.5FA22.5GGBFS15MK	314	93.7

Table 4.12 Free shrinkage and weight loss of the SCCs at w/b ratio of 0.44

Mix ID	Mix Description	Maximum Free Shrinkage [microstrain]	Maximum Weight Loss [gr]
M44	Control-PC	460	80.9
M45	20FA	436	107.3
M46	40FA	392	141.3
M47	60FA	376	148.7
M48	20GGBFS	447	95.2
M49	40GGBFS	426	104.0
M50	60GGBSF	415	119.4
M51	5SF	445	75.1
M52	10SF	475	82.4
M53	15SF	482	57.9
M54	15FA5SF	429	74.6
M55	30FA10SF	440	92.3
M56	45FA15SF	454	108.6
M57	15GGBFS5SF	447	84.5
M58	30GGBFS10SF	431	93.9
M59	45GGBFS15SF	424	81.3
M60	10FA10GGBFS	434	67.1
M61	20FA20GGBFS	402	108.1
M62	30FA30GGBFS	388	96.6
M63	7.5FA7.5GGBFS5SF	433	65.1
M64	15FA15GGBFS10SF	418	95.6
M65	22.5FA22.5GGBFS15SF	429	92.1

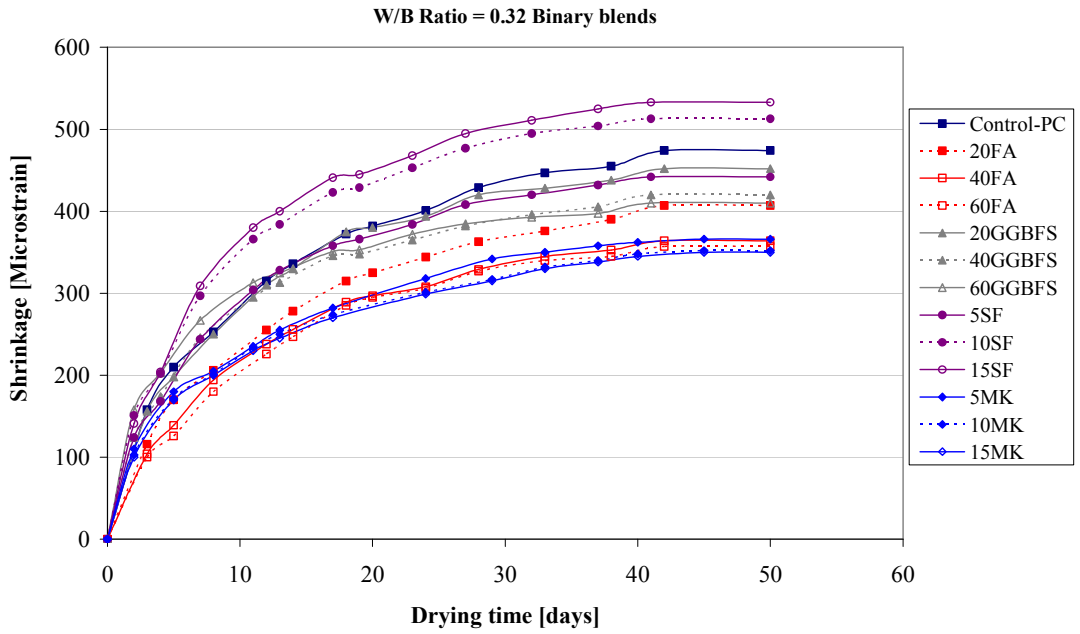


Figure 4.53 Binary effects of mineral admixtures on the free shrinkage of SCCs at w/b ratio of 0.32

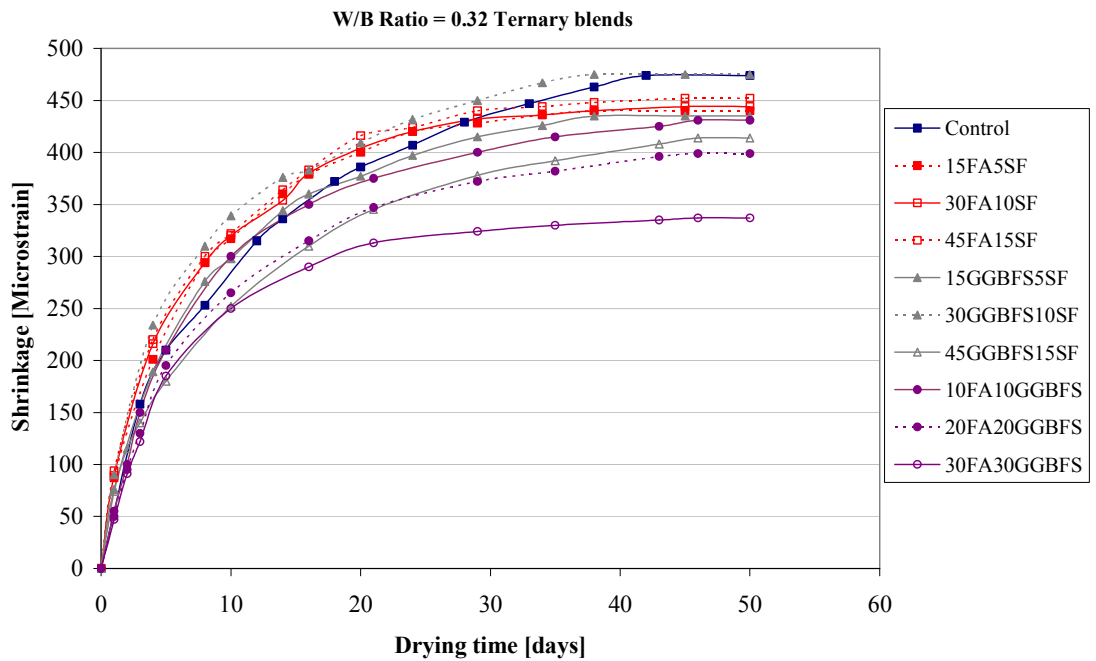


Figure 4.54 Ternary effects of mineral admixtures (PC+FA+SF; PC+GGBFS+SF; PC+FA+GGBFS) on the free shrinkage of SCCs at w/b ratio of 0.32

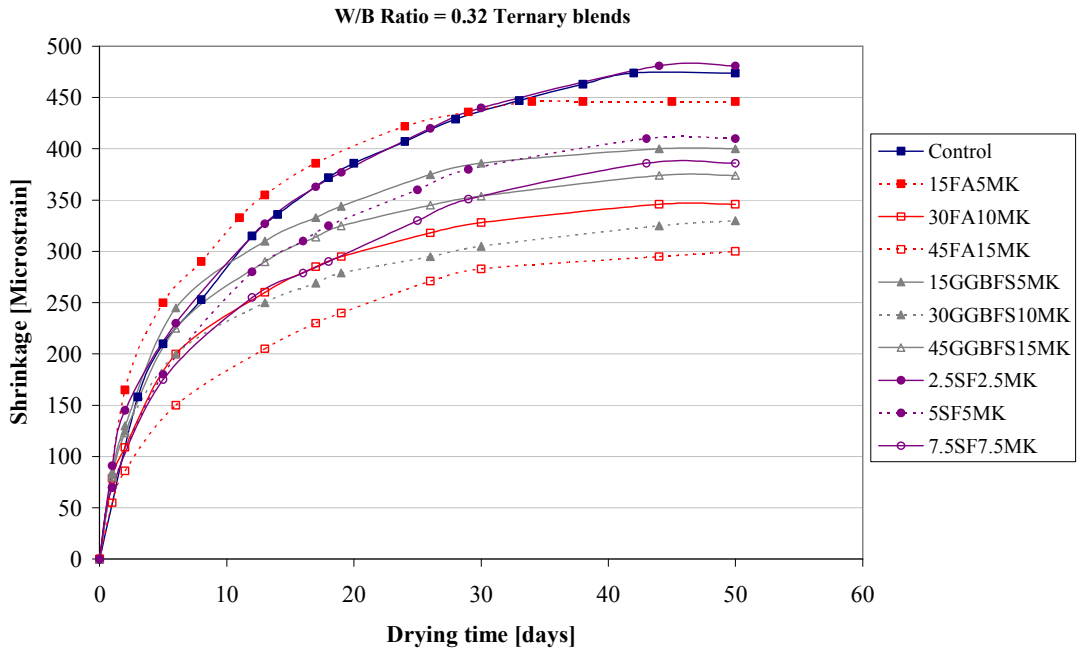


Figure 4.55 Ternary effects of mineral admixtures (PC+FA+MK; PC+GGBFS+MK; PC+SF+MK) on the free shrinkage of SCCs at w/b ratio of 0.32

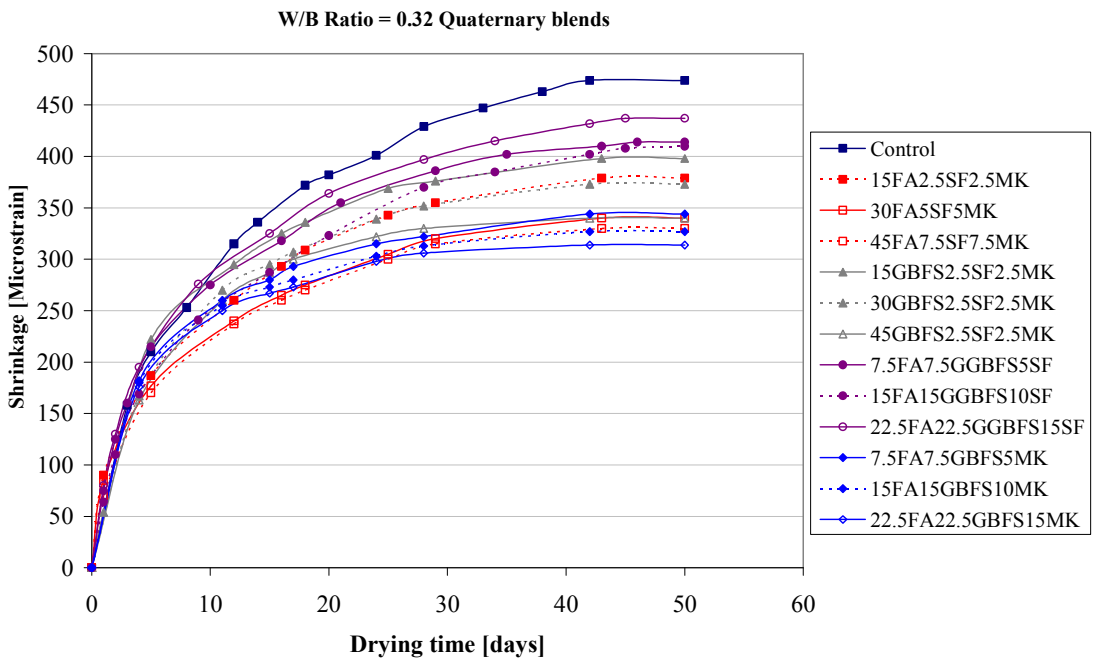


Figure 4.56 Quaternary effects of mineral admixtures on the free shrinkage of SCCs at w/b ratio of 0.32

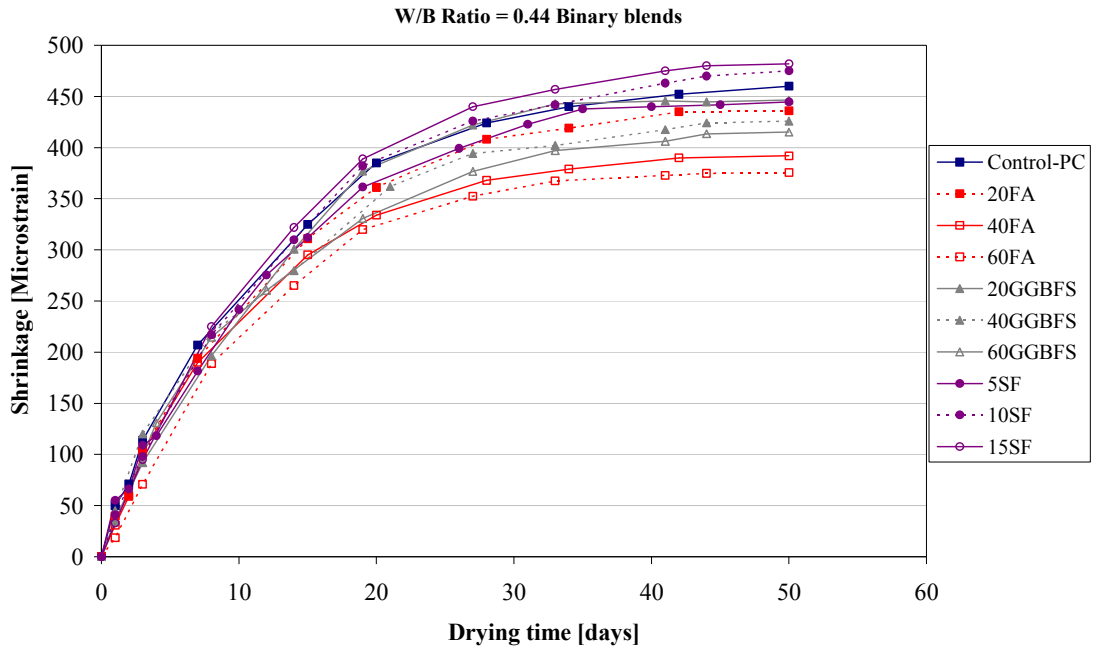


Figure 4.57 Binary effects of mineral admixtures on the free shrinkage of SCCs at w/b ratio of 0.44

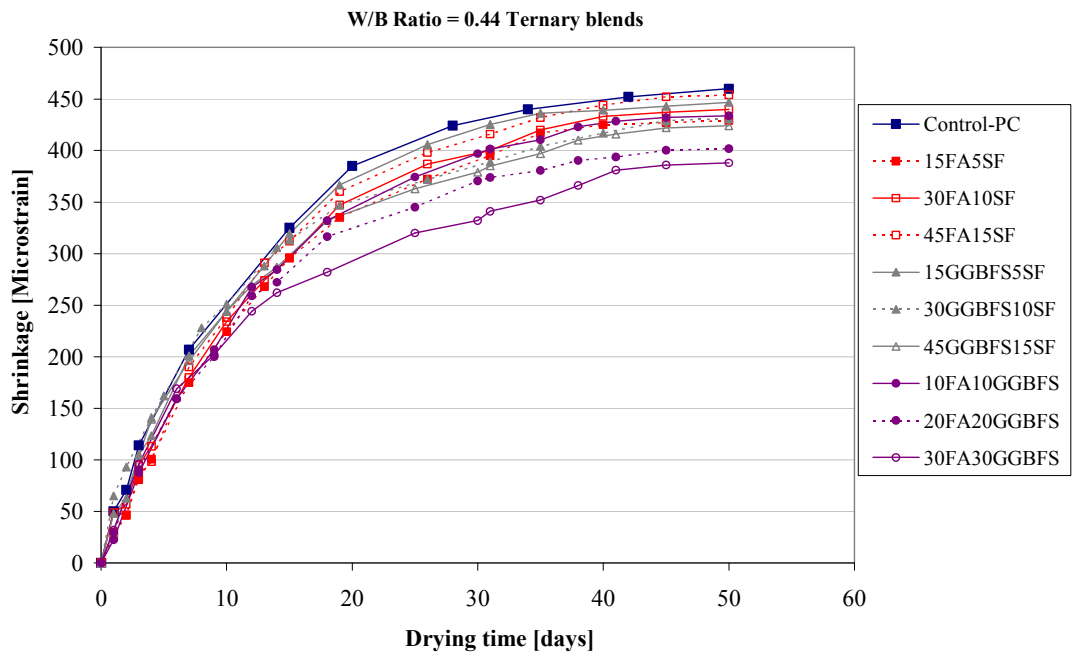


Figure 4.58 Ternary effects of mineral admixtures on the free shrinkage of SCCs at w/b ratio of 0.44

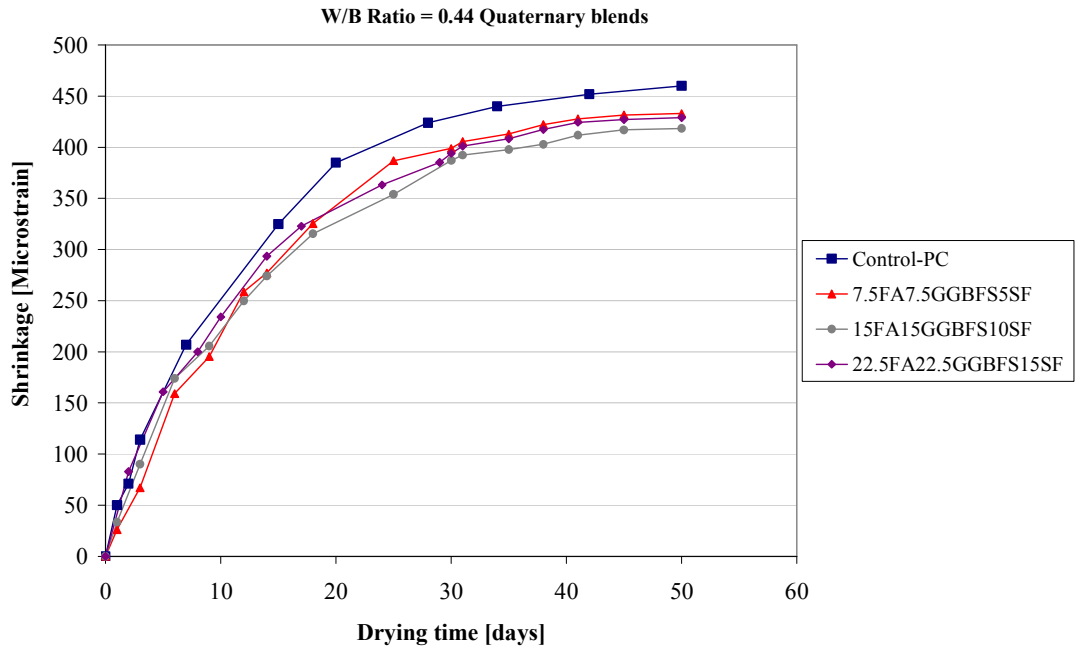


Figure 4.59 Quaternary effects of mineral admixtures on the free shrinkage of SCCs at w/b ratio of 0.44

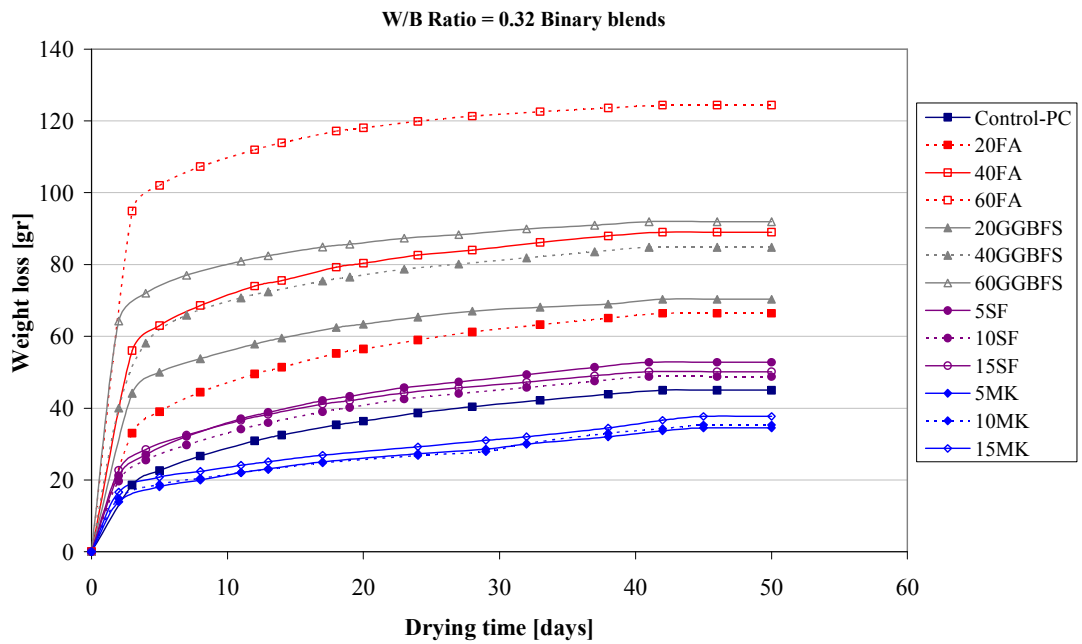


Figure 4.60 Binary effects of mineral admixtures on the weight loss of SCCs at w/b ratio of 0.32

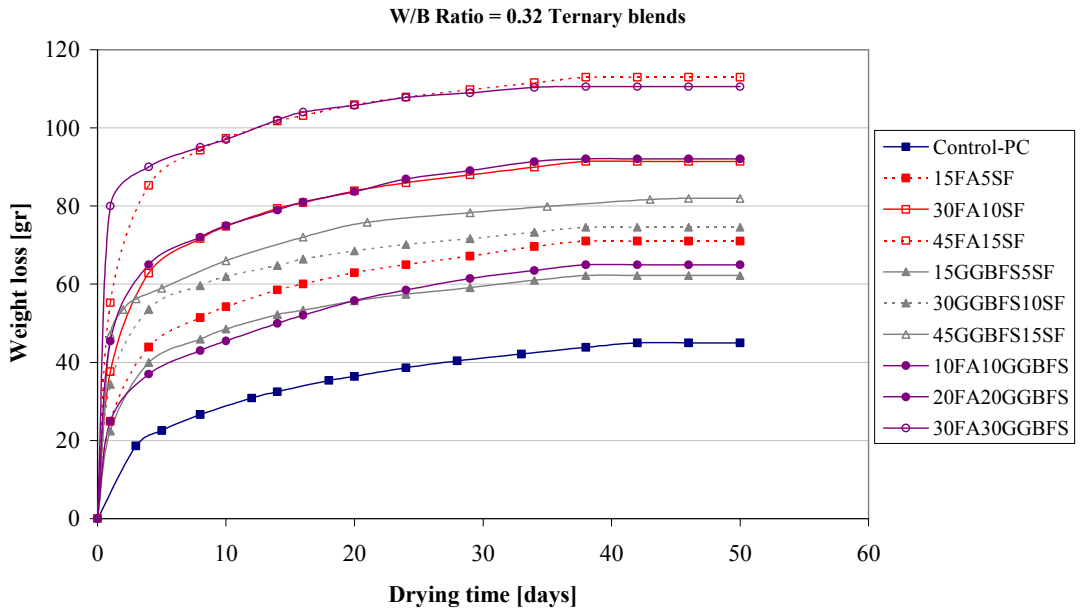


Figure 4.61 Ternary effects of mineral admixtures (PC+FA+SF; PC+GGBFS+SF; PC+FA+GGBFS) on the weight loss of SCCs at w/b ratio of 0.32

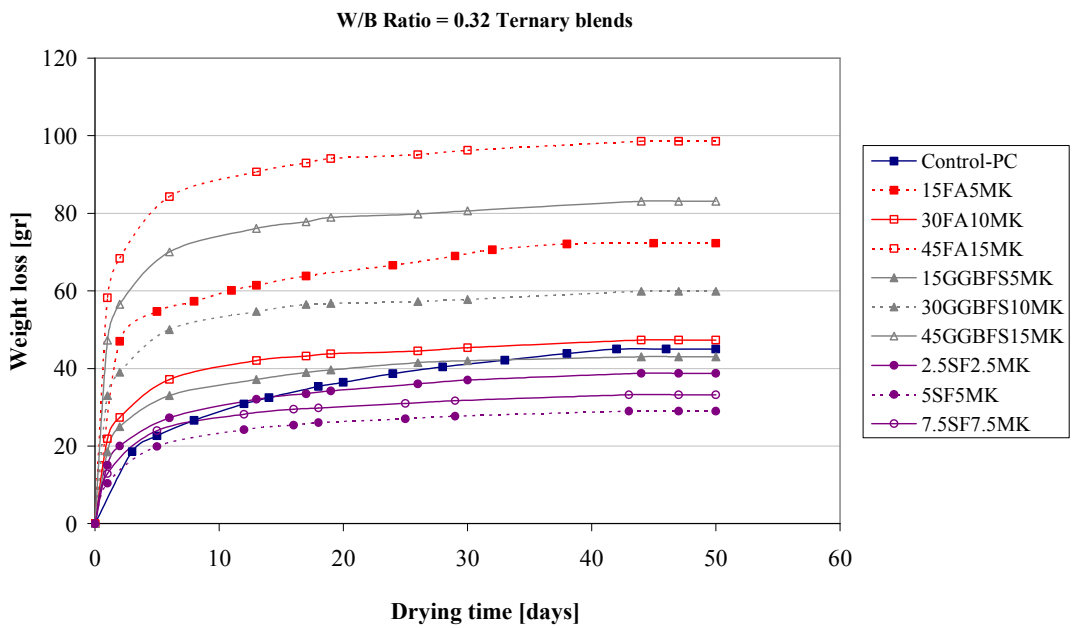


Figure 4.62 Ternary effects of mineral admixtures (PC+FA+MK; PC+GGBFS+MK; PC+SF+MK) on the weight loss of SCCs at w/b ratio of 0.32

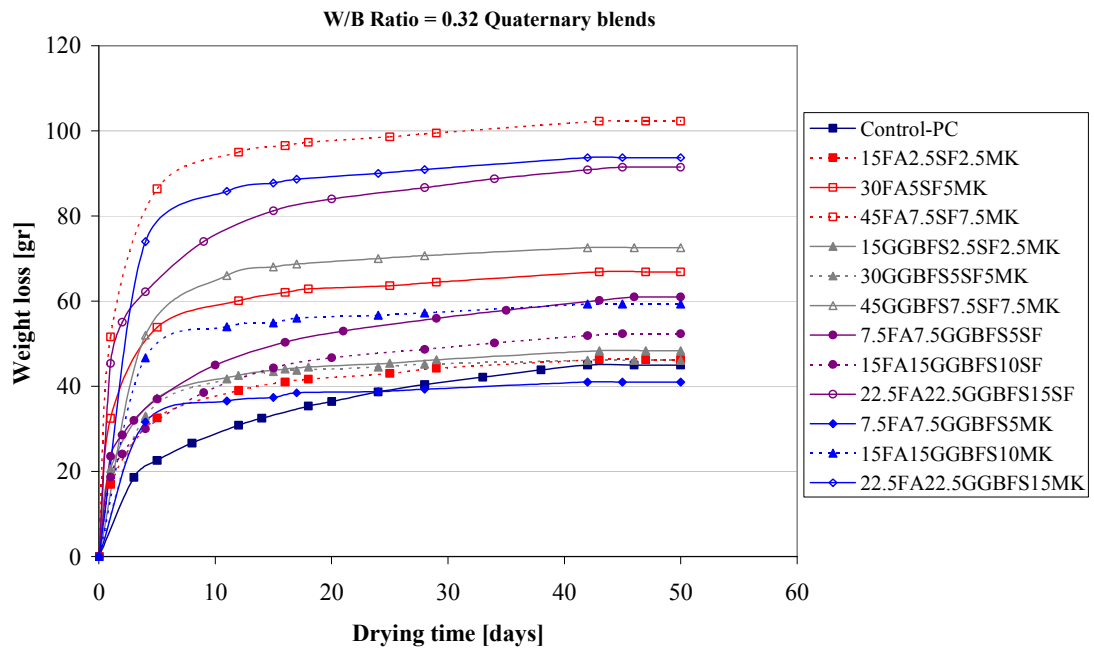


Figure 4.63 Quaternary effects of mineral admixtures on the weight loss of SCCs at w/b ratio of 0.32

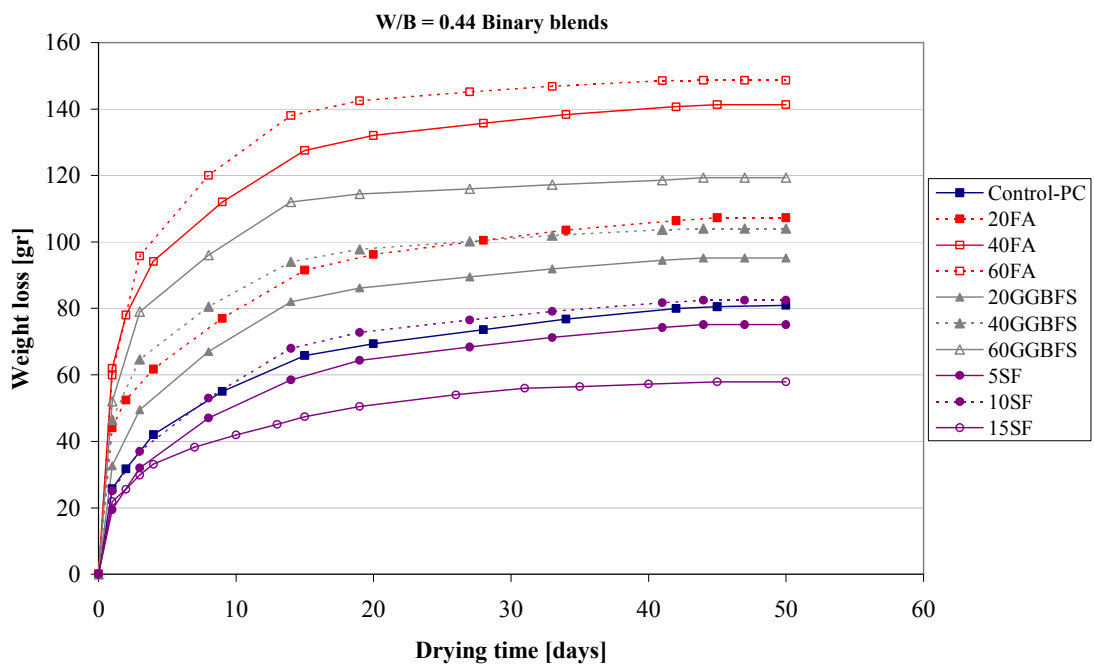


Figure 4.64 Binary effects of mineral admixtures on the weight loss of SCCs at w/b ratio of 0.44

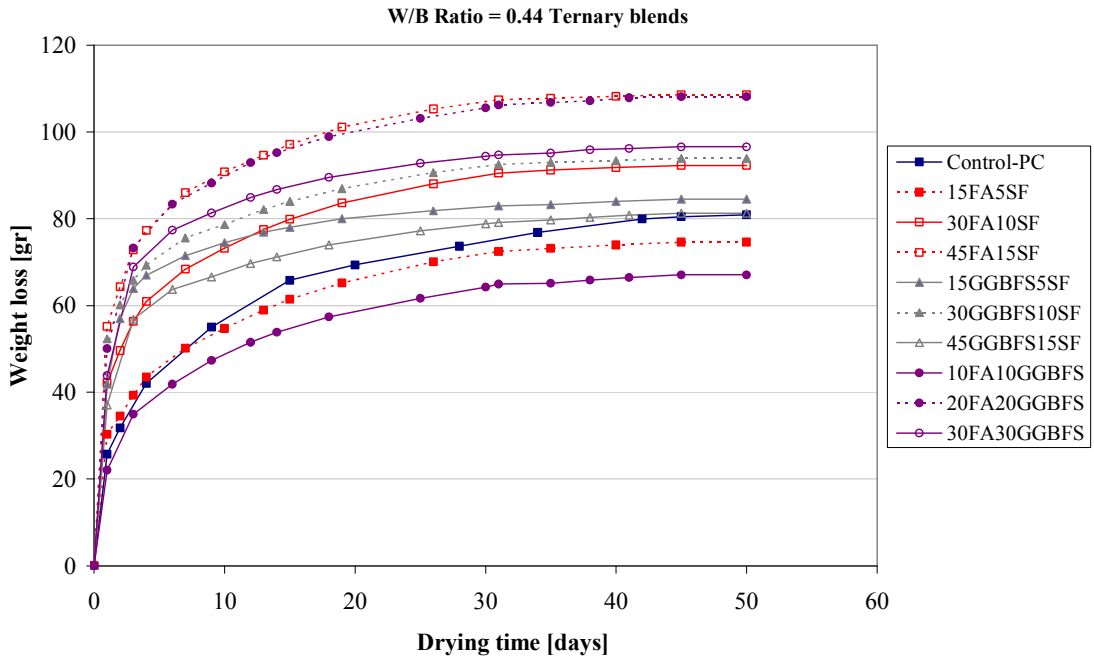


Figure 4.65 Ternary effects of mineral admixtures on the weight loss of SCCs at w/b ratio of 0.44

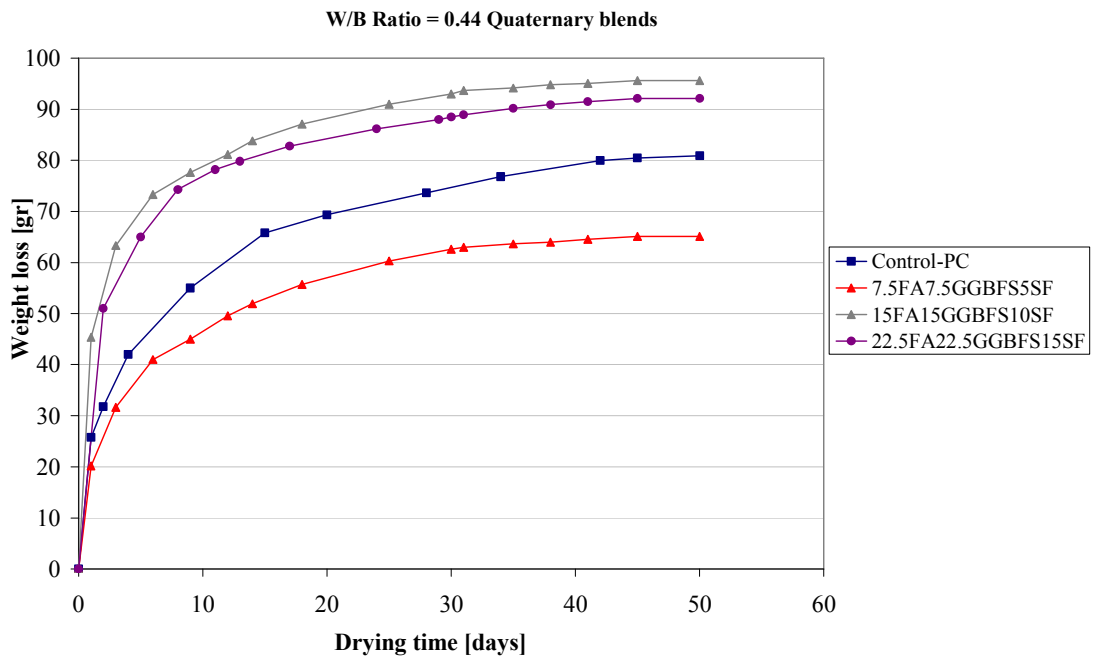


Figure 4.66 Quaternary effects of mineral admixtures on the weight loss of SCCs at w/b ratio of 0.44

4.4 Durability Related Properties

4.4.1 Rapid chloride permeability

The results of rapid chloride ion permeability test are given in Tables 4.13 and 4.14 and Figures 4.67 to 4.73. The calculated total passing charge which is an indication of the concrete's resistance to penetration of the chloride ions ranged from 119 to 1009 coulombs at the low w/b ratio, and from 216 to 2065 at the high w/b ratio. The total charge passed decreased with the use of mineral admixtures irrespective of water-binder ratio. Figure 4.67 clearly shows that the low w/b concretes containing any of the binary blends of mineral admixtures had remarkably higher resistance to chloride ion ingress associated with the lower total charge passed than the plain control concrete. The use of MK appeared to be the most effective in the reducing the chloride ion permeability of the concretes, especially the effect being increased with increasing the MK content. The total charge passed through the concrete made with 15% MK was as low as 164 coulombs while those of the concrete with 60% FA, 60% GGBFS and 15% SF were almost 715, 264, and 229 coulombs, respectively. At low w/b ratio concretes, the total charge passed through the control concrete was about 1009 coulombs which rated the concrete as low. However, the rating of the concretes shifted to very low for all of the concretes with mineral admixtures at low w/b ratio. These results are in good agreement with the findings of the studies reported in the literature in that incorporating supplementary cementitious materials significantly improve the resistance of the concretes penetration of the chloride ions. It was also reported that the concretes made with supplementary cementitious materials such as silica fume, fly ash, and slag are equal to or superior than the control concrete both as regards to strength development and the resistance to chloride ion permeability (Alonso et al., 2000; Güneysi, 2004; Polder and Peelen, 2002; Ramezani-pour and Malhotra, 1995;).

As seen in Table 4.13 and Figure 4.68, in the case of using ternary blends of PC+FA+SF, PC+FA+MK, PC+FA+GGBFS, and PC+SF+MK, the total charge passed decreased with increasing the mineral admixtures content, as well. Interestingly, 30FA30GGBFS mixture (or M28) had very low chloride ion permeability than those of the 60% FA and 60% GGBFS mixtures. The total charge passed was about 3 times less than that of 60%FA and 1.15 times less than that of

60% GGBFS mixtures. Another interesting result was monitored in the concrete with PC+SF+MK, namely M29 (or 2.5SF2.5MK) mixture which appeared to be poorer against chloride ion ingress than the concretes with binary blends of 5% SF (or M8) and 5% MK (or M11). In the case of the ternary blend concretes of PC+GGBFS+SF (M20 to M22) and PC+GGBFS+MK (M23 to M25) mixtures, the chloride ion permeability of concretes initially displayed a remarkable decrease thereafter a gradual rise was observed. Indeed, the total charge passed through the former and the latter were measured to be 160 and 188 C, respectively.

Using the quaternary blends of mineral admixtures provided a marked improvement in resistance to chloride ingress as seen in Figure 4.69. The total charge passed of such concretes was within 2.06 to 8.48 times that of the control concrete. The highest reduction in the chloride ion permeability was achieved for the mixture with 22.5FA22.5GGBFS15SF blend (or M40). However, when compared to the performance of the similar concretes with ternary blends (i.e PC+GGBFS+SF or PC+GGBFS+MK), using PC+GGBFS+SF+MK and PC+FA+GGBFS+MK blends slightly aggravated the resistance to penetration of chloride ions of these concretes.

At high w/b ratio concretes, as expected, relatively higher chloride ion permeability values were calculated when compared to those with the low w/b ratio. However, the behavior displayed by the low w/b concretes was also seen in the concretes with the high w/b ratio. Test results have generally shown that the use of any of the mineral admixtures remarkably reduced the chloride ion permeability of concretes. The rate of reduction appeared to be quite high in the ternary and quaternary blends of mineral admixtures. It was observed in Figure 4.70 that a coulomb value of 2065 rated the control concrete as moderate according to the ASTM 1202. But the rating of concretes presented in Figures 4.70 and 4.71 tended to be the low or very low with incorporating the mineral admixtures. All of the concretes but 15FA5SF (or M54) and 10FA10GGBFS (or M60) can be characterized as very low ratings. The concrete with 60% FA had a coulomb value of as high as 1475 C which reduced to 652 C in the concretes with 45%FA and 15%SF, and to 605 C 30%FA and 30% GGBFS in the concretes with ternary blends. Moreover, for the concretes made with the quaternary blends of 22.5FA22.5GGBFS15SF, this value further decreased to as low as 385 C. Test results indicated that both GGBFS and SF dominated the performance

of the concretes against the chloride ion ingress. Figure 4.72 demonstrates the how the total charge passed through the concrete discs change with the rise in the w/b ratio. As clearly seen in the figure, the chloride ion permeability of concretes increased with increasing the w/b ratio, thus the concretes became poorer against the chloride ion penetration (Güneyisi, 2004).

4.4.2 Electrical resistivity

Electrical resistivity of the concretes measured at 28 and 90 days are given in Tables 4.13 and 4.14 for the low and high w/b ratios, respectively. Moreover, the electrical resistivities of the concretes are graphically depicted in Figures 4.73 to 4.79. The overall resistivity of concretes at low w/b ratio was in the range of 12.8 to 25.8 kohm-cm and 13.4 to 34.4 kohm-cm at the 28 and 90 days, respectively. The concretes at high w/b ratio, on the other hand, had electrical resistivity ranging from 12.1 to 18.9 kohm-cm and from 12.3 to 27.7 kohm-cm. Irrespective of the w/b ratio, the lowest electrical resistivity was measured in the control concrete. It was observed in Figures 4.73 and 4.76 that using any of the mineral admixtures increased the electrical resistivity of SCCs compared to that of the control concrete, especially at higher replacement levels (Gesoglu et al., 2007; Polder and Peelen, 2002). Replacing PC by 20% FA or GGBFS provided an increase in the resistivity of the concretes by as much as 27 and 46% at low w/b ratio, respectively, but the improvement reached about 18% at high w/b ratio, irrespective of the mineral admixture employed. As seen in Table 4.13 and Figure 4.73 that the concretes with binary blends of SF or MK gave much comparable resistivity values at all replacement levels. The concretes with the binary blends 5% SF or MK had higher electrical resistivity up to 48 and 19% than the plain control concrete. At 15% replacement level, however, this beneficial effect reached about 150%. The test results suggested that it was the MK and SF among the mineral admixtures used that governed the increment in the electrical resistivity of the SCCs (Gesoglu et al., 2007).

The concretes made with the ternary cementitious materials have exhibited a behavior much similar to what is seen in the case of the concretes with the binary blends. As seen in Table 4.13 and Figure 4.74 that, all the ternary blended mixture

concretes had higher electrical resistivity than that of the reference concrete. The best compromise was found for the mixture having 45% GGBFS and 15 %SF (M22) which having the resistivity value 25.8 and 32.5 kohm-cm at the 28 and 90 days, respectively, meaning that 2.01 to 2.43 times greater resistance than that of the control concrete. A similar behavior was observed in high w/b ratio concretes (Table 4.14 and Figure 4.77). Indeed, the highest electrical resistivity of all 22 concretes was achieved for the mixture M59 having 45% GGBFS and 15% SF.

When the electrical resistivity performance of the concretes with the ternary blends of PC+FA+SF and PC+GGBFS+SF was compared, it was observed in Figures 4.74 and 4.77 that the ternary use of PC+GGBFS +SF yielded better performance rather than the use of PC+FA+SF, irrespective of the testing age. Moreover, at low w/b ratio concretes, the concretes made with the ternary use PC+FA+GGBFS outperformed those with the binary blends of both PC+FA and PC+GGBFS at the 28 days. However, at the 90 days measurements, it was observed that binary use of PC+GGBFS exhibited superior performance than that of the ternary blends of PC+FA+GGBFS mixtures as seen in Figures 4.73 and 4.74. The ternary use PC+SF+MK showed better electrical resistivity performance than those of the binary use of PC+SF and PC+MK, as well.

Like the case in ternary mixture concretes, using of quaternary blends enhanced the performance of the concretes in terms of electrical resistivity (Figures 4.75 and 4.77). Interestingly, the 28-day resistivity of the concrete containing 30% FA and 30% GGBFS was measured to be 16.3 kohm-cm while that of the concrete made with the quaternary blends of 22.5% FA, 22.5% GGBFS, and 15% MK was 24.7 kohm-cm indicating a 51% enhancement.

As can be clearly seen in Figures 4.78 and 4.79 that, the electrical resistivity of concretes increased with the increasing of testing age but as expected, a gradual decrease was observed with the increasing of w/b ratio (Lopez and Gonzalez, 1993; Saleem et al., 1996).

Table 4.13 Chloride ion permeability of SCCs at w/b ratio of 0.32

Mix ID	Mix Description	Chloride-ion permeability [coulombs]	Rating	Electrical Resistivity [kohm-cm]	
		90 Days	90 Days	28 Days	90 Days
M1	Control-PC1	1009	Low	12.8	13.4
M2	20FA	679	Very low	13.3	17.0
M3	40FA	666	Very low	13.9	17.1
M4	60FA	715	Very low	14.8	20.0
M5	20GGBFS	509	Very low	13.8	19.5
M6	40GGBFS	293	Very low	16.2	22.4
M7	60GGBFS	264	Very low	17.7	25.9
M8	5SF	392	Very low	14.6	19.9
M9	10SF	256	Very low	17.5	25.3
M10	15SF	229	Very low	20.6	34.4
M11	5MK	381	Very low	13.7	16.0
M12	10MK	174	Very low	20.1	26.4
M13	15MK	164	Very low	20.6	33.1
M14	15FA5SF	593	Very low	14.7	18.3
M15	30FA10SF	389	Very low	17.0	23.8
M16	45FA15SF	234	Very low	21.3	25.9
M17	15FA5MK	353	Very low	13.5	22.7
M18	30FA10MK	228	Very low	15.7	26.2
M19	45FA15MK	186	Very low	20.6	30.7
M20	15GGBFS5SF	434	Very low	15.8	21.2
M21	30GGBFS10SF	160	Very low	20.9	28.7
M22	45GGBFS15SF	177	Very low	25.8	32.5
M23	15GGBFS5MK	312	Very low	13.6	23.9
M24	30GGBFS10MK	188	Very low	19.8	29.2
M25	45GGBFS15MK	206	Very low	22.2	31.3
M26	10FA10GGBFS	554	Very low	13.4	17.1
M27	20FA20GGBFS	370	Very low	14.7	23.6
M28	30FA30GGBFS	231	Very low	16.3	27.1
M29	2.5SF2.5MK	507	Very low	15.1	19.5
M30	5SF5MK	257	Very low	20.7	28.0
M31	7.5SF7.5MK	224	Very low	23.7	33.8
M32	15FA2.5SF2.5MK	489	Very low	13.9	17.8
M33	30FA5SF5MK	347	Very low	16.9	26.0
M34	45FA7.5SF7.5MK	476	Very low	18.8	30.3
M35	15GGBFS2.5SF2.5MK	486	Very low	14.5	18.7
M36	30GGBFS5SF5MK	347	Very low	19.3	29.2
M37	45GGBFS7.5SF7.5MK	329	Very low	24.1	34.0
M38	7.5FA7.5GGBFS5SF	490	Very low	15.6	22.3
M39	15FA15GGBFS10SF	300	Very low	17.5	26.8
M40	22.5FA22.5GGBFS15SF	119	Very low	21.0	31.6
M41	7.5FA7.5GGBFS5MK	383	Very low	15.6	25.1
M42	15FA15GGBFS10MK	219	Very low	19.6	30.0
M43	22.5FA22.5GGBFS15MK	208	Very low	24.7	33.2

Table 4.14 Chloride ion permeability of SCCs at w/b ratio of 0.44

Mix ID	Mix Description	Chloride-ion permeability [coulombs]	Rating	Electrical Resistivity [kohm-cm]	
		90 Days	90 Days	28 Days	90 Days
M44	Control-PC 2	2065	Moderate	12.1	12.3
M45	20FA	1224	Low	12.6	14.5
M46	40FA	1083	Low	12.7	15.2
M47	60FA	1475	Low	13.2	16.5
M48	20GGBFS	1053	Low	12.4	14.5
M49	40GGBFS	403	Very low	13.5	15.8
M50	60GGBFS	282	Very low	14.7	17.1
M51	5SF	1118	Low	12.5	14.4
M52	10SF	796	Very low	12.8	15.9
M53	15SF	375	Very low	14.9	18.2
M54	15FA5SF	1184	Low	12.7	14.8
M55	30FA10SF	585	Very low	13.7	15.5
M56	45FA15SF	652	Very low	15.3	17.9
M57	15GGBFS5SF	719	Very low	13.1	15.1
M58	30GGBFS10SF	408	Very low	16.9	19.9
M59	45GGBFS15SF	216	Very low	18.9	27.7
M60	10FA10GGBFS	1040	Low	12.4	14.5
M61	20FA20GGBFS	682	Very low	13.0	15.5
M62	30FA30GGBFS	605	Very low	14.0	17.0
M63	7.5FA7.5GGBFS5SF	743	Very low	14.0	16.5
M64	15FA15GGBFS10SF	463	Very low	15.0	18.5
M65	22.5FA22.5GGBFS15SF	385	Very low	16.0	21.5

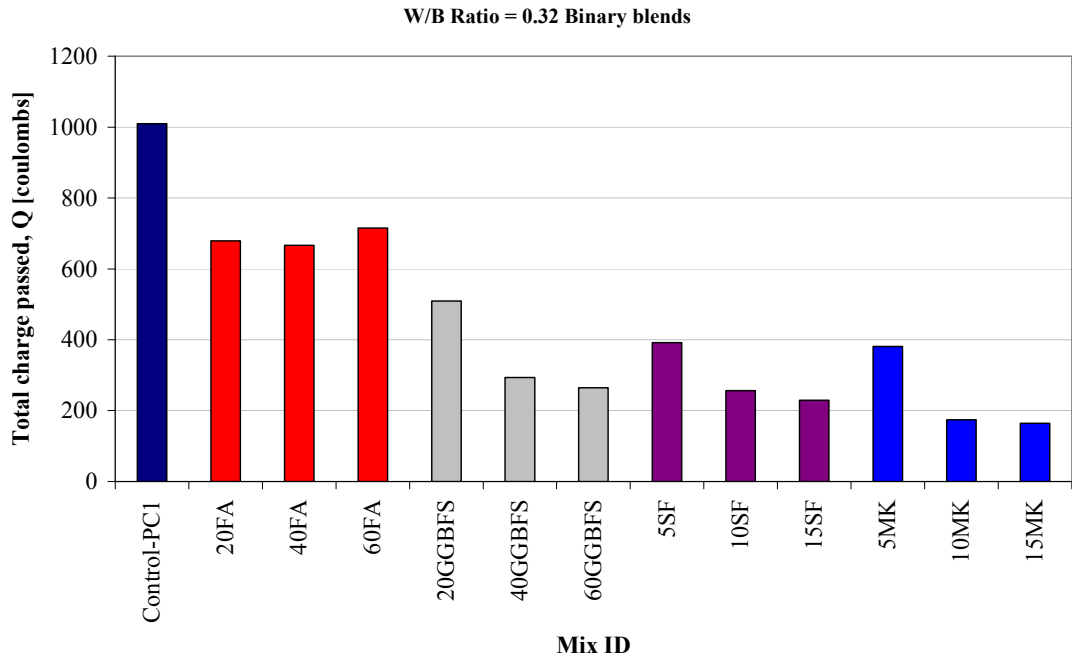


Figure 4.67 Binary effects of mineral admixtures on the chloride ion permeability of SCCs at w/b ratio of 0.32

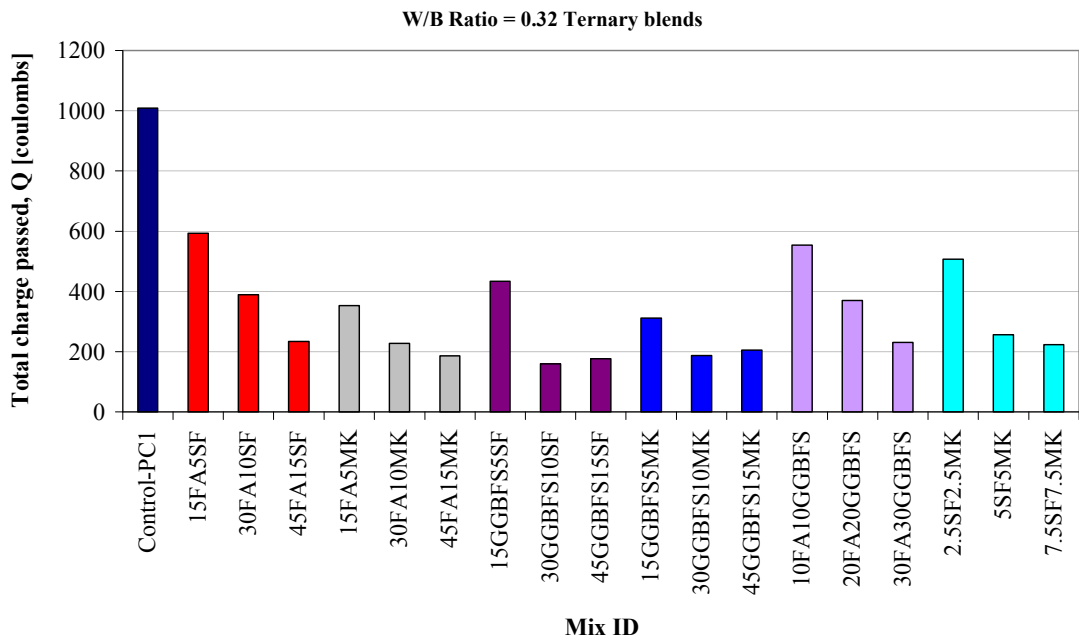


Figure 4.68 Ternary effects of mineral admixtures on the chloride ion permeability of SCCs at w/b ratio of 0.32

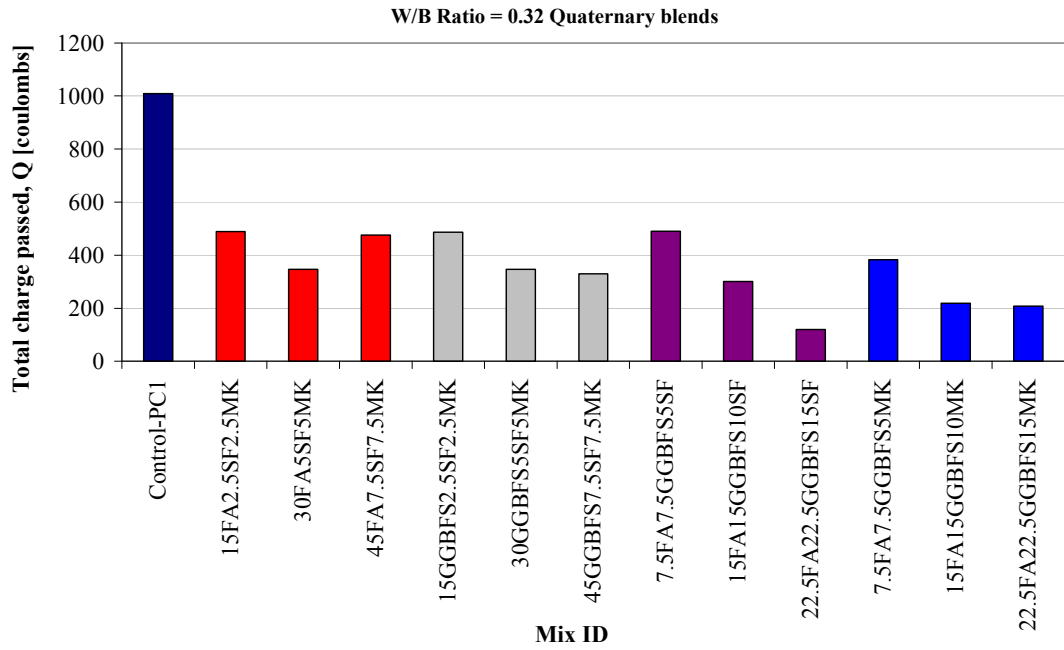


Figure 4.69 Quaternary effects of mineral admixtures on the chloride ion permeability of SCCs at w/b ratio of 0.32

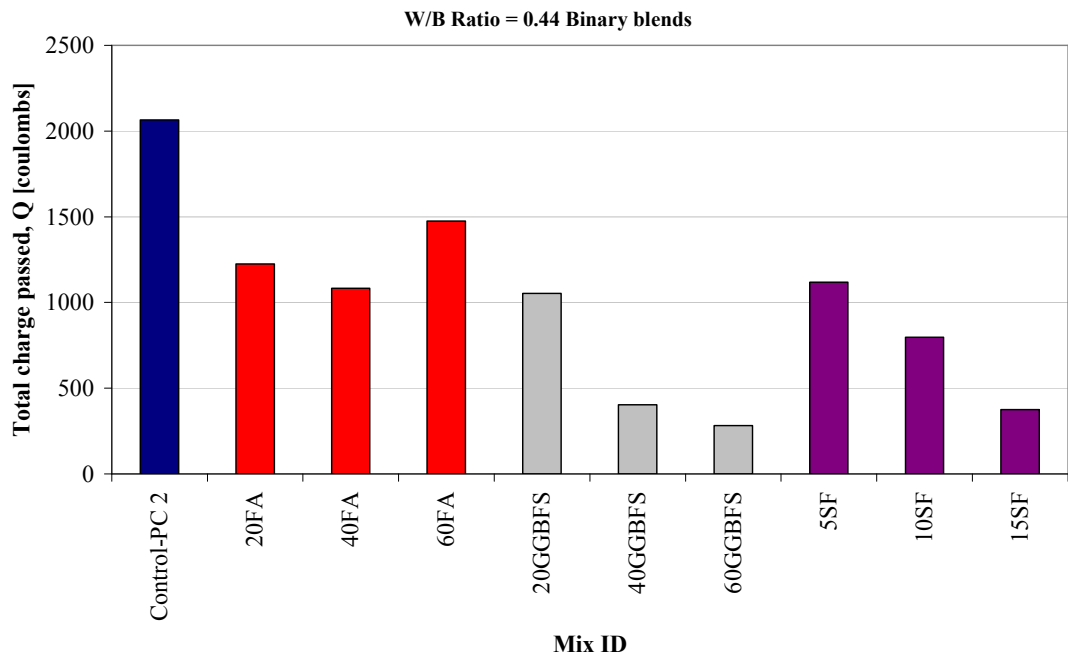


Figure 4.70 Binary effects of mineral admixtures on the chloride ion permeability of SCCs at w/b ratio of 0.44

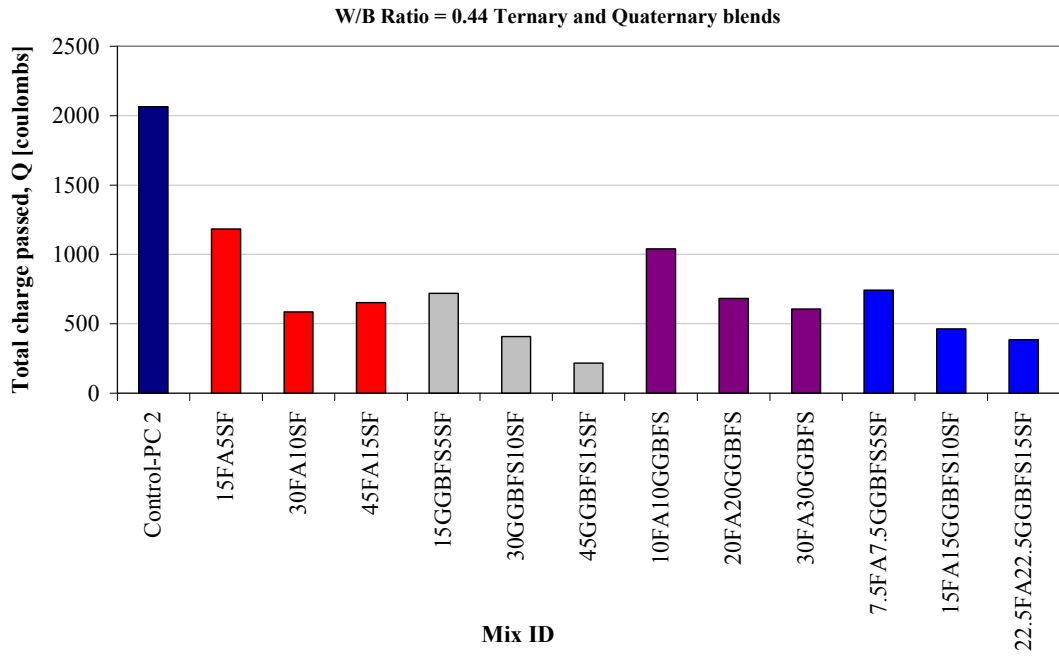


Figure 4.71 Ternary and quaternary effects of mineral admixtures on the chloride ion permeability of SCCs at w/b ratio of 0.44

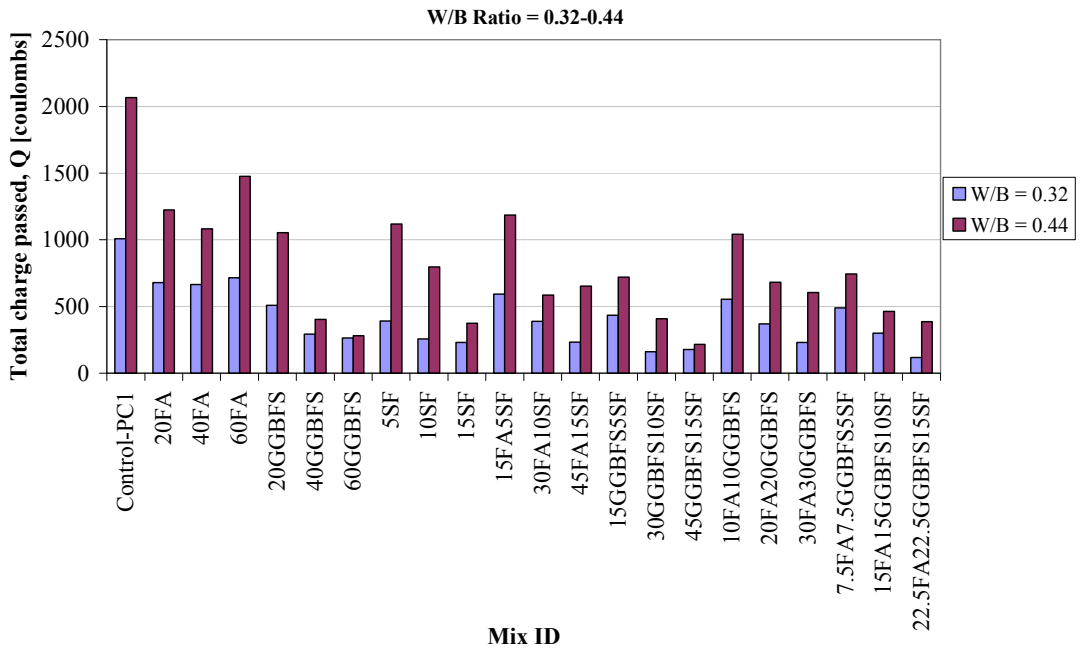


Figure 4.72 Comparison of the chloride ion permeability of SCCs at different w/b ratios

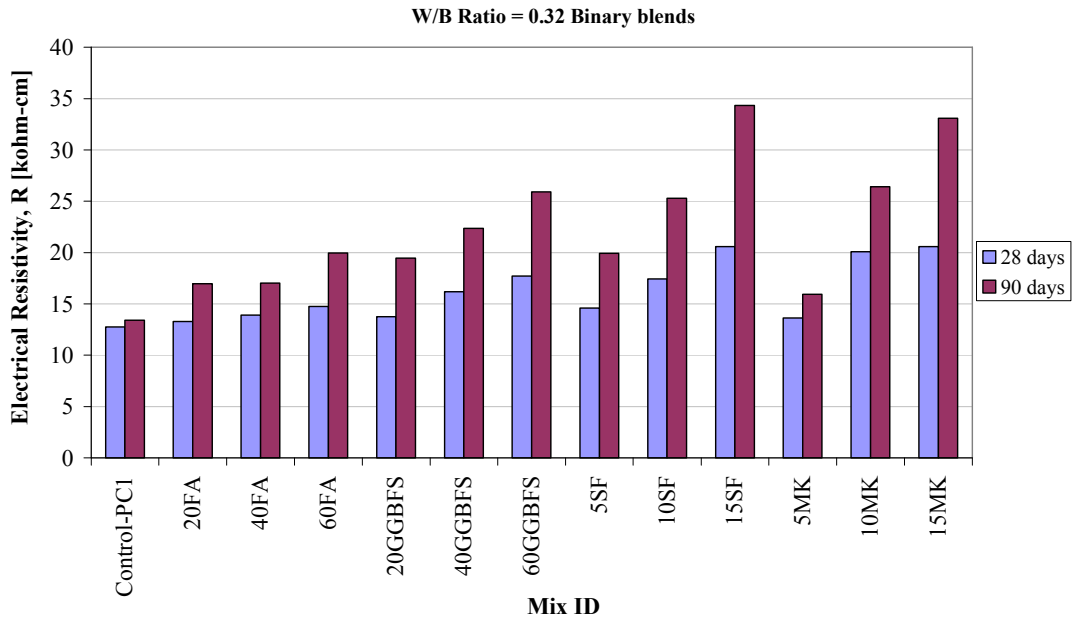


Figure 4.73 Binary effects of mineral admixtures on electrical resistivity of SCCs at w/b ratio of 0.32

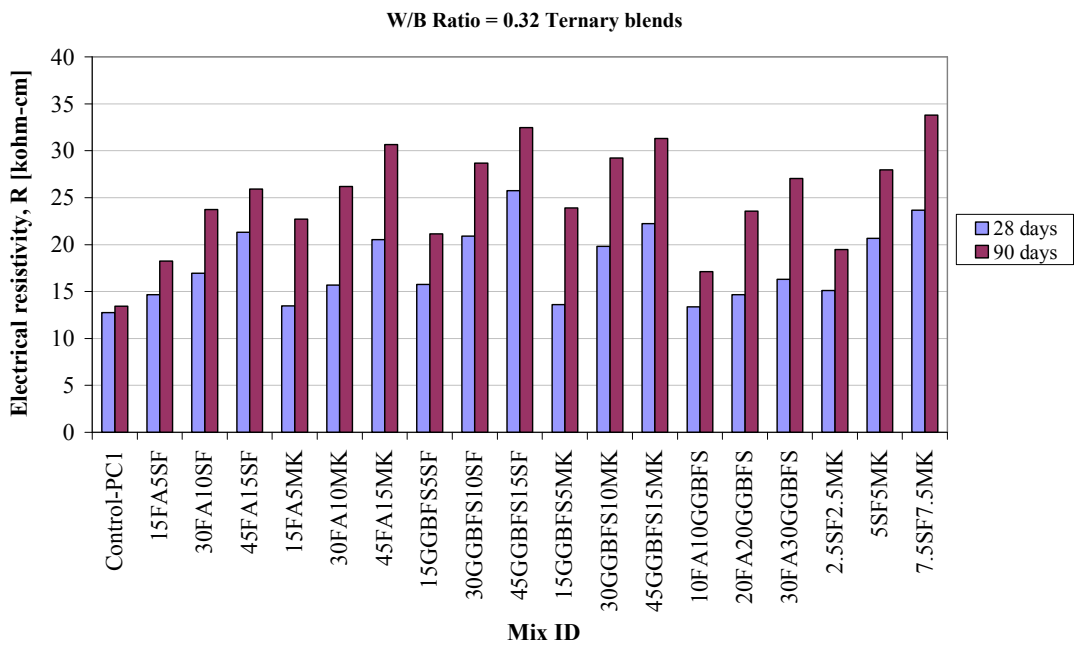


Figure 4.74 Ternary effects of mineral admixtures on electrical resistivity of SCCs at w/b ratio of 0.32

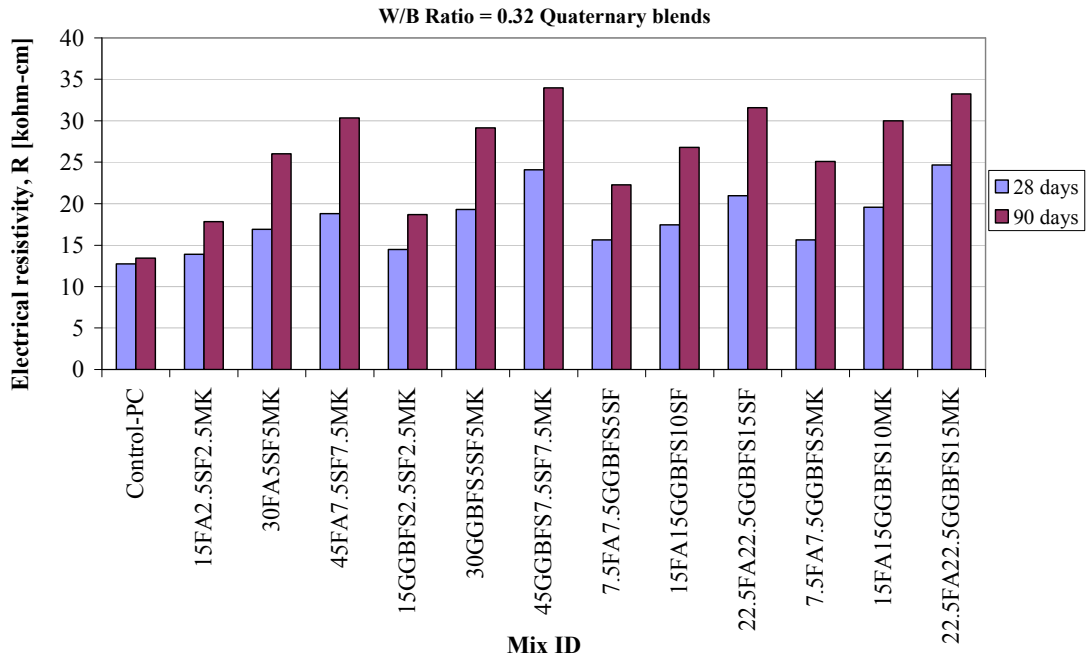


Figure 4.75 Quaternary effects of mineral admixtures on electrical resistivity of SCCs at w/b ratio of 0.32

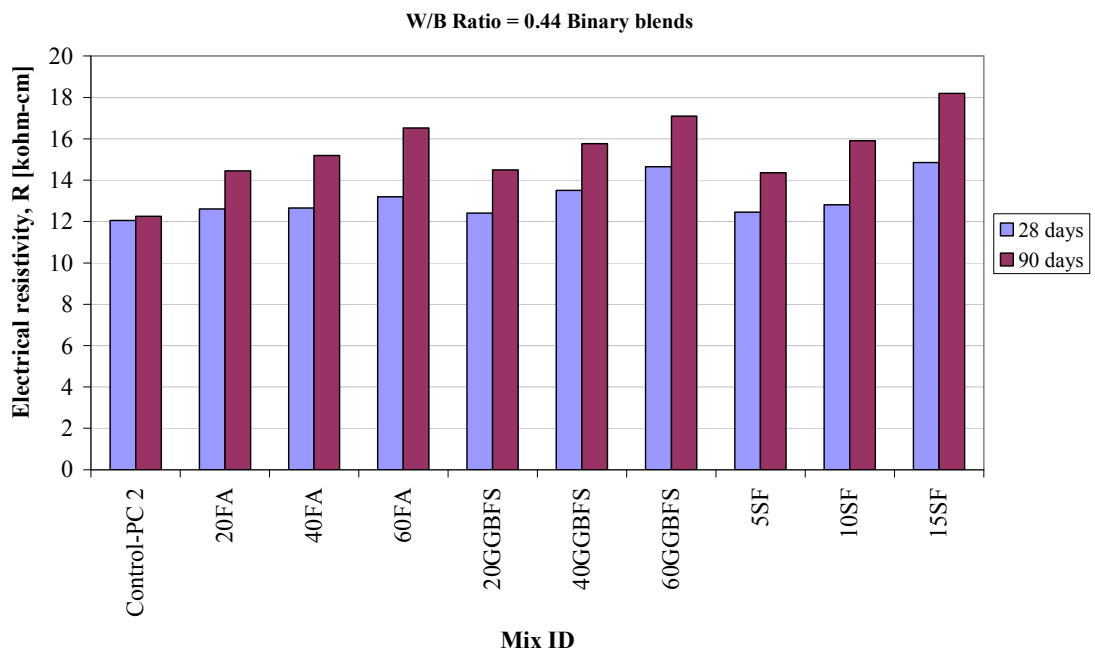


Figure 4.76 Binary effects of mineral admixtures on electrical resistivity of SCCs at w/b ratio of 0.44

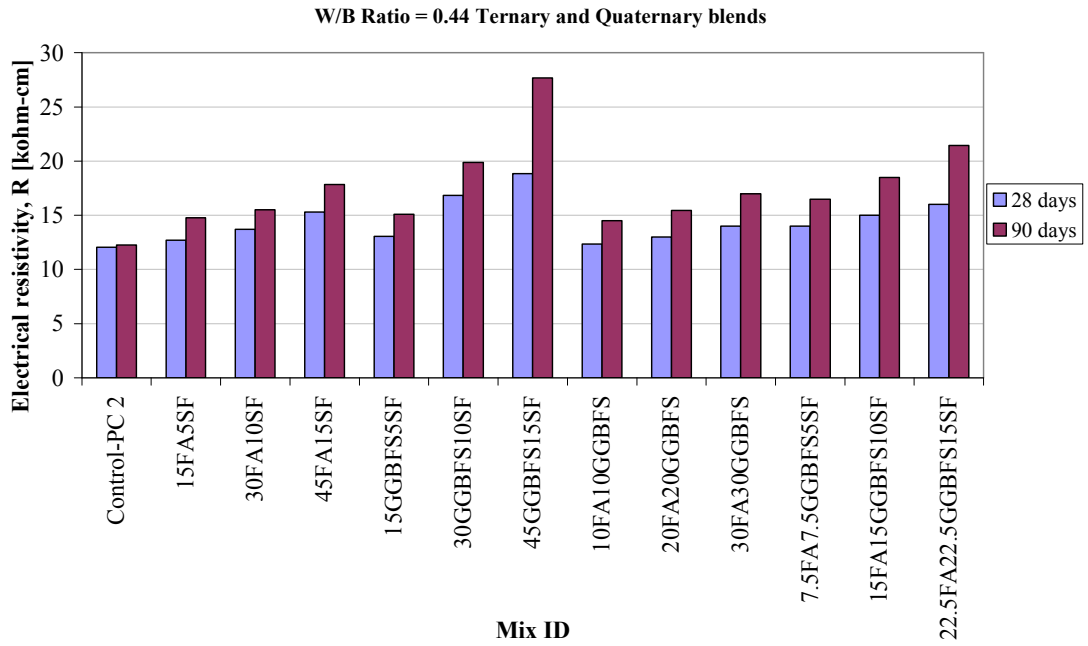


Figure 4.77 Ternary and quaternary effects of mineral admixtures on electrical resistivity of SCCs at w/b ratio of 0.44

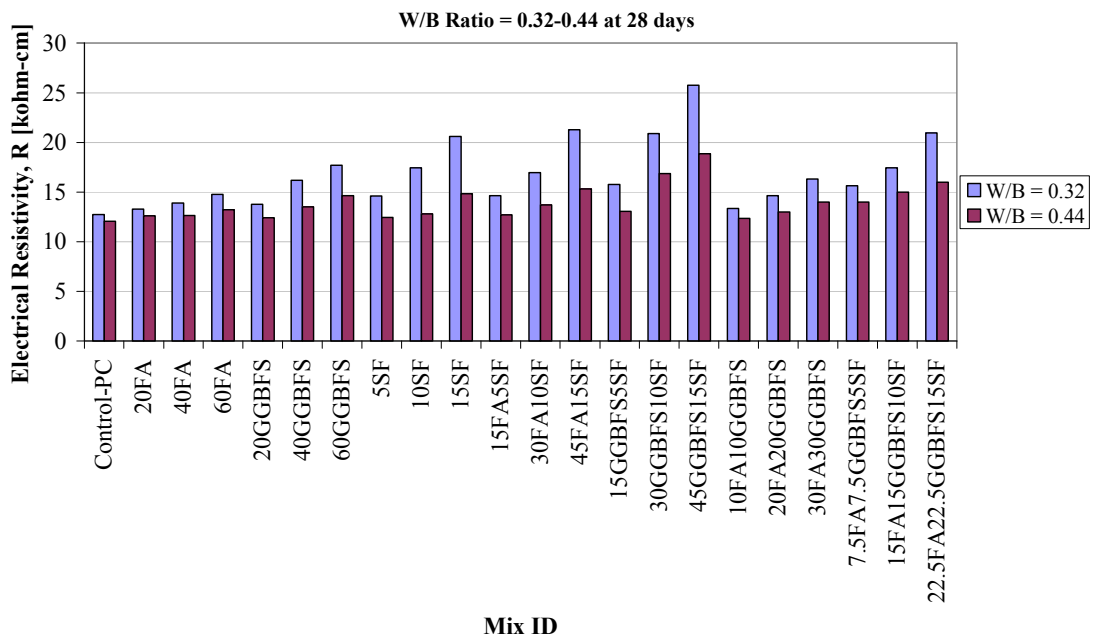


Figure 4.78 Comparison of electrical resistivity of SCCs at 28 days for different w/b ratios

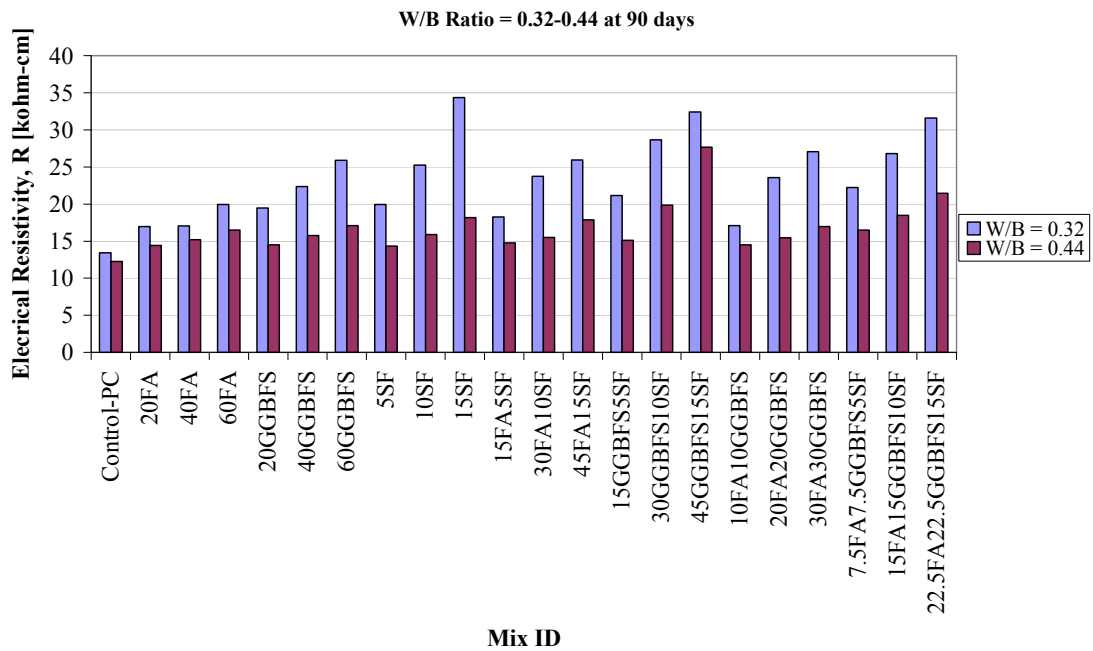


Figure 4.79 Comparison of electrical resistivity of SCCs at 28 days for different w/b ratios

4.4.3 Water absorption

Tables 4.15 and 4.16 give the water absorption of the SCCs measured at 90 days. The variation in water absorption of the concretes with different mineral admixture and replacement levels are shown in Figures 4.80 to 4.85. It is clear from the tables and the figures that the water absorption decreased with increasing of mineral admixtures content. The water absorption of concretes ranged from 1.57 to 4.79% and 2.53% to 7.74 at the low and high w/b ratio concretes, respectively.

As can be seen in Figure 4.80 that the binary use of PC+SF and PC+MK blends significantly reduced the water absorption of concretes at low w/b ratio. Both SF and MK appeared to be the most effective in the reduction of water absorption among the mineral admixtures used; the effect being increased with increasing the replacement level. As expected, the highest water absorption was measured for the control concrete. The reduction in the water absorption indicates superior performance of the concretes made with the ultrafine minerals such as SF and MK. The beneficial effect of MK in reducing the water absorption was noticeable due to the filling effect of ultrafine MK as well as its pozzolanic reaction. Wild et al. (1996) reported that in the

presence of MK, the filling effect is immediate, the acceleration of OPC hydration has its major within the first 24 h, and the level of pozzolanic reaction is considerably high within first 7-14 days for all MK levels. However, the differences in the water absorption characteristics of the plain and MK concretes became more significant at later ages (90 days) and were remarkably lower for MK concrete compared to the plain concrete. This may be explained by the pozzolanic activity of MK since it is well known that the pozzolanic reactions contribute to the refinement of the binder capillary porosity, with its direct consequences on the improvement of the durability characteristics of the concrete (Mermerdaş, 2006). The water absorption of the concretes with the binary blends of PC+FA were very close to that of the control concrete. However, the ternary use of PC+FA+SF and PC+FA+MK reduced the water absorption remarkably according to the binary use of PC+FA as seen in Figure 4.81. Moreover, Figure 4.82 revealed that of all the 43 mixtures in low w/b ratio concretes, the quaternary use of 45GGBFS7.5SF7.5MK gave the lowest water absorption values.

At low w/b ratio concretes, on the other hand, further inclusion of FA into PC+SF and PC+MK mixtures increased the water absorption characteristics of the concretes. Moreover, the rate of increment in the water absorption was higher for the ternary blends of PC+FA+MK. Unlike FA, with inclusion of GGBFS into the PC+MK mixtures, the concretes with the ternary blends of PC+GGBFS+MK exhibited superior water absorption performance over the concretes with the binary blends both PC+GGBFS and PC+MK. Ternary use of PC+FA+GGBFS absorbed more water than the binary blends of PC+GGBFS. However, it absorbed less water than that of the binary blends of PC+FA.

At low w/b ratio concretes, among the quaternary blended mixtures (PC+FA+SF+MK, PC+GGBFS+SF+MK, PC+FA+GGBFS+SF and PC+FA+GGBFS+MK), the lowest absorption belonged to the mixture of PC+GGBFS+SF+MK. The concrete with the quaternary blends of PC+FA+GGBFS+SF exhibited better water absorption performance than the concrete having PC+FA+GGBFS+MK mixture.

As in low w/b ratio concretes, the use of mineral admixtures remarkably reduced the water absorption of the concretes at high w/b ratio as seen in Figures 4.83 and 4.84.

The rate of reduction was very high at the binary use of SF with PC. The use of SF appeared to be the most effective in the reduction of water absorption, especially the effect being increased with increasing SF content. As expected, the highest water absorption value was also measured for the control concrete. Water absorption of the concretes made with binary, ternary and quaternary blends of mineral admixtures significantly decreased compared to the control concrete. Moreover, the binary use of PC+SF gave the lowest water absorption values than those of the ternary and quaternary blends of the mineral admixtures. When compared the performance of ternary and quaternary blends of mineral admixtures, the ternary blends exhibited better performance. As expected increasing the w/b ratio increased the water absorption of concretes as seen in Figure 4.85.

4.4.4 Sorptivity

Sorptivity test are based on water-flow into unsaturated concrete through large connected pores. Thus, it is considered as a relative measure of the permeability. Tables 4.15 to 4.16 and Figures 4.86 to 4.91 present the sorptivity test results of the SCCs measured at 90 days with different mineral admixtures and w/b ratio. As seen in Tables 4.15-4.16 and Figures 4.86 and 4.89 that the plain control concretes (M1 and M44) had the highest sorptivity index for both w/b ratio concretes. However, incorporating the mineral admixtures continuously decreased the sorptivity of SCCs. It is clear from tables and figures that water sorptivity decreased with increasing the amount of mineral admixtures used. The water sorptivity of concretes ranged from 0.027 to 0.082 mm/min^{0.5} and 0.05 to 0.093 mm/min^{0.5} at the low and high w/b ratio concretes, respectively.

As seen in Figure 4.86, in the binary blends of mineral admixtures, the use of MK appeared to be much effective in reducing the sorptivity due to the reduced pore volume (Bai et al., 2002). The influence of MK on the water sorptivity was much clearer on the ternary use of PC+FA+MK and PC+GGBFS+MK as seen in Figure 4.87. Take for example M23 containing 15% GGBFS and 5% MK as mineral admixtures. The sorptivity of this concrete was almost 65% lower than that of the control and 64% less than that the mixture with the binary blends of 20% GGBFS.

The mixture M20 (15% GGBFS+5% SF), similarly, had lower sorptivity than those of the control and the concrete with 20% GGBFS by as much as 26 and 23%, respectively. According to Taşdemir (2003), the beneficial roles of silica fume in concrete were an increase in strength and reduction in the capillary absorption of concrete such that increasing the replacement level of silica fume reduced the sorptivity index of SCCs as seen in Tables 4.15-4.16. As can be seen in Figures 4.86 and 4.87 that the ternary use of PC+SF+MK did not significantly alter the water sorptivity of concretes according to the binary blends of PC+SF. Moreover, the ternary use of PC+SF+MK increased the water sorptivity by a small amount when compared to the binary use of PC+MK. Ternary use of FA and GGBFS with SF exhibited superior performance than those of the binary blends of PC+FA and PC+GGBFS. Besides, increasing the mineral admixtures contents from 10 to 30% for each of the FA and GGBFS in the ternary blends (PC+FA+GGBFS) decreased the water sorptivity coefficient remarkably.

As depicted in Figure 4.88 that the quaternary use of PC+FA+SF+MK and PC+GGBFS+SF+MK had lower water sorptivity index when compared to those of the quaternary blends of PC+FA+GGBFS+SF and PC+FA+GGBFS+MK. As also seen in Figure 4.88 that a systematical decrease was observed by increasing the mineral admixture content in the quaternary blends of PC+FA+GGBFS+SF. The lowest water sorptivity coefficient was monitored at the mixture M37 (or 45GGBFS7.5SF7.5MK) with a $0.027 \text{ mm/min}^{0.5}$ value.

At high w/b ratio concretes, as seen in Table 4.16 and Figures 4.89 and 4.90 that the plain control concrete had the highest sorptivity index. However, incorporating the mineral admixtures continuously decreased the sorptivity of SCCs. The effects of using ternary (PC+GGBFS+SF) and quaternary (PC+FA+GGBFS+SF) blends of mineral admixtures were to decrease the sorptivity of SCCs but increasing the replacement level of mineral admixtures did not change the sorptivity index significantly. In the case of using the ternary blend of PC+FA+GGBFS, water sorptivity remarkably decreased when compared to the binary use of PC+FA and PC+GGBFS. Furthermore, the rate of reduction was much more evident at the binary use of PC+FA. Ternary use of PC, FA, and GGBFS provided lower sorptivity index than the quaternary use of PC, FA, GGBFS, and SF. As expected, increasing the

water binder ratio from 0.32 to 0.44 increased the water sorptivity coefficients of SCCs (Figure 4.91).

4.4.5 Water permeability

Replacing the portland cement with mineral admixtures significantly improved the water permeability of the concretes depending on the type of mineral admixture used and the replacement level. At low w/b ratio concretes, the highest water permeability of 23 mm was achieved for the control concrete (M1) followed by the concretes with binary and ternary blends of FA and/or GGBFS which having a water penetration of 9 to 14 mm. When compared to that of the control concrete, incorporating MK in the binary blends of 5, 10 and 15% caused a reduction of 65, 78, and 82% in the water permeability, respectively.

As seen in Figures 4.92 and 4.93 that the combined use of PC+FA+SF increased slightly the water ingress into concrete when compared to those of the binary blends of PC+SF and PC+MK. Nevertheless, the effect appeared to be insignificant at higher content of mineral admixtures. Interestingly, increasing the mineral admixtures content in the ternary use of PC+FA+MK increased the water permeability of concretes. There was a gradual increase in the depth of water ingress with using ternary blends of PC+SF+MK according to the binary use PC+MK, but and approximately similar water permeability values were recorded in the concretes with the binary blends of PC+SF.

When the water permeability of the concretes with quaternary blends are concerned, it was very interesting to note that the concretes with MK had water permeability less than 5 mm, irrespective of MK, FA, and GGBFS content (Figure 4.94). Therefore, it may be suggested that the MK among the mineral admixtures used governed the reduction in the water permeability of the SCCs. Incorporating quaternary blends generally decreased the water permeability of concretes. The lowest penetration depth was measured in the concretes containing MK, followed by SF.

Table 4.16 and Figures 4.95 to 4.96 present the water permeability of the SCCs at high w/b ratio. It was observed in Table 4.16 that the water permeability of all

concretes was lower than 26 mm, the highest water ingress belonging to the control concrete (M1). However, the concretes with mineral admixtures had a water permeability ranging from 12 to 17 mm. Therefore, using any of the mineral admixtures provided a marked reduction in the water permeability of SCCs when compared to that of the control concrete. Especially, the quaternary use of mineral admixtures in M65 provided a reduction of about 54% in the water penetration depth of the concrete. This result was consistent with the literature. In the study of Khatri et al. (1997) it was revealed that the addition of silica fume to normal portland cement considerably reduced the water permeability, and concretes prepared with high slag blended cement had lower permeability than did those prepared with normal Portland cement.

According to the DIN 1048 and TS EN 12390/8 that, concretes can be accepted resistant to chemical attacks if their water permeability values are less than 30 mm in contact with aggressive media. It can be said that all produced concretes for both w/b ratio are resistant to chemical attacks in aggressive media. In Figure 4.97, it was monitored that increasing the water binder ratio from 0.32 to 0.44 generally increased the water permeability of concretes.

Table 4.15 Results of water absorption, sorptivity and water permeability tests at w/b ratio of 0.32

Mix ID	Mix Description	Water Absorption	Water Sorptivity	Water Permeability
		[%]	[mm/min ^{0.5}]	[mm]
		90 Days	90 Days	90 Days
M1	Control-PC1	4.79	0.082	23
M2	20FA	4.78	0.080	14
M3	40FA	4.71	0.071	12
M4	60FA	4.52	0.062	9
M5	20GGBFS	3.99	0.079	14
M6	40GGBFS	3.68	0.063	11
M7	60GGBFS	3.1	0.057	12
M8	5SF	2.27	0.062	10
M9	10SF	2.18	0.056	5
M10	15SF	2.07	0.051	7
M11	5MK	2.57	0.057	8
M12	10MK	2.43	0.058	5
M13	15MK	2.11	0.039	4
M14	15FA5SF	3.67	0.06	11
M15	30FA10SF	2.88	0.056	12
M16	45FA15SF	2.21	0.055	9
M17	15FA5MK	3.5	0.054	3
M18	30FA10MK	3.01	0.043	7
M19	45FA15MK	2.55	0.051	9
M20	15GGBFS5SF	3.25	0.061	13
M21	30GGBFS10SF	2.74	0.054	13
M22	45GGBFS15SF	2.56	0.05	11
M23	15GGBFS5MK	1.99	0.028	5
M24	30GGBFS10MK	2.76	0.047	5
M25	45GGBFS15MK	2.1	0.039	4
M26	10FA10GGBFS	4.41	0.065	14
M27	20FA20GGBFS	3.79	0.046	13
M28	30FA30GGBFS	2.67	0.041	14
M29	2.5SF2.5MK	2.51	0.066	11
M30	5SF5MK	2.27	0.066	7
M31	7.5SF7.5MK	2.35	0.035	5
M32	15FA2.5SF2.5MK	3.31	0.060	12
M33	30FA5SF5MK	2.29	0.038	11
M34	45FA7.5SF7.5MK	2.87	0.047	10
M35	15GGBFS2.5SF2.5MK	1.92	0.032	10
M36	30GGBFS5SF5MK	1.62	0.050	9
M37	45GGBFS7.5SF7.5MK	1.57	0.027	8
M38	7.5FA7.5GGBFS5SF	3.05	0.063	13
M39	15FA15GGBFS10SF	3.04	0.051	12
M40	22.5FA22.5GGBFS15SF	2.59	0.049	12
M41	7.5FA7.5GGBFS5MK	3.37	0.051	5
M42	15FA15GGBFS10MK	3.33	0.044	5
M43	22.5FA22.5GGBFS15MK	3.54	0.045	4

Table 4.16 Results of water absorption, sorptivity and water permeability tests at w/b ratio of 0.44

Mix ID	Mix Description	Water Absorption	Water Sorptivity	Water Permeability
		[%] 90 Days	[mm/min ^{0.5}] 90 Days	[mm] 90 Days
M44	Control-PC 2	7.74	0.093	26
M45	20FA	6.12	0.090	17
M46	40FA	6.05	0.083	17
M47	60FA	5.87	0.081	13
M48	20GGBFS	4.78	0.088	15
M49	40GGBFS	4.59	0.074	13
M50	60GGBFS	4.33	0.050	14
M51	5SF	3.13	0.076	15
M52	10SF	2.80	0.065	14
M53	15SF	2.53	0.064	13
M54	15FA5SF	5.54	0.084	16
M55	30FA10SF	4.31	0.074	17
M56	45FA15SF	3.77	0.071	16
M57	15GGBFS5SF	3.43	0.067	16
M58	30GGBFS10SF	2.98	0.065	15
M59	45GGBFS15SF	2.67	0.068	16
M60	10FA10GGBFS	4.71	0.065	15
M61	20FA20GGBFS	4.61	0.064	13
M62	30FA30GGBFS	3.73	0.059	14
M63	7.5FA7.5GGBFS5SF	5.70	0.068	17
M64	15FA15GGBFS10SF	4.82	0.063	13
M65	22.5FA22.5GGBFS15SF	4.17	0.062	12

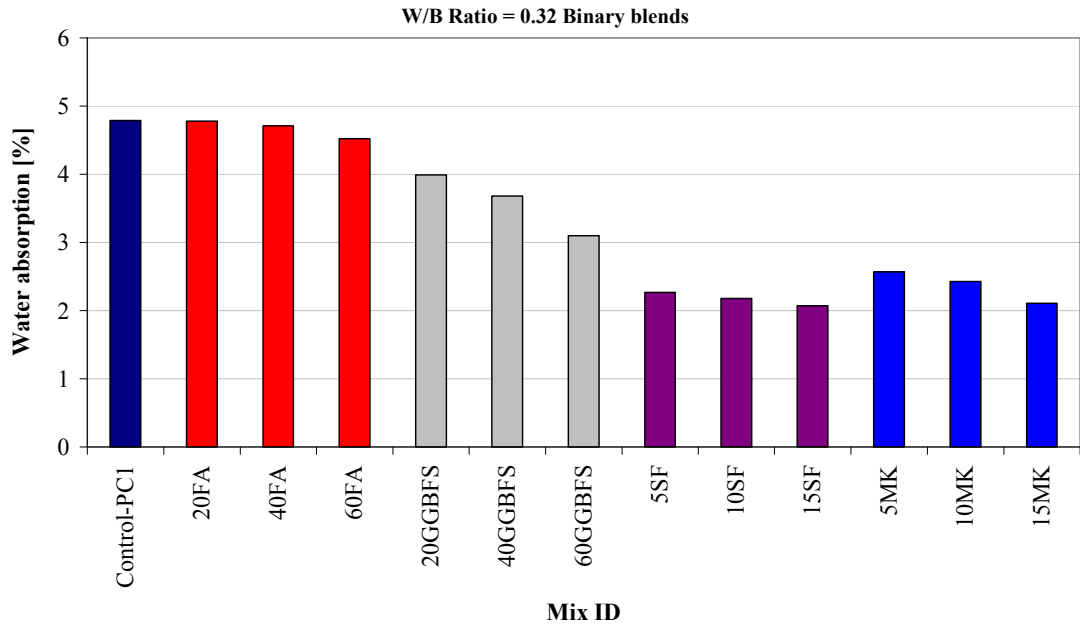


Figure 4.80 Binary effects of mineral admixtures on water absorption of SCCs at w/b ratio of 0.32

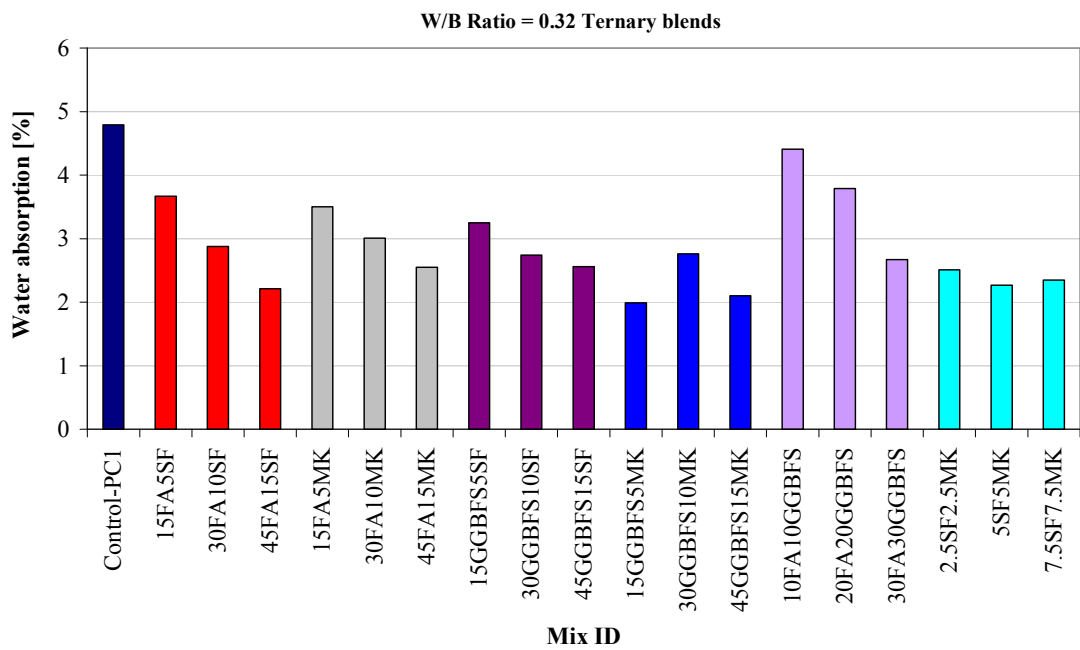


Figure 4.81 Ternary effects of mineral admixtures on water absorption of SCCs at w/b ratio of 0.32

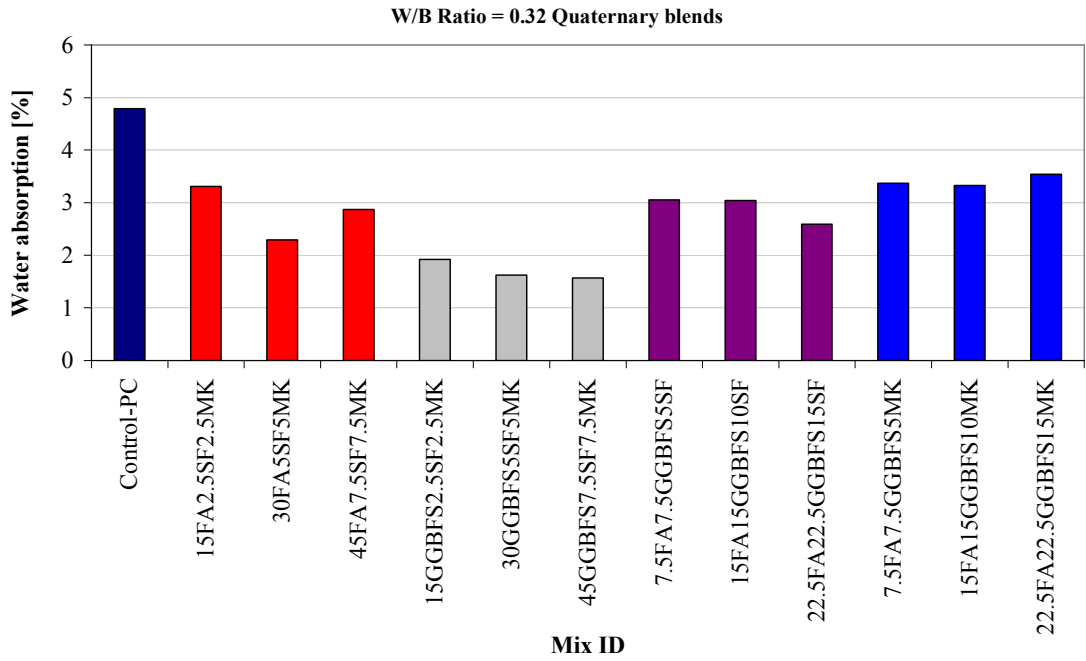


Figure 4.82 Quaternary effects of mineral admixtures on water absorption of SCCs at w/b ratio of 0.32

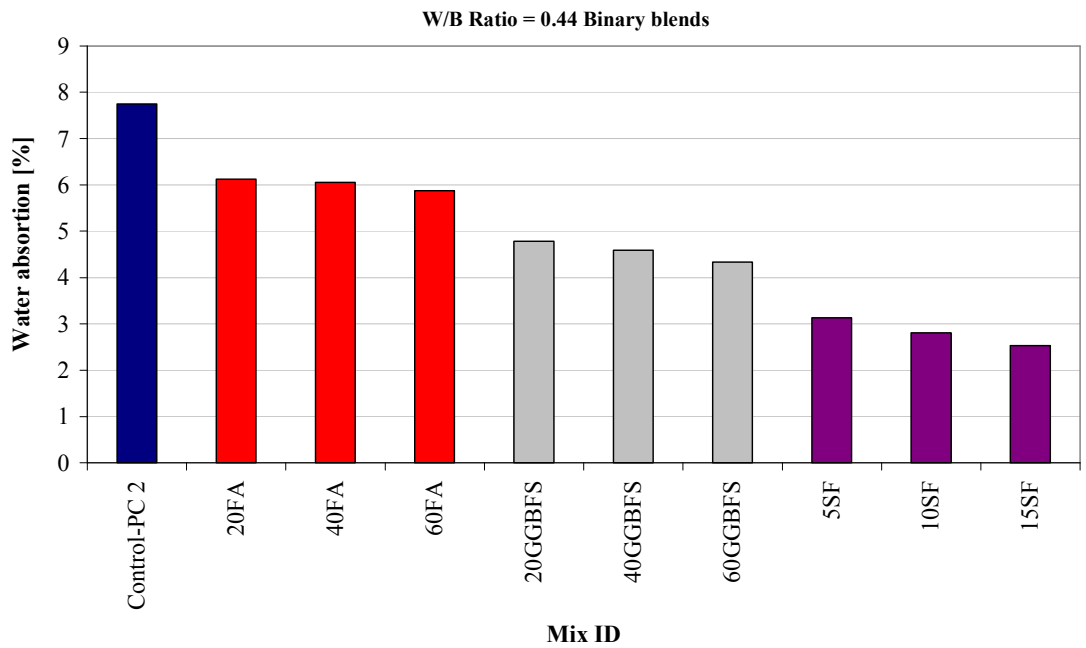


Figure 4.83 Binary effects of mineral admixtures on water absorption of SCCs at w/b ratio of 0.44

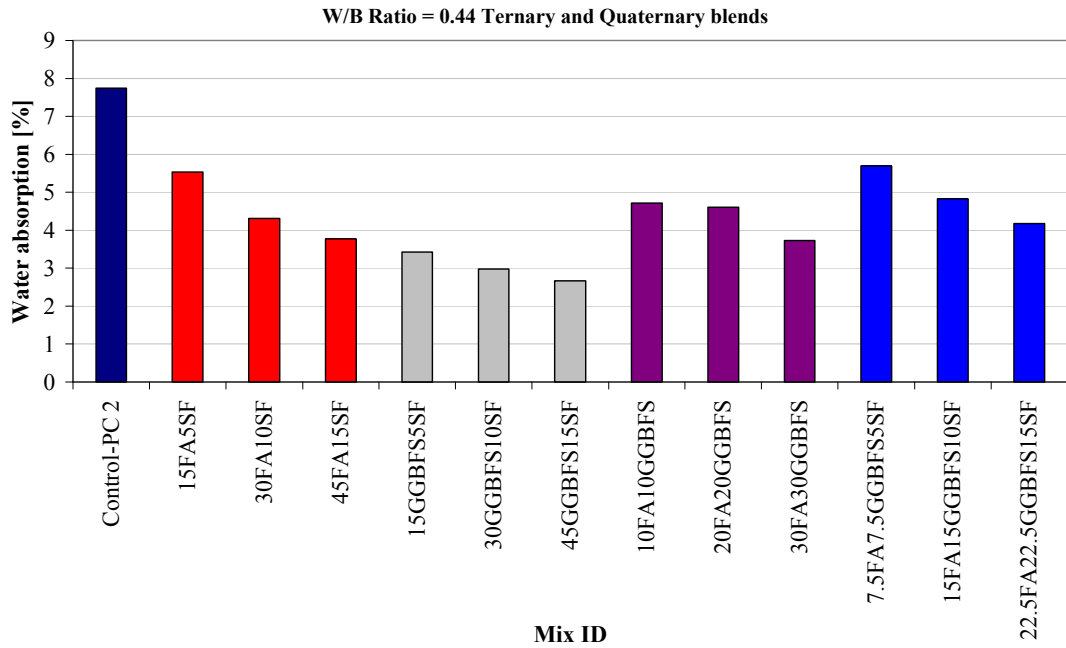


Figure 4.84 Ternary and quaternary effects of mineral admixtures on water absorption of SCCs at w/b ratio of 0.44

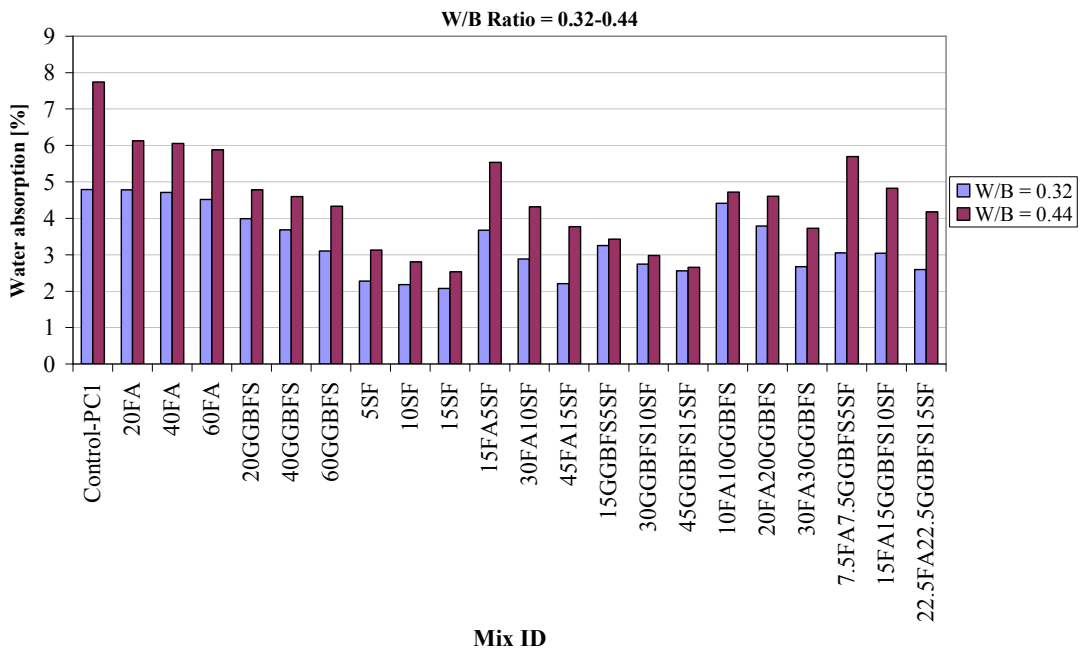


Figure 4.85 Comparison of the water absorption of SCCs at different w/b ratios

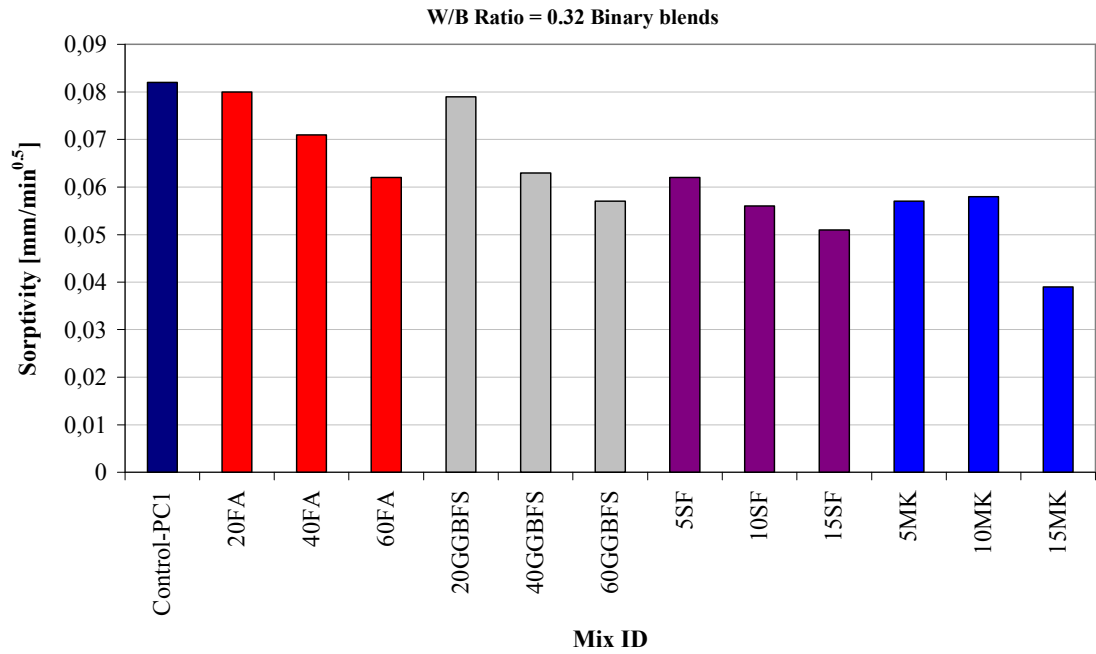


Figure 4.86 Binary effects of mineral admixtures on water sorptivity of SCCs at w/b ratio of 0.32

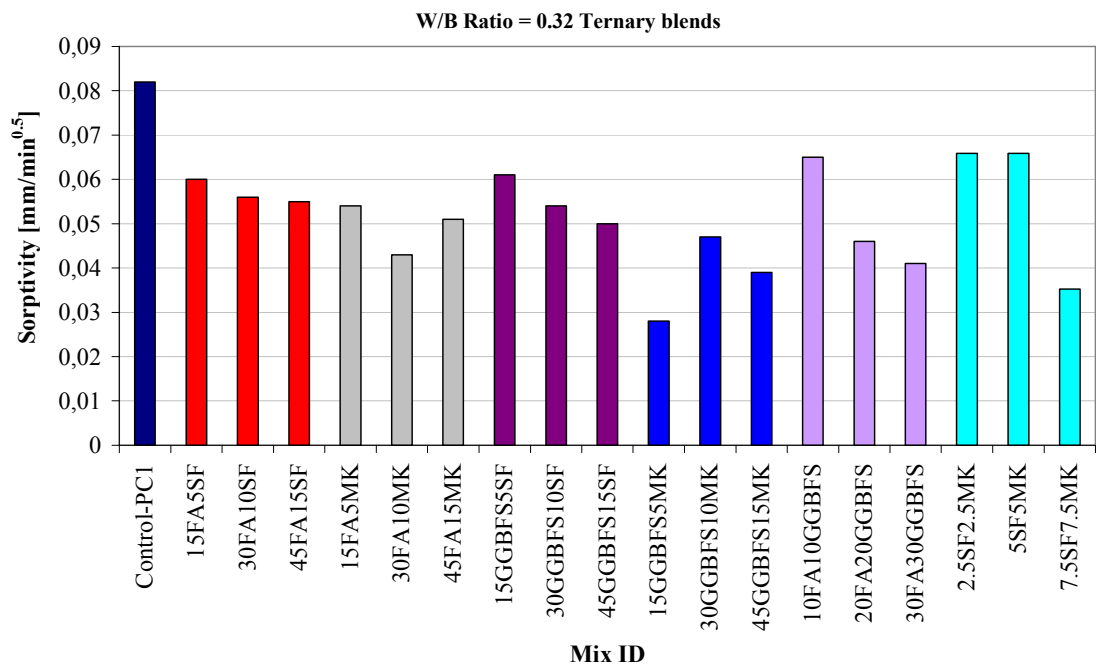


Figure 4.87 Ternary effects of mineral admixtures on water sorptivity of SCCs at w/b ratio of 0.32

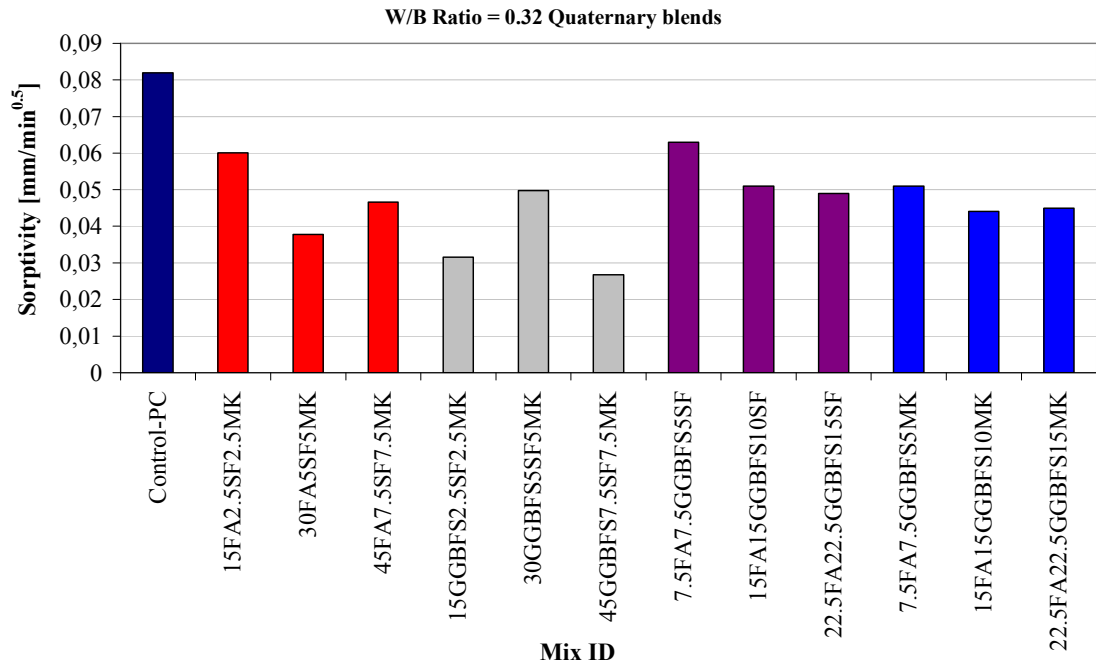


Figure 4.88 Quaternary effects of mineral admixtures on water sorptivity of SCCs at w/b ratio of 0.32

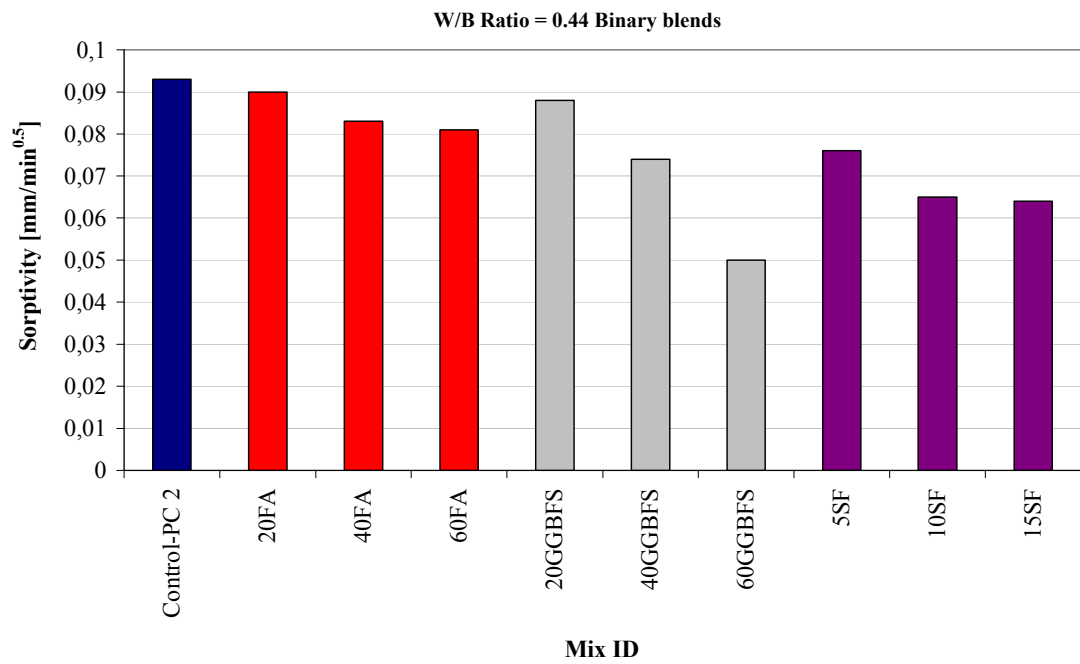


Figure 4.89 Binary effects of mineral admixtures on water sorptivity of SCCs at w/b ratio of 0.44

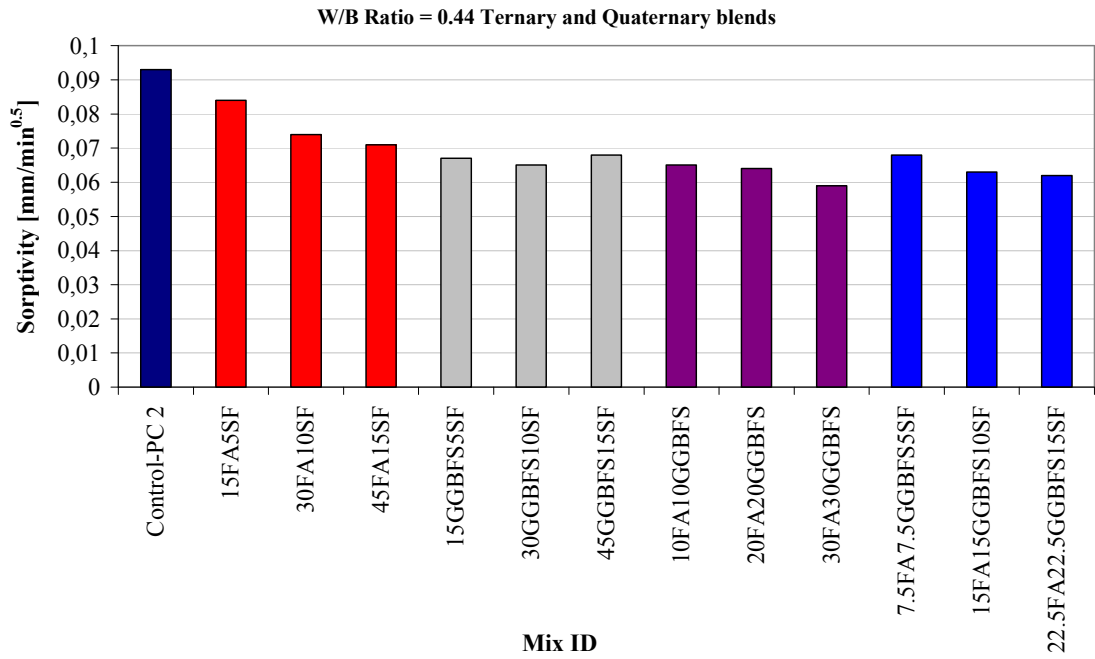


Figure 4.90 Ternary and quaternary effects of mineral admixtures on water sorptivity of SCCs at w/b ratio of 0.44

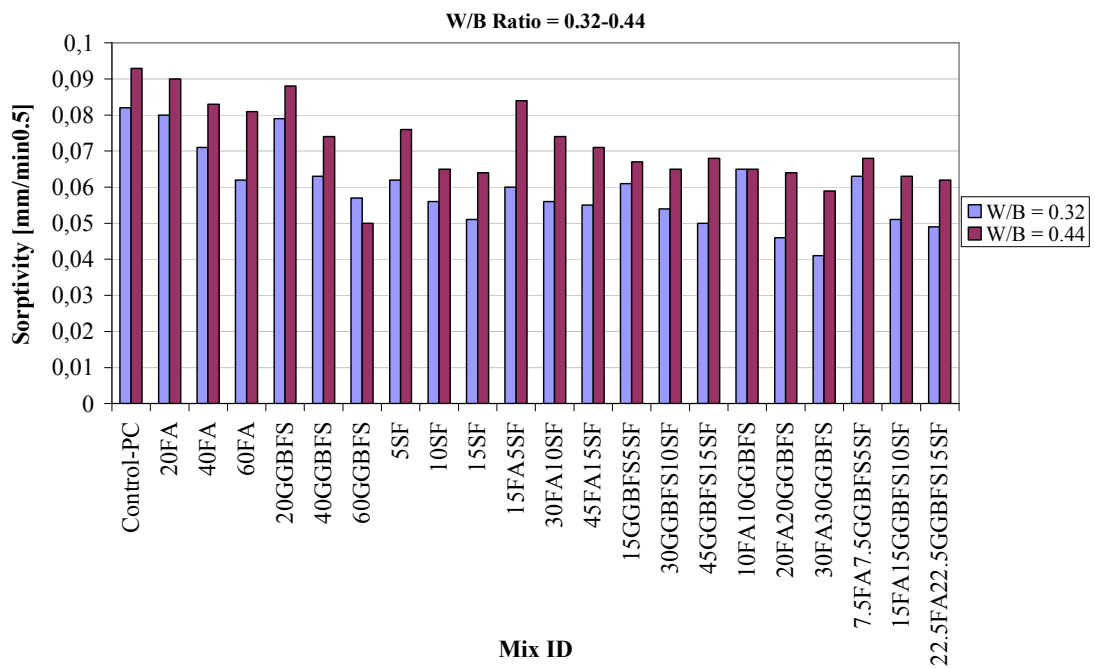


Figure 4.91 Comparison of the water sorptivity of SCCs at different w/b ratios

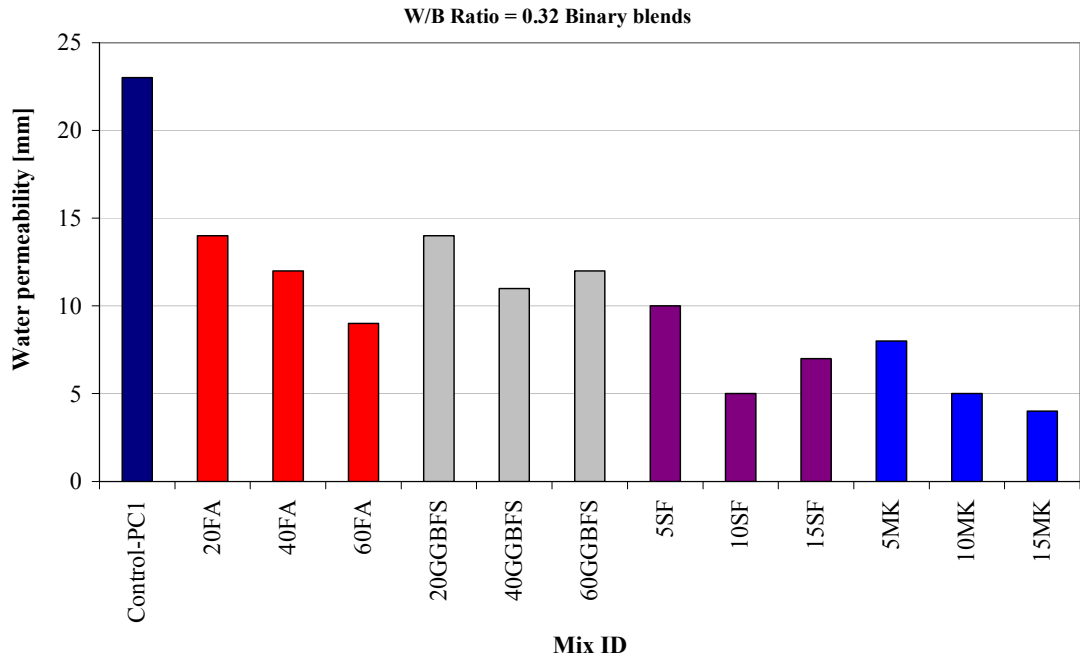


Figure 4.92 Binary effects of mineral admixtures on water permeability of SCCs at w/b ratio of 0.32

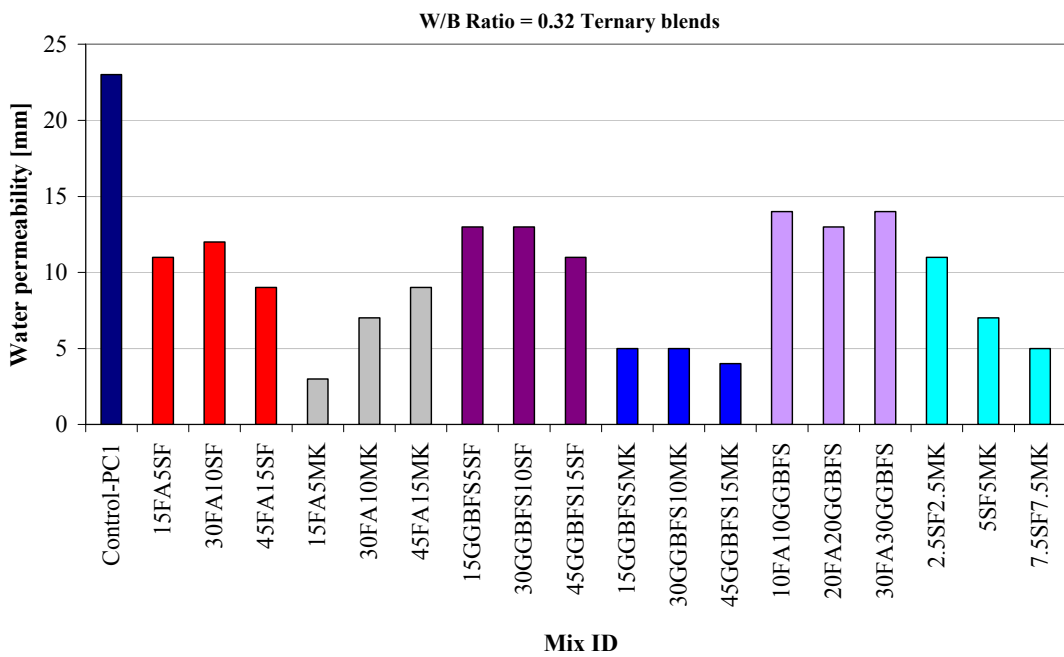


Figure 4.93 Ternary effects of mineral admixtures on water permeability of SCCs at w/b ratio of 0.32

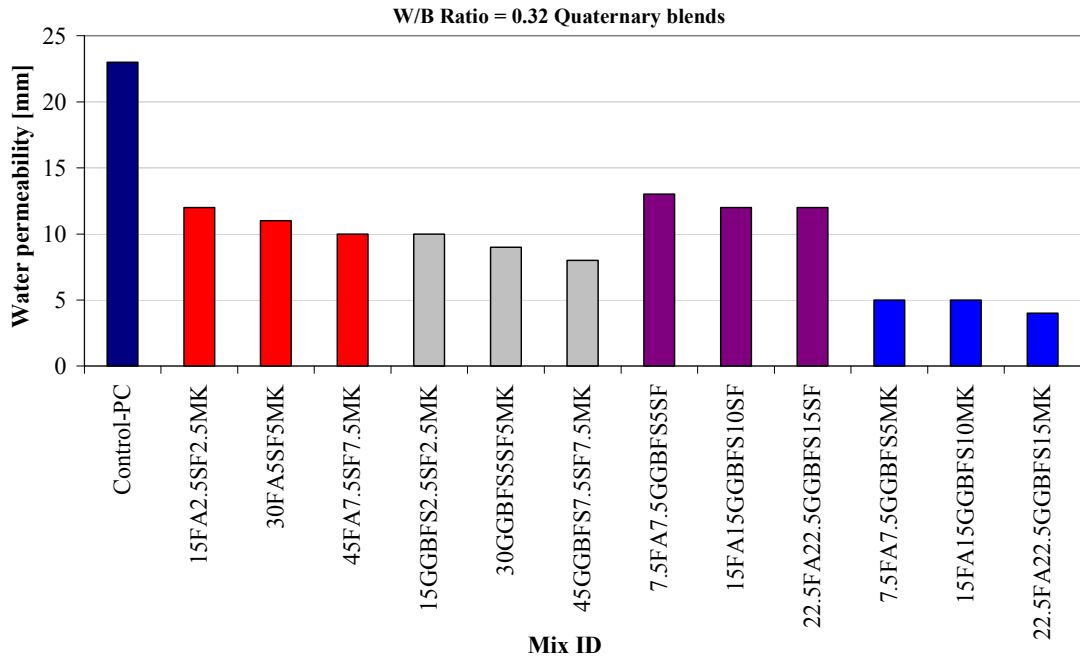


Figure 4.94 Quaternary effects of mineral admixtures on water permeability of SCCs at w/b ratio of 0.32

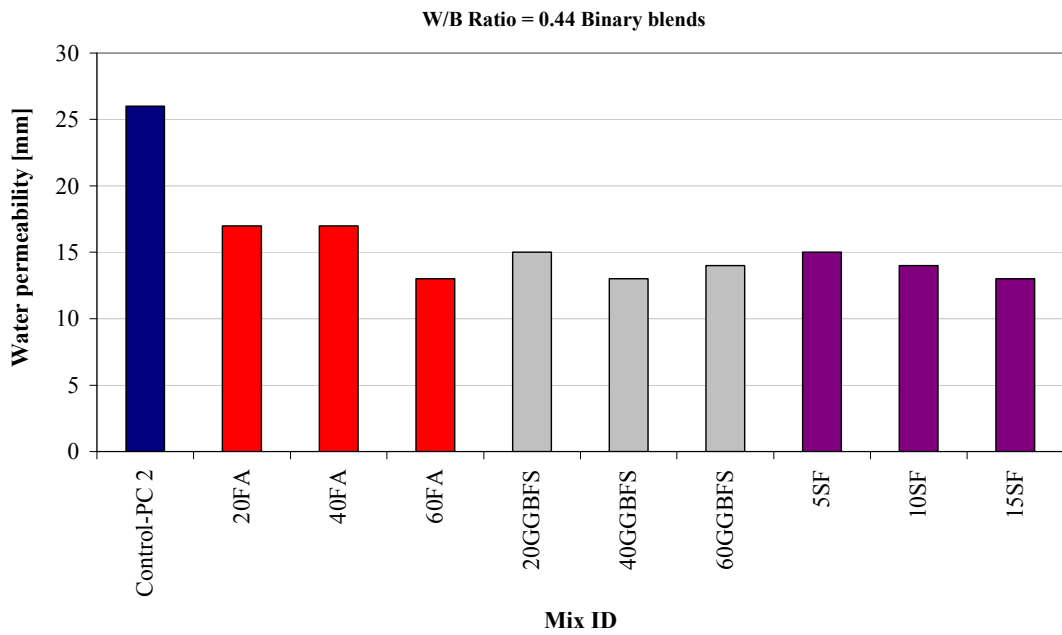


Figure 4.95 Binary effects of mineral admixtures on water permeability of SCCs at w/b ratio of 0.44

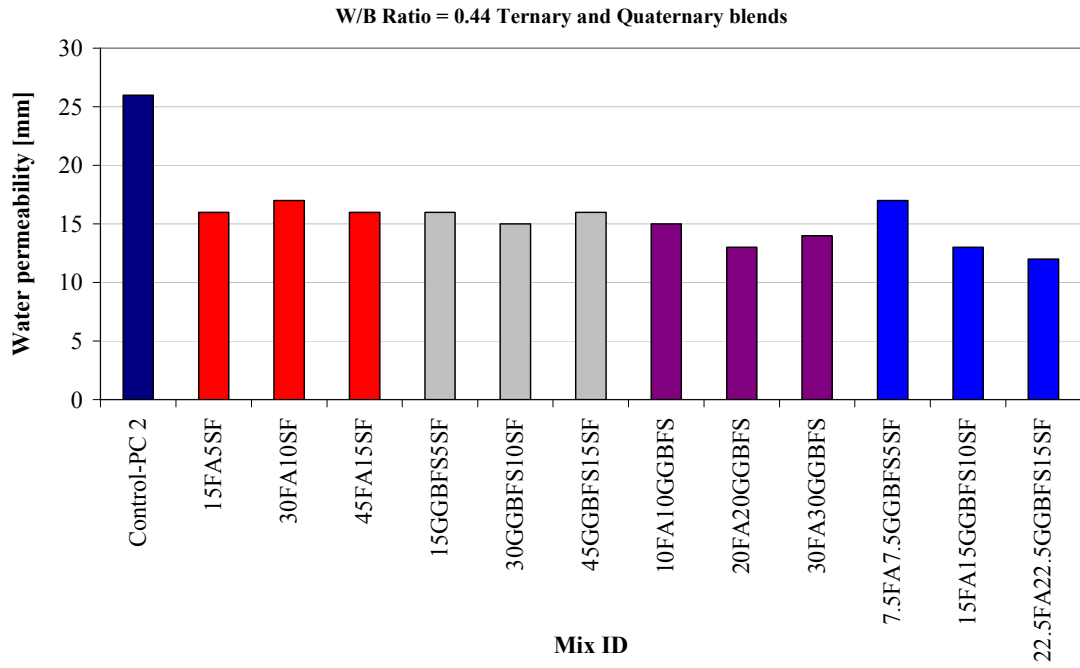


Figure 4.96 Ternary and quaternary effects of mineral admixtures on water permeability of SCCs at w/b ratio of 0.44

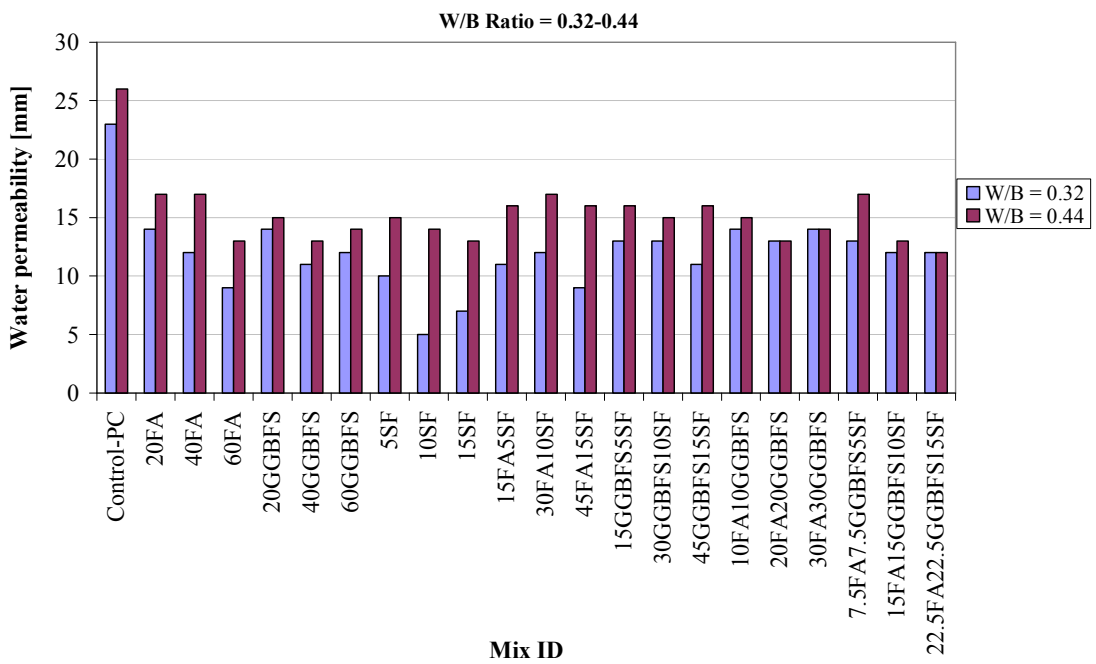


Figure 4.97 Comparison of the water permeability of SCCs at different w/b ratios

4.5 Correlations between Properties of SCCs

4.5.1 Correlations between fresh properties of SCCs

To identify any possible correlation between the fresh properties of SCCs, the correlation coefficients (R) between any of the two fresh tests were calculated and presented in Figures 4.98 to 4.100. The closer the correlation coefficient is to one, the more the points will fall along a line stretching from the lower left to the upper right. The closer the correlation coefficient is to negative one, the more the points will fall along a line stretching from the upper left to the lower right. The closer the correlation coefficient is to zero, the less the points fall on a straight line. For obtaining viscosity related relationship between the T_{50} slump flow time, V-funnel flow time and L-box H_2/H_1 ratio, viscosity values at five revolutions per minute was used.

T_{50} slump flow time value describes the flowability of a fresh mixture in unconfined conditions. Visual observations during the measurement of the T_{50} time can give additional information on the segregation resistance, uniformity of each delivery and viscosity of concrete. Viscosity of SCCs can be assessed by the T_{50} slump flow time during the slump-flow test or assessed by the V-funnel flow time. For this, the durations obtained from both slump flow and V-funnel flow do not measure the viscosity of SCC directly but they are related to it by describing the rate of flow. Concrete with a low viscosity will have a very quick initial flow and then stop. Concrete with a high viscosity, on the other hand, may continue to creep forward over an extended time (EFNARC, 2002). Therefore, in order to estimate the relations among the T_{50} slump flow time, V-funnel flow time, and viscosity at 5 rpm, linear regressions were applied to the test results measured in the experimental stage of this work. Linear regression made for 65 observations between the T_{50} slump flow time and V-funnel flow time gave a correlation coefficient (R) of 0.76 as shown in Figure 4.98. As seen from the Figure 4.98 that increasing the T_{50} slump flow time extended the V-funnel flow time of SCCs gradually.

As mentioned earlier, T_{50} slump flow and V-funnel flow times do not directly measure the viscosity of SCCs but they may give an idea about the flow rate of SCCs. Figures 4.99 and 4.100 showed linear relationships between the T_{50} slump

flow time versus viscosity and V-funnel flow time versus viscosity, respectively. Almost the same correlation coefficients were obtained between those properties and viscosity. It was observed in the figures that increasing both T_{50} and V-funnel flow times increased the viscosity of concretes.

4.5.2 Correlations between mechanical properties of SCCs

The broad relationships among the mechanical properties of concrete are well known but there are no agreements on the precise form of the relation. In this part of the study, the relationships among the compressive strength, splitting tensile strength and ultrasonic pulse velocity were explored on the experimental test results of study. The regression results among these properties are depicted in Figures 4.101 to 4.103. Figure 4.101 shows the relationship between the compressive strength and splitting tensile strength of the SCCs. It can be concluded from the figure that these two mechanical properties are highly correlated to each other. As expected, increasing the compressive strength increased the splitting tensile strength of SCCs. Compressive strength and ultrasonic pulse velocity relation was presented in Figure 4.102, the correlation coefficient being 0.81. The lowest relation among the mechanical properties was observed between the splitting tensile strength and ultrasonic pulse velocity with correlation coefficient (R) of 0.71 as seen in Figure 4.103.

4.5.3 Correlation between chloride ion permeability and electrical resistivity

It is generally agreed that the ingress of chloride ions into concrete leads, in many structures, to long-term deterioration. In other words, the chloride permeability of the concrete is one such intrinsic property of the concrete that needs to be assessed independently, especially in the design and construction of structures to be built in a salt-laden environment. When the chloride concentration of concrete exceeds a certain threshold value, depassivation of the steel occurs and reinforcing steel starts to corrode (Thomas, 1996; Alonso et al., 2000). From theoretical and experimental work there appears to be a correlation between concrete resistivity and chloride ion permeability. In general, the chloride ion permeability of concrete is inversely

proportional to the concrete electrical resistivity. Within a particular structure, more permeable zones will have a comparatively lower resistivity and higher chloride ion penetration (Polder and Peelen, 2002). A relation in the form of power function between the electrical resistivity and chloride ion permeability was determined by curve fitting on the 65 test results and given in the Figure 4.104. There is a strong relationship with correlation coefficient of 0.87 between these two tests.

4.5.4 Correlations between permeation properties

Theoretically, the main factors that control the permeation properties of concrete materials are the relative volume of paste matrix, the pore structure of the bulk matrix and the interfacial zone around the aggregate particles. It is thought that due to the enhanced stability of the fresh mixture and/or the use of additional fine mineral admixtures, together with the elimination of vibration, SCC mixes should have more homogeneous microstructures and denser interfacial zones since more efficient packing and less water bleeding and trapping may be expected (Wenzhong and Bartos, 2003). Water absorption, water sorptivity and water permeability tests are based on the measuring the ingress of water to the capillary pores of an unsaturated concrete. These three tests are much related to each others. The relationship among these permeation tests were investigated in this part on the 65 SCCs mixtures. As seen in Figures 4.105 to 4.107, the curve fitting applied on the tests results provided very similar correlations with quite high coefficients among such properties of the concretes. As seen in Figures 4.105 to 4.107, the highest correlation coefficient of 0.80 among the permeation tests was observed between the water absorption and water sorptivity. Correlation coefficients of water sorptivity-water permeability and water absorption-water permeability were 0.76 and 0.75, respectively.

4.5.5 Correlations between electrical and permeation properties

In this part of the thesis, correlations among the electrical properties such as chloride ion permeability and electrical resistivity, and water permeation properties such as water absorption, water sorptivity and water permeability were investigated. It is generally accepted that the durability of concrete is related to the characteristics of its

pore structure. Degradation mechanisms of concrete often depend on the way potentially aggressive substances can penetrate into the concrete, possibly causing damage. The permeability of the concrete is depending on the porosity, and on the connectivity of the pores. The more open the pore structure of the concrete, the more vulnerable the material is to degradation mechanisms caused by penetrating substances (Schutter and Audenaert, 2004).

Torii and Kavamura (1994) stated that the water permeability test data may not be used to predict the concrete resistance to the chloride-ion penetration and vice versa. The discrepancy may be related to the different transport mechanisms involved in the water permeability test and the chloride penetration tests. Schutter and Audenaert (2004) established a weak correlation between water absorption by immersion and chloride migration. They concluded that no significant correlation exist between water absorption and chloride migration (R was about 0.45). Schutter and Audenaert (2004), finally, concluded that the water absorption by immersion is not a reliable parameter for the estimation of concrete durability issue like chloride migration. The water absorption by immersion until saturation gives an estimation of the total pore volume of the concrete, but gives no accurate indication on the concrete permeability, which is more important with regard to chloride migration.

Contrary to the abovementioned references, better correlations are obtained among the chloride ion permeability and water permeation properties. Obtained correlations are depicted in Figures 4.108 to 4.110. As can be seen in Figure 4.108 that the significant correlation exists between chloride ion permeability and water absorption ($R = 0.82$). The correlation coefficients between chloride ion permeability-water sorptivity and chloride ion permeability-water permeability were 0.78 and 0.73, respectively (Figures 4.109 and 4.110). As also known from Figures 4.105 to 4.107, the relations among permeations properties had high correlation coefficients. These results showed that chloride ion permeability and permeation properties (water absorption, water sorptivity and water permeability) appeared to be closely related properties.

The electrical resistivity of concrete is known to be sensitive to the degree of saturation (Lopez and Gonzalez, 1993) and to chloride variations in concrete (Saleem et al., 1996). Since concrete is an artificial rock, Archie's law may be used to

describe the dependence of its electrical resistivity on water content, porosity and pore solution salinity

$$\rho = a\phi^{-m}S^{-n}\rho_w \quad (4.1)$$

As presented above, Archie's law is an empirical power law involving the electrical resistivity of the concrete ρ , the concrete porosity ϕ , the degree of saturation S , the electrical resistivity of the pore solution ρ_w , and parameters (a, m, n) computed by regression on experimental data (Sbartai et al., 2007). As it mentioned earlier the main factors that control the permeation properties of concrete materials are the relative volume of paste matrix, the pore structure of the bulk matrix, and the interfacial zone around the aggregate particles so as stated by Sbartai et al, there is a relation among the electrical resistivity and permeation properties of concretes. Figures 4.111 to 4.113 present the correlations among the electrical resistivity and water permeation properties of produced 65 SCC mixtures. As for the chloride ion permeability, the relationships among electrical resistivity and water permeation properties exhibited quite high correlation coefficients. The electrical resistivity versus water sorptivity, water absorption, and depth of pressurized water penetration were 0.81, 0.79 and 0.76, respectively.

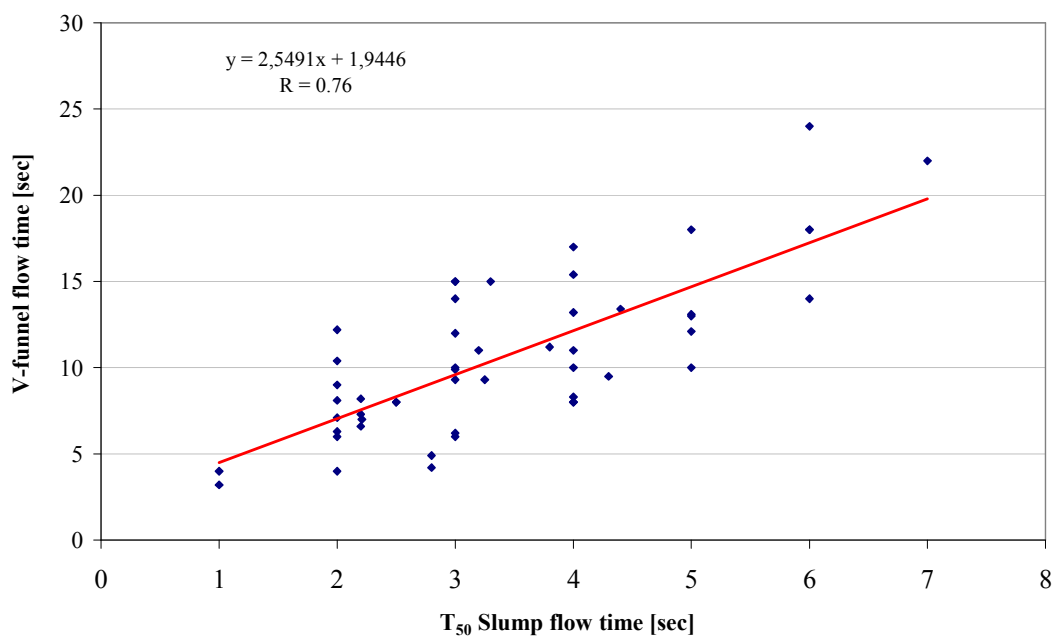


Figure 4.98 Correlation between T₅₀ slump flow time and V-funnel flow time

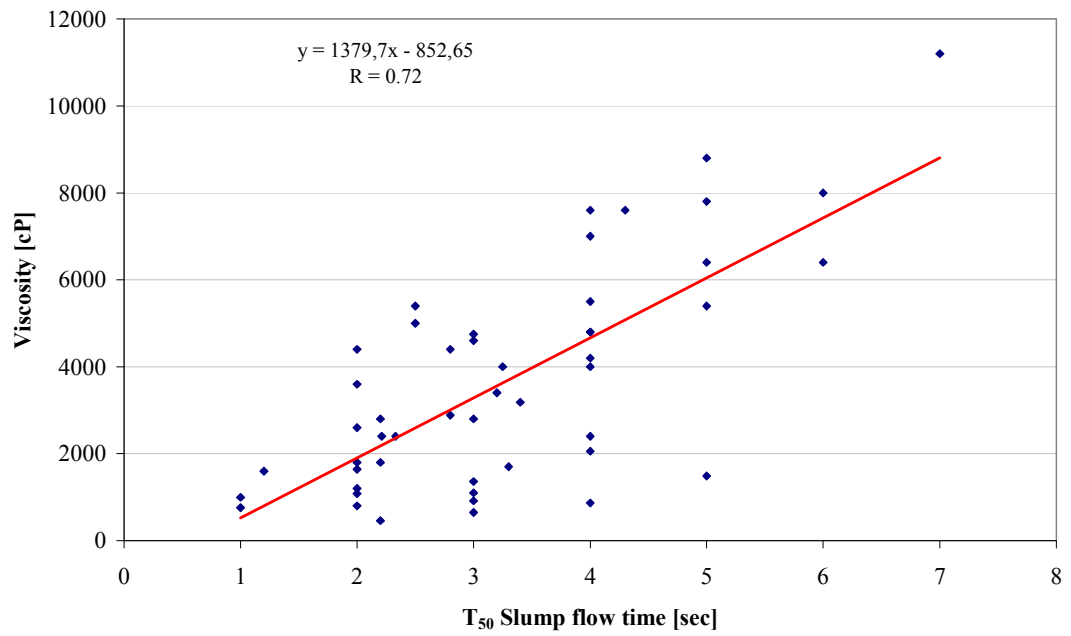


Figure 4.99 Correlation between T₅₀ slump flow time and viscosity at 5 rpm

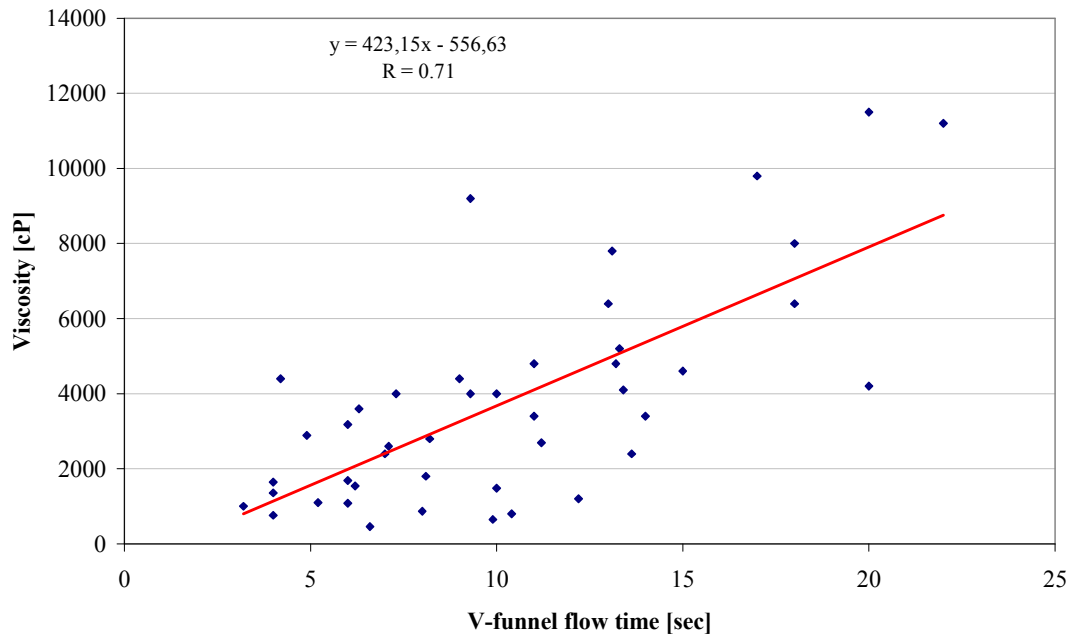


Figure 4.100 Correlation between V-funnel flow time and viscosity at 5 rpm

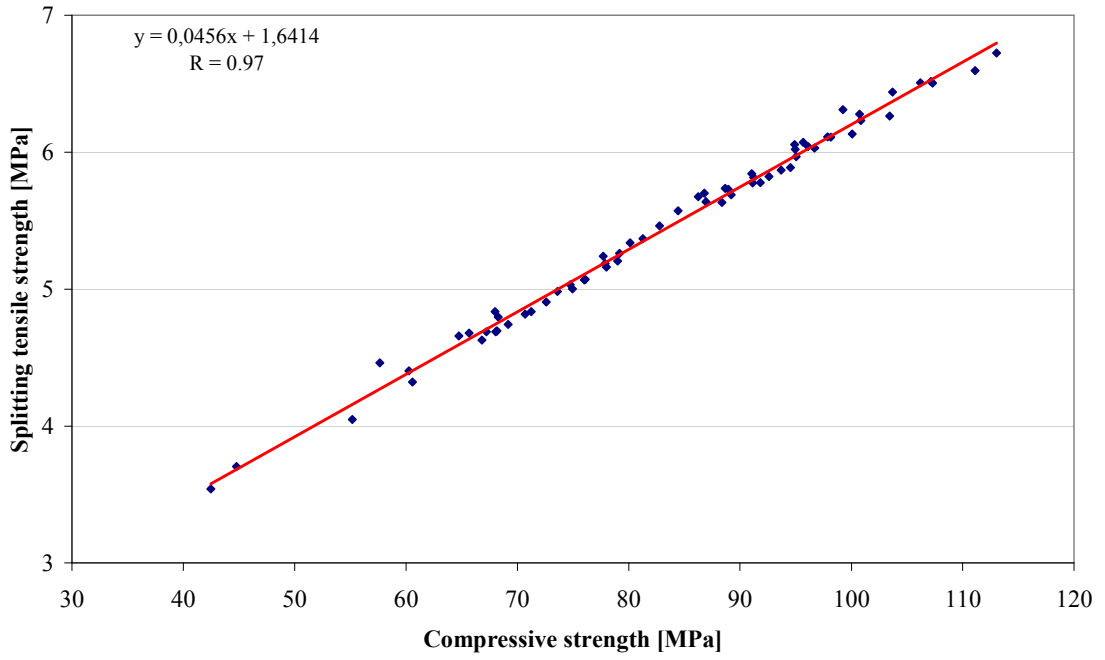


Figure 4.101 Correlation between compressive and splitting tensile strengths at 90 days

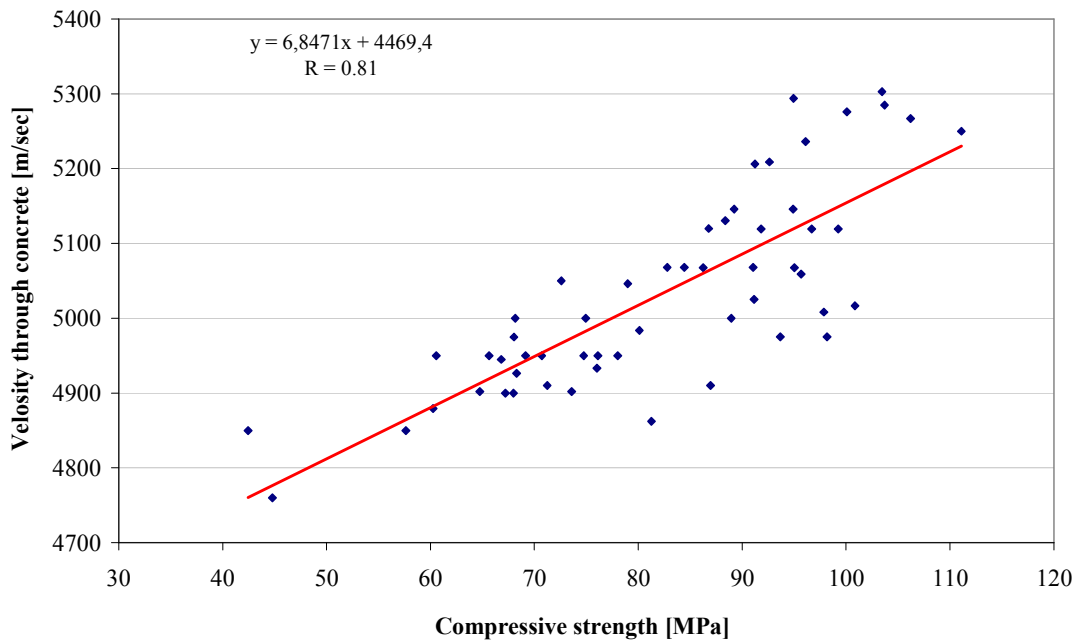


Figure 4.102 Correlation between compressive strength and ultrasonic pulse velocity at 90 days

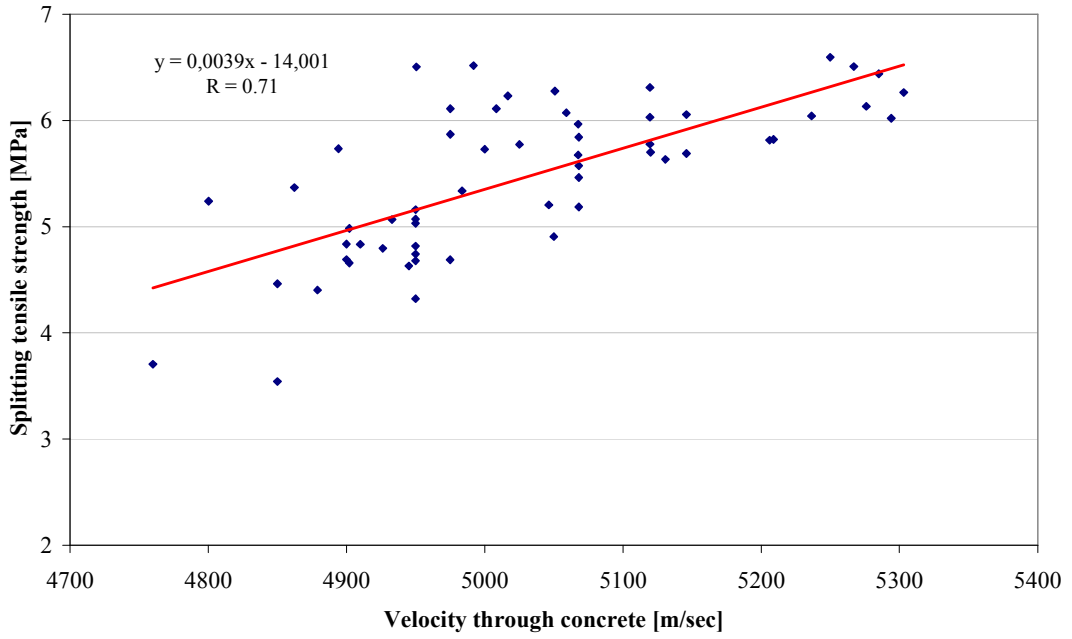


Figure 4.103 Correlation between ultrasonic pulse velocity and splitting tensile strength at 90 days

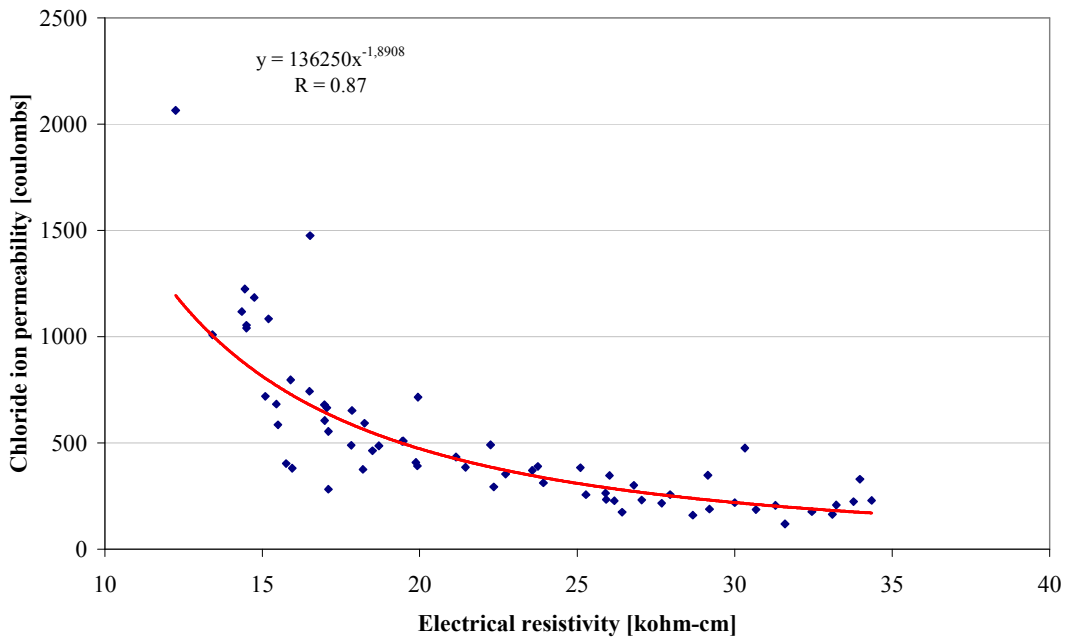


Figure 4.104 Correlation between electrical resistivity and chloride ion permeability

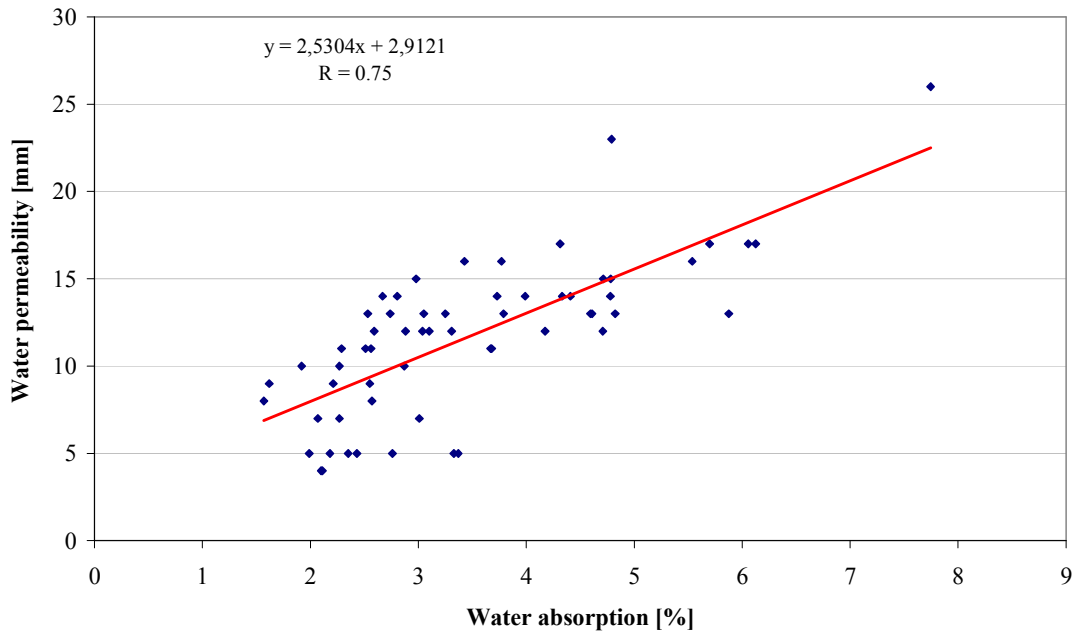


Figure 4.105 Correlation between water absorption and water permeability

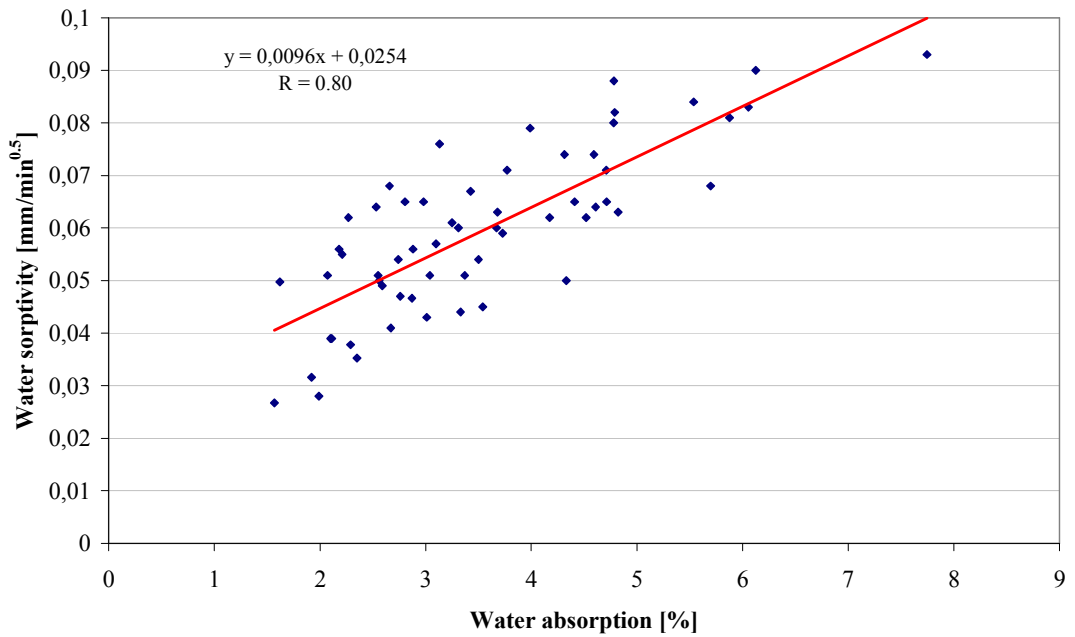


Figure 4.106 Correlation between water absorption and water sorptivity

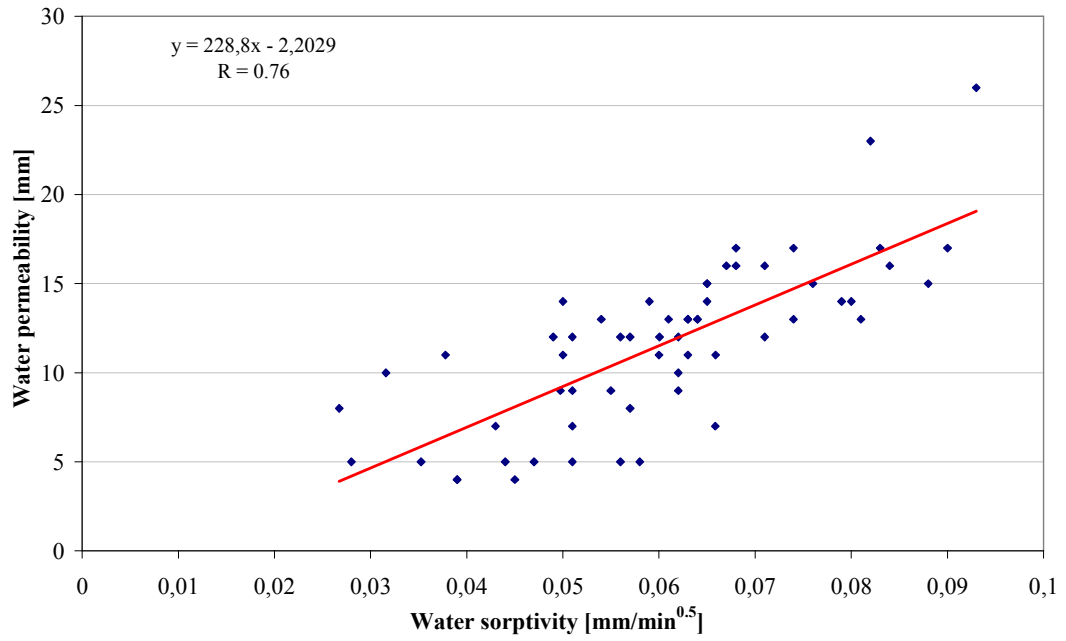


Figure 4.107 Correlation between water sorptivity and water permeability

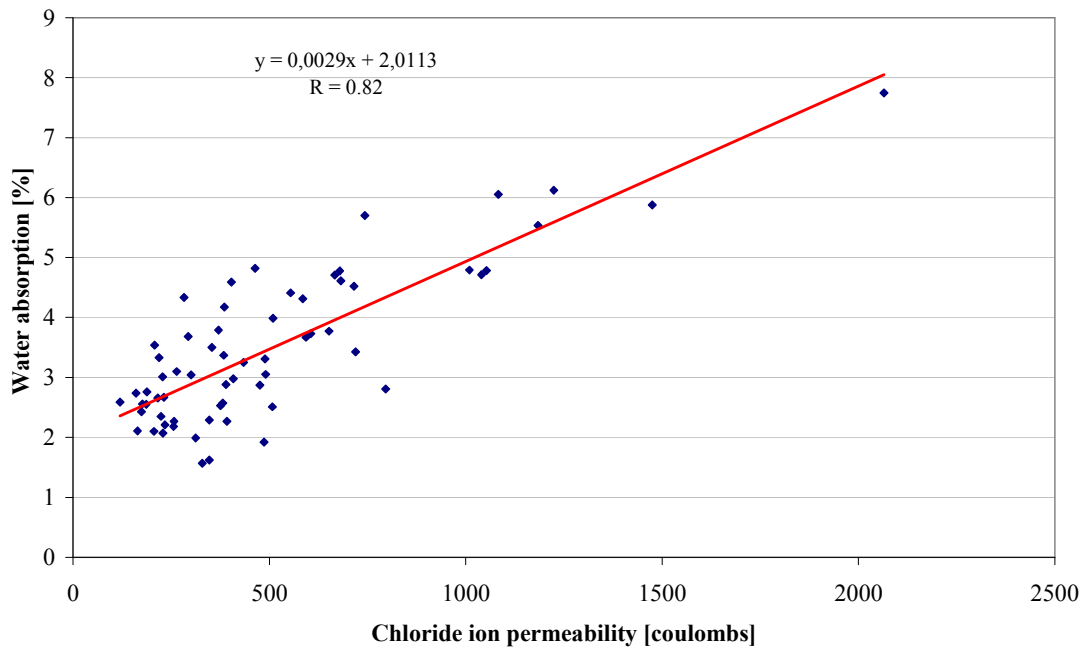


Figure 4.108 Correlation between chloride ion permeability and water absorption

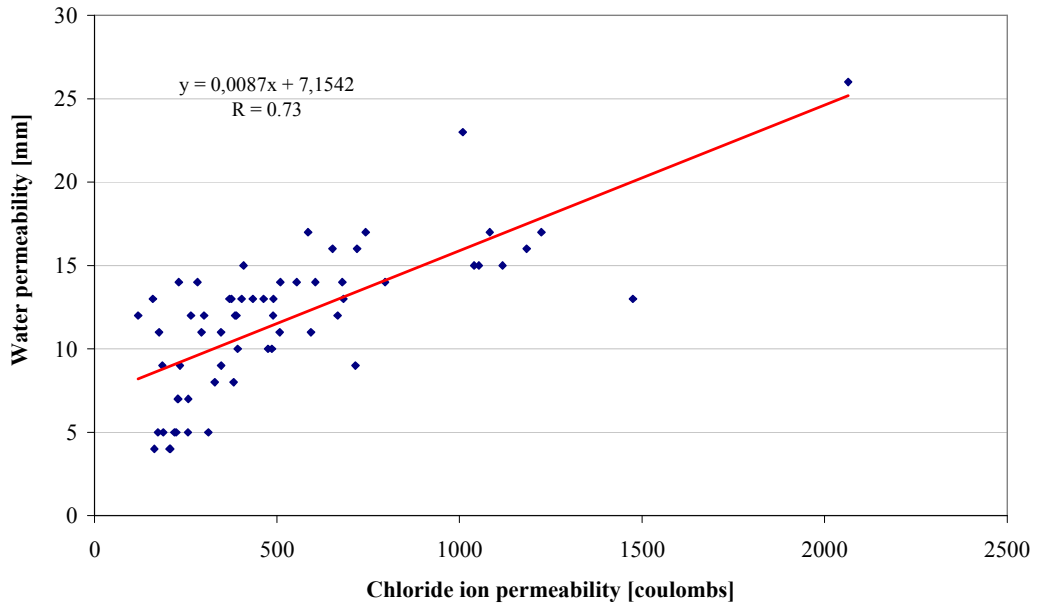


Figure 4.109 Correlation between chloride ion permeability and water permeability

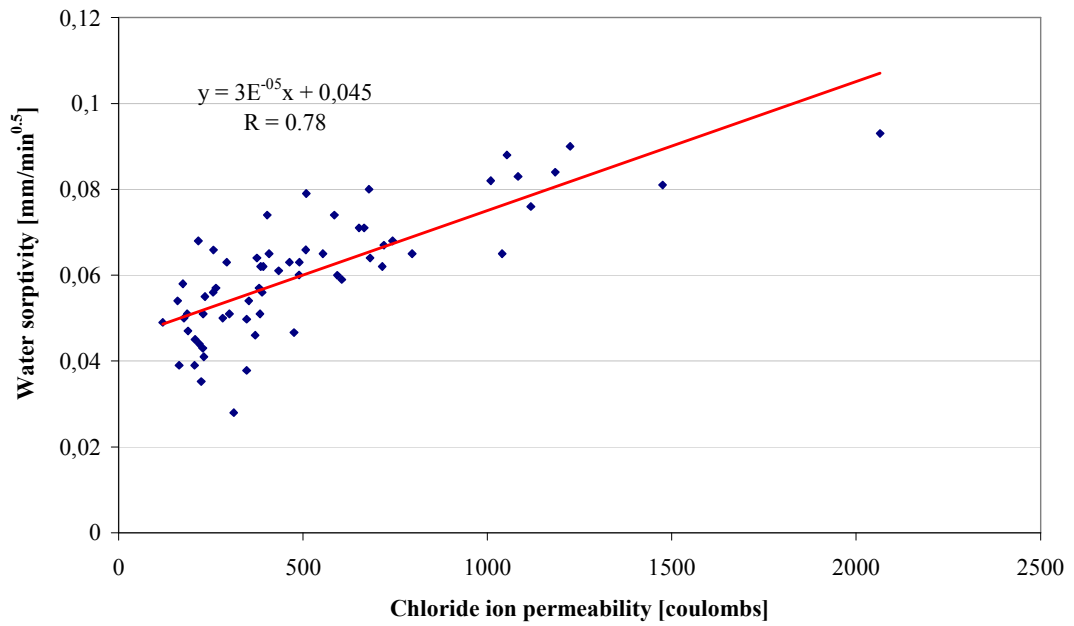


Figure 4.110 Correlation between chloride ion permeability and water sorptivity

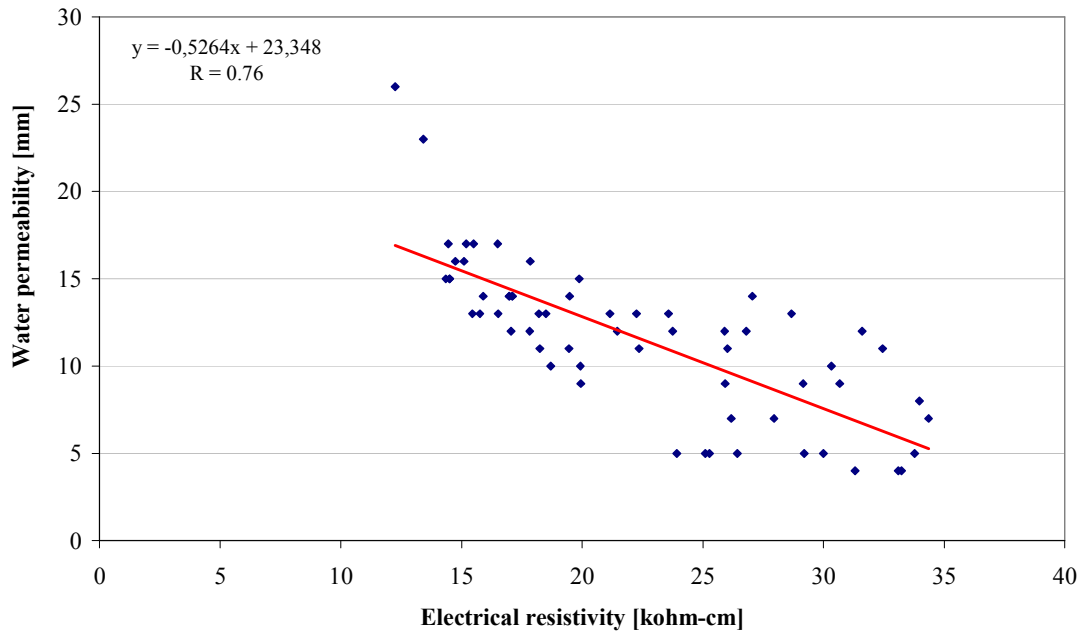


Figure 4.111 Correlation between electrical resistivity and water permeability

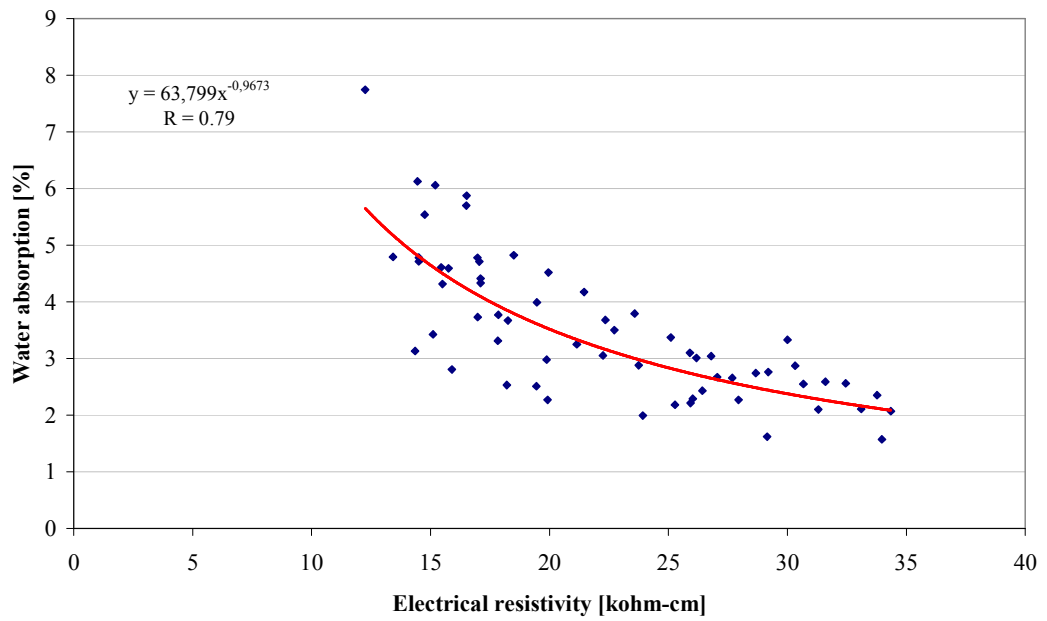


Figure 4.112 Correlation between electrical resistivity and water absorption

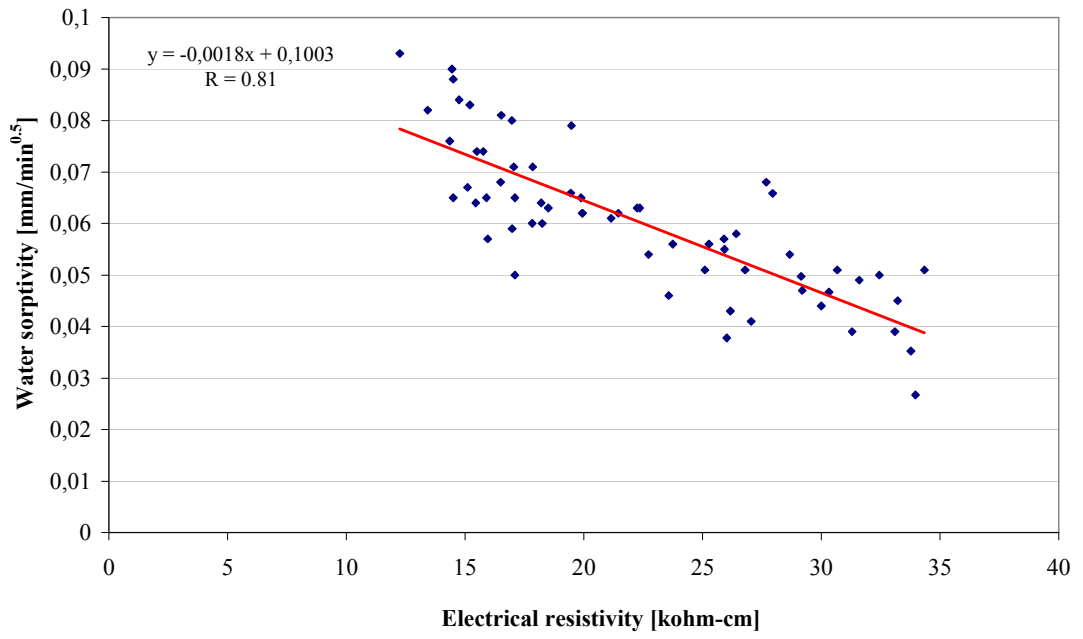


Figure 4.113 Correlation between electrical resistivity and water sorptivity

5. PREDICTION OF SELF COMPACTING CONCRETE PROPERTIES BY SOFT COMPUTING TECHNIQUES

5.1 Soft Computing Techniques

According to Zadeh (1994) ‘soft computing is a collection of methodologies that aim to exploit the tolerance for imprecision and uncertainty to achieve tractability, robustness, and low solution cost. Its principal constituents are fuzzy logic, neurocomputing, and probabilistic reasoning. Soft computing is likely to play an increasingly important role in many application areas, including software engineering. The role model for soft computing is the human mind. The fuzzy logic, genetic algorithm, genetic programming, neural network can be accepted as the main techniques of soft computing. In this thesis two of them namely neural network and genetic programming were used for prediction and to obtain explicit formulations for properties of self compacting concretes. The background of both techniques will be explained briefly in the following parts of the manuscript.

5.2 An Overview of Artificial Neural Networks

5.2.1 General

An Artificial Neural Network (ANN) is an information processing paradigm that is inspired by the way biological nervous systems, such as the brain, process information. The key element of this paradigm is the novel structure of the information processing system. It is composed of a large number of highly interconnected processing elements (neurons) working in unison to solve specific problems. ANNs, like people, learn by example. An ANN is configured for a specific application, such as pattern recognition or data classification, through a learning process. Learning in biological systems involves adjustments to the synaptic connections that exist between the neurons.

Artificial neural network (ANN) models may be used as an alternative method in engineering analysis and predictions. ANNs mimic somewhat the learning process of a human brain. They operate requiring no detailed information about the system. Instead, they learn the relationship between the input parameters and the controlled and uncontrolled variables by studying previously recorded data. ANNs have ability to handle large and complex systems with many interrelated parameters. They seem simply to ignore excess data that are of minimal significance and concentrate instead on the more important inputs (Kalogirou, 1999).

5.2.2 Artificial neural networks

Artificial neural networks are computational systems that simulate the microstructure (neurons) of a biological nervous system. The most basic components of ANNs are modeled after the structure of the brain, and therefore even the terminology is borrowed from neuroscience. It is necessary to give a fundamental description of natural nerve system (Zhang and Friedrich, 2003). A biological neuron is shown in Figure 5.1. The power of the brain comes from the numbers of these basic components and the multiple connections between them. All natural neurons have four basic components, which are dendrites, soma, axons, and synapses. In the brain, there is a flow of coded information (using electrochemical media, the so-called neurotransmitters) from the synapses towards the axon. The axon of each neuron transmits information to a number of other neurons. The neuron receives information at the synapses from a large number of other neurons. It is estimated that each neuron may receive stimuli from as many as 10,000 other neurons. Groups of neurons are organized into subsystems and the integration of these subsystems forms the brain. It is estimated that the human brain has got around 100 billion interconnected neurons (Kalogirou, 1999).

Inspired by biological neurons, ANNs are composed of simple elements operating in parallel, i.e. ANNs are the simple clustering of the primitive artificial neurons. This clustering occurs by creating layers, which are then connected to one another. How these layers connect may also vary. Basically, all ANNs have a similar topological structure. Some of the neurons interface with the real world to receive its input, and the other neurons provide the real world with the network's output. All the rest of the

neurons are hidden from view. As in nature, the network function is determined largely by the interconnections between neurons, which are not simple connections, but some non-linear functions. Each input to a neuron has a weight factor of the function that determines the strength of the interconnection, and thus the contribution of that interconnection to the following neurons. ANNs can be trained to perform a particular function by adjusting the values of these weight factors between the neurons, either by the information from outside the network or by the neurons themselves in response to the input. This is the key to the ability of ANNs to achieve learning and memory (Zhang and Friedrich, 2003).

Artificial neural networks (ANN) have been developed as generalizations of mathematical models of biological nervous systems. A first wave of interest in neural networks (also known as connectionist models or parallel distributed processing) emerged after the introduction of simplified neurons by McCulloch and Pitts (1943). The basic processing elements of neural networks are called artificial neurons, or simply neurons or nodes. In a simplified mathematical model of the neuron, the effects of the synapses are represented by connection weights that modulate the effect of the associated input signals, and the nonlinear characteristic exhibited by neurons is represented by a transfer function. The neuron impulse is then computed as the weighted sum of the input signals, transformed by the transfer function. The learning capability of an artificial neuron is achieved by adjusting the weights in accordance to the chosen learning algorithm.

Figure 5.2 shows a highly simplified model of an artificial neuron, which may be used to simulate some important aspects of the real biological neuron. An ANN is a group of interconnected artificial neurons, interacting with one another in a concerted manner. In such a system, excitation is applied to the input of the network. Following some suitable operation, it results in a desired output. At the synapses, there is an accumulation of some potential, which in the case of the artificial neurons, is modeled as a connection weight. These weights are continuously modified, based on suitable learning rules.

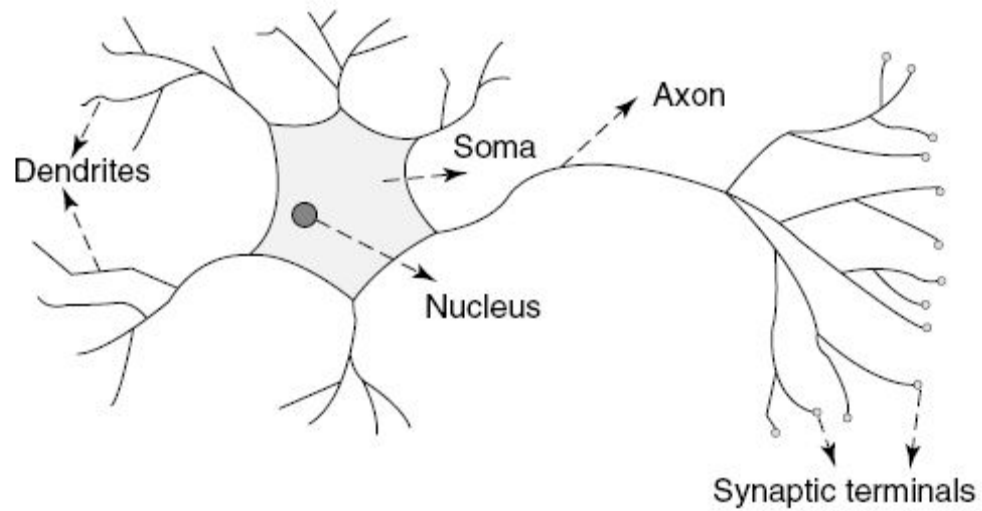


Figure 5.1 A simplified model of a biological neuron

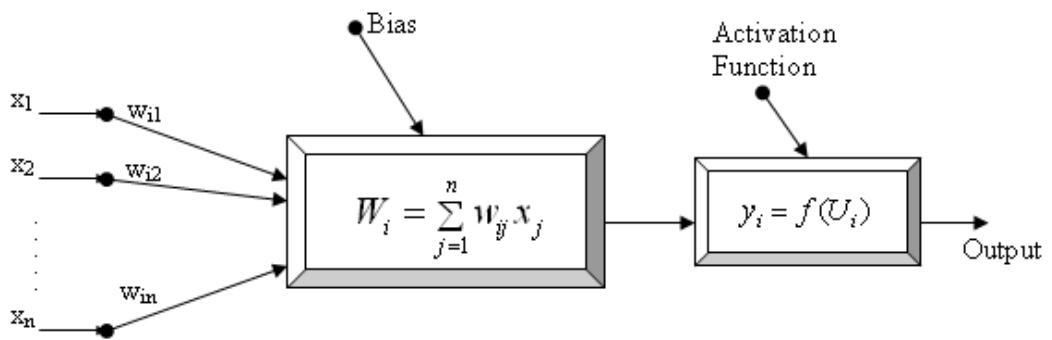


Figure 5.2 Basic elements of an artificial neuron

5.2.3 Artificial neural network principles

According to Haykin (1998), a neural network is a massively parallel distributed processor that has a natural propensity for storing experimental knowledge and making it available for use. It resembles the human brain in two respects; the knowledge is acquired by the network through a learning process, and inter-neuron connection strengths known as synaptic weights are used to store the knowledge.

As seen in Figure 5.3, ANN generally consists of a number of layers: the layer where the input patterns are applied is called the input layer, the layer where the output is obtained is the output layer, and the layers between the input and output layers are

the hidden layer. There may be one or more hidden layers, which are so named because their outputs are not directly observable. The addition of hidden layers enables the network to extract higher-order statistics which are particularly valuable when the size of the input layer is large (Fausett, 1994).

Neurons in each layer are fully or partially interconnected to preceding and subsequent layer neurons with each interconnection having an associated connection strength (or weight). The input signal propagates through the network in a forward direction, on a layer-by-layer basis. These networks are commonly referred to as multilayer perception (Aleksander and Morton, 1990; Fausett, 1994; Skapura, 1996).

The weighted sum of input components as shown in Figure 5.2 can be calculated as in equation.5.1

$$F_j = \sum_{i=1}^n w_{ij} * x_i + b \quad (5.1)$$

where w_{ij} represents the weight coefficient between i^{th} and j^{th} neurons, n is the total number of the input neurons that comes to a cell; b is called the bias and is used to model the threshold. In various ANN models, different activation function has been proposed to process the net input obtained from a sum function which in turn determines the cell output. Activation function is a function that processes the net input obtained from the sum function and determines the cell output. In this thesis, tangent-sigmoid transfer function is employed in the proposed ANN models. The output of the j^{th} neuron after activation can be evaluated by using the equation 5.2:

$$y_i = f(Net_j) = \frac{2}{1 + e^{-2U_i}} - 1 \quad (5.2)$$

The learning capability of an artificial neuron is achieved by adjusting the weights in accordance to the chosen learning algorithm. Most applications of neural networks fall into the following categories (Abraham, 2001):

- **Prediction:** Use input values to predict some output
- **Classification:** Use input values to determine the classification
- **Data Association:** Like classification, but it also recognizes data that contains errors

- **Data conceptualization:** Analyze the inputs so that grouping relationships can be inferred.

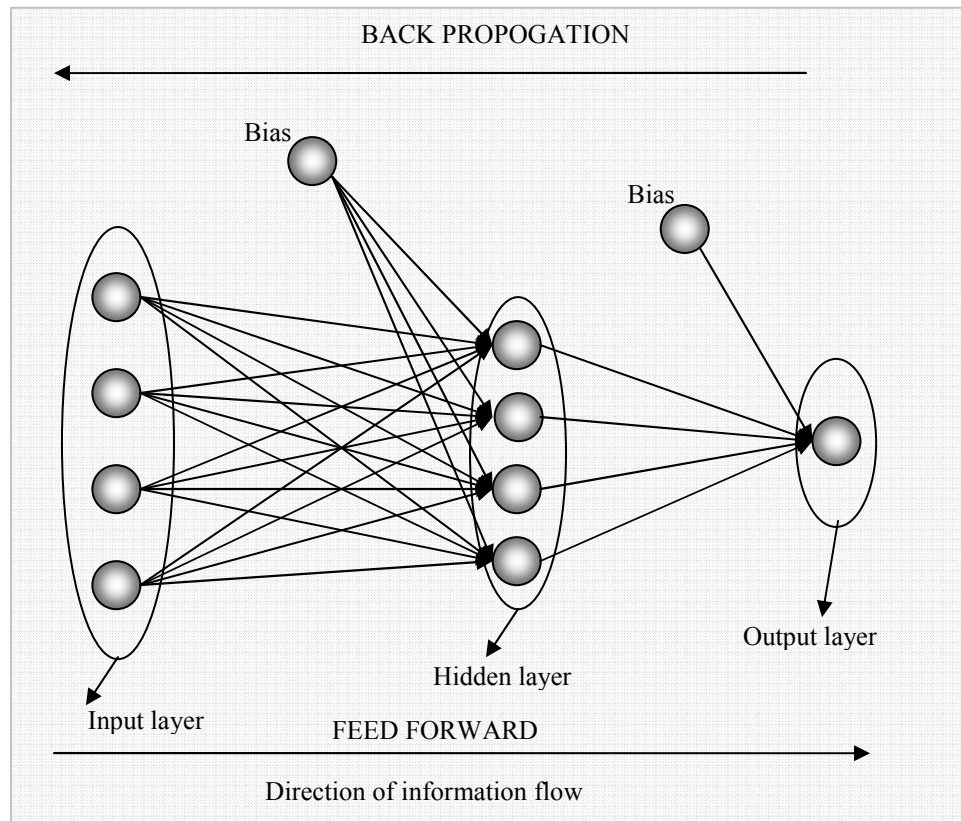


Figure 5.3 Multilayered artificial neural network

ANNs are commonly classified by their network topology, (i.e. feedback, feed forward) and learning or training algorithms (i.e. Supervised, Unsupervised). For example, a multilayer feed forward neural network with back propagation indicates the architecture and learning algorithm of the neural network (Figure 5.3).

5.2.3.1 Feed forward neural networks

In feed-forward networks, the signal flow is from input to output units, strictly in a feed-forward direction. The data processing can extend over multiple (layers of) units, but no feedback connections are present, that is, connections extending from outputs of units to inputs of units in the same layer or previous layers.

5.2.3.2 Back propagation algorithm

A back propagation algorithm can be used to train multilayer feed-forward networks with differentiable transfer functions to perform function approximation, pattern association, and pattern classification. The term back propagation refers to the process by which derivatives of network error, with respect to network weights and biases, can be computed (Schalkoff, 1997). The training of ANNs by back propagation involves three stages (Schalkoff, 1997): (i) the feed forward of the input training pattern, (ii) the calculation and back propagation of the associated error, and (iii) the adjustment of the weights. This process can be used with a number of different optimization strategies. The error between the output of the network and the target value is propagated backward during the backward pass and used to update the weights of the previous layers as shown in Figure 5.4 (Haykin, 2000; Hebb, 1949).

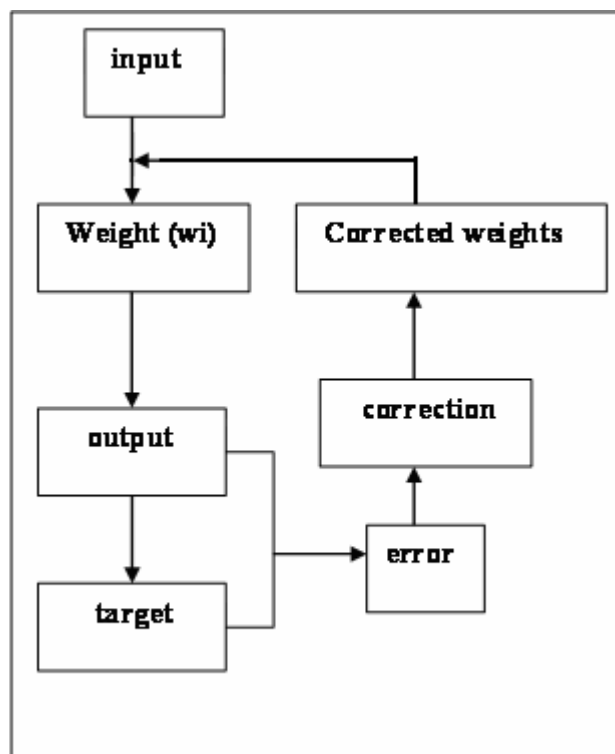


Figure 5.4 Schematic presentation of weight correction in BPNN

5.2.3.3 Supervised, unsupervised and reinforcement training

The learning situations in neural networks may be classified into three distinct sorts of learning:

- Supervised
- Unsupervised
- Reinforcement

In supervised learning, an input vector is presented at the inputs together with a set of desired responses, one for each node, at the output layer. A forward pass is done and the errors or discrepancies, between the desired and actual response for each node in the output layer, are found. These are then used to determine weight changes in the net according to the prevailing learning rule. The term ‘supervised’ originates from the fact that the desired signals on individual output nodes are provided by an external teacher. The best-known examples of this technique occur in the back propagation algorithm, the delta rule, and perceptron rule (Abraham, 2001).

In unsupervised learning (or self-organization), a (output) unit is trained to respond to clusters of pattern within the input. In this paradigm, the system is supposed to discover statistically salient features of the input population (Kohonen, 1998). Unlike the supervised learning paradigm, there is no a priori set of categories into which the patterns are to be classified; rather, the system must develop its own representation of the input stimuli.

Reinforcement learning is learning what to do – how to map situations to actions – so as to maximize a numerical reward signal. The learner is not told which actions to take, as in most forms of machine learning, but instead must discover which actions yield the most reward by trying them. In the most interesting and challenging cases, actions may affect not only the immediate reward but also the next situation and, through that, all subsequent rewards. These two characteristics, trial-and-error search and delayed reward, are the two most important distinguishing features of reinforcement learning (Abraham, 2002).

5.2.3.4 Training and testing artificial neural networks

A training set is a group of matched input and output patterns used for training the network, usually by suitable adaptation of the synaptic weights. The outputs are the

dependent variables that the network produces for the corresponding input. It is important that all the information the network needs to learn is supplied to the network as a data set. When each pattern is read, the network uses the input data to produce an output, which is then compared to the training pattern, i.e. the correct or desired output. If there is a difference, the connection weights (usually but not always) are altered in such a direction that the error is decreased. After the network has run through all the input patterns, if the error is still greater than the maximum desired tolerance, the ANN runs again through all the input patterns repeatedly until all the errors are within the required tolerance. When the training reaches a satisfactory level, the network holds the weights constant and uses the trained network to make decisions, identify patterns, or define associations in new input data sets not used to train it (Kalogirou and Bojic, 2000).

After training a network, the performance of the ANN model can be tested on data that the network was not trained with. This data set is called as testing data. To test the network one must freeze the weights after the training phase and apply data that the network has not seen before. If the training is successful and the network's topology is correct, it will apply its 'past experience' to this data and still produce a good solution. If this is the case, then the network will be able to generalize based on the training set. What is interesting is that a network with enough weights will always learn the training set better as the number of iterations is increased. However, neural network researchers have found that this decrease in the training set error was not always coupled to better performance in the test set. When the network is trained too much, the network 'memorizes' the training patterns and does not generalize well.

During learning, the network is going to discover the best mapping between the input data and the desired performance. If the data used in the training set is not representative of the input data class, it can expect poor performance with the test set, even though performance can be excellent with the training set.

5.2.4 Performance evaluation of ANN models

The artificial neural network performance can be evaluated by using the some statistical parameters. The quality of the prediction can normally be characterized by the mean square error (MSE) of the predicted values from the real measured data. The smaller the MSE of the both data sets (train and test) is the higher is the predictive quality. As an improvement, the correlation coefficient (R), mean absolute error (MAE) and mean absolute percentage error (MAPE) have been introduced to evaluate ANNs quality. Statistical formulations of these parameters are given in equations 5.3 to 5.6, respectively. The coefficient “R” describes the fit of the ANN’s output variable approximation curve to the actual test data output variable curve. Higher R coefficients indicate an ANN with better output approximation capabilities. Lower MAE and MAPE values also show the robustness of the proposed ANN models.

$$MSE = \frac{\sum_{i=0}^n (m_i - p_i)^2}{n} \quad (5.3)$$

$$R = \frac{\sum (m_i - m')(p_i - p')}{\sqrt{\sum (m_i - m')^2 \sum (p_i - p')^2}} \quad (5.4)$$

$$MAE = \left(\sum \left| \frac{m_i - p_i}{m_i} \right| \right) / n \quad (5.5)$$

$$MAPE = \frac{1}{n} \sum_{i=1}^n \left| \frac{m_i - p_i}{m_i} \right| * 100 \quad (5.6)$$

where m' and p' are mean values of measured (m_i) and predicted (p_i) values

5.2.5 Review on ANN applications in construction materials area

For years, researches have been carried out using various methods in order to anticipate the cement and concrete properties in advance. In this part of the study, artificial neural network based studies in the field of construction materials was

summarized to highlight how the ANN can be used on the experimental dataset acquired in the experimental part of the thesis.

Yeh (2007) modelled the slump flow of high performance concrete using second-order regressions and artificial neural networks. In that study, it was concluded that slump flow model based on ANN is much more accurate than that based on regression analysis. Hewayde et al. (2007) examined the feasibility of using artificial neural networks (ANNs) to predict the compressive strength of concrete and its degradation under exposure to sulphuric acid of various concentrations. Results showed that the ANN model successfully predicted the weight loss of concrete specimens subjected to sulphuric acid attack, not only for mixtures used in the training process, but also for new mixtures unfamiliar to the ANN model designed within the practical range of the input parameters used in the training process. Yeh (2006) investigated the potential of using design of experiments and artificial neural networks to determine the effect of fly ash replacements, from 0 to 50%, on the early and the late compressive strength, from 3 to 56 days, of low- and high-strength concrete, at water-cementitious material ratios in the range of 0.3–0.7. It was reported that high correlations between the compressive strength and the component composition of concrete can be developed using the generalization capabilities of the neural networks. Kewalramani and Gupta (2006) conducted a study for prediction of compressive strength of concrete based on weight and UPV for two different concrete mixtures involving specimens of two different sizes and shapes as a result of the need for rapid test method for predicting long-term compressive strength of concrete. The prediction is done using multiple regression analysis and artificial neural networks. A comparison between two methods depicted that the artificial neural network can be used to predict the compressive strength of concrete more effectively.

Alqedra and Ashour (2005) proposed a feed forward back-propagation neural network model for predicting the shear capacity of anchor bolts located near a concrete edge. In the developed neural network, the neurons of the input layer represent the anchor outside diameter, concrete compressive strength, anchor embedment depth, and the edge distance from the anchor bolt to the edge of concrete in the direction of the shear force. One neuron is used in the output layer to represent

the concrete shear capacity of the anchor bolts. Predictions of the concrete shear capacity of anchors using the trained neural network are in good agreement with experimental results and those calculated from the concrete capacity design method.

Tarefder et al. (2005) constructed and applied a four-layer feed-forward neural network to determine a mapping associating mix design and testing factors of asphalt concrete samples with their performance in conductance to flow or permeability. The network is trained using the Levenberg-Marquardt algorithm. At the end of the study, it is believed that the developed ANN model will be a useful tool in the study of asphalt pavement construction and maintenance.

Bai et al. (2003) developed a neural network model that provides effective predictive capability in respect of the workability of concrete incorporating metakaolin (MK) and fly ash (FA). The predictions produced reflect the effect of graduated variations in pozzolanic replacement in portland cement (PC) of up to 15% MK and 40% FA. The results show that the models are reliable and accurate, and illustrate how neural networks can be used to beneficially predict the workability parameters of slump, compacting factor and Vebe time across a wide range of PC–FA–MK compositions.

Jun et al. (2002) studied the feasibility of using a neural network as an adaptive synthesizer as well as an estimator to predict the chloride profiles diffused through concrete specimens. ANN predictions are in good agreement with the test results in both steady and unsteady states. Moreover, the investigation results demonstrate that the addition of fly ash and micro silica improves the resistance of mixtures to chloride diffusion. However, the addition of calcium nitrite solution degrades the improvement caused by the incorporation of these mineral admixtures, so calcium nitrite should be used in practical engineering with caution.

Haj-Ali et al. (2001) developed an ANN model to predict the long-term expansion response of concrete cylinders while exposed to a 2.1% Na_2SO_4 solution. The experimental data used in that study was collected by the U.S. Bureau of Reclamation (USBR) during a long-term (40+ years), non-accelerated test program. The ANN was constructed such that it provided for the expansion of the concrete as an output while its input vector includes time and two mixture parameters: the water-cement ratio (w/c), and the tricalcium aluminate content of the cement. At the end of

the research, it was concluded that ANN could effectively learn and predict the expansion of the concrete samples within a practical range of the two mixture parameters, during a span of up to 40 years, despite the described limitations of using the USBR data for ANN training.

5.3 An Overview of Genetic Programming

Genetic programming is a domain-independent method that genetically breeds a population of computer programs to solve a problem. Specifically, genetic programming iteratively transforms a population of computer programs into a new generation of programs by applying analogs of naturally occurring genetic operations. The genetic operations include crossover (sexual recombination), mutation, reproduction, gene duplication, and gene deletion. Analogous of developmental processes that transform an embryo into a fully developed entity are also employed. Genetic programming is an extension of the genetic algorithm into the arena of computer programs (Koza, 2005).

As seen in Figure 5.5, there are five major preparatory steps for the basic versions of genetic programming (Koza, 1992a). They require the human user to specify

- the set of terminals (e.g., the independent variables of the problem, zero-argument functions, and random constants) for each branch of the program to-be-evolved,
- the set of primitive functions for each branch of the to-be-evolved program,
- the fitness measure (for explicitly or implicitly measuring the fitness of individuals in the population),
- certain parameters for controlling the run, and
- the termination criterion and method for designating the result of the run

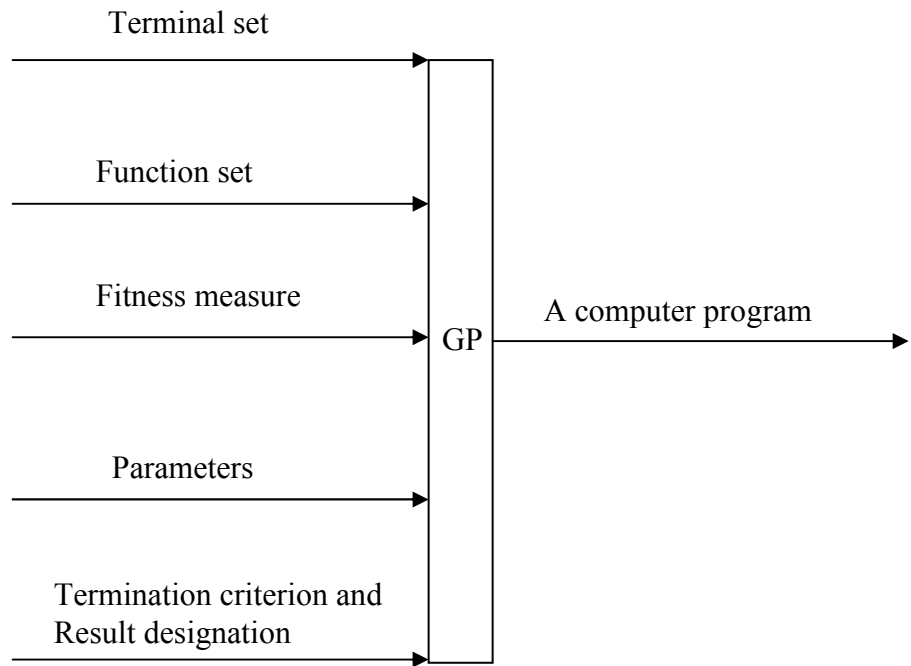


Figure 5.5 Five major preparatory steps for the basic versions of genetic programming.

After the user has performed the preparatory steps for a problem, the run of genetic programming can be launched. Once the run is launched, a series of well-defined, problem-independent steps is executed. The executional steps of genetic programming are as follows (Koza, 2005):

1. Randomly create an initial population (generation 0) of individual computer programs composed of the available functions and terminals.
2. Iteratively perform the following sub-steps (called a generation) on the population until the termination criterion is satisfied:
 - a. Execute each program in the population and ascertain its fitness (explicitly or implicitly) using the problem's fitness measure.
 - b. Select one or two individual program(s) from the population with a probability based on fitness (with reselection allowed) to participate in the genetic operations in.
 - c. Create new individual program(s) for the population by applying the following genetic operations with specified probabilities:

- i. Reproduction: Copy the selected individual program to the new population.
- ii. Crossover: Create new offspring program(s) for the new population by recombining randomly chosen parts from two selected programs.
- iii. Mutation: Create one new offspring program for the new population by randomly mutating a randomly chosen part of one selected program.
- iv. Architecture-altering operations: Choose an architecture-altering operation from the available repertoire of such operations and create one new offspring program for the new population by applying the chosen architecture-altering operation to one selected program.

3. After the termination criterion is satisfied, the single best program in the population produced during the run (the best-so-far individual) is harvested and designated as the result of the run. If the run is successful, the result may be a solution (or approximate solution) to the problem.

Genetic programming (GP) is a search technique which allows the solution of problems by automatically generating algorithms and expressions. These expressions are coded or represented as a tree structure with its terminals (leaves) and nodes (functions) (Koza, 1992b).

Gene-Expression Programming (GEP) is a natural extension of Genetic Programming (GP) and was recently developed by Ferreira (2006). A standard GP is a search strategy based on the rules of natural genetic evolution (Castilho et al., 2005). The GP works with population of individuals each representing a possible solution to a given problem. Each candidate solution, or individual, is represented as a string of bits analogous to chromosomes and genes in the evolution theory. A fitness score is assigned to each individual (Al-Tabtabai and Alex, 1999). On the other hand a GEP starts with an *expression tree* (ET) written in the so-called Karva

notation. For example, the algebraic expression given in equation 5.7 can be represented by an ET as shown in Figure 5.6

$$\left(c0\left(d0/d4\right)\right) \times \sin(d6(\text{atan}(d3))) \quad (5.7)$$

To read the tree given in Figure 5.6, we start at the bottom and move up. The left leaf indicates $d0/d4$ as the lowest expression. It then is multiplied by $c0$ to give the expression in the first set of parentheses. The right leaf starts with defining arc-tangent of $d3$ which then is multiplied by $d6$ and the resulting expression is then used as the argument to the sine function. The expressions from the two leafs are then multiplied to get the final expression. A GEP algorithm begins with the random values of parameters in the ET and applies standard genetic operations of selection, crossover, and mutation to find the best fit (Al-Tabtabai and Alex, 1999).

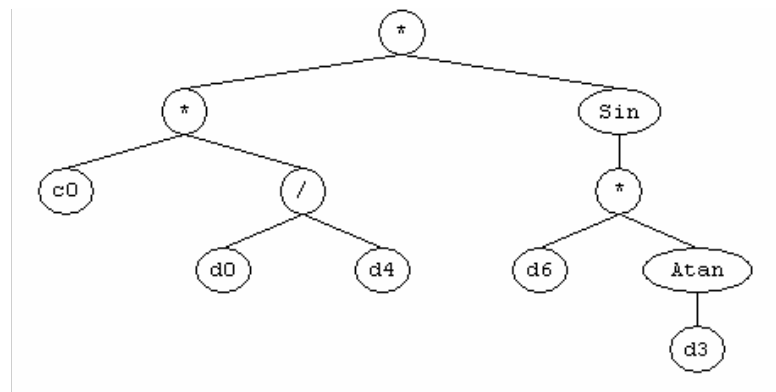


Figure 5.6 A typical example of the GEP expression tree

5.4 Applications of Soft Computing Techniques on the Data Set

5.4.1 General

The database obtained in the experimental part was used for modeling the fresh, physical, mechanical, and durability properties of SCCs. The major task herein is to define the hidden function connecting the input variables (water, cement, fly ash, ground granulated blast furnace slag, silica fume, and metakaolin contents, amounts of fine and coarse aggregates, and superplasticizer used) and the outputs (slump flow diameter, T_{50} slump flow time, V-funnel flow time, L box height ratio, initial and final setting times, compressive and splitting tensile strengths, ultrasonic pulse

velocity, free shrinkage, chloride ion permeability, electrical resistivity, water absorption, water sorptivity, and water permeability). The expected empirical models may be written in the form of following equation

$$Y_i = f(W, PC, FA, GGBFS, SF, MK, fa, ca, SP) \quad (5.8)$$

In order to construct empirical models and to show the generalization capability of ANN and GEP, the database produced in the experimental part is subdivided into two sets so called training and test sets. The empirical formulations were developed based on the former while the latter was employed to test the proposed models so as to measure their generalization capabilities. Of all 65 concrete mixtures, the training and testing sets consisted of randomly selected 50 and 15 mixtures, respectively.

5.4.2 Construction of ANN models

Two different ANN architectures were constructed for the prediction of SCC properties. When constructing the ANN architectures, the following two main points were taken into account:

1. Construct the ANN model with minimum number of neurons in the hidden layer to shorten the proposed explicit artificial neural network formulations for the properties of SCCs,
2. Get correlation coefficients (R) as low as 0.990 and above for the training set data

For each target properties of SCCs, an ANN model was constructed. At the beginning, ANN models were constructed with four neurons for each response. A number of four is the lowest number of neurons proposed by the used commercial software. Constructed ANN models were trained up to 20000 learning cycle and then the training process were stopped. After that the predefined architecture designation criteria was controlled and if it was found satisfactory, the trial ANN architecture was chosen as the final ANN model for that property of SCCs.

At the end of designation process of the ANN, 9-6-1 and 9-7-1 ANN architectures fulfilled the defined criteria as shown in Figures 5.7 and 5.8, respectively. Those architectures indicate that there are 9 nodes in the input layer corresponding to 9 factors from water content to amount of superplasticizer used, 6 or 7 neurons in the hidden layer, and 1 in the output layer corresponding target properties of SCCs. Slump flow diameter, compressive strength, splitting tensile strength, chloride ion permeability, water absorption, water permeability, and electrical resistivity of SCCs were predicted with six neurons in the hidden layer as seen in Figure 5.7. However, T_{50} slump flow time, V-funnel flow time, L-box H_2/H_1 ratio, initial setting time, final setting time, velocity through concrete, free shrinkage, and water sorptivity properties were predicted with seven neurons in the hidden layer as shown in Figure 5.8.

The input parameters were normalized in the range of (-0.95; 0.95) via equation 5.9 in order to acquire accurate results prediction prior to the execution of the training process of the ANN:

$$\Gamma_{normalized} = c\Gamma + d \quad (5.9)$$

where Γ represents the parameters used in the ANN training process, c and d are normalization coefficients of that particular parameter. The normalization coefficients of each parameter utilized in the SCC properties are given in Table 5.1. It must be kept in mind that the proposed empirical equations are valid for the ranges of training set, thus providing upper and lower limit of the parameters in Table 5.1.

In this study, a feed-forward back-propagation network model was used to predict properties of SCCs. Training was carried out using a supervised manner, whereby the networks were provided with sets of (input/target) training patterns along with measured outputs for each input vector, and the network was told what to learn. The training mechanism was based on the back propagation in which the error between the predicted and desired outputs is minimized using a Levenberg Marquardt (LM) learning algorithm with a tangent sigmoid transfer function, which was given in equation 5.2.

5.4.3 Construction of GEP model

The major task herein was also to define the hidden functions connecting the input variables or mix constituents to the outputs or the target properties SCCs. The GEP models proposed in this study were constructed using the GEP software “GeneXproTools 4.0” developed by Ferreira (2001). The same training and testing sets used in ANN models were employed in the GEP applications.

As mentioned in section 5.3 (an overview of genetic programming), there are five major steps in preparing to use gene expression programming. The first step is to choose the appropriate fitness function. For this, in all constructed GEP models for the SCC properties, the fitness “ f_i ” of an individual program “ i ” is measured by

$$f_i = \sum_{j=1}^{C_t} (M - |C_{(i,j)} - T_j|) \quad (5.10)$$

where M is the range of selection, $C_{(i,j)}$ is the value returned by the individual chromosome i for fitness case j (out of C_t fitness cases) and T_j is the target value for fitness case j . If $|C_{(i,j)} - T_j|$ (the precision) is less than or equal to 0.01, then the precision is equal to zero, and $f_i = f_{max} = C_t M$. In this case, $M = 100$ was used, therefore, $f_{max} = 1000$. The advantage of this kind of fitness functions is that the system can find the optimal solution by itself.

The second major step consists of choosing the set of terminals “ T ” and the set of functions “ F ” to create the chromosomes. In this problem, the terminal set consists obviously of the independent variables, i.e., $T = \{W, PC, FA, GGBFS, SF, MK, fa, ca, SP\}$. The choice of the appropriate function set is not so obvious. However, a good guess can always be helpful in order to include all the necessary functions. In this study, four basic arithmetic operators (+, -, *, /) associated with some basic mathematical functions ($\sqrt{\quad}$, $\ln(x)$, $\log(x)$, e^x , 10^x , power, Sine, Cosine, Arctangent, $1/x$) were utilized.

The third major step in GEP is to choose the chromosomal architecture, i.e., the length of the head and the number of genes. Length of the head and number genes changed according to properties of SCC to be estimated.

The fourth major step is to choose the linking function. In this study, the sub-ETs were linked by addition except for slump flow diameter and water sorptivity formulations. High correlation coefficients could not be found for such properties of SCCs with addition-linking function so that the multiplication-linking function was tried and a better performance with respect to addition-linking was obtained.

Finally, the fifth major step is to choose the set of genetic operators that cause variation and their rates. In this study, all of the proposed GEP based formulations, mutation rate, inversion rate, one and two point recombination rates were selected as 0.044, 0.1, 0.3, and 0.3, respectively.

5.4.4 Proposed formulations and performance of the models

According to the explained criteria in the sections 5.4.2 and 5.4.3, explicit artificial neural networks and genetic programming based formulations were obtained for the fresh, physical, mechanical, and durability properties of SCCs. ANN and GEP based explicit mathematical formulations for the slump flow diameter of SCCs were given in equation 5.11 and 5.12, respectively. ANN and GEP based explicit formulations for the other properties of SCCs were given in Appendix A and B, respectively. It should be noted that the proposed formulations with both methods are valid for the parameters ranging between minimum and maximum values given in Table 5.1.

A total of fifty training pattern were used to train the ANN and GEP models. Satisfactory completion of the training process was verified by requiring the ANN and GEP models to predict the target properties of SCCs in the training process, and the resulting responses are illustrated in Figures 5.9a to 5.23a. In these figures, natural axis shows the data order in the training data, vertical axis demonstrates the values of target properties of SCCs that was compared with the predictions of ANN and GEP models. It can be observed in Figures 5.9a to 5.23a that ANN based models for all target properties have successfully learned the relationships between the input parameters and the associated targets. As can be seen from the figures, there is a close match between the actual and predicted properties. The ANN functions are able to very closely follow the trend of the actual data. As also seen in Figures 5.9a to

5.23a that GEP functions follow the trend of the actual data but the performance of GEP was found to be worse than the ANN functions.

The models developed through ANN and GEP were then tested on 15 new input vectors, randomly selected from the total of 65 data, to examine their ability to generalize their predictions beyond the training data. In the testing process, only input vectors of 9 elements unfamiliar to the network were presented to the trained ANN model and no knowledge of the actually measured corresponding properties were provided. The predictions of the both ANN and GEP models are illustrated with the experimentally measured data in Figures 5.9b to 5.23b. As seen from the figures that the performance of the proposed ANN models showed almost similar pattern with that of the experimental data in the test set. The proposed ANN models were generally well agreed with the experimental data for testing data sets. The test set results of the proposed GEP formulations are also shown in Figures 5.9b to 5.23b. As seen in the figures, the performance of the GEP based formulations were rather poor in quality according to the experimental and ANN predicted results. GEP based formulations generally estimated the trend of experimental data but in some cases high fluctuations were observed, especially in the fresh properties such as slump flow diameter, T_{50} slump flow time, L-box H_2/H_1 ratio, and initial and final setting times.

Table 5.2 demonstrates the statistical performance of the both ANN and GEP models. Mean square error (MSE), mean absolute error (MAE), mean absolute percentage error (MAPE), and correlation coefficients of training and testing sets for both methods are tabulated in Table 5.2. As mentioned in the ANN architecture designation criteria, ANN models were constructed to get a correlation coefficient as low as 0.990 for the training set. As seen in the Table 5.2 that training set of ANN models for all SCC properties had higher correlation coefficients than 0.990. As seen in Table 5.2 that the highest and the lowest correlation coefficients in the training set of ANN models were obtained for the electrical resistivity (0.999) and initial setting times (0.991), respectively. It was observed that the test set provided approximately the same correlation coefficients. As also seen in Table 5.2 that the test set of initial setting time had the lowest correlation coefficient of 0.969. Except for the initial setting times and slump flow diameter, the other SCCs properties had correlation coefficients as high as 0.993. The ultrasonic pulse velocity had the lowest mean

absolute percentage error for both training and testing sets. MAPE values for ultrasonic pulse velocity for training and testing sets are 0.099 and 0.054, respectively. The results in Table 5.2 showed that proposed ANN models and explicit formulations have successfully learned the hidden relations between the concrete mixture constituents and associated target SCCs properties.

When the statistical outcomes of the GEP models were evaluated, it was observed in Table 5.2 that the prediction capability of GEP models for both training and testing sets was much higher for the hardened properties of the concretes than that of fresh properties. As seen in Table 5.2 that correlation coefficients of empirical models for both the training and test sets were generally higher than 0.506. When the correlation coefficients of testing sets are considered, the highest R of 0.973 was obtained for the compressive strength while the lowest R of 0.506 belonged to the L-box H_2/H_1 ratio. When compared the MAPE values of GEP models for both sets, it was seen that the highest mean absolute percentage error of 23.43 was obtained for the test set of T_{50} slump flow time while the lowest MAPE of 0.845 belonged to the train set of ultrasonic pulse velocity.

$$\text{Slump flow diameter} = \left(\left(\frac{2}{1 + e^{-2F}} - 1 \right) - (-14.1) \right) / (0.2) \quad (5.11)$$

$$F = (-1.20924) * \left(\frac{2}{1 + e^{-2F_1}} - 1 \right) + (3.44676) * \left(\frac{2}{1 + e^{-2F_2}} - 1 \right) + (1.70937) * \left(\frac{2}{1 + e^{-2F_3}} - 1 \right) + (0.68719) * \left(\frac{2}{1 + e^{-2F_4}} - 1 \right) + (0.65973) * \left(\frac{2}{1 + e^{-2F_5}} - 1 \right) + (-4.43815) * \left(\frac{2}{1 + e^{-2F_6}} - 1 \right) + (-1.08743) \quad (5.11a)$$

$$F_1 = (W) * (1.82747) + (PC) * (1.38432) + (FA) * (-3.32956) + (GGBFS) * (1.15651) + (SF) * (-0.17783) + (MK) * (1.92799) + (fa) * (-8.1266) + (ca) * (-6.63277) + (SP) * (-1.61664) + (-0.50069) \quad (5.11b)$$

$$F_2 = (W) * (11.59421) + (PC) * (-2.33617) + (FA) * (1.39392) + (GGBFS) * (-0.76741) + (SF) * (-2.87603) + (MK) * (0.48180) + (fa) * (-6.50805) + (ca) * (11.01144) + (SP) * (1.46403) + (-0.62487) \quad (5.11c)$$

$$F_3 = (W) * (-5.49772) + (PC) * (-3.65732) + (FA) * (7.60974) + (GGBFS) * (-2.98757) + (SF) * (0.72669) + (MK) * (0.92524) + (fa) * (15.5623) + (ca) * (9.00065) + (SP) * (0.62847) + (0.69496) \quad (5.11)$$

$$F_4 = (W) * (0.89015) + (PC) * (-7.04079) + (FA) * (-2.1978) + \\ (GGBFS) * (15.45796) + (SF) * (4.77733) + (MK) * (-3.81026) + \\ (fa) * (1.33507) + (ca) * (-0.16917) + (SP) * (-3.37922) + (-4.1962) \quad (5.11e)$$

$$F_5 = (W) * (1.87442) + (PC) * (-19.67239) + (FA) * (-2.01424) + \\ (GGBFS) * (12.03451) + (SF) * (-0.66377) + (MK) * (-14.08656) + \\ (fa) * (-0.27435) + (ca) * (-8.62817) + (SP) * (25.72725) + (10.32457) \quad (5.11f)$$

$$F_6 = (W) * (7.84692) + (PC) * (-4.58438) + (FA) * (5.55180) + \\ (GGBFS) * (-2.21353) + (SF) * (-0.75397) + (MK) * (0.28662) + \\ (fa) * (3.04761) + (ca) * (16.84529) + (SP) * (0.88493) + (-0.24173) \quad (5.11g)$$

$$\text{Slump flow diameter} = F_1 * F_2 * F_3 * F_4 * F_5 * F_6 * F_7 \quad (5.12)$$

$$F_1 = 89.3588 * (W - e^{((\text{Sin}(274.1+(ca-W))) * \text{Arctan}(ca))}) \quad (5.12a)$$

$$F_2 = [ca + (\sqrt{GGBFS} + fa)] + \text{Cos}(3.82056 * ca) \quad (5.12b)$$

$$F_3 = W + [fa - \text{Cos}[9.365 + [(PC - GGBFS) * (FA + W)]]] \quad (5.12c)$$

$$F_4 = \sqrt[4]{FA} + [\text{Cos}(SF) + [\text{Cos}(SF) + (W + 4.08)]] \quad (5.12d)$$

$$F_5 = (W - \sqrt{PC + 8.1895}) + [fa + (-8.1895 * \text{Cos}(SP))] \quad (5.12e)$$

$$F_6 = ca + [[PC - (-2.5437 - SP)] - [ca + (-2.5437 - SF)]] \quad (5.12f)$$

$$F_7 = \left[\frac{1}{\text{Cos}[(W - MK) * SF] - fa} + fa \right]^{3.64865} \quad (5.12g)$$

Table 5.1 Normalization coefficient and data range of parameters for ANN models

Parameters	Lower limit	Upper limit	Normalization coefficient	
			c	d
W	176	198	0.08181	-15.29999
PC	180	550	0.00486	-1.77567
FA	0	330	0.00545	-0.9
GGBFS	0	330	0.00545	-0.9
SF	0	82.5	0.02181	-0.9
MK	0	82.5	0.02181	-0.9
fa	684.9	826.1	0.01274	-9.63101
ca	827.7	934.6	0.01683	-14.83695
SP	2.8	12	0.19565	-1.447826

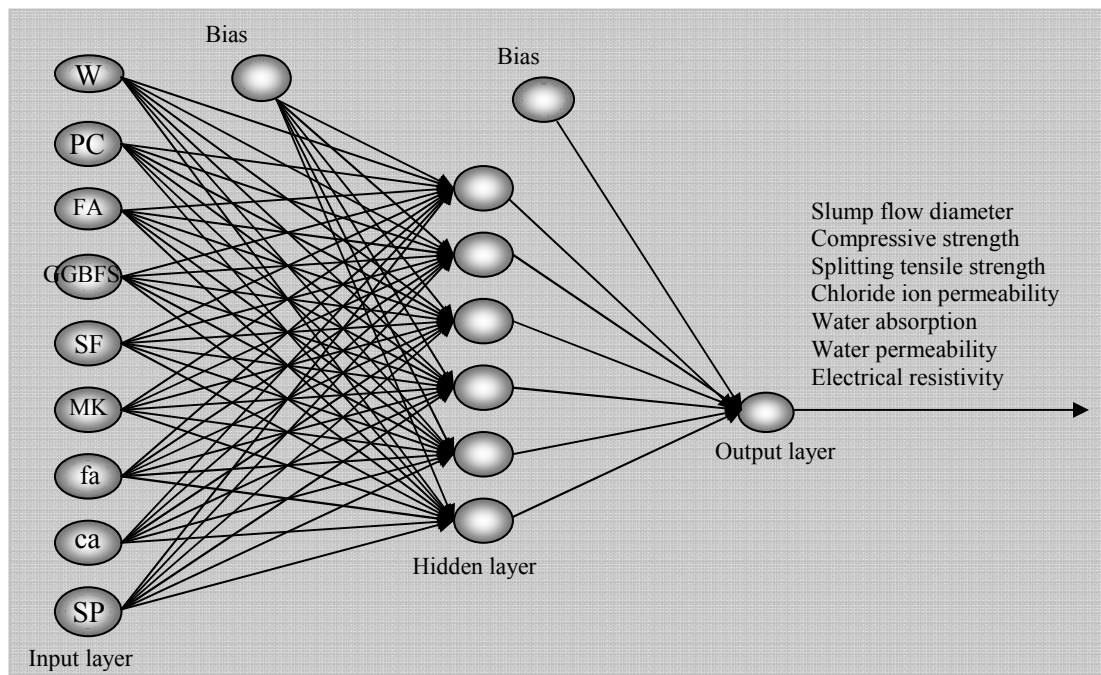


Figure 5.7 Proposed ANN architecture for prediction of slump flow diameter, compressive strength, splitting tensile strength, chloride ion permeability, water absorption, water permeability, and electrical resistivity of SCC

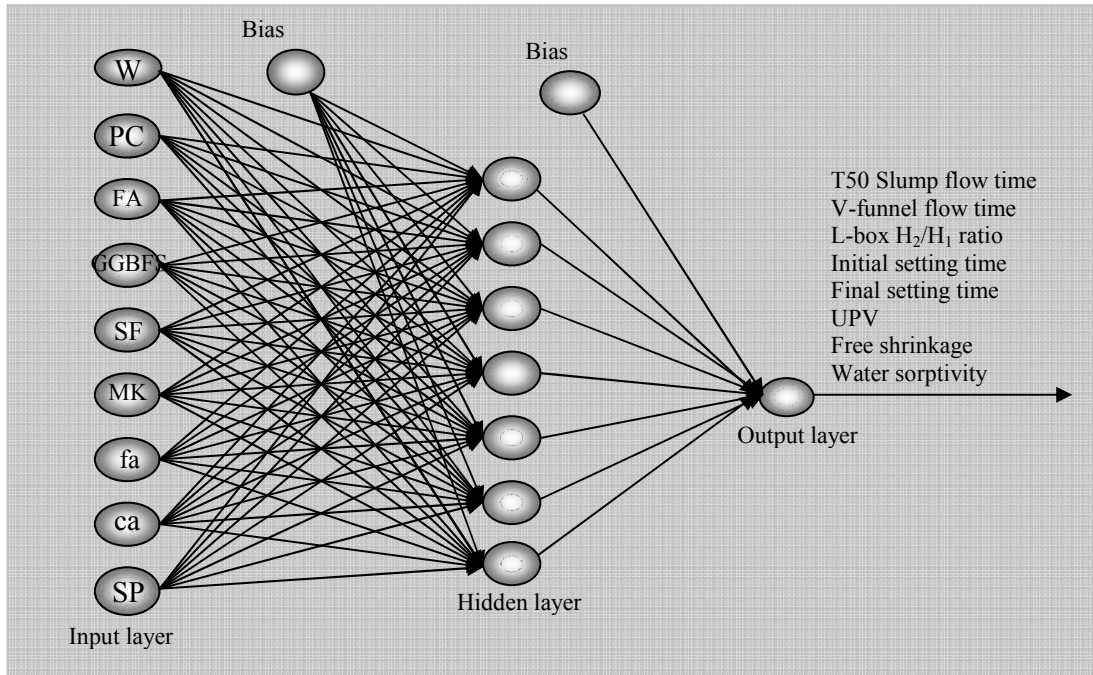
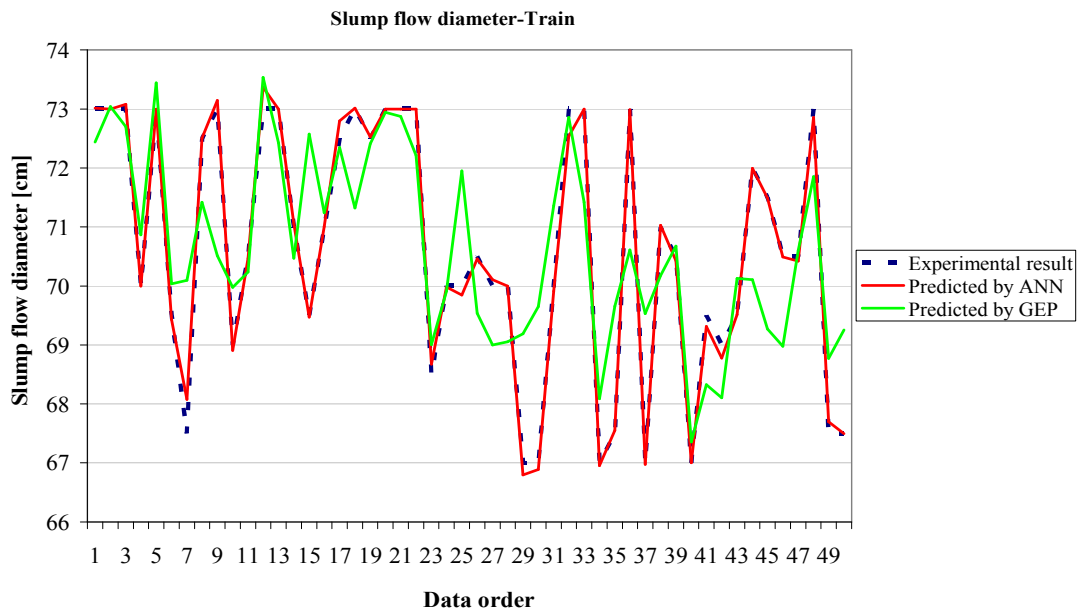


Figure 5.8 Proposed ANN architecture for prediction of T_{50} slump flow time, V-funnel flow time, L-box H_2/H_1 ratio, initial setting time, final setting time, ultrasonic pulse velocity, free shrinkage and water sorptivity of SCC

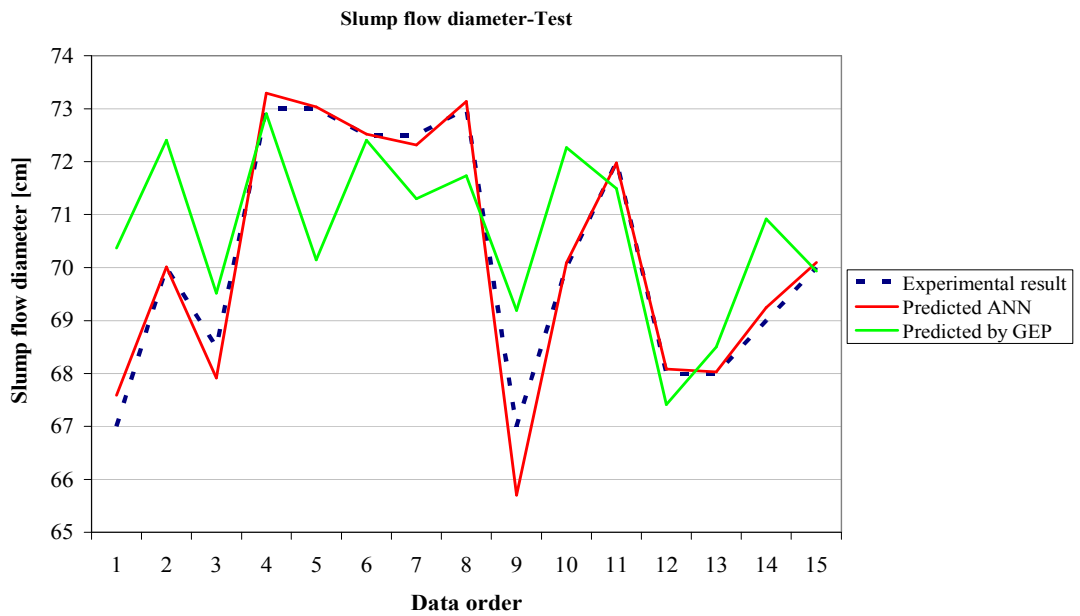
Table 5.2 Statistical performance of the proposed ANN and GEP formulations for prediction SCCs properties

SCC Properties	ANN						GEP									
	Train			Test			Train			Test						
	MSE	MAE	MAPE	R	MSE	MAE	MAPE	R	MSE	MAE	MAPE	R				
Slump flow diameter	0.022	0.001	0.122	0.997	0.173	0.004	0.361	0.985	1.840	0.015	1.530	0.764	2.922	0.019	1.945	0.662
T ₅₀ Slump flow time	0.015	0.026	2.584	0.995	0.005	0.024	2.399	0.999	0.468	0.191	19.092	0.830	0.875	0.234	23.43	0.778
V-funnel flow time	0.413	0.056	5.624	0.995	0.279	0.030	3.075	0.998	7.658	0.229	22.969	0.894	10.63	0.206	20.62	0.917
L box H ₂ /H ₁ ratio	0.000	0.003	0.332	0.997	0.000	0.003	0.284	0.998	0.002	0.042	4.202	0.793	0.002	0.041	4.080	0.506
Initial setting time	572.3	0.043	4.285	0.990	1024	0.049	4.939	0.969	5823	0.116	11.59	0.886	4081	0.141	14.07	0.862
Final setting time	123.6	0.018	1.806	0.998	129.7	0.016	1.591	0.998	9131	0.114	11.35	0.867	6974	0.157	15.75	0.829
Compressive strength	1.420	0.010	0.998	0.997	1.801	0.012	1.174	0.997	17.44	0.034	3.443	0.964	16.69	0.038	3.785	0.973
Ultrasonic pulse velocity	66.63	0.001	0.099	0.998	18.24	0.001	0.054	0.999	2959	0.008	0.845	0.915	3350	0.009	0.950	0.868
Splitting tensile strength	0.009	0.011	1.059	0.991	0.002	0.007	0.731	0.998	0.039	0.028	2.760	0.961	0.043	0.028	2.753	0.966
Free shrinkage	22.56	0.008	0.759	0.994	7.270	0.005	0.498	0.999	401.1	0.038	3.814	0.899	563.3	0.038	3.757	0.920
Chloride ion permeability	597.6	0.053	5.312	0.998	414.1	0.047	4.708	0.998	11349	0.196	19.64	0.961	9777	0.158	15.80	0.962
Electrical resistivity	0.073	0.009	0.899	0.999	0.050	0.009	0.880	0.999	4.514	0.086	8.571	0.938	6.138	0.080	8.000	0.913
Water absorption	0.010	0.025	2.502	0.997	0.010	0.024	2.400	0.995	0.136	0.087	8.681	0.962	0.154	0.093	9.278	0.935
Water sorptivity	0.000	0.009	0.915	0.999	0.000	0.009	0.899	0.997	0.000	0.116	11.58	0.847	0.000	0.074	7.368	0.910
Water permeability	0.320	0.055	5.504	0.992	0.301	0.050	5.067	0.993	3.788	0.153	15.30	0.904	4.078	0.101	10.14	0.909

- MSE: Mean square error
- MAE: Mean absolute error
- MAPE: Mean absolute percentage error
- R: Correlation coefficient

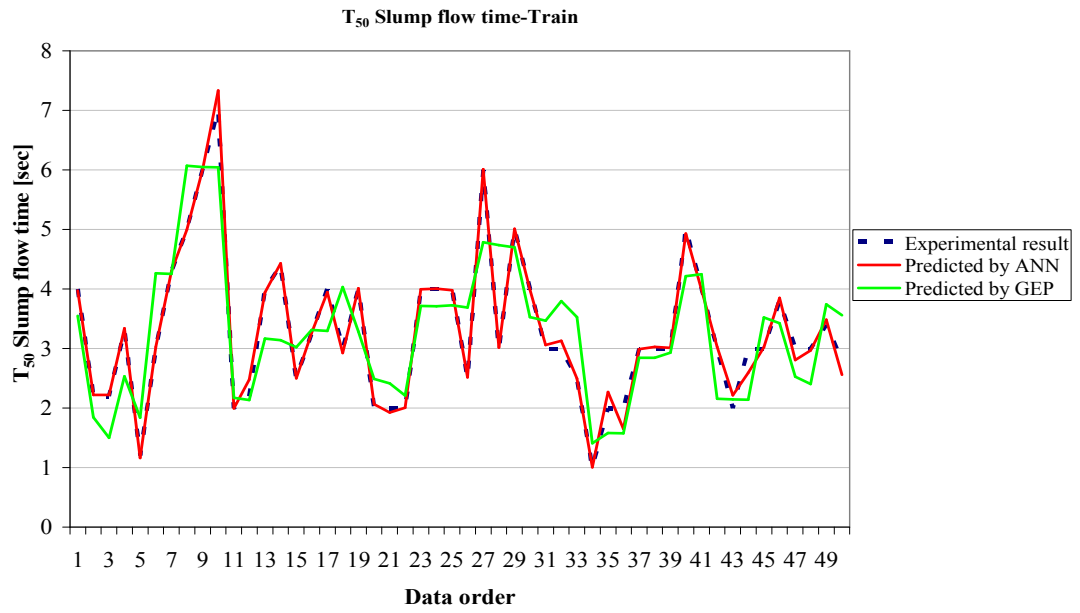


a)

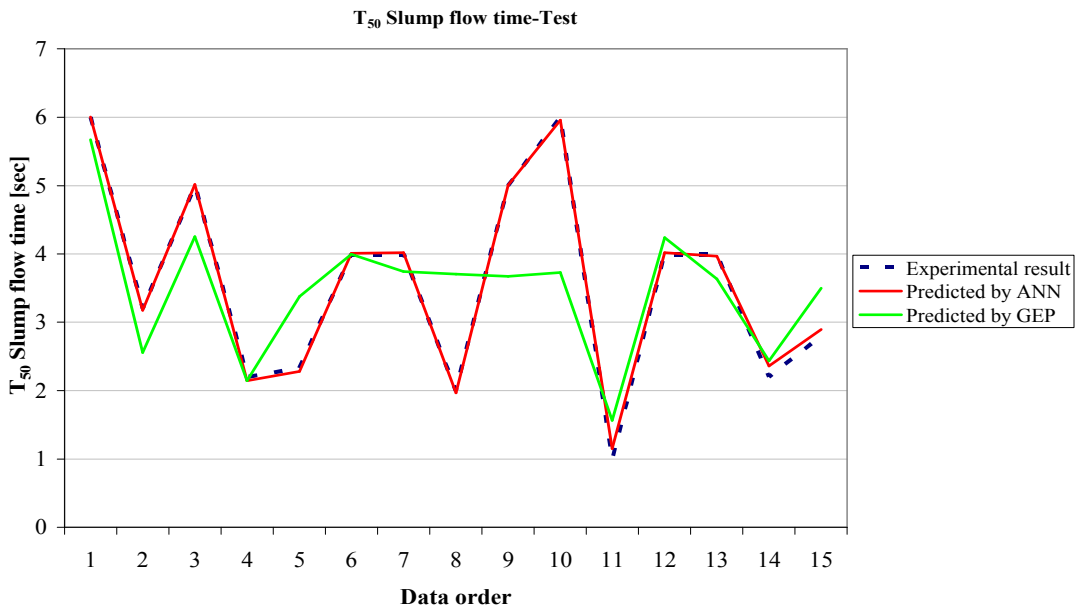


b)

Figure 5.9 Performance of the formulation of slump flow diameter of SCC a) train set b) test set

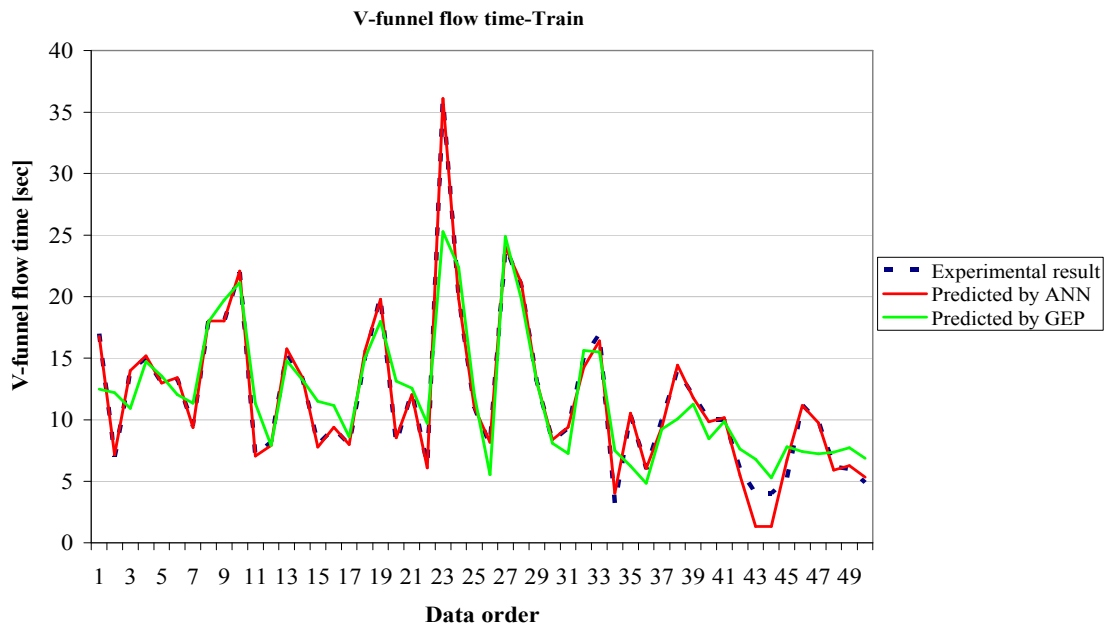


a)

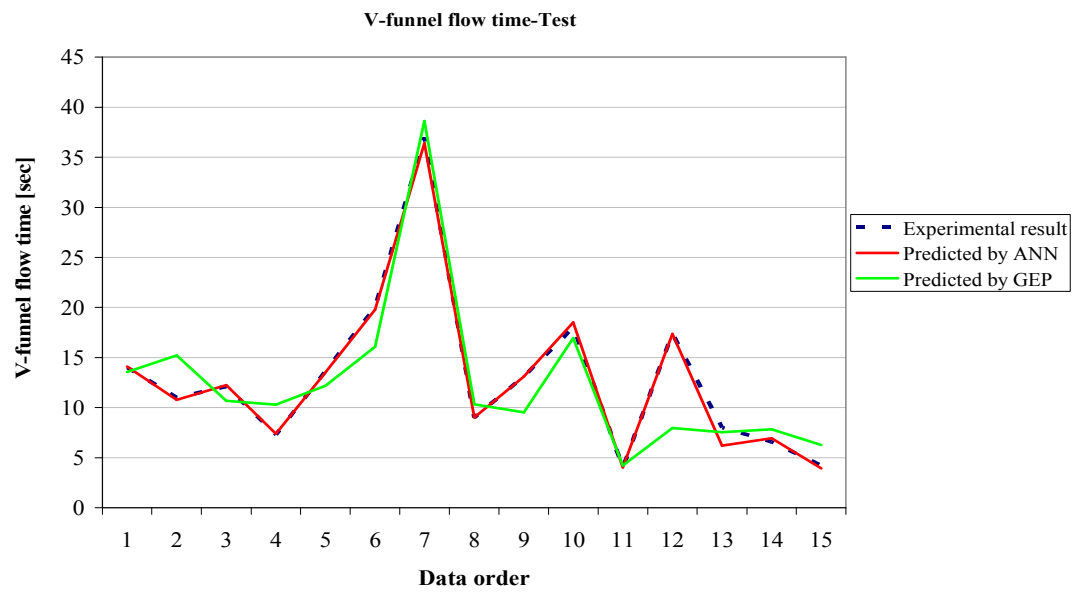


b)

Figure 5.10 Performance of the formulation of T₅₀ slump flow time of SCC a) train set b) test set

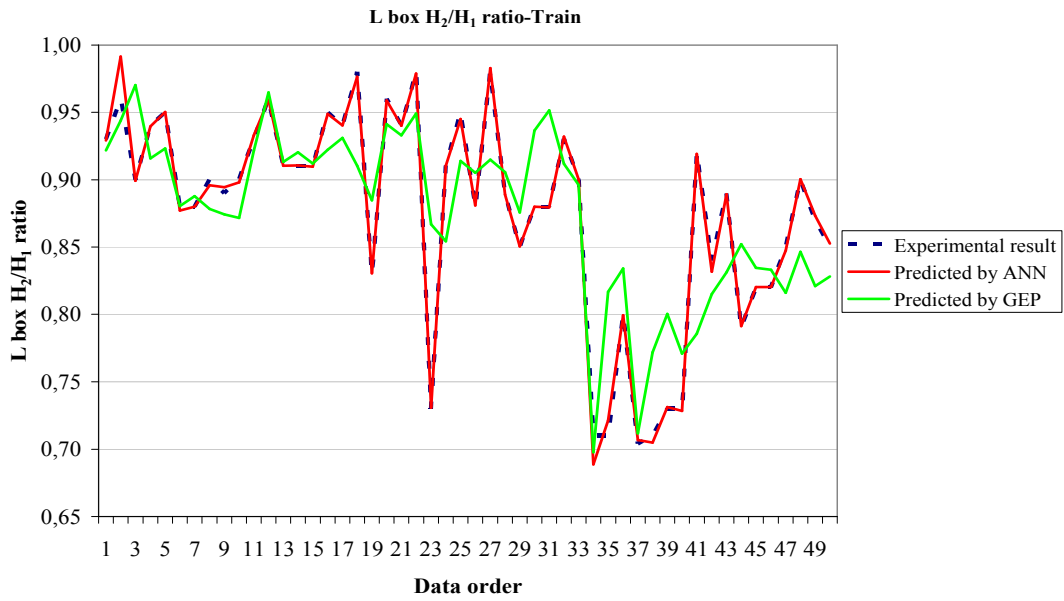


a)

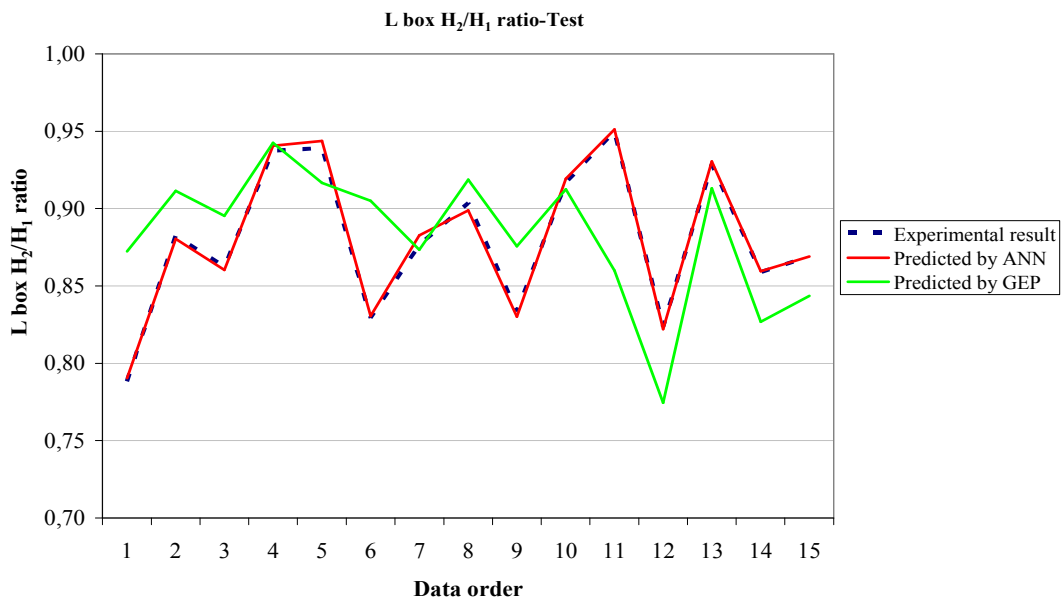


b)

Figure 5.11 Performance of the formulation of V-funnel flow time of SCC a) train set b) test set

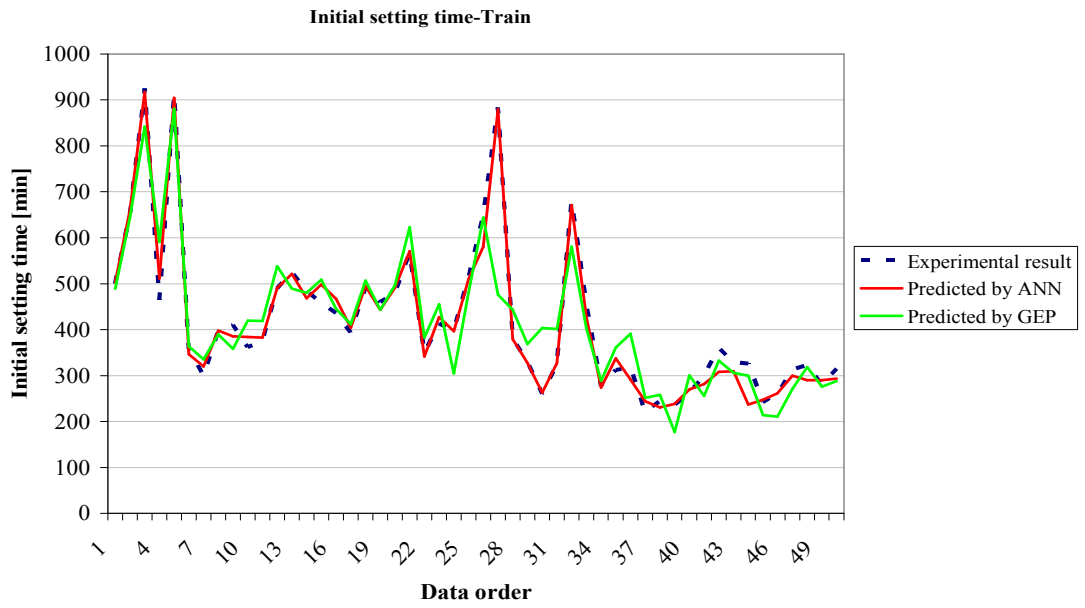


a)

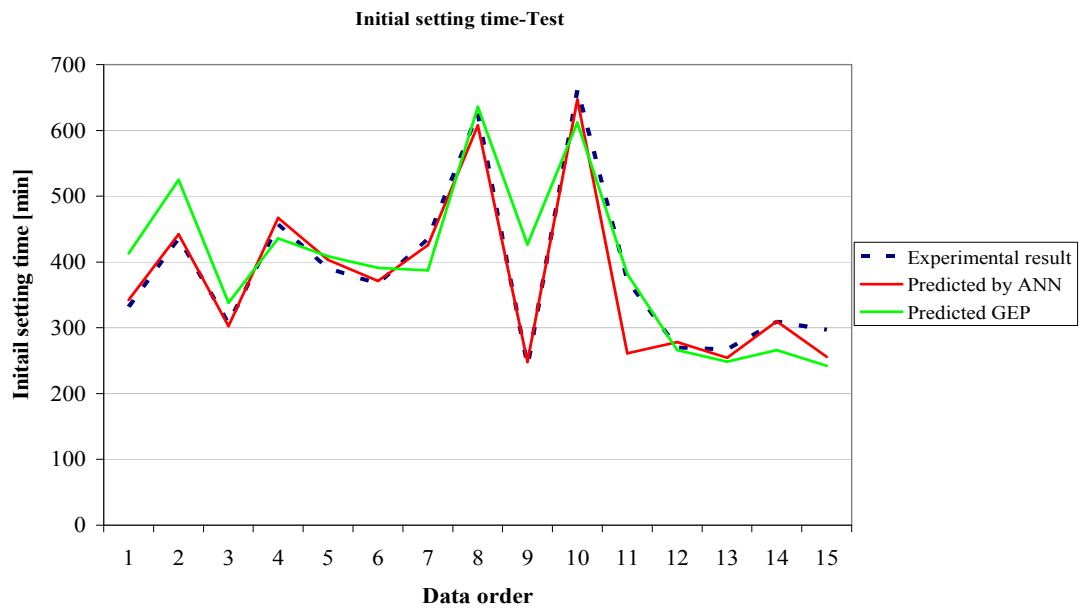


b)

Figure 5.12 Performance of the formulation of L-box height ratio (H_2/H_1) of SCC a) train set b) test set

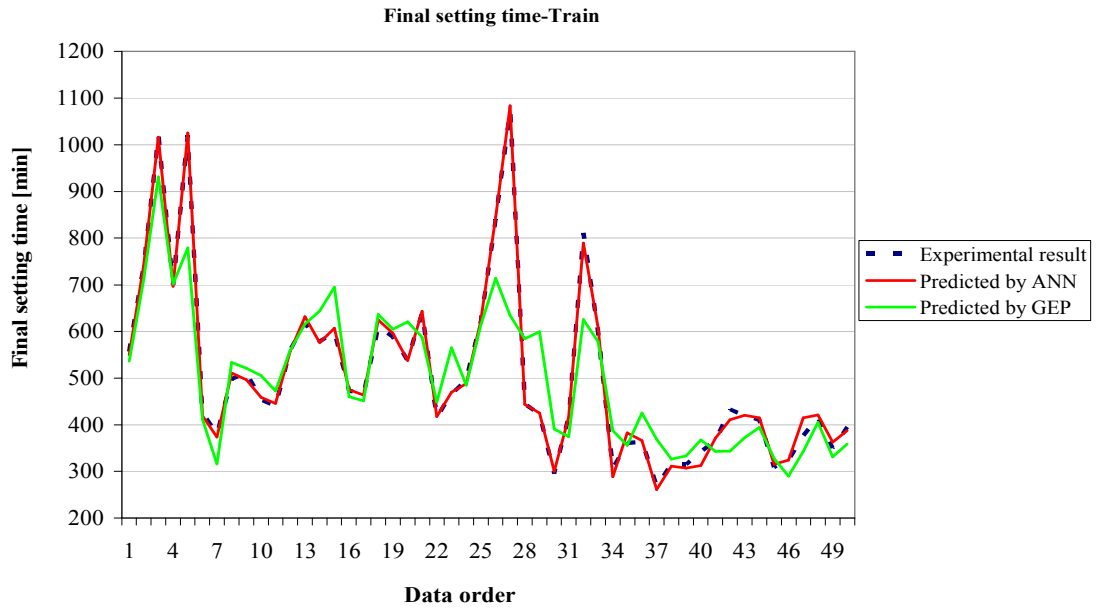


a)

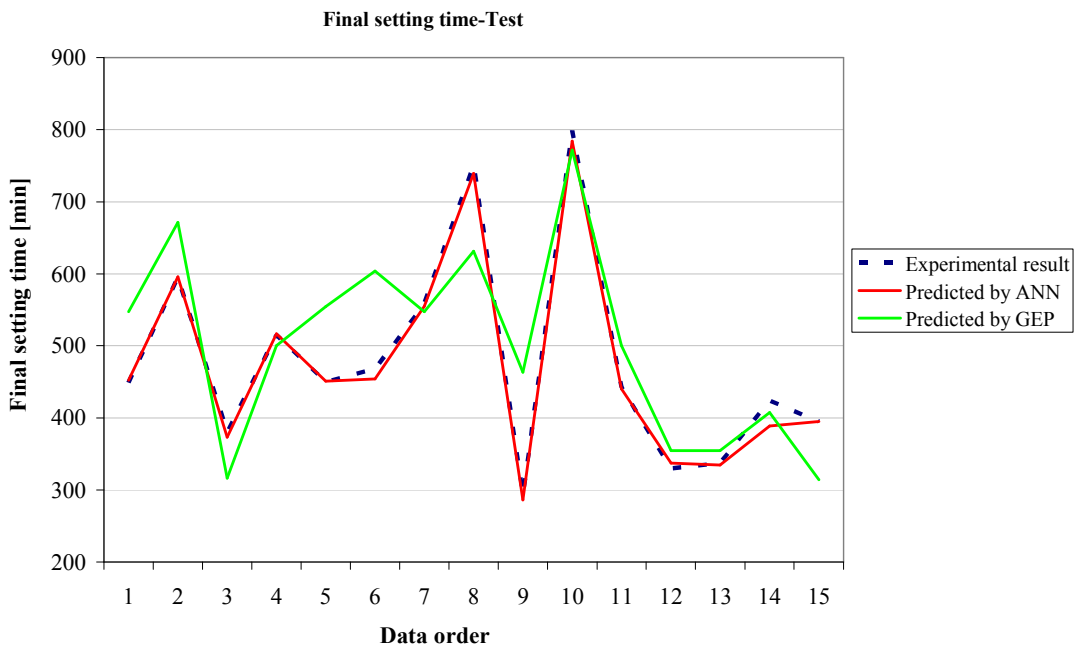


b)

Figure 5.13 Performance of the formulation of initial setting time of SCC a) train set
b) test set

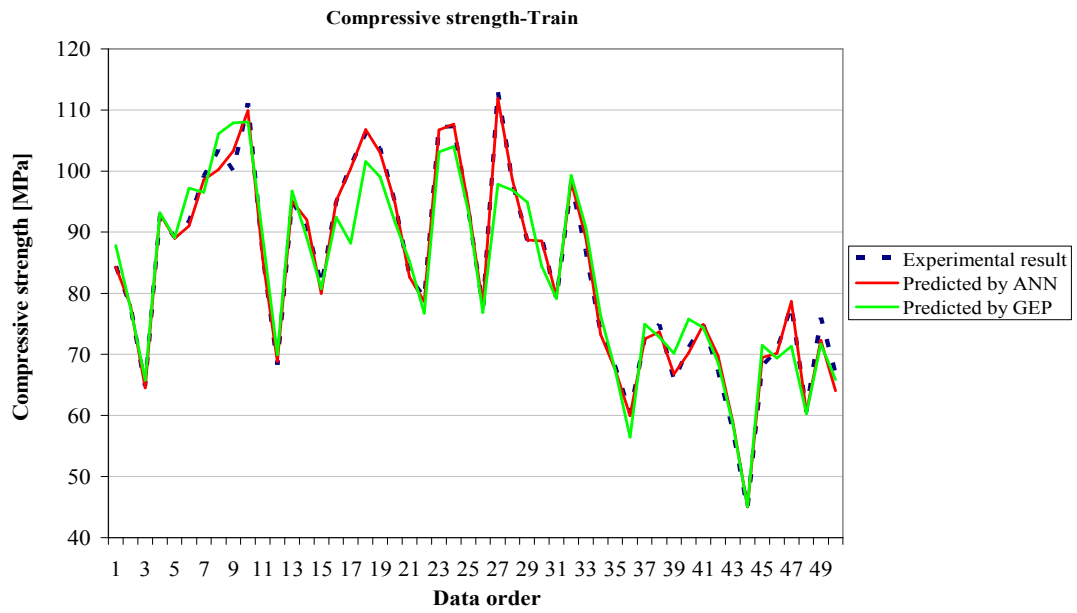


a)

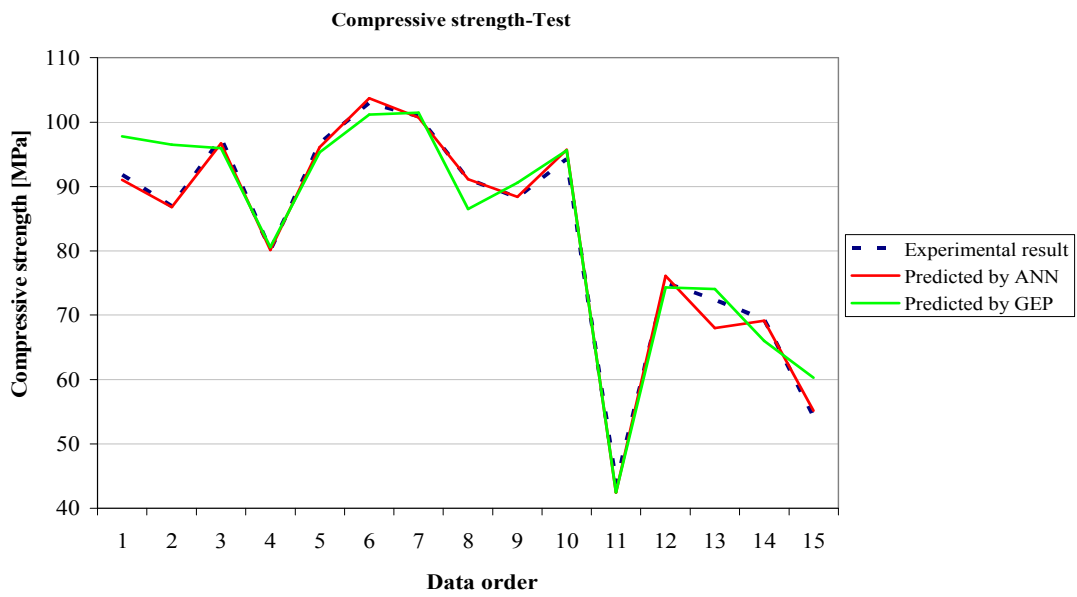


b)

Figure 5.14 Performance of the formulation of final setting time of SCC a) train set b) test set

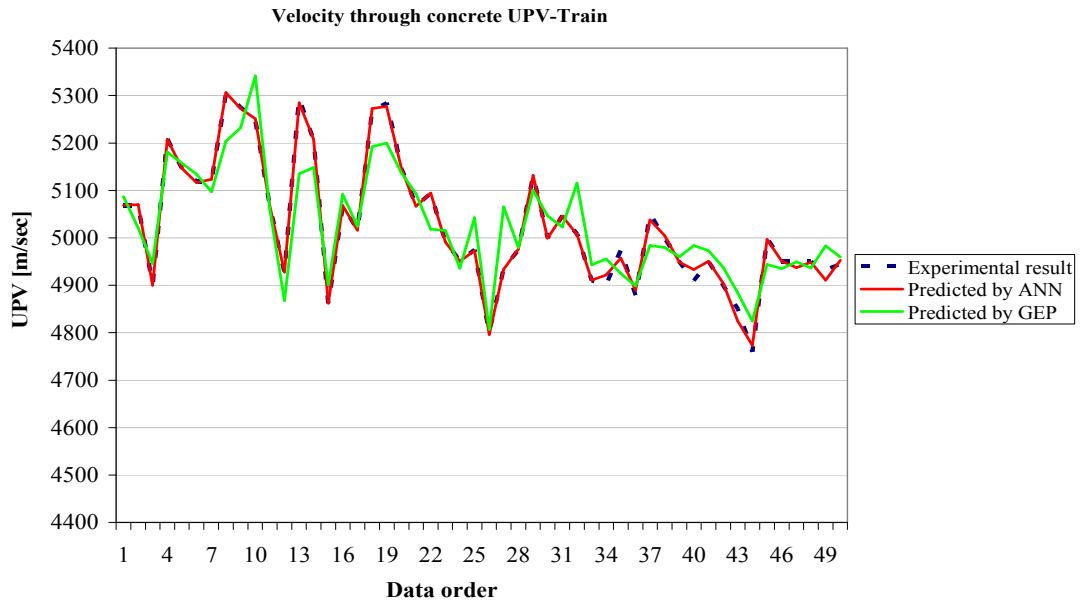


a)

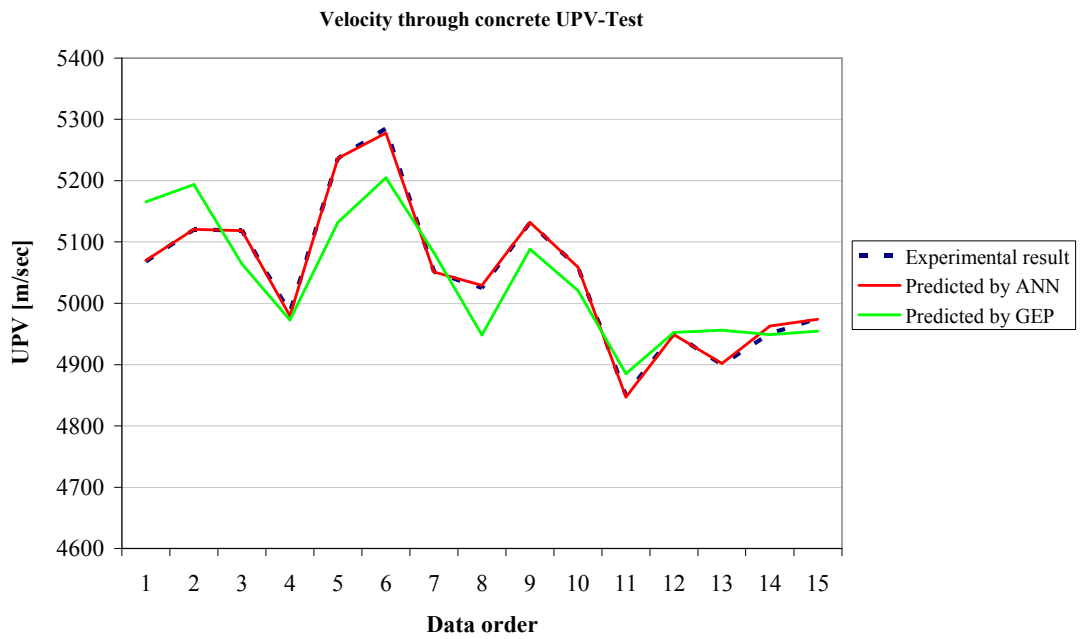


b)

Figure 5.15 Performance of the formulation of compressive strength of SCC a) train set b) test set

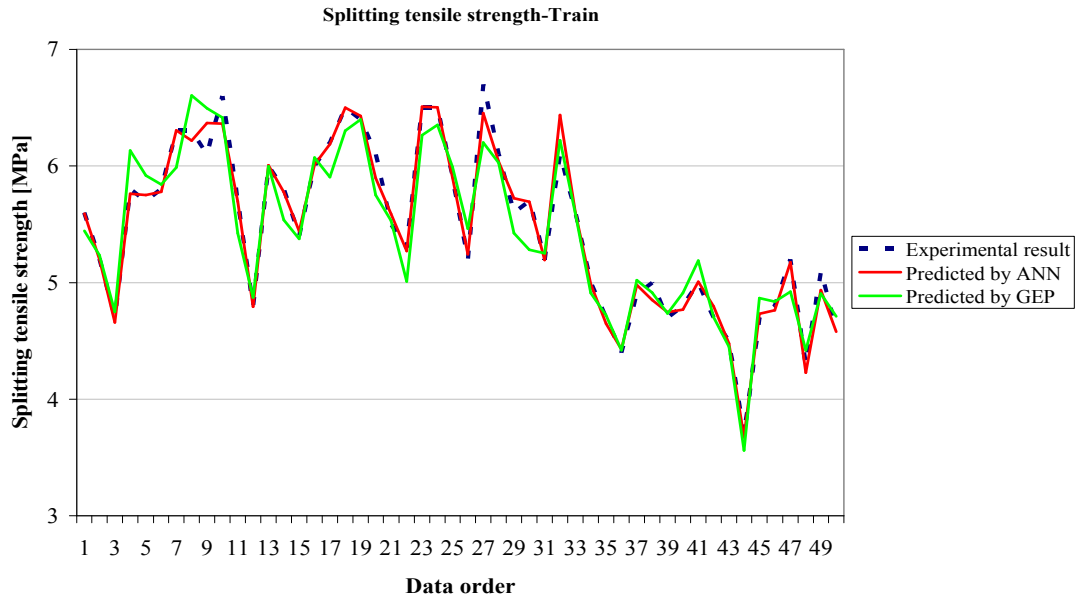


a)

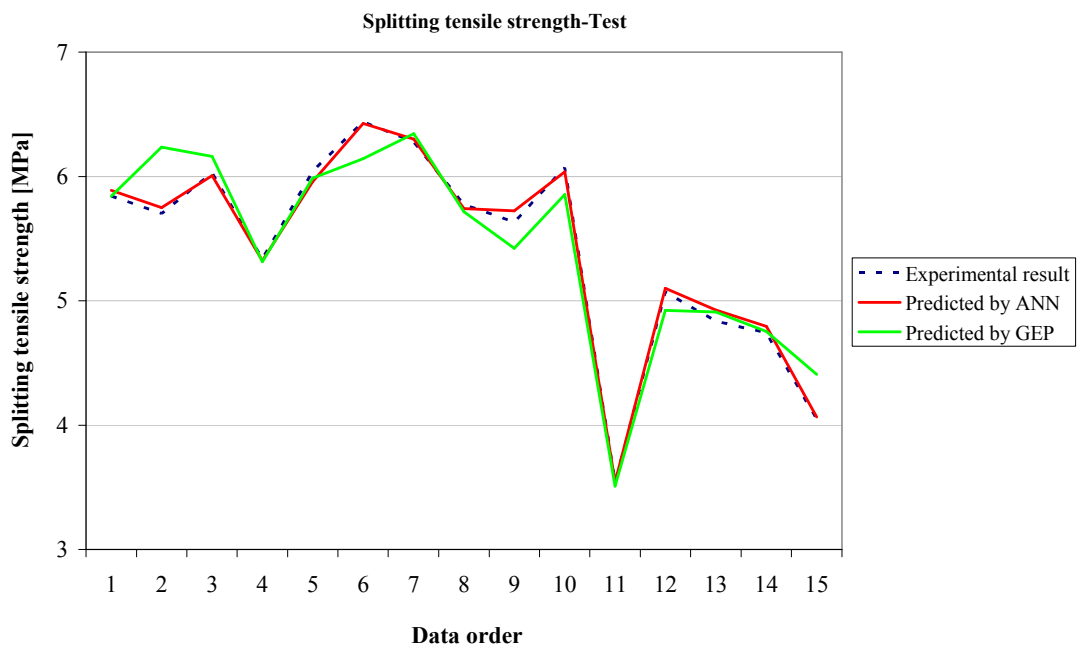


b)

Figure 5.16 Performance of the formulation of UPV of SCC a) train set b) test set

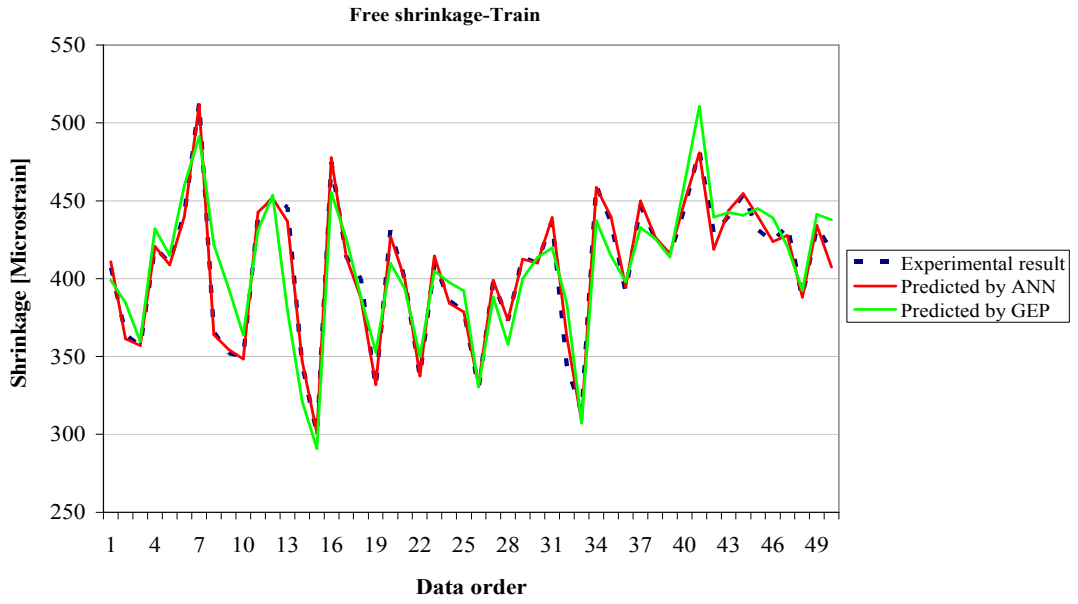


a)

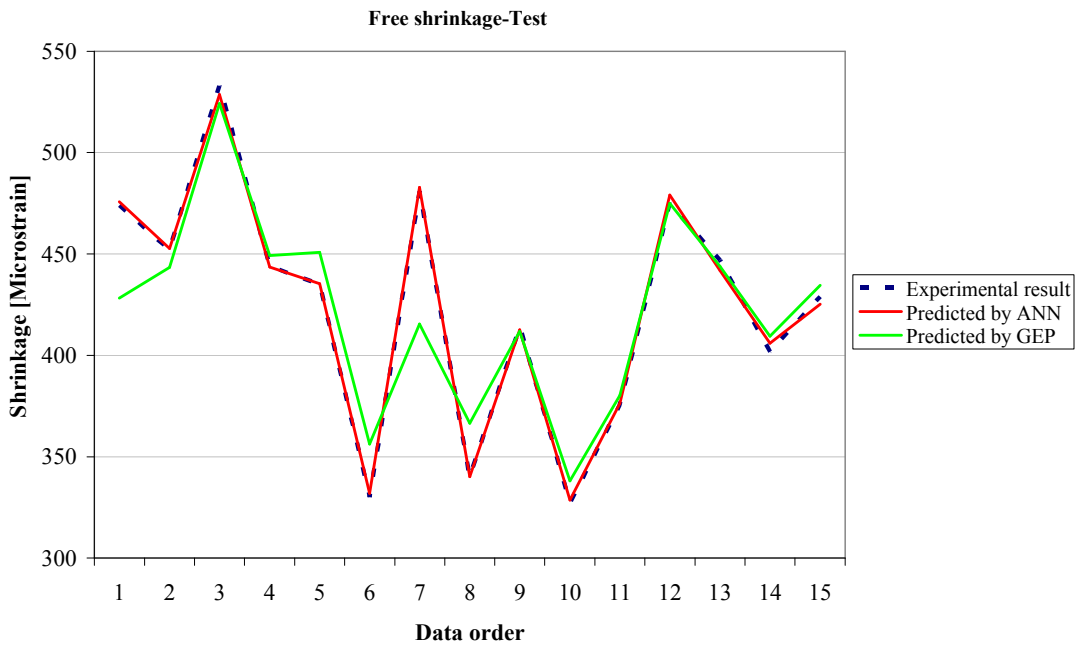


b)

Figure 5.17 Performance of the formulation of splitting tensile strength of SCC a) train set b) test set

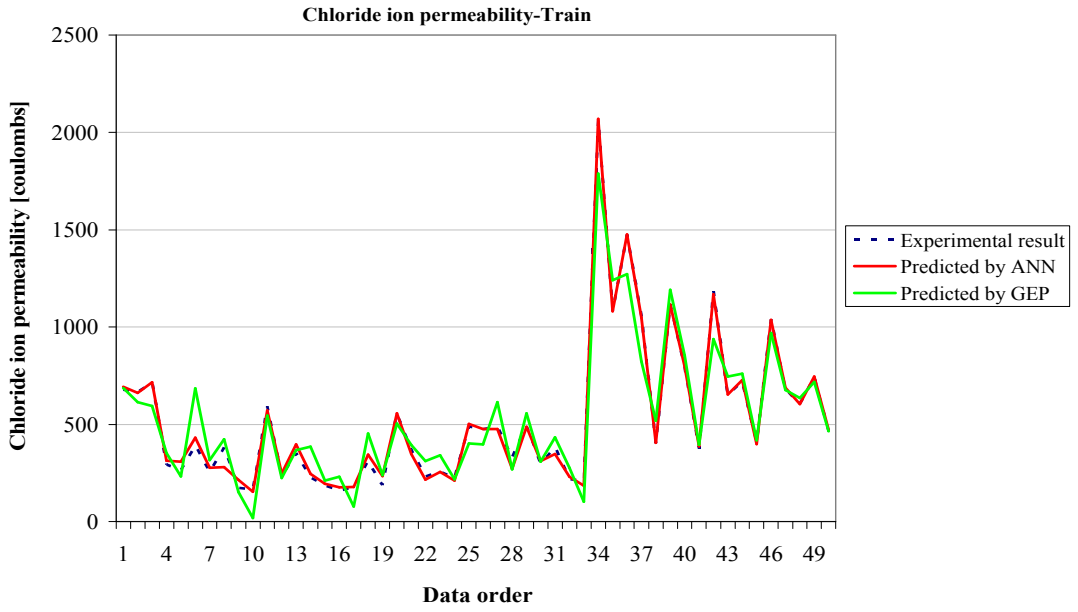


a)

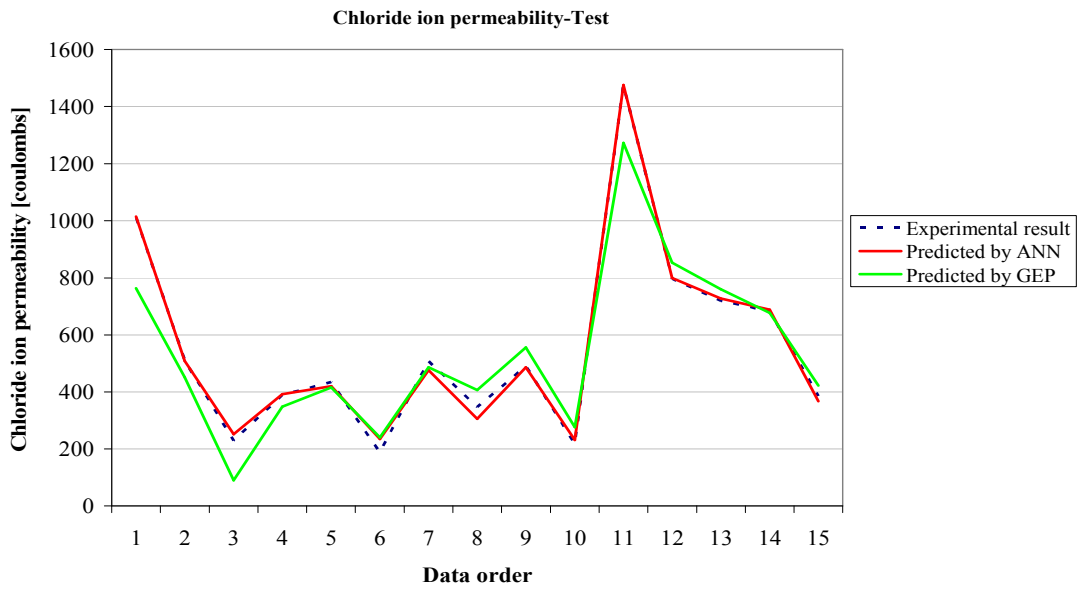


b)

Figure 5.18 Performance of the formulation of free shrinkage of SCC a) train set b) test set

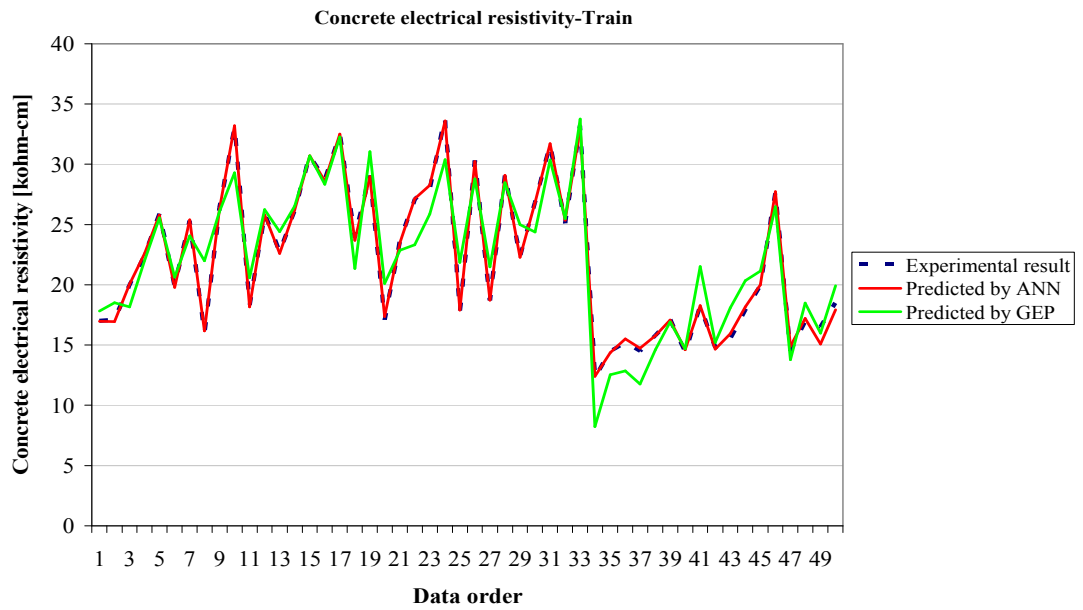


a)

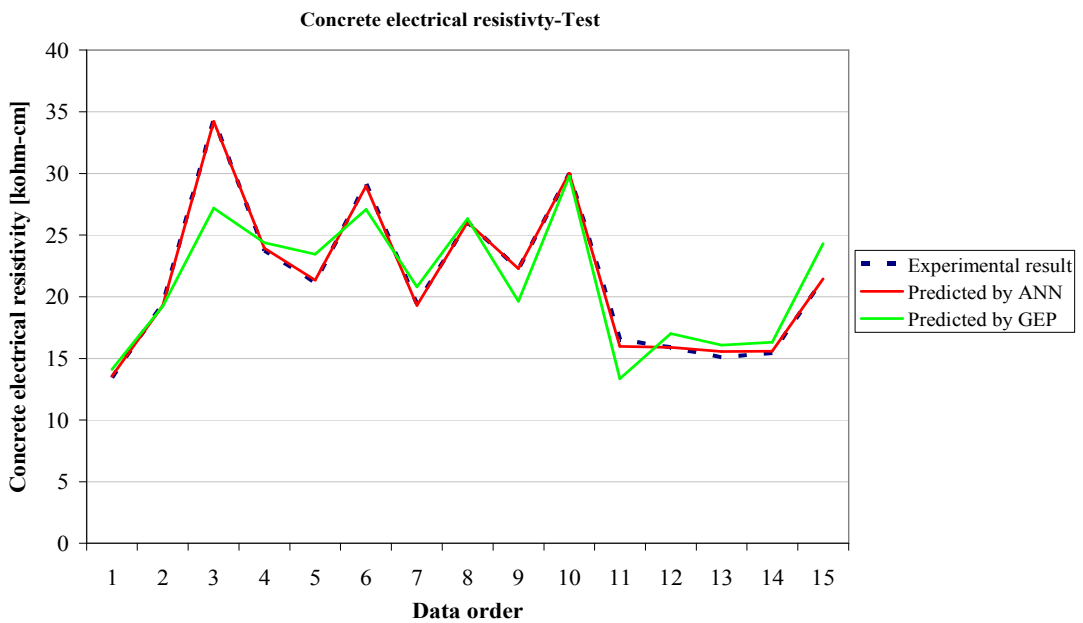


b)

Figure 5.19 Performance of the formulation of chloride ion permeability of SCC a) train set b) test set

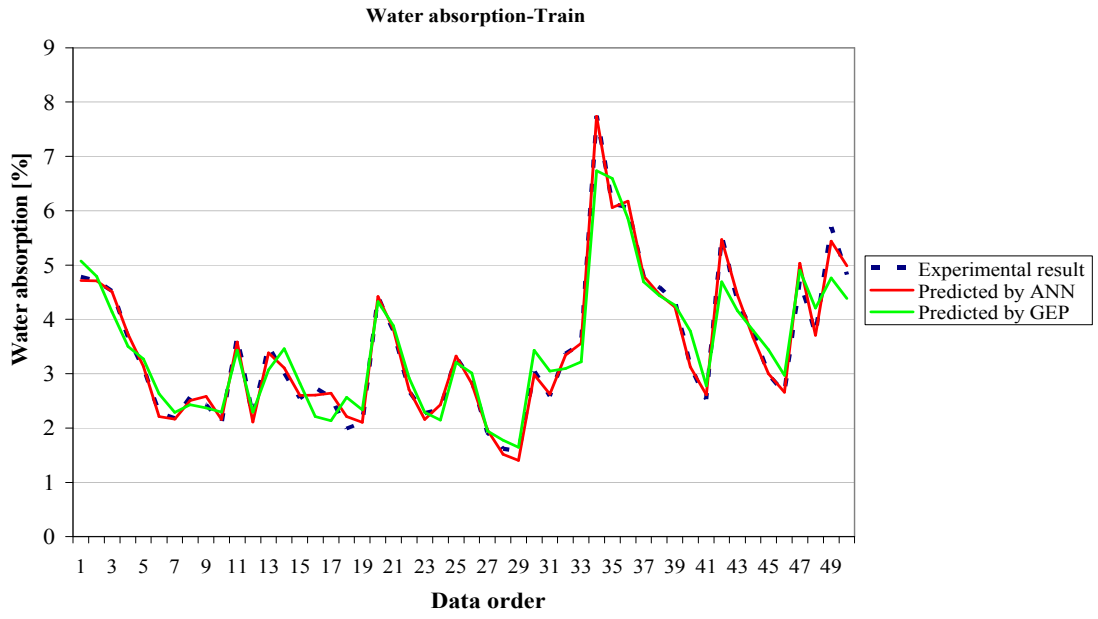


a)

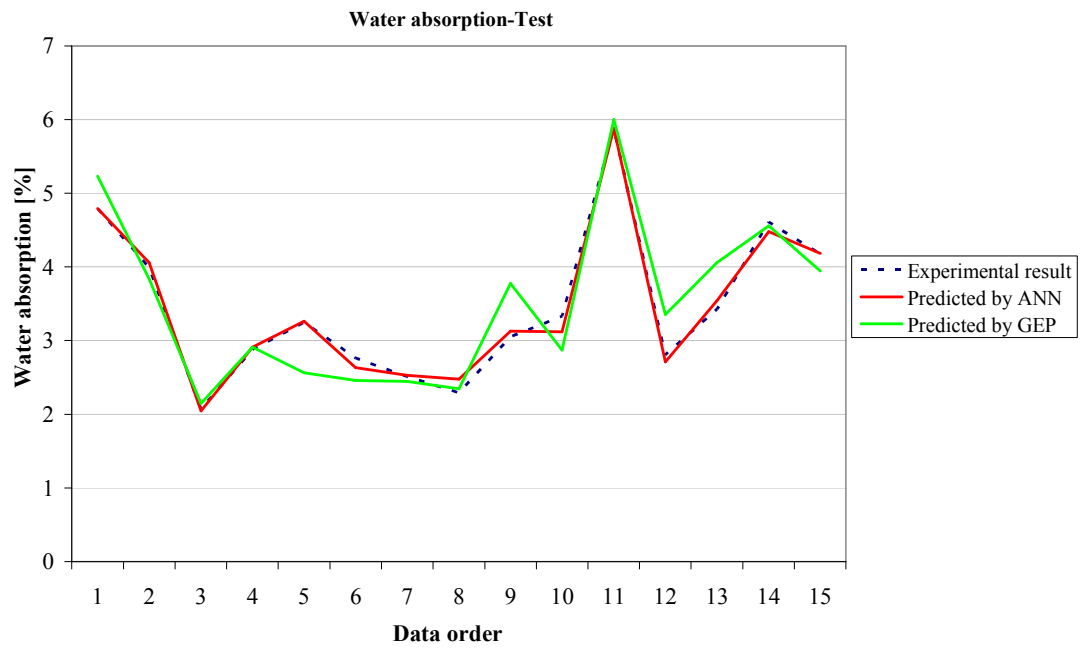


b)

Figure 5.20 Performance of the formulation of electrical resistivity of SCC a) train set b) test set

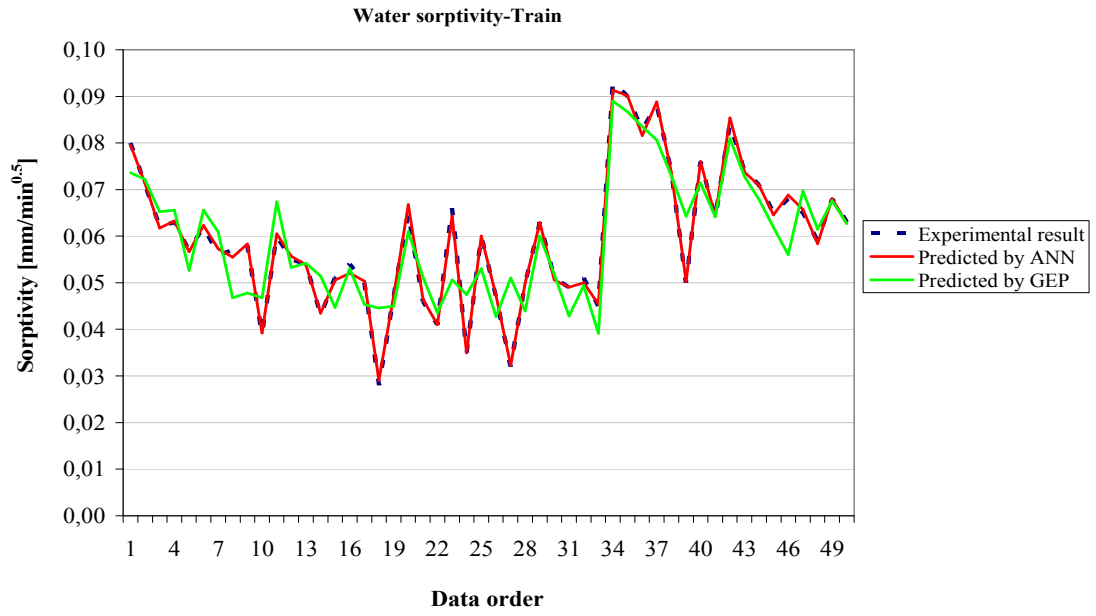


a)

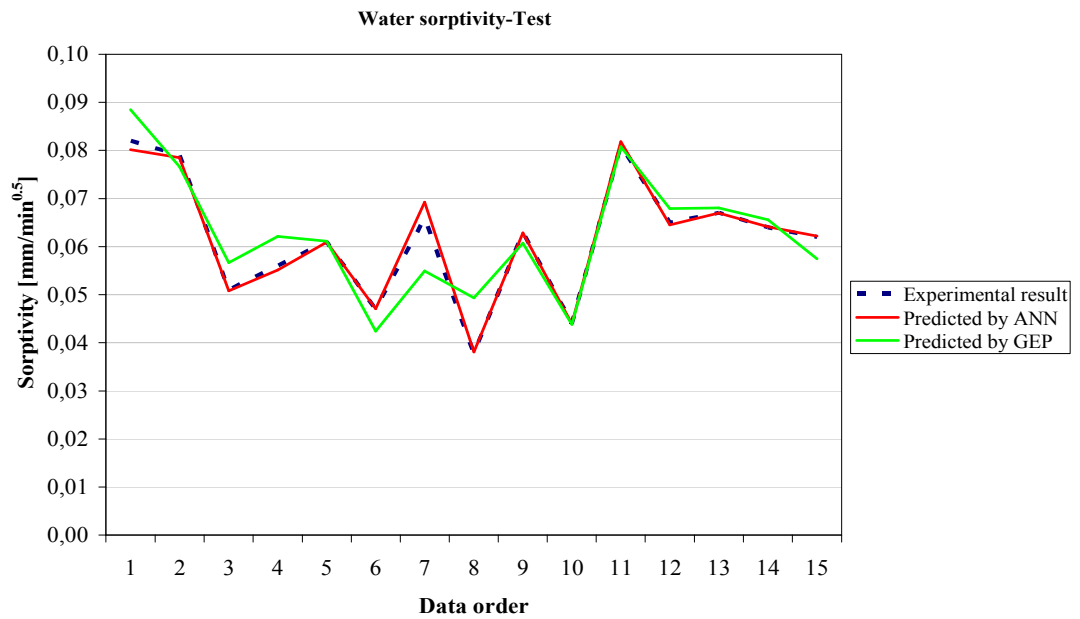


b)

Figure 5.21 Performance of the formulation of water absorption of SCC a) train set b) test set

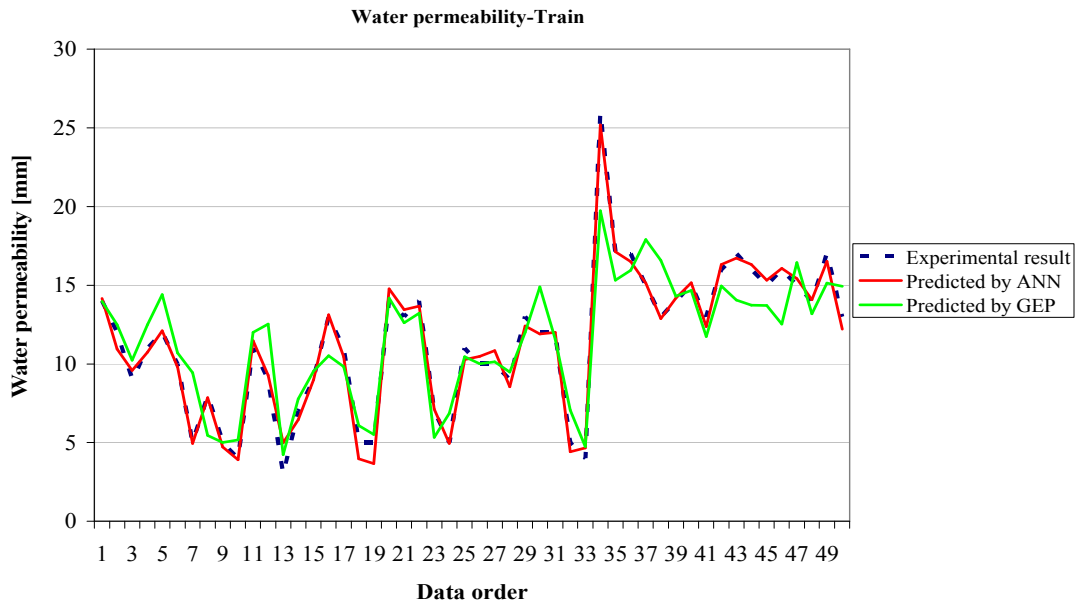


a)

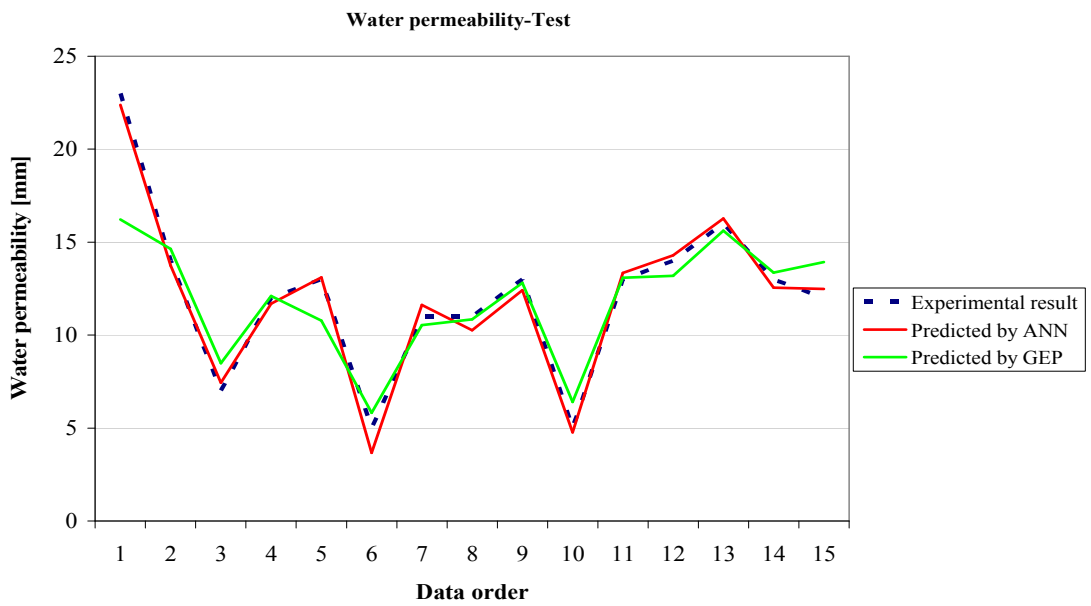


b)

Figure 5.22 Performance of the formulation of water sorptivity of SCC a) train set b) test set



a)



b)

Figure 5.23 Performance of the formulation of water permeability of SCC a) train set
b) test set

5.4.5 Comparisons of correlations obtained by soft computing models

In this part of the study, the correlations between the experimental test results as well as the relationships between the predicted values obtained using ANN and GEP techniques are explored. As it was explained section 5.4.1, when constructing the ANN and GEP models, the database involving the experimental results were subdivided into two groups, namely, training and testing sets. Training set was used for the training network, thereafter its performance was tested using the data in test set. When drawing the correlations in Figures 5.24 to 5.36, aforementioned two sets (training and test) were combined to acquire meaningful comparisons among the experimental results and soft computing techniques.

As it was known from the Table 5.2, ANN method had very high correlation coefficients so that predicting the actual experimental result better than GEP. Therefore, as seen in Figures 5.24 to 5.36 that the relationships between experimental results and those obtained for the corresponding ANN predictions were comparably similar, thus leading to approximately similar coefficients of correlations. ANN and GEP predictions along with the experimental results for T_{50} slump flow time and V-funnel flow time are given in Figure 5.24. It was observed in Figure 5.24 that the correlation coefficients for the relationships determined for the experimental results and ANN predictions are remarkably similar ($R = 0.76$) while GEP model had comparably low correlation coefficient of as low as 0.61.

Figure 5.25 presents the compressive strength versus ultrasonic pulse velocity relation based on the actual data as well as the predictions via ANN and GEP models. According to Figure 5.25, the compressive strength was highly correlated with the UPV values for both experimental results and the values predicted by ANN model. Interestingly, GEP model resulted in a better correlation for these properties of the concretes in spite of the relatively poor prediction performance of GEP. Therefore, a good correlation for the two inputs may be found although the GEP models poorly estimated the response values. Similar findings were also observed in Figures 5.26, 5.28, 5.29, 5.30, 5.32, 5.34, and 5.36. Figure 5.26 shows the comparison of the correlation between ultrasonic pulse velocity and splitting tensile strength on the basis of the experimental data, ANN, and GEP predictions. As seen in Figure 5.26, the correlation coefficients were almost similar. They had comparably

low correlation coefficients with respect to the compressive strength-ultrasonic pulse velocity relationship.

In Figure 5.27 it was observed that the electrical resistivity and chloride ion permeability had a relation in terms of a power function based on the experimental results as well as ANN and GEP predictions. This relation showed that increasing the electrical resistivity decreased the chloride ion transportation of SCCs. The correlation coefficients for the actual data and the ANN predictions were of comparable values. However, the GEP model had comparatively lower correlation coefficient.

It was observed in Figure 5.28 that there is a linear relationship between the water absorption and water sorptivity. In the comparisons of experimental results, ANN and GEP model predictions, it was seen that all of them had nearly same correlation coefficients. Comparison of the correlations for the water absorption and water permeability through the experimental results, ANN and GEP models is given in Figure 5.29. It was monitored in Figure 5.29 that correlation in ANN models had lower correlation coefficient with respect to the correlation obtained using the experimental results. However, the correlation developed using the predictions of GEP gave rise to slightly higher correlation coefficient. The highest coefficient of correlation for the water permeability of SCCs were obtained for the GEP model as seen in Figure 5.30.

Figure 5.31 shows the comparison of chloride ion permeability versus water absorption based on the experimental result, and estimations of ANN and GEP models. There was a quite similar variation between such properties of SCCs such that the correlation coefficient being about 0.80, irrespective of the data employed. The relation between the chloride ion permeability and water sorptivity test results is demonstrated in Figure 5.32. The relations are given for actual experimental result, ANN and GEP models predictions. As seen in Figure 5.32 that the proposed GEP model provided the best relationship along with a correlation coefficient of about 0.82. Figure 5.33 presents the relations between the chloride ion permeability and water permeability. As seen in Figure 5.33, there was a poor correlation the chloride ion permeability and water permeability of the concretes, irrespective of the data

employed. Nevertheless, using of ANN model and actual results led to better correlation than GEP model.

A relation in the form of power function between the electrical resistivity and water absorption test results is observed as seen in Figure 5.34. The behavior was almost similar for all of the three models (actual results, ANN and GEP predictions). It was observed in Figure 5.34, correlation coefficient of the relation developed using the GEP model had relatively higher. As it was presented in Table 5.2, prediction performance of GEP model was comparatively poor with respect to the ANN model. Therefore, this finding suggests that a good correlation between two relatively poor GEP models may be obtained. Figure 5.35 demonstrates the relation between electrical resistivity and water sorptivity test results. Moreover, the correlations of ANN and GEP models predictions of these two tests are also given in Figure 5.35. GEP model predictions of electrical resistivity and water sorptivity test results had relatively higher correlation coefficient of as high as 0.92. The relationships constructed using the actual results and ANN model were of a correlation coefficient of 0.81. In figure 5.36 the correlations between the electrical resistivity and water permeability tests are given. According to the Figure 5.36, there is a linear relation between these two tests. If the models were ranked according to the coefficients of correlation, GEP model had higher correlation coefficient of 0.79 followed by the actual data and ANN model, coefficient of correlation being the same for both of them ($R = 0.76$).

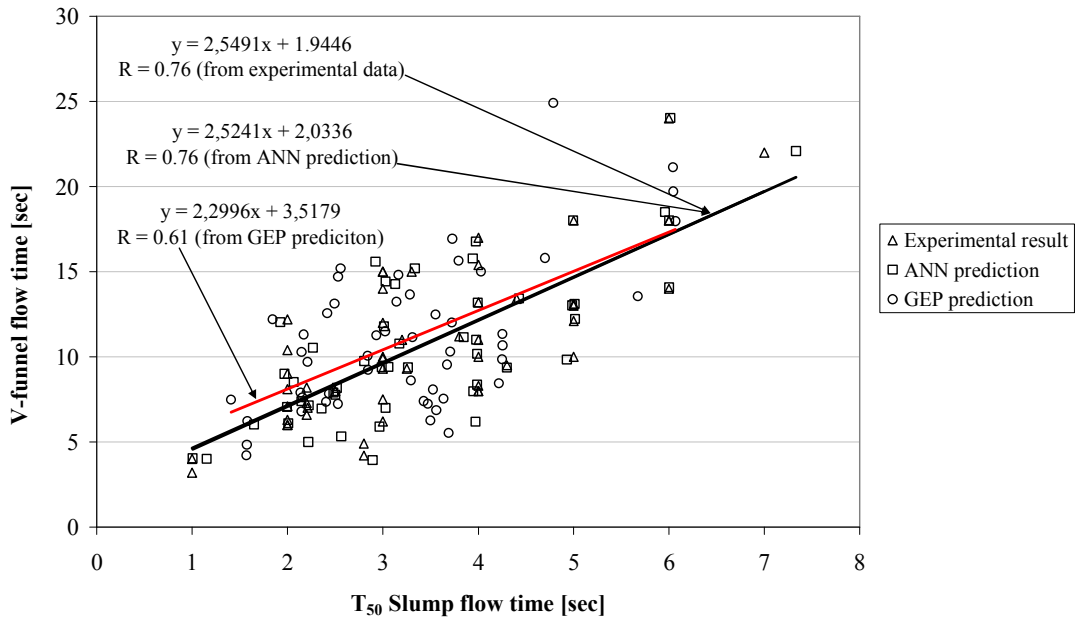


Figure 5.24 T₅₀ slump flow time and V-funnel flow time tests based comparisons of prediction performance of soft computing techniques

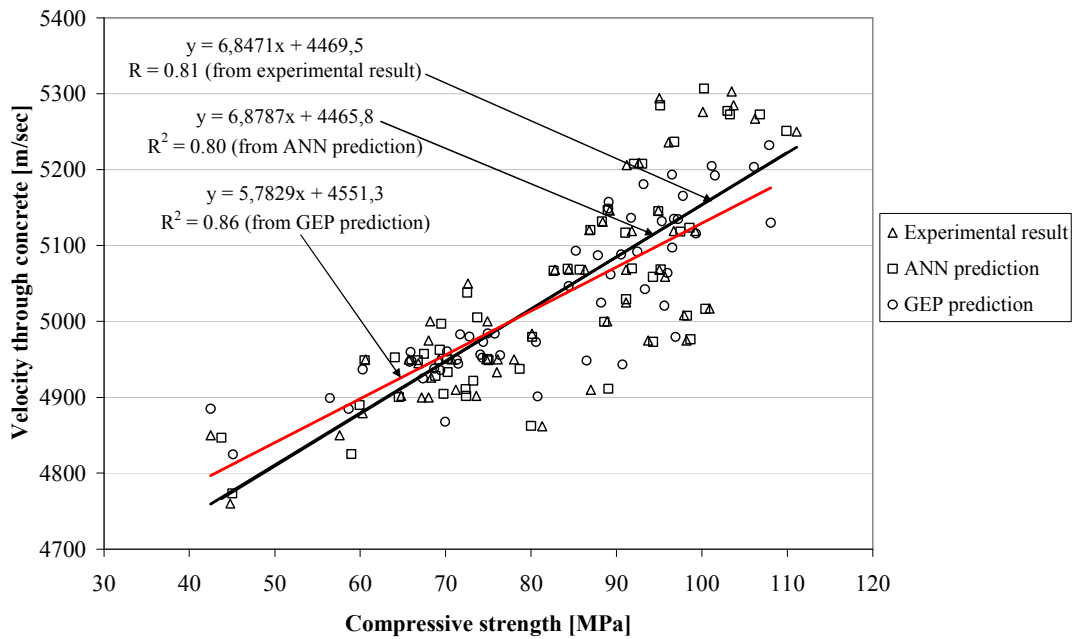


Figure 5.25 Compressive strength and velocity through concrete tests based comparisons of prediction performance of soft computing techniques

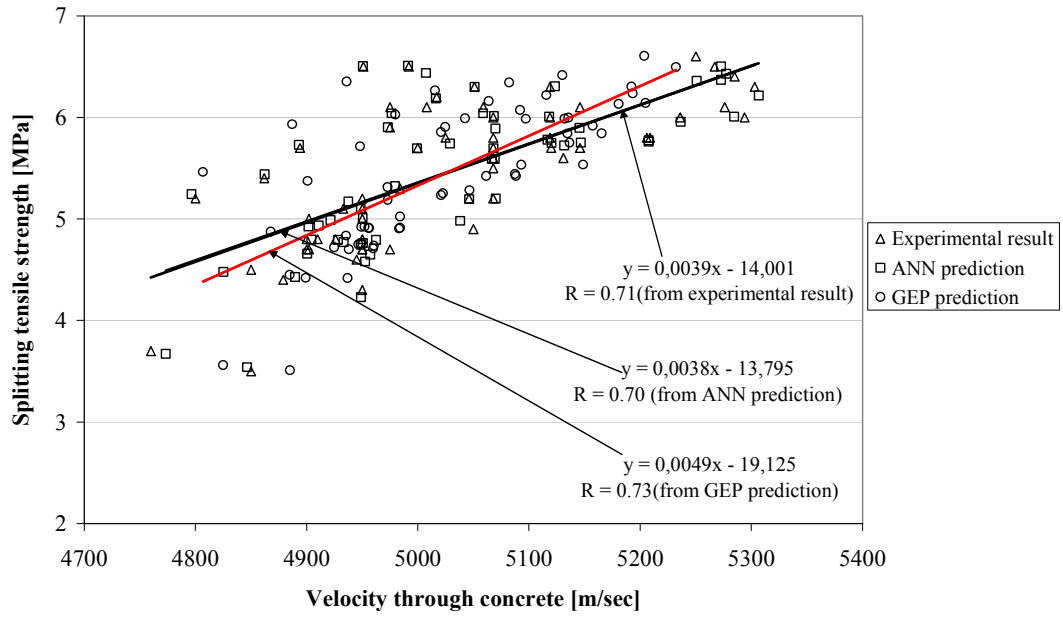


Figure 5.26 Velocity through concrete and splitting tensile strength tests based comparisons of prediction performance of soft computing techniques

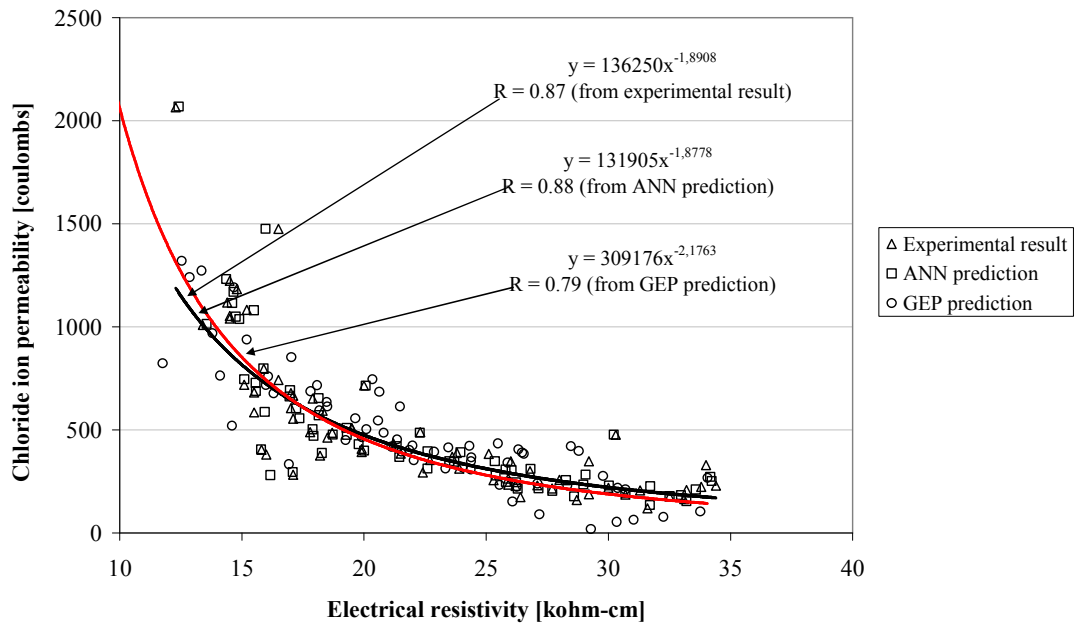


Figure 5.27 Electrical resistivity and chloride ion permeability tests based comparisons of prediction performance of soft computing techniques

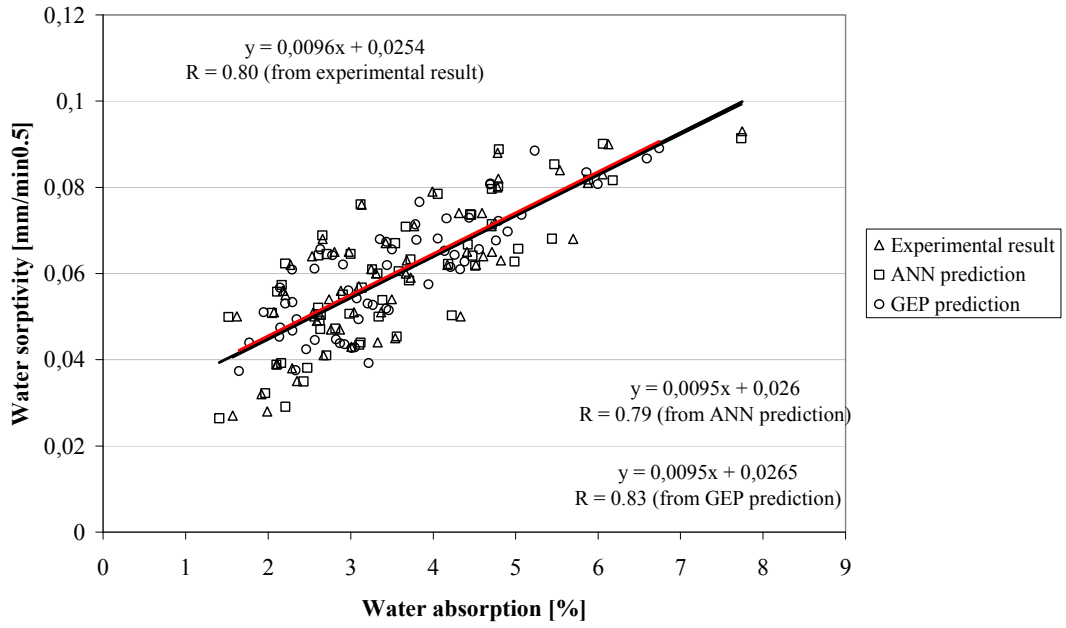


Figure 5.28 Water absorption and water sorptivity tests based comparisons of prediction performance of soft computing techniques

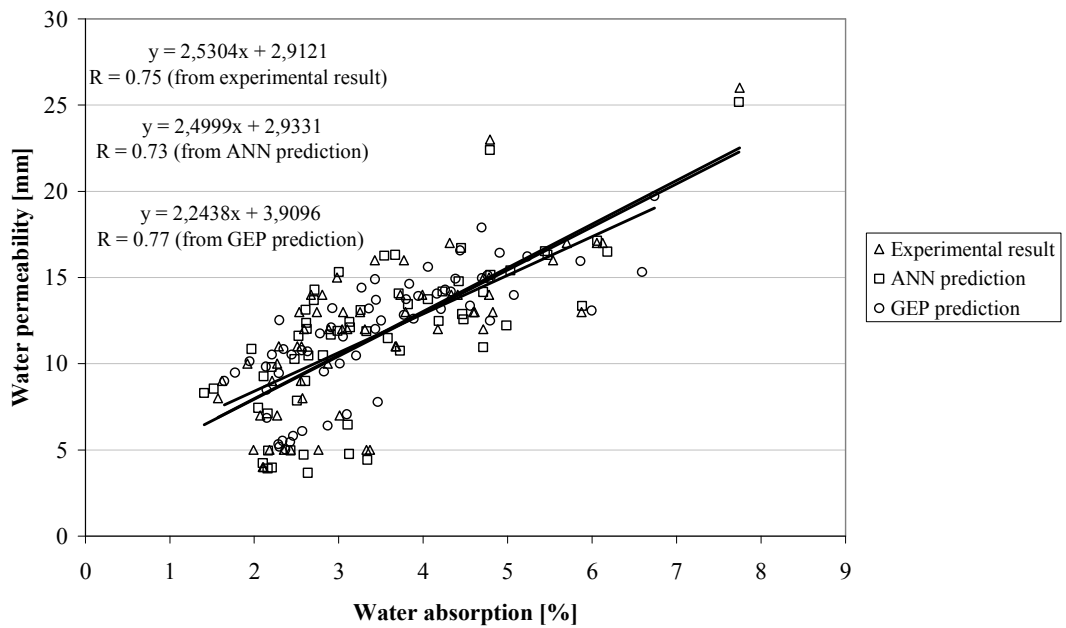


Figure 5.29 Water absorption and water permeability tests based comparisons of prediction performance of soft computing techniques

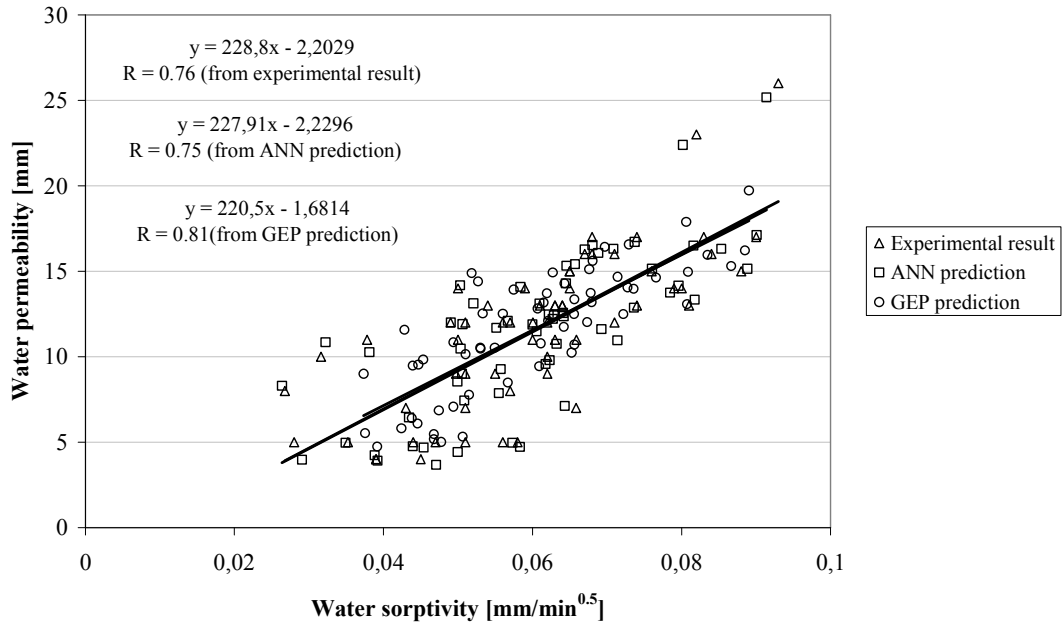


Figure 5.30 Water sorptivity and water permeability tests based comparisons of prediction performance of soft computing techniques

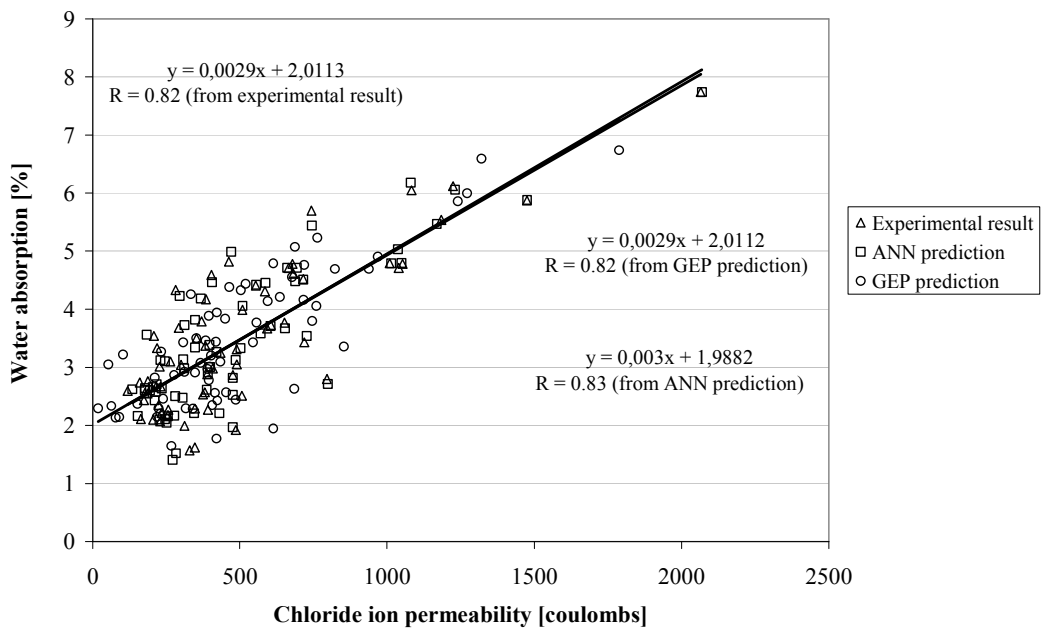


Figure 5.31 Chloride ion permeability and water absorption tests based comparisons of prediction performance of soft computing techniques

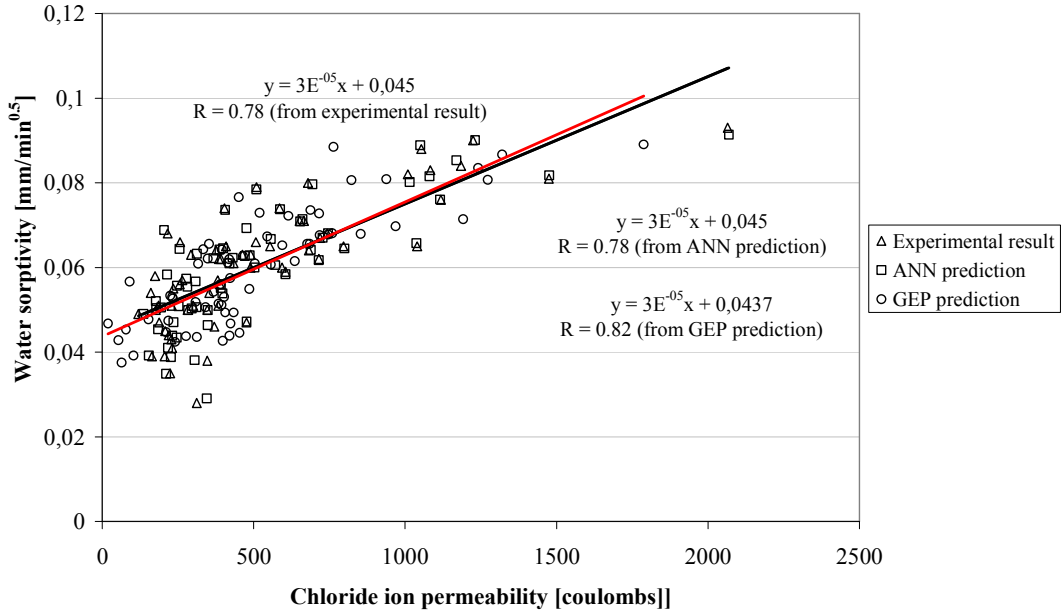


Figure 5.32 Chloride ion permeability and water sorptivity tests based comparisons of prediction performance of soft computing techniques

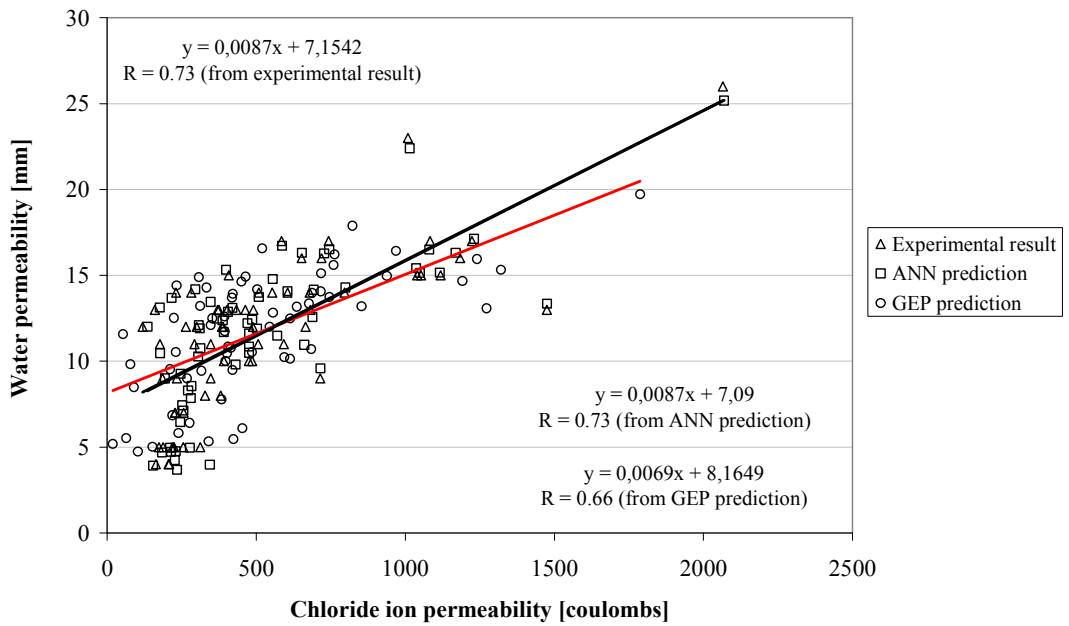


Figure 5.33 Chloride ion permeability and water permeability tests based comparisons of prediction performance of soft computing techniques

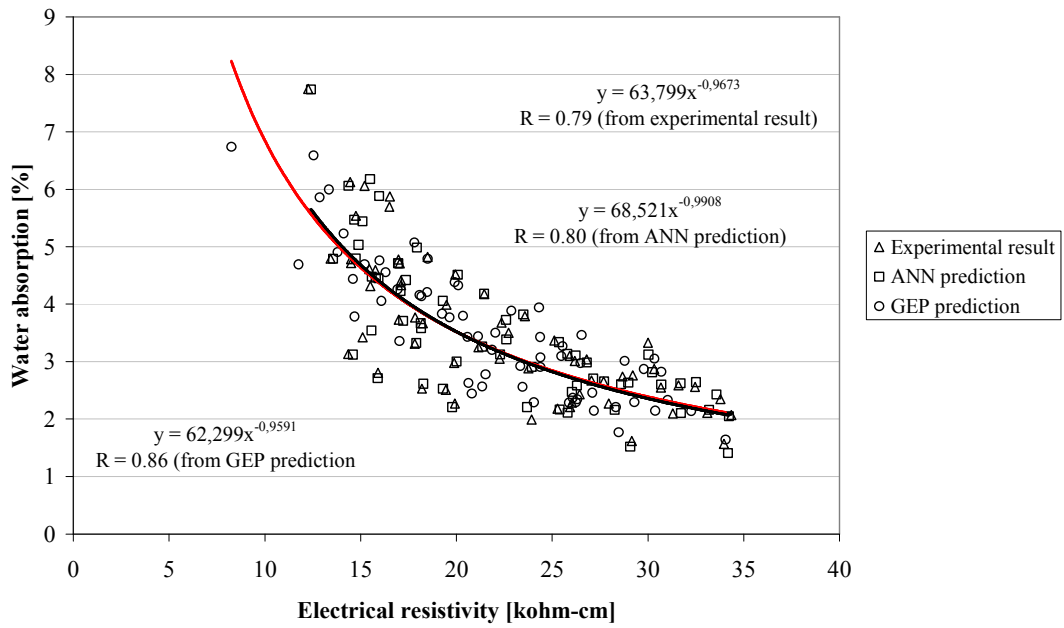


Figure 5.34 Electrical resistivity and water absorption tests based comparisons of prediction performance of soft computing techniques

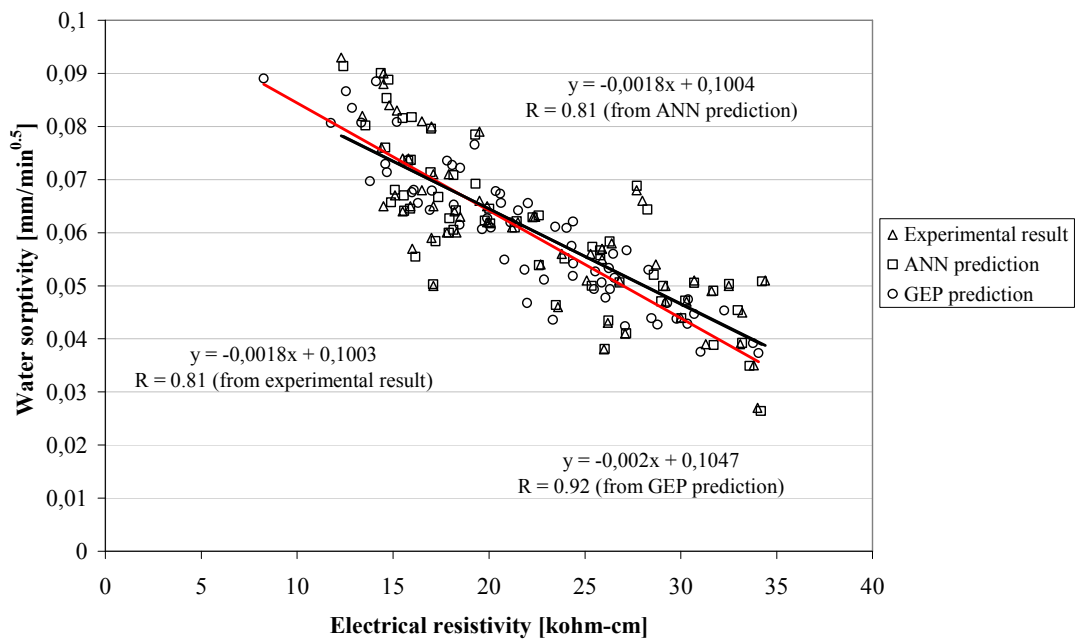


Figure 5.35 Electrical resistivity and water sorptivity tests based comparisons of prediction performance of soft computing techniques

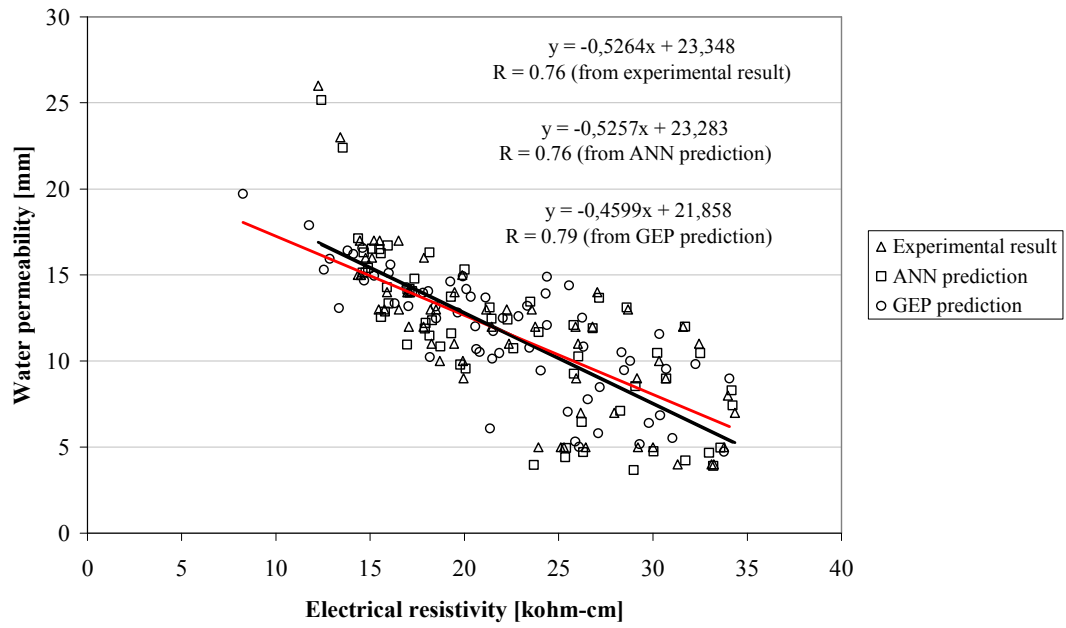


Figure 5.36 Electrical resistivity and water permeability tests based comparisons of prediction performance of soft computing techniques

6. OPTIMIZING CONCRETE MIXTURE PROPORTIONS

6.1 General

Mix proportions of SCCs were performed on the basis of single objective and multi objectives, respectively. Before constructing the optimization, properties of SCCs must be defined in the form of mathematical expressions as a function of the concrete mixture constituents. As explained in Chapter 5, properties of SCCs were predicted by using two well known soft computing techniques, namely artificial neural network and genetic programming. Considering the high prediction and generalization capability of artificial neural network (ANN), explicit formulations developed through this method were employed in the optimization studies.

6.2 Optimization Based on Single Response

Single objective optimization was performed to minimize the material cost of one cubic meter of SCCs. For this purpose, the material cost of 65 concrete mixtures in experimental database of the study was determined. Then, the optimum mix proportions were obtained to minimize the cost of concrete under the predefined constraints.

6.2.1 Cost calculation of self compacting concretes

Since there may be various expenses involved in concrete production, the first step in this part of the work was to identify the overall cost parameters affecting the cost of a 1 m³ of SCCs. For this, a very simple approach was used in order to compare the cost of concrete mixtures. The cost of one cubic meter of SCC was assessed only by considering the manufacturer point of view. The curing, erection and placing costs were not considered in the cost calculation in this research because these costs must be supplied by the purchaser. Furthermore, transportation and administrative costs

were not taken into account. Therefore, using the mix proportions of 65 concrete mixtures produced in the experimental part, the raw material costs of each mixture was calculated. Unit prices of each raw material were determined taking into account the economic rates in Turkey in June 2007. When defining cost of the raw materials involved in the concrete production, interviews were implemented with the managers of OYAK ready mixed concrete plants in Adana and the obtained unit costs were tabulated in Table 6.1. Based on the expenses for the raw materials, the cost of 1 m³ of SCC was then calculated for each mixture using the equation 6.1.

$$\text{Cost} = M_w * UP_w + M_{PC} * UP_{PC} + M_{FA} * UP_{FA} + M_{GGBFS} * UP_{GGBFS} + M_{SF} * UP_{SF} + M_{MK} * UP_{MK} + M_{fa} * UP_{fa} + M_{ca} * UP_{ca} + M_{SP} * UP_{SP} \quad (6.1)$$

where M denoted the mass of raw material e.g M_w mass of water, UP denotes the unit price of raw materials e.g UP_w unit price of water.

Table 6.1 Unit prices of raw materials

Materials	Unit price(YTL/kg)
Water (W)	0.003
Portland Cement(PC)	0.13
Fly ash (FA)	0.025
Ground granulated blast furnace slag (GGBFS)	0.03375
Silica fume (SF)	0.6075
Metakaolin (MK)	0.7425
Fine Aggregate(fa)	0.01
Coarse Aggregate(ca)	0.009
Superplasticizer(SP)	4.563

6.2.2 Optimization model for cost minimization

An optimization problem is formulated to determine the variables of SCC in order to obtain the mix proportion/proportions with the minimum cost. As known before there are nine design variables described as follows:

Water content (W)
Portland cement content (PC)
Fly ash content (FA)
Ground granulated blast furnace slag content (GGBFS)
Silica fume content (SF)
Metakaolin content (MK)
Fine aggregate content (fa)
Coarse aggregate content (ca)
Superplasticizer content (SP)

The cost of SCCs in terms of these variables is determined by using equation 6.1. Thus, the objective function for the optimization problem is to determined as

$$\text{Minimize } f_{\text{cost}} \quad (6.2)$$

The resulting concrete must meet the fresh, physical, mechanical, and durability requirements of the SCCs mentioned in the experimental part. For this purpose, acceptance criteria of EFNARC for the fresh properties such as T_{50} slump flow time, V-funnel flow time, and L box height ratio were defined as the constraints for fresh concrete. However, physical, mechanical and durability properties of SCCs in the optimization problem were defined within the range of experimental results. All of the constrains defined for the properties of SCCs were given in Table 6.2. Furthermore, the variables in SCCs must meet upper and lower limits of experimental database given Table 6.2. For the solution of this constrained optimization problem, the optimization process was carried out through a commercially available software package known as Design-Expert (2006).

Table 6.2 Design variables and responses constraints in the single objective optimization

No	Variables and responses	Goal	Lower limit	Upper limit	Constraint lower limit	Constraint upper limit
1	W	In range	176	198	176	198
2	PC	In range	180	550	180	550
3	FA	In range	0	330	0	330
4	GGBFS	In range	0	330	0	330
5	SF	In range	0	82.5	0	82.5
6	MK	In range	0	82.5	0	82.5
7	fa	In range	685	826	685	826
8	ca	In range	828	935	828	935
9	SP	In range	2.8	12	2.8	12
10	Slump flow diameter	In range	67	73	67	73
11	T50 Slump flow time	In range	1	7	2	5
12	V-funnel flow time	In range	3.2	37	6	12
13	L box H ₂ /H ₁ ratio	In range	0.704	0.976	0.8	1
14	Initial setting time	In range	220	925	220	925
15	Final setting time	In range	268	1074	268	1074
16	Compressive strength	In range	42.5	113.1	42.5	113.1
17	UPV	In range	4760	5303	4760	5303
18	Splitting tensile strength	In range	3.5	6.7	3.5	6.7
19	Free shrinkage	In range	300	533	300	533
20	Chloride ion permeability	In range	119	2065	119	2065
21	Electrical resistivity	In range	12.25	34.35	12.25	34.35
22	Water absorption	In range	1.57	7.75	1.57	7.75
23	Water sorptivity	In range	0.027	0.093	0.027	0.093
24	Water permeability	In range	3	26	3	26
25	Cost	Minimize	59.77	188.31	-----	-----

6.2.3 Desirability function

A useful approach for the optimization of single objective and/or multi objective optimization problems is to use desirability functions which reflect the levels of each response in terms of minimum and maximum desirability. Desirability is an objective function that ranges from zero, if it is outside the range, to one provided that the goal has been achieved. In case of maximizing and minimizing the individual responses, d_i is defined by equations 6.3 and 6.4, respectively (Bayramov et al., 2006).

$$d_i = \begin{cases} 0 & Y_i \leq \min f_i \\ \left[\frac{Y_i - \min f_i}{\max f_i - \min f_i} \right]^t & \text{and } 0 < d_i < 1 \\ 1 & Y_i \geq \max f_i \end{cases} \quad (6.3)$$

$$d_i = \begin{cases} 1 & Y_i \leq \min f_i \\ \left[\frac{\max f_i - Y_i}{\max f_i - \min f_i} \right]^t & \text{and } 0 < d_i < 1 \\ 0 & Y_i \geq \max f_i \end{cases} \quad (6.4)$$

The numerical optimization finds a point or points that maximize the desirability function. The characteristics of a goal may be altered by adjusting the weight or importance. All the target responses are combined into a desirability function as in equation 6.5. If any of the responses or factors falls outside their desirability range, the overall function becomes zero (Design-Expert, 2006).

$$D = (d_1 \times d_2 \times d_3 \times \dots \times d_n)^{1/n} \quad (6.5)$$

According to Myers and Montgomery (2002), it must not be distracted by trying to get a very high desirability value. The value is completely dependent on how closely the lower and upper limits are set relative to the actual optimum. The goal of optimization is to find a good set of conditions that will meet all the goals, not to get to a desirability value of 1. Desirability is simply a mathematical method to find the optimum (Myers and Montgomery, 2002). The goal field for responses must be one of choices, namely, none, maximum, minimum, target or in range. Factors will always be included in the optimization, at their design range by default, or as a maximum or minimum of target goal. According to Myers and Montgomery 2002) the meanings of the goal parameters are:

Maximum

$d_i = 0$ if response < low value

$0 \leq d_i \leq 1$ as response varies from low to high

$d_i = 1$ if response > high value

Minimum

$d_i = 1$ if response < low value

$0 \leq d_i \leq 1$ as response varies from low to high

$d_i = 0$ if response > high value

Target

$d_i = 0$ if response < low value

$0 \leq d_i \leq 1$ as response varies from low to target

$0 \leq d_i \leq 1$ as response varies from target to high

$d_i = 0$ if response > high value

Range

$d_i = 0$ if response < low value

$d_i = 1$ as response varies from low to high

$d_i = 0$ if response > high value

Where d_i for “in range” are included in the product of the desirability function but are not counted in determining n in Eqn.6.5. If the goal is none, the response will not be used for the optimization.

6.2.4 Results of cost minimization optimization

For the solution of predefined single objective constrained optimization problem, a commercially available software package known as Design-Expert 7.0.2 (2006) was used. At the end of the optimization process, 10 different solutions which satisfied the specified constraints and limits could be obtained. The desirability of the functions ranged from 0.78 to 1. Optimum mixtures were ordered according to the highest desirability and given in Table 6.3. The graphically demonstration of desirability function was depicted in Figure 6.1. In Figure 6.1, the variation of desirability is given as the function of silica fume and metakaolin. The other seven parameters were kept constant at the optimum levels of optimum mix proportion in

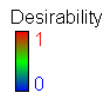
line 1 of Table 6.3. Moreover, the predicted responses for these ten mixtures are given in Table 6.4.

Table 6.3 Optimum mix proportions for cost minimization

No	W	C	FA	GGBFS	SF	MK	Binder	W/B	fa	ca	SP	D*
1	176	254	75	28	69	3	429	0.41	688	859	11	1
2	182	248	18	14	77	28	385	0.47	795	866	12	1
3	181	243	6	173	49	6	477	0.38	690	901	5.7	1
4	180	292	109	120	47	1	569	0.32	693	931	6.3	1
5	182	233	55	20	44	7	359	0.50	707	846	12	1
6	176	324	0	8	81	3	416	0.43	823	932	5.7	1
7	186	356	0	0	83	0	439	0.42	759	931	7.2	0.985
8	184	220	0	61	83	19	383	0.48	733	839	3	0.857
9	187	366	34	0	53	60	513	0.37	826	910	4.1	0.803
10	188	287	9	0	16	74	386	0.49	823	828	12	0.780

* Desirability

Design-Expert® Software



X1 = E: SF
X2 = F: MK

Actual Factors
A: W = 176.24
B: C = 254.24
C: FA = 74.86
D: GGBFS = 28.06
G: fa = 687.54
H: ca = 859.38
J: SP = 11.34

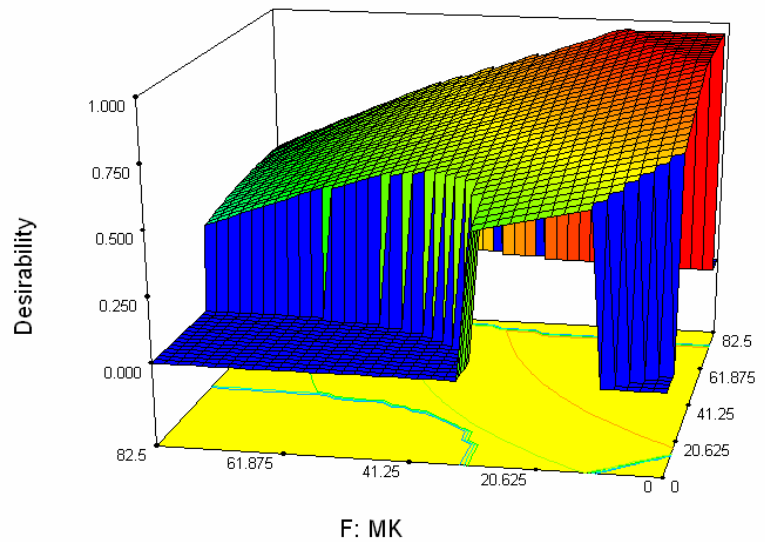


Figure 6.1 Graphically demonstration of changing of desirability function with SF and MK

Table 6.4 Predicted response values of the SCC properties according to ten optimal mixtures

SCC Property	OM1*	OM2	OM3	OM4	OM5	OM6	OM7	OM8	OM9	OM10
Slump flow diameter [cm]	67.9	68.2	70.0	71.9	68.2	70.5	69.9	69.3	70.2	71.8
T50 Slump flow time [sec]	3.3	2.6	3.2	3.8	2.9	3.2	2.9	2.9	3.1	2.1
V-funnel flow time [sec]	6.6	8.8	7.9	6.4	7.7	8.8	8.1	8.4	12.0	8.1
L box H ₂ /H ₁ ratio	0.862	0.844	0.809	0.885	0.868	0.875	0.831	0.812	0.800	0.953
Initial setting time [min]	294	367	326	361	279	318	306	368	379	580
Final setting time [min]	436	502	423	464	417	409	406	477	455	731
Compressive strength [MPa]	69.9	71.2	57.1	57.8	74.0	70.6	56.5	75.2	72.3	93.2
UPV [m/sec]	4971	4927	4850	4900	4935	4914	4765	4937	4924	4986
Splitting tensile Strength [MPa]	4.8	5.0	4.2	4.2	5.0	4.9	4.3	5.1	4.9	5.9
Free shrinkage [Microstrain]	451	469	409	391	443	376	414	429	375	424
Chloride ion permeability [Coulombs]	980	733	1019	854	655	688	904	685	802	181
Electrical resistivity [kohm-cm]	16.0	18.1	15.7	17.0	17.1	25.2	17.5	14.0	20.8	27.3
Water absorption [%]	5.57	4.38	4.95	4.58	4.88	2.92	4.00	4.57	3.87	1.97
Water sorptivity [mm/min ^{0.5}]	0.082	0.076	0.076	0.069	0.072	0.055	0.074	0.073	0.064	0.045
Water permeability [mm]	16	14	18	15	14	11	17	17	13	9
Cost [YTL/m ³]	48.3	57.3	58.6	59.2	59.4	59.7	61.7	78.1	85.1	88.0
Desirability function value	1	1	1	1	1	1	0.985	0.857	0.803	0.780

*Optimum Mixture

6.3 Multi Objective Optimization Based on Several Responses

6.3.1 General

In the previous section (section 6.2), the mixture proportioning problem was solved according to the only one objective function. However, many design problems require simultaneous optimization of multiple, and in many cases conflicting, objectives. For example, mixture proportioning of the self compacting concrete involves several objectives which cannot be combined into a single objective function. These usually include fresh, physical, mechanical and durability properties as well as economical aspects. In the optimization literature, such kinds of problems are known as multi objective optimization (MOO). Generally a MOO problem is of the following form:

$$\begin{aligned} &\min \text{ or } \max \quad Y(X) \\ &\text{such that;} \\ &X \in S = \left[X \mid X \in A^n, g_i(X) \leq a_i, h_j(X) = b_j \right] \quad i = 1, 2, \dots, m \quad j = 1, 2, \dots, n \end{aligned}$$

where, X is an n -dimensional vector of the decision variables; $Y(X) = \{Y_1(X), Y_2(X), \dots, Y_k(X)\}$ is the set of objective functions; and S is the set of feasible solutions, bounded by m inequality constraints (g_i) and n equality (h_j) constraints, a_i and b_j are constants. For continuous variables $A = \mathbb{R}$, A contains the set of permissible values in the case of for discrete variables.

Several studies have been conducted regarding the implementation of MOO in the field of construction materials. Muthukumar and Mohan (2004) optimized mix proportions of polymer concrete to have minimum void. For each polymer concrete combination, the mechanical properties such as compressive strength, and flexural and splitting strengths were studied using the multi-objective optimization technique for maximum values and compared with the experimental data. Once having maximum values in all the responses, a combined optimization was done and a mix design was recommended. Chung et al. (2004) proposed a MOO methodology which simultaneously considers the mechanical performance and the manufacturing cost from the early stage of design of composite laminated plates. Sahab et al. (2005) optimized the cost of reinforced concrete flat slab buildings. The objective function was the total cost of the building including the cost of floors, columns, and

foundations. The cost of each structural element covers that of material and labor for reinforcement, concrete and formwork. Karihaloo and Lange-Kornbak (2005) demonstrated how rigorous mathematical programming techniques can be employed in the design of fibre-reinforced concrete mixtures which have both high tensile strength and high ductility. Bayramov et al. (2004) optimized the fracture parameters of steel fibre reinforced concretes to obtain a more ductile behavior than that of plain concrete. The effects of the aspect ratio and volume fraction of steel fibre on fracture properties of concrete in bending were investigated by measuring the fracture energy and characteristic length. For optimization, three-level full factorial experimental design and response surface method were used. The results show that the effects of fibre volume fraction and aspect ratio on fracture energy and characteristic length are very significant.

6.3.2 Multi objective optimization model

An optimization problem is formulated to determine the SCC variables in order to obtain the mix proportion/proportions with several responses. As known from section 6.2, there exist nine design variables in this study. As also known from the chapter five, fresh, physical, mechanical and durability properties of SCCs were estimated with high precision by using artificial neural network (ANN). Therefore, multi objective optimizations of SCC mix proportion were performed using explicit ANN formulations.

The mixture constituents of SCCs were optimized simultaneously for minimization of chloride ion permeability, water absorption, water sorptivity, water permeability, free shrinkage strain, and cost while for maximization of compressive strength, ultrasonic pulse velocity, splitting tensile strength, and electrical resistivity. Moreover, T_{50} slump flow time, V-funnel flow time and L box height ratio were defined as constraints of fresh properties in the range of EFNARC (2002). All of the objective functions and constrains defined in the problem were given in Table 6.5. As in the case of single objective optimization, the design variables in SCCs must meet the upper and lower limits of the experimental database given Table 6.5.

Table 6.5 Design variables and responses constraints in the multi objective optimization

No	Variables and responses	Goal	Lower limit	Upper limit	Constraint lower limit	Constraint lower limit
1	Water	In range	176	198	176	198
2	Cement	In range	180	550	180	550
3	Fly ash	In range	0	330	0	330
4	Ground granulated blast furnace slag	In range	0	330	0	330
5	Silica fume	In range	0	82.5	0	82.5
6	Metakaolin	In range	0	82.5	0	82.5
7	Fine aggregate	In range	685	826	685	826
8	Coarse aggregate	In range	828	935	828	935
9	Superplasticizer	In range	2.8	12	2.8	12
10	Slump flow diameter	In range	67	73	67	73
11	T50 Slump flow time	In range	1	7	2	5
12	V-funnel flow time	In range	3.2	37	6	12
13	L box H2/H1 ratio	In range	0.704	0.976	0.8	1
14	Initial setting time	In range	220	925	220	925
15	Final setting time	In range	268	1074	268	1074
16	Compressive strength	Maximize	42.5	113.1	----	----
17	UPV	Maximize	4760	5303	----	----
18	Splitting tensile strength	Maximize	3.5	6.7	----	----
19	Free shrinkage	Minimize	300	533	----	----
20	Chloride ion permeability	Minimize	119	2065	----	----
21	Electrical resistivity	Maximize	12.25	34.35	----	----
22	Water absorption	Minimize	1.57	7.75	----	----
23	Water sorptivity	Minimize	0.027	0.093	----	----
24	Water permeability	Minimize	3	26	----	----
25	Cost	Minimize	59.77	188.31	----	----

6.3.3 Results of multi objective optimization

Similar to the single objective optimization, the solution of multi objective optimization problem was performed via a commercially available software package known as Design-Expert 7.0.2 (2006) which provided the overall desirability function. The responses in the optimization were considered to have an equal importance ($t=1$) in equations 6.3 and 6.4. At the end of the optimization process, four different solutions which satisfied the specified constraints and the limits could

be acquired. The desirability of the functions ranged from 0.564 to 0.655. The optimum mixtures were ordered according to the highest desirability and given in Table 6.6 and the graphically demonstrated in Figure 6.2., the variation of overall desirability function is given as the function of silica fume and metakaolin as shown in Figure 6.2. However, the other seven parameters were kept constant at the optimum levels of mixture proportioning given in the first line of Table 6.6. Moreover, the predicted responses for the mixtures having optimal constituents are given in Table 6.7.

Table 6.6 Optimum mix proportions for multi objective optimization

No	W	C	FA	GGBFS	SF	MK	Binder	W/B	fa	ca	SP	D*
1	194	245	305	0	0	0	550	0.35	685	829	6.3	0.655
2	184	246	213	0	0	46	505	0.36	825	935	12	0.616
3	180	274	0	0	45	82	401	0.45	685	828	6.5	0.599
4	188	224	276	8	14	9	532	0.35	826	913	3.7	0.564

*Desirability

Table 6.7 Predicted response values of the SCC properties according to four optimal mixtures

SCC Property	Optimum Mix 1	Optimum Mix 2	Optimum Mix 3	Optimum Mix 4
Slump flow diameter [cm]	70.4	71.2	71.6	71.0
T50 Slump flow time [sec]	3.0	4.2	3.4	4.1
V-funnel flow time [sec]	11.9	11.0	9.8	12.0
L box H ₂ /H ₁ ratio	0.910	0.923	0.939	0.879
Initial setting time [min]	337	362	273	498
Final setting time [min]	446	446	397	662
Compressive strength [MPa]	82.6	93.4	90.2	83.4
UPV [m/sec]	4957	5277	5000	4951
Splitting tensile Strength [MPa]	5.4	5.9	5.6	5.4
Free shrinkage [Microstrain]	351	401	414	311
Chloride ion permeability [Coulombs]	157	473	260	462
Electrical resistivity [kohm-cm]	28.8	18.8	23.1	20.4
Water absorption [%]	2.30	3.23	2.74	3.52
Water sorptivity [mm/min ^{0.5}]	0.052	0.053	0.063	0.064
Water permeability [mm]	10	15	11	10
Cost [YTL/m ³]	118.8	117.3	120.1	127.9
Desirability function value	0.655	0.616	0.599	0.564

Design-Expert® Software

Desirability



X1 = E: SF
X2 = F: MK

Actual Factors
A: W = 194.08
B: C = 244.56
C: FA = 304.59
D: GGBFS = 0.32
G: fa = 685.04
H: ca = 828.96
J: SP = 6.27

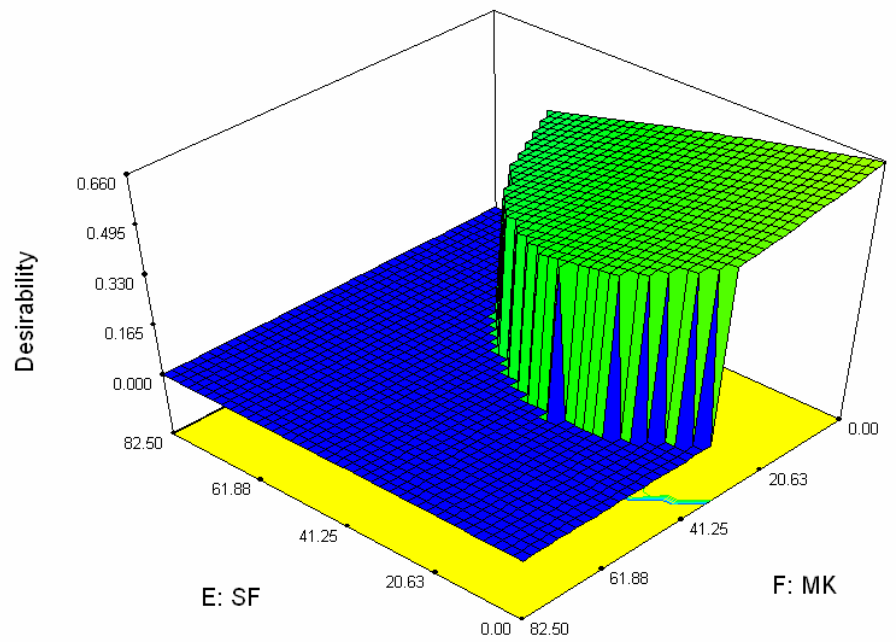


Figure 6.2 Graphically demonstration of changing of overall desirability function with SF and MK

7. CONCLUSIONS

An experimental program was conducted to investigate the effects of mineral admixtures used in binary (two components), ternary (three components), and quaternary (four components) cementitious blends on the mechanical, physical, and durability properties of self compacting concretes. In this context, four mineral admixtures, namely fly ash, ground granulated blast furnace slag, silica fume, and metakaolin were employed. A total of 65 self compacting concrete mixtures were designed at 0.32 and 0.44 water/binder ratios. Moreover, based on the test results, the fresh and hardened properties of self compacting concretes were predicted depending on the mixture constituents of SCCs using artificial neural network and genetic programming techniques. Using the explicit artificial neural networks based mathematical expressions single and multi objective optimization problems are formulated and solved to obtain the best possible values for ingredient of SCCs for single and several responses. Based on the findings of this study the following conclusions were drawn:

1. All of the concrete mixtures were designed to give a slump flow diameter of 70 ± 3 cm which was realized by using superplasticizer at varying amounts. Therefore, the slump flow diameter of the concretes ranged from 67 to 73 cm. Slump flow times (T_{50}) of all produced concretes were less than 7 sec. Binary blends of FA, GGBFS and SF had generally lower slump flow time (T_{50}) than the control concrete. However, the concretes containing MK had similar T_{50} duration with the control concrete at w/b ratio of 0.32 concretes.
2. The ternary and quaternary systems improved the flow characteristics of the SF and MK concretes in that T_{50} durations were significantly reduced by the combined use of FA, GGBFS, SF, and MK at w/b ratio of 0.32 concretes. The binary use of FA, GGBFS, and SF with portland cement generally increased the slump flow time of SCC when compared to that of the control mixture at w/b ratio of 0.44 concretes. Using the ternary and quaternary blends of the mineral admixtures provided better performance than the binary blends.

3. Apart from the control concrete, the mixtures particularly containing binary blends of FA, GGBFS, SF, and MK did not fulfill the EFNARC recommendation in terms of V-funnel flow time. However, the concretes made with the ternary or quaternary blends of FA, GGBFS, SF, and MK generally yielded more satisfactory performance at the w/b ratio of 0.32. Except for the 40% GGBFS mixture, all the concretes satisfied the upper acceptance limit of EFNARC but because of the lack of cohesion some of them did not fulfill the lower limit recommendation of EFNARC at the w/b ratio of 0.44.
4. L-box H_2/H_1 height ratio ranged from 0.704 to 0.976 depending mainly on binder used in concrete and w/b ratio. At high w/b ratio concretes, binary (PC+FA, PC+GGBFS, PC+SF) and ternary use of (PC+FA+GGBFS) mineral admixtures in the production of SCCs increased the H_2/H_1 ratio with the increasing of replacement level of mineral admixtures. Conversely, a reducing trend was monitored in the ternary blends of PC+GGBFS+SF blends at high replacement ratios. The ratio of H_2/H_1 was in the range of 0.8–1 for almost all of the concrete mixtures containing one or more of the supplementary cementitious materials at low w/b ratio.
5. There is a clear trend that the binary use of FA or GGBFS with ordinary PC significantly prolonged the initial and final setting times of the SCCs. The effect of SF was to reduce both initial and final setting times of the SCCs especially when used at 10 and 15% replacement levels. The setting times of MK concretes at low w/b ratio slightly increased with increasing MK content from 5 to 10%. When the amount of MK, however, further increased to 15%, there was a marginal reduction in both initial and final setting times in comparison to those of the concrete having 5 or 10% MK content. Even though using the mineral admixtures in the ternary blends reduced the setting time, the mixture incorporating quaternary blends of the mineral admixtures had the shortest setting times, even below those of the control mixture. Test results suggested that SF governed the reduction in the setting time of mixtures.

6. Combined use of FA and GGBFS with PC decreased the viscosity, irrespective of time of measurement at both w/b ratios. However, the silica fume and metakaolin concretes had consistently higher viscosity values than those of the control concretes. When the binary effects of the mineral admixtures on the viscosity of SCCs were ranked, it was listed in the order of SF, MK, and FA or GGBFS. There were no significant differences in the viscosity of FA and GGBFS blended concretes.
7. The overall compressive strength ranged from 30.3 to 98.6 and 42.5 to 113.1 MPa at 28 and 90 days, respectively. There was a marked reduction in the compressive strength of the concretes with increasing FA content while the concretes having GGBFS had comparable strength values to that of the control concrete. The SF and MK concretes, on the other hand, had consistently higher compressive strength than the control concrete. MK is the most effective mineral admixture on the compressive strength of SCC for both testing ages.
8. In the case of ternary use of PC+FA+SF and PC+FA+MK, the compressive strength also slightly decreased with the replacement ratio but the rate of reduction was much less compared to the case in the binary use of PC and FA. However, the ternary use of PC+GGBFS+SF and PC+GGBFS+MK provided a positive effect on the compressive strength, especially at higher replacement levels.
9. The overall pulse velocity ranged from 4644 to 5172 m/sec and 4800 to 5303 m/sec at the w/b ratio of 0.32 concretes at 28 and 90 days testing time, respectively. However, the high w/b ratio concretes had pulse velocities varying from 4738 to 4999 m/sec and 4760 to 5050 m/sec at 28 and 90 days, respectively. The concretes produced in this study had UPV values of greater than 4500 m/sec for both w/b ratios so that the rating of the concretes was found to be excellent.
10. As for compressive strength, the splitting tensile strength of SCCs exhibited a gradual decrease with the increase in the replacement level of FA, irrespective of w/b ratio. However, quite similar strengths were measured at

all replacement levels of GGBFS. Furthermore, this value was much close to the splitting tensile strength of the control concrete. Incorporating MK or SF, on the other hand, gave rise to increase in the strength values. The negative effect of FA on the splitting tensile strength remarkably reduced when the ternary blends of mineral admixtures used. The highest splitting tensile strength values at low w/b ratio concretes were monitored at the ternary blends of PC+SF+MK.

11. The effects of replacing the PC by FA, GGBFS or MK were to reduce the free shrinkage of SCCs remarkably at low w/b ratio. The shrinkage of the concrete with binary use of PC+MK exhibited the highest reduction in comparison to the control concrete. It was pointed out that the higher the replacement level of FA, GGBFS, and MK, the higher reduction in shrinkage. However, the binary use of SF with PC increased the shrinkage of SCCs. All of the mixtures in ternary use of the mineral admixtures have low drying shrinkage values when compared to the control concrete. The negative effect of SF on the shrinkage of SCCs was relatively eliminated with the ternary use and entirely eliminated of in the quaternary use of mineral admixtures.
12. Increasing the replacement level of FA and GGBFS in the binary use of PC+FA and PC+GGBFS increased the weight loss of SCCs gradually. When the weight loss of the concretes with the binary blends of PC+SF or PC+MK were considered, the effect of replacement level on the water loss of these concretes was significantly lower. All mixtures in the ternary use of mineral admixtures exhibited higher weight loss than the control concrete. It may be postulated that the weight loss of the concretes with ternary or quaternary blends were generally dominated by FA, GGBFS of both of them.
13. The calculated total passing charge ranged from 119 to 1009 coulombs at the low w/b ratio, and from 216 to 2065 at the high w/b ratio. The total charged passed decreased with the use of mineral admixtures. The use of MK appeared to be the most effective in the reducing the chloride permeability of the concretes, especially the effect being increased with increasing the MK content.

14. The overall resistivity of concretes at low w/b ratio was in the range of 12.8 to 25.8 kohm-cm and 13.4 to 34.4 kohm-cm at the 28 and 90 days, respectively. The concretes at high w/b ratio, on the other hand, had electrical resistivity ranging from 12.1 to 18.9 kohm-cm and from 12.3 to 27.7 kohm-cm. Irrespective of the w/b ratio, the lowest electrical resistivity was measured in the control concrete. Using any of the mineral admixtures increased the electrical resistivity of SCCs compared to that of the control concrete, especially at higher replacement levels. The test results suggested that it was the MK and SF among the mineral admixtures used that governed the increment in the electrical resistivity of the SCCs. All the ternary blended mixture concretes had higher electrical resistivity than that of the reference concrete. Like the case in ternary mixture concretes, using of quaternary blends enhanced the performance of the concretes in terms of electrical resistivity. The electrical resistivity of concretes increased with the increasing of testing age but as expected, a gradual decrease was observed with the increasing of w/b ratio.
15. The water absorption of concretes ranged from 1.6 to 4.8% and 2.5 to 7.7% at the low and high w/b ratio concretes, respectively. The use of mineral admixtures remarkably reduced the water absorption of the concretes irrespective of w/b ratio. Both SF and MK appeared to be the most effective in the reduction of water absorption among the mineral admixtures used; the effect being increased with increasing the replacement level. The water absorption of the concretes with the binary blends of PC+FA were very close to that of the control concrete. However, the ternary use of PC+FA+SF and PC+FA+MK reduced the water absorption remarkably according to the binary use of PC+FA. Unlike FA, with inclusion of GGBFS into the PC+MK mixtures, the concretes with the ternary blends of PC+GGBFS+MK exhibited superior performance over the concretes with the binary blends both PC+GGBFS and PC+MK. When compared the performance of ternary and quaternary blends of mineral admixtures, the ternary blends exhibited better performance.

16. The water sorptivity of concretes ranged from 0.027 to 0.082 mm/min^{0.5} and 0.05 to 0.093 mm/min^{0.5} at the low and high w/b ratio concretes, respectively. Incorporating the mineral admixtures continuously decreased the sorptivity of SCCs. In the binary blends of mineral admixtures, the use of MK appeared to be much effective in reducing the sorptivity due to the reduced pore volume. The influence of MK on the water sorptivity was much clearer on the ternary blends of mineral admixtures.
17. Replacing the portland cement with mineral admixtures, significantly improved the water permeability of the concretes depending on the type of mineral admixture used and the replacement level. Among the mineral admixture MK caused the highest reduction in the water permeability of SCCs. It can be said that all produced concretes for both w/b ratios are resistant to chemical attacks in aggressive media.
18. The properties of SCCs were predicted by two well known soft computing techniques, namely ANN and GEP. Both of these techniques predicted the SCCs properties with high correlation coefficients but the developed ANN models had better prediction performance than the GEP models owing to the higher coefficient of correlation and the lower mean absolute percentage of error. However, the GEP suggested a much shorter and more user-friendly model than ANN.
19. Two different types of optimization were performed, one for cost minimization under fresh and hardened properties constraints, and the second for multi objective. Several responses optimized simultaneously in which fresh properties were kept in the acceptance criteria of EFNARC, mechanical properties maximized, and permeation properties were minimized with the cost of SCCs. At the end of the cost optimization process, ten different mixtures which satisfied the specified constraints and limits could be obtained. At the end of the multi objective optimization process, four different mixtures satisfied the defined constraints and objectives.

8. FUTURE WORK

Regarding the self compacting concretes, further investigations may be carried out on the following main topics:

- Influence of different maximum aggregate size on the rheological properties of self compacting concretes may be studied.
- Influence of mineral admixtures on the durability related properties of self compacting concretes such as alkali aggregate reaction, freeze-thaw resistance, salt scaling etc. may be studied.
- A new experimental program can be developed considering the particle packing of the mineral admixtures to better understand their combined effects on the properties of self compacting concretes.
- Optimum mixture proportions of the self compacting concretes can be obtained according to the different optimization algorithms or techniques such as genetic algorithms.
- In this study, the feasibility of using four different types of mineral admixtures in the design and production of self compacting concretes were studied. In future, the combined use of the other mineral admixtures such as limestone filler, marble powder, etc. may be utilized in the production of self compacting concretes.
- The effects of using mineral admixtures on the microstructure of self compacting concretes was not studied in this work. In future, however, a comprehensive microstructural investigation in terms of SEM, ESEM, EDX, and TDG should be conducted.

REFERENCES

- Abraham, A. (2001). Neuro-fuzzy systems: state-of-the art modeling techniques, connectionist models of neurons, learning processes, and artificial intelligence. *Lecture Notes in Computer Science*, **2084**, 269–276
- Abraham, A. (2002). Recent advances in intelligent paradigms and applications, in studies in fuzziness and soft computing. In A. Abraham, L. Jain and J. Kacprzyk (Eds.), *Intelligent systems: architectures and perspectives*.
- Abraham, A. (2005). Handbook for Measurement Systems Design. In P. Sydenham and R. Thorn (Eds.), *Nature and Scope of AI Techniques*. London: John Wiley and Sons Ltd.
- Aleksander, I. and Morton, H. (1990). *An introduction to neural computing*. London: Chapman and Hall.
- Alexander, M.G. and Magee, B.J. (1999). Durability performance of concrete containing condensed silica fume. *Cement and Concrete Research*, **29**, 917-922
- Al-Khaja, W.A. (1994). Strength and time-dependended deformations of silica fume concrete for use in Bahrain. *Construction and Building Materials*, **8**, 169-172
- Alonso, C., Andrade, C., Castellote, M. and Castro, P. (2000). Chloride threshold values to depassivate reinforcing bars embedded in a standardized OPC mortar. *Cement and Concrete Research*, **30**, 1047–1055
- Alqedra, M.A. and Ashour, A.F. (2005). Prediction of shear capacity of single anchors located near a concrete edge using neural networks. *Computers and Structures*, **83**, 2495-2502
- Alshamsi, A.M., Sabouni, A.R., and Bushlaibi, A.H. (1993). Influence of set-retarding superplasticizers and micro-silica on the setting times of pastes at various temperature. *Cement and Concrete Research*, **23**, 592–598
- Al-Tabtabai, H. and Alex, P.A. (1999). Using genetic Algorithm to solve optimization problems in construction. *Engineering Construction and Architectural Management*, **6**, 121-32
- American Concrete Institute. (1993). *Application of super workable concrete to reinforced concrete structures with difficult construction conditions ACI Report SP-140*. Detroit: Mlura, N., Akeda, N., Chlkamatsu, R. and Sogo, S.
- American Concrete Institute. (1995). *Ground Granulated Blast-Furnace Slag as a Cementitious Constituent in Concrete*. ACI 233R-95.
- American Concrete Institute. (1996). *Guide for the Use of Silica Fume in Concrete*. ACI 234R-96.
- American Concrete Institute. (1996). *Use of Fly Ash in Concrete*. ACI 232.2R-96.

- American Society for Testing and Materials. (2002). *ASTM C 618 Standard Specification for Coal Fly Ash and Raw or Calcined Natural Pozzolan for use as a Mineral Admixture in Concrete*. West Conshohocken, PA.
- Babu, K.G. and Rao, G.S.N. (1994). Early strength of fly ash concrete. *Cement Concrete Research*, **24**, 277–84
- Bai, J., Wild, S. and Safir, B.B. (2002). Sorptivity and strength of air-cured and water cured PC-PFA-MK concrete and the influence of binder composition on carbonation depth. *Cement and Concrete Research*, **32**, 1813-1821
- Bai, J., Wild, S., Ware, J.A. and Sabir, B.B. (2003). Using neural networks to predict workability of concrete incorporating metakaolin and fly ash. *Advances in Engineering Software*, **34**, 663-669
- Baker, M. (1984). Evaluation on the utilization options, combustion by products utilization manual. EPRI report no. CS-3122.
- Batis, G., Pantazopoulou, P., Tsvilis, S. and Badogiannis, E. (2005). The effect of Metakaolin on the corrosion behavior of cement mortars. *Cement and Concrete Composites*, **27**, 458-467
- Bayramov, F., Tasdemir, C. and Tasdemir, M.A. (2004). Optimization of steel fiber reinforced concretes by means of statistical response surface method. *Cement and Concrete Composites*, **26**, 665-675
- Bhanja, S. and Sengupta, B. (2005). Influence of silica fume on the tensile strength of concrete. *Cement and Concrete Research*, **35**, 743-747
- Bilodeau, A., and Malhotra, V.M. (2000). High-volume fly ash system: Concrete solution for sustainable development. *ACI Material Journal*, **97**, 41–48
- Bilodeau, A., Sivasundaram, V., Painter, K. and Malhotra, V.M. (1994). Durability of concrete incorporating high volumes of fly ash from sources in the US. *ACI Materials Journal*, **91**, 3-12
- Bouzoubaa, N., and Lachemi, M. (2001). Self-compacting concrete incorporating high volumes of class F fly ash Preliminary results. *Cement and Concrete Research*, **31**, 413-420
- Brooks, J.J. and Megat Johari, M.A. (2001). Effect of metakaolin on creep and shrinkage of concrete. *Cement and Concrete Composites*, **23**, 495-502
- Brooks, J.J., Megat, J.M.A., and Mazloom, M. (2000). Effect of admixtures on the setting time of high-strength concrete. *Cement and Concrete Composites*, **22**, 293–301,
- Cabrera, J.G. (1986). The use of pulverized fuel ash to produce durable concrete. Institute of Civil Engineering in Improvement of Concrete Durability, 29-59
- Canada Energy Mines and Resources. (1986). *Thermal crack control of mass concrete*. MSL Division Report MSL 86-93 (IR). Ottawa: Sivasundaram, V.
- Carette, G.G., and Malhotra, V.M. (1983). Mechanical properties, durability, and drying shrinkage of portland cement concrete incorporating silica fume. *Cement, Concrete, and Aggregates*, **5**, 3-13

- Castilho, V.C., Nicoletti, M.C. and Debs, M.K. (2005). An investigation of the use of three selection-based genetic algorithm families when minimizing the production cost of hollow core slabs. *Computer Methods in Applied Mechanics and Engineering*, **194**, 4651-4667
- Chen, B., Zhang, Y. and Guo, L. (2007). Investigation of drying shrinkage of high volume fly ash concrete. *Journal of Southeast University*, **37**, 334-338
- Chung, H.P., Woo, I.L., Woo, S.H. and Alain, V. (2004). Simultaneous optimization of composite structures considering mechanical performance and manufacturing cost. *Composite Structures*, **65**, 117-127
- Coleman, N.S. and Page, C.L. (1997). Aspects of the pore solution chemistry of hydrated cement pastes containing metakaolin. *Cement and Concrete Research*, **27**, 147-154
- De Almeida, I.R. and Gonvalves, A.F. (1990). Proceedings of the RILEM colloquium on properties of fresh concrete. In H.J. Wierig (ed.). *Properties of freshly mixed high-strength concrete*.
- Delage, P., and Aitcin, P.C. (1983). Influence of Condensed Silica Fume on the Pore-Size Distribution of Concretes. *Industrial and Engineering Chemistry Product Research and Development*, **22**, 286-290
- Design-Expert V 7.0.2. (2006). Stat-Ease incorporation. Minneapolis, USA.
- Domone, P.L. (2007). A review of the hardened mechanical properties of self-compacting concrete. *Cement and Concrete Composites*, **29** (1), 1-12
- ECC International product document. (1996) *A new pozzolanic material for the cement and concrete industry, use of meta-star for the production of highly durable concrete and mortars*, England: St Austell.
- EFNARC (2002). *Specification and guidelines for self compacting concrete*. <http://www.efnarc.org>
- Eren, O., Brooks, J.J. and Celik, T. (1995). Setting of fly ash and slag-cement concretes as affected by curing temperature. *Cement, Concrete, and Aggregates*, **17**, 11-17
- Fausett, L.V. (1994). *Fundamentals of neural networks*. New Jersey: Prentice Hall.
- Felekoglu, B., Tosun, K., Baradan, B., Akin, A. and Uyulgan, B. (2006). The effect of fly ash and limestone fillers on the viscosity and compressive strength of self-compacting repair mortars. *Cement and Concrete Research*, **36**, 1719-1726
- Ferraris, C.F. (1999). Measurement of the Rheological Properties of High Performance Concrete: State of the Art Report. *Journal of Research of the National Institute of Standards and Technology*, 104 (5), 461-478
- Ferraris, C.F. (1999). RILEM international symposium proceedings. In J.G. Cabrera and R.R. Rivera-Villarreal (Eds.), *Role of admixtures in high performance concrete*.
- Ferreira, C. (2001). Gene Expression programming: a new adaptive algorithm for solving problems. *Complex Systems*, **13**, 87-129
- Ferreira, C. (2006). *Gene expression programming: mathematical modeling by an artificial intelligence*. (2nd ed.). Germany: Springer-Verlag.

- FIP Commission on Concrete. (1988). *State of Art Report on Condensed silica fume in concrete*. London: Thomas Telford.
- Gesoglu, M. (2004). Effects of lightweight aggregate properties on the mechanical, fracture, and physical behavior of lightweight concrete. PhD thesis, Bogazici University, Istanbul.
- Gesoğlu, M. and Özbay, E. (2007). Effects of mineral admixtures on fresh and hardened properties of self-compacting concretes: binary, ternary and quaternary systems. *Materials and Structures*, DOI 10.1617/s11527-007-9242-0.
- Gesoğlu, M., Güneyisi, E. and Mermerdaş, K. (2007). Effects of metakaolin content and curing conditions on the compressive strength and electrical resistivity of concretes. *Journal of Ready Mixed Concrete*, **80**, 72-76
- Güneyisi, E. (2004). Mechanical and durability performance of plain and blended cement concrete exposed to chlorides and different curing regimes. PhD thesis, Bogazici University, Istanbul.
- Güneyisi, E. and Gesoglu, M. (2007). Improving strength, drying shrinkage, and pore structure of concrete using Metakaolin. *Materials and Structures*, Article in Press.
- Haj-Ali, R.M., Kurtis, K.E. and Sthapit, A.R. (2001). Neural network modeling of concrete expansion during long-term sulfate exposure. *ACI Materials Journal*, **98**, 36-43
- Haykin, S. (2000). *Neural networks: a comprehensive foundation*. New Jersey: Macmillan College Publications Cooperation.
- Haykin, S.S. (1998). *Neural networks: a comprehensive foundation*. (2nd ed.). New Jersey: Prentice Hall
- Hebb, D.O. (1949). *The organization of behavior*. New York: John Wiley and Sons Inc.
- Helland, S., Hoff, A. and Einstabland, T. (1983). High strength concrete. Presented at Norsk Betongdag, Trondheim, Norway.
- Hewayde, E., Nehdi, M., Allouche, E. and Nakhla, G. (2007). Neural network prediction of concrete degradation by sulphuric acid attack. *Structure and Infrastructure Engineering*, **3**, 17-27
- Hogan, F.J. and Meusel, J.W. (1981). Evaluation for durability and strength development of a ground granulated blast-furnace slag. *Cement, Concrete, and Aggregates*, **3**, 40-52
- <http://www.metakaolin.com/23.04.2007>.
- Jianyong, L. and Yan, Y. (2001). A study on creep and drying shrinkage of high performance concrete. *Cement and Concrete Research*, **31**, 1203-1206
- Jun, P., Zongjin, L. and Baoguo, M. (2002). Neural network analysis of chloride diffusion in concrete. *Journal of Materials in Civil Engineering*, **14**, 327-333
- Kalogirou, S. and Bojic, M. (2000). Artificial neural networks for the prediction of the energy consumption of a passive solar building. *Energy-The International Journal*, **25**, 479-491
- Kalogirou, S.A. (1999). Applications of artificial neural networks in energy systems: a review. *Energy Conversion and Management*, **40**, 1073-1087

- Karihaloo, B.L. and Kornbak, D.L. (2001). Optimization techniques for the design of high-performance fiber-reinforced concrete. *Structural Multi Disciplinary Optimization*, **21**, 32–39
- Kewalramani, M.A. and Gupta, R. (2006). Concrete compressive strength prediction using ultrasonic pulse velocity through artificial neural networks. *Automation in Construction*, **15**, 374-379
- Khatib, J.M. and Hibbert, J.J. (2005). Selected engineering properties of concrete incorporating slag and metakaolin. *Construction and Building Materials*, **19**, 460-472
- Khatib, J.M. and Wild, S. (1996). Pore size distribution of metakaolin paste. *Cement and Concrete Research*, **26**, 1545–1553
- Khatib, J.M. and Wild, S. (1998). Sulphate resistance of metakaolin mortar. *Cement and Concrete Research*, **28**, 83–92.
- Khatri, R.P., Sirivivatnanon, V. and Yu, L.K. (1997) Effect of curing on water permeability of concretes prepared with normal portland cement and with slag and silica fume. *Magazine of Concrete Research*, **49**, 167-172
- Khayat, K.H., Bickley, J. and Lessard, M. (2000). Performance of self-consolidating concrete for casting basement and foundation walls. *ACI Materials Journal*, **97**, 374-380
- Khayat, K.H., Manai, K. and Trudel, A. (1997). In situ mechanical properties of wall elements cast using self consolidating concrete. *ACI Materials Journal*, **94**, 492-500
- Khedr, S.A., and Abou-Zeid, M.N. (1994). Characteristics of silica-fume concrete. *Journal of Materials in Civil Engineering*, **6**, 357–375
- Kim, H.S., Lee, S.H. and Moon, H.Y. (2007). Strength properties and durability aspects of high strength concrete using Korean metakaolin. *Construction and Building Materials*, **6**, 1229-1237
- Kim, J.K., Han, S.H., Park, Y.D., Noh, J.H., Park, C.L., and Kwon, Y.H. (1996). Production Methods and Workability of Concrete. In P.J.M. Bartos, D.L. Marris, and D.J. Cleland (Eds.). *Experimental research on the material properties of super flowing concrete*.
- Kohonen, T. (1988). *Self-organization and Associative Memory*. New York: Springer-Verlag.
- Kostuch, J.A., Walters, G.V. and Jones, T.R. (1993). High performance concrete incorporating metakaolin: a review. *Concrete 2000*, **2**, 1799-1811
- Koza, J.R. (1992). Foundations of Genetic Algorithms 2. In W. Darrell (ed.), *Hierarchical automatic function definition in genetic programming*. San Mateo, CA: Morgan Kaufmann Publishers.
- Koza, J.R. (1992). *Genetic Programming: on the programming of computers by means of natural selection*. Cambridge, MA: MIT Press.
- Koza, J.R. (2005). *Genetic Programming IV*. New York: Springer Science and Business Media Inc.

- Kriven, W.M., Bell, J.L. and Gordon, M. (1994). Advances in Ceramic Matrix Composites. In N.P. Bansal, J.P.Singh, W.M. Kriven, and H. Schneider (Eds.), *Microstructure and Microchemistry of Fully-Reacted Geopolymers and Geopolymer Matrix Composites*.
- Kuder, K.G., Özyurt, N., Mu, E.B., and Shah, S.P. (2007). Rheology of fiber-reinforced cementitious materials. *Cement and Concrete Research*, **37**,191–199
- Lachemi, M., Hossain, K.M.A., Lambros, V., Nkinamubanzi, P.C., and Bouzoubaa, N. (2004). Performance of new viscosity modifying admixtures in enhancing the rheological properties of cement paste. *Cement and Concrete Research*, **34** (2), 185–193
- Lee, A.R. (1974). *Blast furnace and steel slag: Production, properties and uses*. London: Edward Arnold Ltd.
- Lopez, W. and Gonzalez, J.A. (1993). Influence of the degree of pore saturation on the resistivity of concrete and the corrosion rate of steel reinforcement. *Cement and Concrete Research*, **23**, 368–376
- MacCulloch, W.S.Y. and Pitts, W. (1943). A logical calculus of the ideas of immanent in nervous activity. *Bulletin of Mathematical Biophysics*, **5**, 115-133
- Malhotra, V.M. (1986). Superplasticizer fly ash concrete for structural applications. *Concrete International*, **8**, 28–31.
- Malhotra, V.M. (2000). Concrete technology for a sustainable development in the 21st century. In O.E. Gjorv, and K. Sakai (Eds.), *Role of supplementary cementing materials in reducing Greenhouse gas emissions*.
- Mazloom, M., Ramezaniapour, A.A. and Brooks, J.J. (2004). Effect of silica fume on mechanical properties of high-strength concrete. *Cement and Concrete Composites*, **26**, 347-357
- McCarthy, M.J. and Dhir, R.K. (2005). Development of high volume fly ash cements for use in concrete construction. *Fuel*, **84**, 1423-1432.
- Mehta, P.K. (2000). Second international symposium on cement and concrete technology in the 2000s. *Reflections on recent advancements in concrete technology*.
- Mermerdaş, K. (2006). Effectiveness of metakaolin on the strength and durability properties of air-cured and water-cured concretes. MSc thesis, Gaziantep University, Gaziantep.
- Mokarema, D.W., Weyers, R.E. and Lane, D.S (2005). Development of a shrinkage performance specifications and prediction model analysis for supplemental cementitious material concrete mixtures. *Cement and Concrete Research*, **35**, 918–925
- Muthukumar, M. and Mohan, D. (2004). Optimization of mechanical properties of polymer concrete and mix design recommendation based on design of experiments. *Journal of Applied Polymer Science*, **94**, 1107–1116
- Myers, R.H. and Montgomery, D.C. (2002). *Response surface methodology process and product optimization using designed experiments*. New York: John Willey & Sons Inc.
- Naik, T. R., and Singh, S. S. (1997). Flowable slurry containing foundry sands. *Journal of Materials in Civil Engineering*, **9** (2), 93 –102

- Naik, T.R. and Singh, S.S. (1997). Influence of fly ash on the setting and hardening characteristics of concrete systems. *ACI Material Journal*, **94**, 355-360
- Naveen, K.C., John, K.V., Vengala, J., and Ranganath, R.V. (2006). Self-compacting concrete with fly ash and metakaolin. *Indian Concrete Journal*, **80**, 33-39
- Neville, A.M. (1996). *Properties of Concrete*. New York: John Wiley and Sons Inc.
- Okamura, H. (1997). Self-compacting high performance concrete, *Concrete International*, **19**, 50–54
- Okamura, H., (1999). *Self-Compacting High Performance Concrete*. Tokyo: Social System Institute.
- Okamura, H., and Ozawa, K. (1995). Mix-design for self-compacting concrete. *Concrete Library of Japanese Society of Civil Engineering*, **25**, 107–120
- Okamura, H., Maekawa, K., and Ozawa, K. (1993). *High Performance Concrete*. Tokyo: Gihoudou Press.
- Ozawa, K., Maekawa, K., Kunishima, M., and Okumura, H. (1989) Proceedings of the second East-Asia and Pacific Conference on the Structural Engineering and Construction (EASEC-2). *Development of High performance concrete based on the durability design of concrete structures*.
- Özbay, E., Gesoglu, M. and Güneyisi, E. (2007). Empirical modeling of fresh and hardened properties of self compacting concretes by genetic programming. *Construction and Building Materials*, Article in Press.
- Park, C.K., Noh, M.H., and Park, T.H. (2005). Rheological properties of cementitious materials containing mineral admixtures. *Cement and Concrete Research*, **35**, 842–849
- Pera, J., Rols, S., Chabannet, M., and Ambraise, J. (1998). Materials Science of Concrete. In M.Cohen, S. Mindess, J. Skolny (Eds.), *Influence of the cement type on the resistance of concrete to an agricultural environment*.
- Persson, B. (2001). A comparison between mechanical properties of self-compacting concrete and the corresponding properties of normal concrete. *Cement and Concrete Research*, **31**, 193-198
- Pigeon, M., Pleau, R., Aitcin, P.C. (1986). Freeze-thaw durability of concrete with and without silica fume in ASTM C 666 (Procedure A) test method: internal cracking versus scaling. *Cement, Concrete and Aggregate*, **8**, 76-85
- Pistilli, M.F., Wintersteen, R., Cechner, R. (1984). The uniformity and influence of silica fume from a U.S. source on the properties of portland cement concrete. *Cement, Concrete and Aggregates*, **6**, 120–124.
- Polder, R.B. and Peelen, W.H.A. (2002). Characterization of chloride transport and reinforcement corrosion in concrete under cyclic wetting and drying by electrical resistivity. *Cement and Concrete Composites*, **24**, 427-435
- Poon, C.S., Koua, S.C. and Lam, L. (2006). Compressive strength, chloride diffusivity and pore structure of high performance metakaolin and silica fume concrete. *Construction and Building Materials*, **20**, 858–865

- Ramezaniou, A.A. and Malhotra, V.M. (1995). Effect of curing on the compressive strength, resistance to chloride ion penetration and porosity of concretes incorporating slag, fly ash, or silica fume. *Cement and Concrete composites*, **17**, 125-133
- Razak, H.A., Chai, H.K. and Wong, H.S. (2004). Near surface characteristics of concrete containing supplementary cementing materials. *Cement and Concrete Composites*, **26**, 883-889
- RILEM TC Final Report 188-CSC. (2006). Casting of self compacting concrete. *Materials and Structures*, **39**, 937-954
- Sabir, B.B., Wild, S., and Bai, J. (2001). Metakaolin and calcined clays as pozzolans for concrete a review. *Cement and Concrete Composites*, **23**, 441-454
- Sahab, M.G., Ashour, A.F. and Toropov, V.V. (2005). Cost optimization of reinforced concrete flat slab buildings. *Engineering Structures*, **27**, 313-322.
- Şahmaran, M. (2006). Self compacting concrete with high volumes of fly ash. PhD Thesis, Middle East Technical University, Ankara.
- Sakata, S., Maruyama, K., and Minami, M. (1996). Proceedings of RILEM International conference production methods and workability of Concrete. In: P.J.M. Bartos, D.L. Marris, and D.J. Cleland (Eds.), *Basic properties and effects of welangum on self compacting concrete*. London: E&FN Spon, 1-24
- Saleem, M., Shameem, M., Hussain, S.E. and Maslehuddin, M. (1996). Effect of moisture, chloride and sulphate contamination on the electrical resistivity of portland cement concrete. *Construction and Building Materials*, **10**, 209-214
- Saraswathy V., Muralidharan, S., Thangavel, K., and Srinivasan, S. (2003). Influence of activated fly ash on corrosion-resistance and strength of concrete. *Cement and Concrete Composites*, **25**, 673-680
- Sari, M., Prat, E., and Labastire, J.F. (1999). High strength self-compacting concrete: original solutions associating organic and inorganic admixtures. *Cement and Concrete Research*, **29**, 813-818
- Saric-Coric, M., Khayat, K.H., Tagnit-Hamou, A. (2003). A Performance characteristics of cement grouts made with various combinations of high-range water reducer and cellulose-based viscosity modifier. *Cement and Concrete Research*, **33** (12), 1999-2008
- Sbartai, Z.M., Laurens, S., Rhazi J., Balayssac J.P. and Arliguie, G. (2007). Using radar direct wave for concrete condition assessment: correlation with electrical resistivity. *Journal of Applied Geophysics*, Article in press
- Scali, M.J., Chin, D., and Berke, N.S. (1987). Proceedings of ninth international conference on cement microscopy. *Effect of Micro silica and Fly Ash upon the Microstructure and Permeability of Concrete*. International Cement Microscopy Association, Duncanville, Texas.
- Schalkoff, R.J. (1997). *Artificial neural networks*. Columbus: McGraw-Hill.
- Schutter, G.D. and Audenaert, K. (2004). Evaluation of water absorption of concrete as a measure for resistance against carbonation and chloride migration, *Materials and Structures*, **37**, 591-596

- Sekino, S., and Narita, T. (2003). Study on mix design and properties of self-compacting concrete containing high volume fly ash. *Journal of the Taiheiyo Cement Corporation*, **145**, 18-35
- Sellevoid, E.J. and Nilsen, T. (1987). Supplementary Cementing Materials for Concrete. In V.M. Malhotra (ed.). *Condensed Silica Fume in Concrete*.
- Şengül, Ö. (2005). Effects of pozzolanic materials on the mechanical properties and chloride diffusivity of concrete. PhD thesis, Istanbul Technical University, Istanbul.
- Shah, S.P., Karaguler, M.E. and Sarigaphuti, M. (1992). Effects of shrinkage reducing admixtures on restrained shrinkage cracking of concrete. *ACI Materials Journal*, **89**, 289-195
- Shames, I.H. (1992). *Mechanics of Fluids*. (3th ed.). Singapore: McGraw-Hill.
- Shi, Y.X., Matsui, I. and Guo, Y.J. (2004). A study on the effect of fine mineral powders with distinct vitreous contents on the fluidity and rheological properties of concrete. *Cement and Concrete Research*, **34**, 1381-1387
- Skapura, D. (1996). *Building neural networks*. New York: Addison-Wesley ACM Press.
- Sonebi, M. (2004). Medium strength self-compacting concrete containing fly ash: modelling using factorial experimental plans. *Cement and Concrete Research*, **34**, 1199–1208.
- Sun, Z., Voigt, T. and Shah, S.P. (2006). Rheometric and ultrasonic investigations of viscoelastic properties of fresh portland cement pastes. *Cement and Concrete Research*, **36**, 278–287
- Symons, M.G. and Fleming, K.H. (1980). Effect of post Augusta fly ash on concrete shrinkage. *Australian Civil Engineering Transactions*, **22**, 181-185
- Tarefder, R.A., White, L. and Zaman, M. (2005). Neural network model for asphalt concrete permeability. *Journal of Materials in Civil Engineering*, **17**, 19-27
- Tasdemir, C. (2003). Combined effects of mineral admixtures and curing conditions on the sorptivity coefficient of concrete. *Cement and Concrete Research*, **33**, 2637-1642
- Tattersall, G.H. (1991). *Workability and Quality Control of Concrete*. London: E & FN Spon.
- Thomas, M. (1996). Chloride thresholds in marine concrete. *Cement and Concrete Research*, **26**, 513–519
- Torii, K. and Kawamura, M. (1994). Pore structure and chloride ion permeability of mortars containing silica fume. *Cement and Concrete Composites*, **16**, 279-286
- US Bureau of Reclamation. (1984). *Fly ash and fly ash concrete*. Report REC-ERC-82-1. Colorado: Edwin, D.
- Wenzhong, Z. and Bartos, P.J.M. (2003). Permeation properties of self-compacting concrete. *Cement and Concrete Research*, **33**, 921-926
- Whitehurst, E.A. (1951). Soniscope tests concrete structures. *Journal of American Concrete Institute*, **47**, 443–444

- Wiegrink, K., Marikunte, S. and Shah, S.P. (1996). Shrinkage cracking of high strength concrete. *ACI Material Journal*, **93**, 409-415
- Wild, S. and Khatib, J.M. (1997). Portlandite consumption in metakaolin cement pastes and mortars. *Cement and Concrete Research*, **27**, 127-146
- Wild, S., Khatib, J.M. and Jones, A. (1996). Relative strength pozzolanic activity and cement hydration in superplasticised metakaolin concrete. *Cement and Concrete Research*, **26**, 1537-1544
- Wild, S., Sabir, B.B. and Khatib, J.M. (1995). Factors influencing strength development of concrete containing silica fume. *Cement and Concrete Research*, **25**, 1567-1580
- Wood, K. (1981). Symposium on Slag Cement. *Twenty Years of Experience with Slag Cement*.
- Xie, Y., Liu, B., Yin, J., and Zhou, S. (2002). Optimum mix parameters of high-strength self-compacting concrete with ultra-pulverized fly ash. *Cement and Concrete Research*, **32**, 477-480
- Yazıcı, H. (2007). The effect of silica fume and high-volume Class C fly ash on mechanical properties, chloride penetration and freeze-thaw resistance of self-compacting concrete. *Construction and Building Materials*, Article in press
- Yeh, I.C. (2006). Analysis of strength of concrete using design of experiments and neural networks. *Journal of Materials in Civil Engineering*, **18**, 597-604
- Yeh, I.C. (2007). Modeling slump flow of concrete using second-order regressions and artificial neural networks. *Cement and Concrete Composites*, **29**, 474-480
- Zadeh, L.A. (1994). Soft computing and fuzzy logic. *IEEE Software*, **11**, 48-56
- Zhang, H. and Malhotra, V.M. (1995). Characteristics of a thermally activated alumino-silicate pozzolanic material and its use in concrete. *Cement and Concrete Research*, **25**, 1713-1725
- Zhang, Z. and Friedrich, K. (2003). Artificial neural networks applied to polymer composites: a review. *Composites Science and Technology*, **63**, 2029-2044

APPENDIX A

ANN based explicit formulations for the properties of SCCs concretes:

$$T_{50} \text{ slump flow time} = \left(\left(\frac{2}{1 + e^{-2F}} - 1 \right) - (-1.2) \right) / (0.2999) \quad (1)$$

$$F = (3.03491) \left(\frac{2}{1 + e^{-2F_1}} - 1 \right) + (-5.29392) \left(\frac{2}{1 + e^{-2F_2}} - 1 \right) + (4.04873) \left(\frac{2}{1 + e^{-2F_3}} - 1 \right) + (-2.96447) \left(\frac{2}{1 + e^{-2F_4}} - 1 \right) + (-1.6994) \left(\frac{2}{1 + e^{-2F_5}} - 1 \right) + (3.16098) \left(\frac{2}{1 + e^{-2F_6}} - 1 \right) + (2.51221) \left(\frac{2}{1 + e^{-2F_7}} - 1 \right) + (2.33063) \quad (1a)$$

$$F_1 = W * (0.50068) + PC * (1.19375) + FA * (0.32101) + GGBFS * (0.59264) + SF * (1.04466) + MK * (-3.31269) + fa * (-1.75593) + ca * (-0.0506) + SP * (-2.51993) + (-1.66637) \quad (1b)$$

$$F_2 = W * (-1.74947) + PC * (1.55875) + FA * (-0.11917) + GGBFS * (1.18206) + SF * (-2.1369) + MK * (0.49127) + fa * (0.60484) + ca * (-2.50622) + SP * (-1.19772) + (-0.72382) \quad (1c)$$

$$F_3 = W * (-1.13225) + PC * (4.66712) + FA * (0.39171) + GGBFS * (1.16854) + SF * (-4.48306) + MK * (3.86679) + fa * (-1.78941) + ca * (0.01612) + SP * (-6.61832) + (-4.45307) \quad (1d)$$

$$F_4 = W * (-1.8343) + PC * (-0.58204) + FA * (0.58052) + GGBFS * (-0.55925) + SF * (0.15973) + MK * (0.10701) + fa * (1.52701) + ca * (0.36653) + SP * (-1.94306) + (0.85689) \quad (1e)$$

$$F_5 = W * (-2.23019) + PC * (5.15953) + FA * (1.18136) + GGBFS * (0.72681) + SF * (-6.06863) + MK * (0.23406) + fa * (-0.34422) + ca * (2.47521) + SP * (-1.24917) + (-3.50512) \quad (1f)$$

$$F_6 = W * (-1.01807) + PC * (-1.28265) + FA * (0.62993) + GGBFS * (-0.28773) + SF * (-2.28795) + MK * (3.50506) + fa * (2.733) + ca * (3.21445) + SP * (-1.18224) + (0.85348) \quad (1g)$$

$$F_7 = W * (0.74358) + PC * (0.79148) + FA * (0.25039) + \\ GGBFS * (0.6167) + SF * (-2.27611) + MK * (-0.52053) + \\ fa * (-0.35127) + ca * (0.90942) + SP * (0.52932) + (-0.46514) \quad (1h)$$

$$V - \text{funnel flow time} = \left(\left(\frac{2}{1 + e^{-2F}} - 1 \right) - (-1.0704142) \right) / (0.053254437) \quad (2)$$

$$F = (1.52499) * \left(\frac{2}{1 + e^{-2F_1}} - 1 \right) + (-1.45593) * \left(\frac{2}{1 + e^{-2F_2}} - 1 \right) + (1.03979) * \left(\frac{2}{1 + e^{-2F_3}} - 1 \right) + \\ (-0.8876) * \left(\frac{2}{1 + e^{-2F_4}} - 1 \right) + (-1.34771) * \left(\frac{2}{1 + e^{-2F_5}} - 1 \right) + (1.44305) * \left(\frac{2}{1 + e^{-2F_6}} - 1 \right) + \\ (1.71446) * \left(\frac{2}{1 + e^{-2F_7}} - 1 \right) + (-0.81694) \quad (2a)$$

$$F_1 = W * (19.27682) + PC * (-2.64716) + FA * (-0.18113) + \\ GGBFS * (-1.83314) + SF * (1.62905) + MK * (0.91696) + \\ fa * (-7.86803) + ca * (19.45453) + SP * (1.8338) + (-1.44097) \quad (2b)$$

$$F_2 = W * (-13.5586) + PC * (-2.80853) + FA * (5.5016) + \\ GGBFS * (-1.39153) + SF * (0.66363) + MK * (4.13053) + \\ fa * (21.03457) + ca * (6.71366) + SP * (-2.02563) + (1.79861) \quad (2c)$$

$$F_3 = W * (-6.30994) + PC * (1.11529) + FA * (3.44821) + \\ GGBFS * (0.81416) + SF * (-1.91805) + MK * (-1.53947) + \\ fa * (-1.03181) + ca * (0.47425) + SP * (-4.72691) + (-2.10142) \quad (2d)$$

$$F_4 = W * (6.10529) + PC * (2.24048) + FA * (-0.63467) + \\ GGBFS * (0.55764) + SF * (-4.8165) + MK * (-4.09361) + \\ fa * (-7.17332) + ca * (-4.66205) + SP * (1.36374) + (-1.24274) \quad (2e)$$

$$F_5 = W * (10.5313) + PC * (-3.32712) + FA * (-0.35326) + \\ GGBFS * (1.49377) + SF * (-2.1335) + MK * (0.76464) + \\ fa * (-3.86912) + ca * (12.03457) + SP * (0.79498) + (-0.00398) \quad (2f)$$

$$F_6 = W * (-6.7431) + PC * (-4.72025) + FA * (0.56176) + \\ GGBFS * (-3.28525) + SF * (-6.89104) + MK * (12.82926) + \\ fa * (3.53483) + ca * (-1.8365) + SP * (-0.66999) + (5.79162) \quad (2g)$$

$$F_7 = W * (2.15815) + PC * (-3.73894) + FA * (2.07643) + \\ GGBFS * (0.94369) + SF * (-0.69373) + MK * (-0.0647) + \\ fa * (6.00774) + ca * (11.29461) + SP * (0.36659) + (0.84846) \quad (2h)$$

$$L - \text{box } H_2/H_1 \text{ ratio} = \left(\left(\frac{2}{1 + e^{-2F}} - 1 \right) - (-5.4913043) \right) / (6.52173913) \quad (3)$$

$$F = (3.10491) * \left(\frac{2}{1 + e^{-2F_1}} - 1 \right) + (-4.61231) * \left(\frac{2}{1 + e^{-2F_2}} - 1 \right) + (3.06293) * \left(\frac{2}{1 + e^{-2F_3}} - 1 \right) + (-8.15005) * \left(\frac{2}{1 + e^{-2F_4}} - 1 \right) + (-8.85693) * \left(\frac{2}{1 + e^{-2F_5}} - 1 \right) + (7.92492) * \left(\frac{2}{1 + e^{-2F_6}} - 1 \right) + (10.87087) * \left(\frac{2}{1 + e^{-2F_6}} - 1 \right) + (-7.89957) \quad (3a)$$

$$F_1 = W * (-1.66457) + PC * (7.39521) + FA * (0.08954) + GGBFS * (-5.61638) + SF * (2.61376) + MK * (-0.80107) + fa * (0.1708) + ca * (2.28324) + SP * (-5.002) + (-2.22881) \quad (3b)$$

$$F_2 = W * (1.41274) + PC * (-0.96395) + FA * (0.99296) + GGBFS * (0.94249) + SF * (-0.14038) + MK * (-0.12331) + fa * (0.19864) + ca * (5.11117) + SP * (-0.72808) + (-0.25544) \quad (3c)$$

$$F_3 = W * (-3.28057) + PC * (-3.61581) + FA * (-0.44334) + GGBFS * (3.86239) + SF * (-0.74486) + MK * (0.22151) + fa * (1.9396) + ca * (-3.33992) + SP * (-0.53883) + (1.01744) \quad (3d)$$

$$F_4 = W * (4.30477) + PC * (-0.50236) + FA * (0.21332) + GGBFS * (-1.19128) + SF * (1.02042) + MK * (0.326) + fa * (-2.01483) + ca * (3.20355) + SP * (-0.59722) + (0.19956) \quad (3e)$$

$$F_5 = W * (-0.2696) + PC * (3.7829) + FA * (-2.41314) + GGBFS * (1.40295) + SF * (-1.33973) + MK * (-0.12105) + fa * (-5.06285) + ca * (-6.29093) + SP * (-0.82324) + (-1.42126) \quad (3f)$$

$$F_6 = W * (1.80238) + PC * (0.91125) + FA * (-1.70099) + GGBFS * (0.82566) + SF * (0.4701) + MK * (0.68159) + fa * (-5.25416) + ca * (-0.76956) + SP * (0.84149) + (-0.33075) \quad (3g)$$

$$F_7 = W * (1.02687) + PC * (2.07089) + FA * (-1.71016) + GGBFS * (0.45679) + SF * (-1.60209) + MK * (-0.82042) + fa * (-1.80057) + ca * (-4.24777) + SP * (-1.65125) + (0.08138) \quad (3h)$$

$$\text{Initial setting time} = \left(\left(\frac{2}{1 + e^{-2W}} - 1 \right) - (-1.46170) \right) / (0.00255319) \quad (4)$$

$$\begin{aligned} W = & (2.38148) * \left(\frac{2}{1 + e^{-2F_1}} - 1 \right) + (1.57138) * \left(\frac{2}{1 + e^{-2F_2}} - 1 \right) + (2.33459) * \left(\frac{2}{1 + e^{-2F_3}} - 1 \right) + \\ & (2.70547) * \left(\frac{2}{1 + e^{-2F_4}} - 1 \right) + (1.02219) * \left(\frac{2}{1 + e^{-2F_5}} - 1 \right) + (0.99261) * \left(\frac{2}{1 + e^{-2F_6}} - 1 \right) + \\ & (-0.97335) * \left(\frac{2}{1 + e^{-2F_7}} - 1 \right) + (-0.59213) \end{aligned} \quad (4a)$$

$$\begin{aligned} F_1 = & W * (-15.44816) + PC * (10.42199) + FA * (4.58872) + GGBFS * (10.28025) + \\ & SF * (0.32471) + MK * (4.70649) + fa * (-21.83563) + ca * (2.86397) + \\ & SP * (2.57539) + (-15.93504) \end{aligned} \quad (4b)$$

$$\begin{aligned} F_2 = & W * (12.22619) + PC * (6.72129) + FA * (-14.42879) + GGBFS * (6.42993) + \\ & SF * (-7.29315) + MK * (-6.10004) + fa * (-35.23368) + ca * (-30.76830) + \\ & SP * (1.33509) + (-0.15071) \end{aligned} \quad (4c)$$

$$\begin{aligned} F_3 = & W * (9.68577) + PC * (-2.32632) + FA * (1.70214) + GGBFS * (-1.36008) + \\ & SF * (-0.00145) + MK * (-1.16160) + fa * (-5.64691) + ca * (7.67377) + \\ & SP * (0.51702) + (-0.64097) \end{aligned} \quad (4d)$$

$$\begin{aligned} F_4 = & W * (-31.71286) + PC * (-24.21330) + FA * (38.76150) + GGBFS * (-13.23405) + \\ & SF * (12.53830) + MK * (5.02493) + fa * (95.10946) + ca * (70.30323) + \\ & SP * (-3.02200) + (4.43283) \end{aligned} \quad (4e)$$

$$\begin{aligned} F_5 = & W * (-22.53239) + PC * (76.59926) + FA * (-9.79800) + GGBFS * (-223.43611) + \\ & SF * (-55.59353) + MK * (-53.77757) + fa * (-10.30949) + ca * (4.75532) + \\ & SP * (-0.80940) + (120.35931) \end{aligned} \quad (4f)$$

$$\begin{aligned} F_6 = & W * (21.02795) + PC * (-2.79646) + FA * (20.06394) + GGBFS * (14.74024) + \\ & SF * (-38.92818) + MK * (12.22469) + fa * (-9.03512) + ca * (19.06386) + \\ & SP * (4.97394) + (-19.86231) \end{aligned} \quad (4g)$$

$$\begin{aligned} F_7 = & W * (-2.74354) + PC * (39.88165) + FA * (-39.09114) + GGBFS * (8.71283) + \\ & SF * (-8.81715) + MK * (0.81880) + fa * (-72.839) + ca * (-100.19986) + \\ & SP * (-5.77195) + (-7.71952) \end{aligned} \quad (4h)$$

$$\text{Final setting time} = \left(\left(\frac{2}{1 + e^{-2F}} - 1 \right) - (-1.49851) \right) / (0.00223325) \quad (5)$$

$$F = (-5.28991) * \left(\frac{2}{1 + e^{-2F_1}} - 1 \right) + (3.19700) * \left(\frac{2}{1 + e^{-2F_2}} - 1 \right) + (5.05708) * \left(\frac{2}{1 + e^{-2F_3}} - 1 \right) + \\ (-1.38526) * \left(\frac{2}{1 + e^{-2F_4}} - 1 \right) + (2.15401) * \left(\frac{2}{1 + e^{-2F_5}} - 1 \right) + (3.02339) * \left(\frac{2}{1 + e^{-2F_6}} - 1 \right) + \\ (2.91857) * \left(\frac{2}{1 + e^{-2F_7}} - 1 \right) + (-0.1884) \quad (5a)$$

$$F_1 = W * (5.18682) + PC * (0.10415) + FA * (-1.67979) + GGBFS * (-2.18145) + \\ SF * (-1.26898) + MK * (1.06631) + fa * (-2.83219) + ca * (3.23502) + \\ SP * (1.67757) + (0.86002) \quad (5b)$$

$$F_2 = W * (3.88815) + PC * (-3.03156) + FA * (2.18252) + GGBFS * (-2.58224) + \\ SF * (2.65297) + MK * (-0.83777) + fa * (2.27332) + ca * (9.62177) + \\ SP * (1.30868) + (0.59175) \quad (5c)$$

$$F_3 = W * (4.17340) + PC * (-0.63129) + FA * (-0.03148) + GGBFS * (-1.89537) + \\ SF * (-1.62796) + MK * (0.75776) + fa * (0.53194) + ca * (4.14887) + \\ SP * (3.73939) + (1.40896) \quad (5d)$$

$$F_4 = W * (0.11074) + PC * (2.42057) + FA * (0.16413) + GGBFS * (-1.56345) + \\ SF * (0.18053) + MK * (-3.00566) + fa * (-2.40362) + ca * (-6.23281) + \\ SP * (1.34864) + (-0.42207) \quad (5e)$$

$$F_5 = W * (-11.06126) + PC * (-0.67915) + FA * (1.38415) + GGBFS * (1.97736) + \\ SF * (-0.48484) + MK * (1.12438) + fa * (10.59) + ca * (-3.5336) + \\ SP * (-3.30249) + (0.69531) \quad (5f)$$

$$F_6 = W * (-2.58283) + PC * (-6.34839) + FA * (7.48684) + GGBFS * (-3.42734) + \\ SF * (1.63419) + MK * (1.70956) + fa * (14.50944) + ca * (14.04038) + \\ SP * (-0.28474) + (1.55076) \quad (5g)$$

$$F_7 = W * (-1.86445) + PC * (-1.06) + FA * (4.47936) + GGBFS * (-0.94952) + \\ SF * (1.68069) + MK * (-1.50626) + fa * (9.46015) + ca * (9.16367) + \\ SP * (0.44181) + (-1.06118) \quad (5h)$$

$$\text{Compressive strength} = \left(\left(\frac{2}{1 + e^{-2F}} - 1 \right) - (-1.983569) \right) / (0.02549575) \quad (6)$$

$$F = (-4.287) * \left(\frac{2}{1 + e^{-2F_1}} - 1 \right) + (2.59881) * \left(\frac{2}{1 + e^{-2F_2}} - 1 \right) + (4.20677) * \left(\frac{2}{1 + e^{-2F_3}} - 1 \right) + (-0.19533) * \left(\frac{2}{1 + e^{-2F_4}} - 1 \right) + (2.53952) * \left(\frac{2}{1 + e^{-2F_5}} - 1 \right) + (-4.2225) * \left(\frac{2}{1 + e^{-2F_6}} - 1 \right) + (-3.84915) \quad (6a)$$

$$F_1 = W * (1.64399) + PC * (-0.15230) + FA * (0.37746) + GGBFS * (0.24669) + SF * (0.01677) + MK * (-0.02498) + fa * (-1.66406) + ca * (0.44893) + SP * (-0.02493) + (-1.24922) \quad (6b)$$

$$F_2 = W * (0.59629) + PC * (2.31959) + FA * (1.86881) + GGBFS * (-1.67438) + SF * (-3.98697) + MK * (3.49895) + fa * (0.40763) + ca * (1.61329) + SP * (-0.88518) + (-1.52855) \quad (6c)$$

$$F_3 = W * (1.05337) + PC * (-1.61046) + FA * (1.32181) + GGBFS * (-2.75817) + SF * (0.55776) + MK * (0.51062) + fa * (-3.36449) + ca * (-1.92045) + SP * (-3.61605) + (1.80248) \quad (6d)$$

$$F_4 = W * (2.25062) + PC * (5.26445) + FA * (2.03801) + GGBFS * (-2.23411) + SF * (1.60262) + MK * (-6.02158) + fa * (1.89172) + ca * (-0.29423) + SP * (0.70191) + (-4.00867) \quad (6e)$$

$$F_5 = W * (-0.35047) + PC * (-3.53187) + FA * (-0.54213) + GGBFS * (1.59314) + SF * (4.62025) + MK * (-3.31327) + fa * (1.46845) + ca * (2.19521) + SP * (-0.08588) + (1.93798) \quad (6f)$$

$$F_6 = W * (-0.36293) + PC * (-3.22176) + FA * (3.27567) + GGBFS * (-3.42496) + SF * (0.66351) + MK * (0.65447) + fa * (0.85258) + ca * (0.68625) + SP * (-4.76187) + (2.30387) \quad (6g)$$

$$\text{Velocity through concrete, UPV} = \left(\left(\frac{2}{1 + e^{-2F}} - 1 \right) - (-16.679) \right) / (0.0033149) \quad (7)$$

$$F = (2.55783) * \left(\frac{2}{1 + e^{-2F_1}} - 1 \right) + (-1.97533) * \left(\frac{2}{1 + e^{-2F_2}} - 1 \right) + (2.82999) * \left(\frac{2}{1 + e^{-2F_3}} - 1 \right) + (-1.71899) * \left(\frac{2}{1 + e^{-2F_4}} - 1 \right) + (-4.74028) * \left(\frac{2}{1 + e^{-2F_5}} - 1 \right) + (3.89394) * \left(\frac{2}{1 + e^{-2F_6}} - 1 \right) + (3.53004) * \left(\frac{2}{1 + e^{-2F_7}} - 1 \right) + (0.78796) \quad (7a)$$

$$F_1 = W * (1.06641) + PC * (0.56463) + FA * (1.79111) + GGBFS * (-1.90096) + SF * (-0.68614) + MK * (-1.47441) + fa * (0.47838) + ca * (0.05648) + SP * (0.32991) + (-0.65518) \quad (7b)$$

$$F_2 = W * (-3.01671) + PC * (0.75726) + FA * (0.34909) + GGBFS * (-0.30854) + SF * (1.47583) + MK * (-1.7535) + fa * (1.45437) + ca * (-2.15122) + SP * (-1.00933) + (0.57305) \quad (7c)$$

$$F_3 = W * (1.21908) + PC * (0.52106) + FA * (1.09166) + GGBFS * (-1.22435) + SF * (-1.06627) + MK * (-1.53563) + fa * (-3.18645) + ca * (-0.53627) + SP * (4.1) + (-0.40623) \quad (7d)$$

$$F_4 = W * (0.07783) + PC * (0.80578) + FA * (0.1987) + GGBFS * (-2.36923) + SF * (1.39399) + MK * (0.01962) + fa * (1.00318) + ca * (-0.47564) + SP * (-2.15969) + (0.70466) \quad (7e)$$

$$F_5 = W * (-0.68202) + PC * (-0.07282) + FA * (1.56502) + GGBFS * (-1.62513) + SF * (-0.71623) + MK * (0.20769) + fa * (2.29458) + ca * (-0.30181) + SP * (0.6477) + (0.48144) \quad (7f)$$

$$F_6 = W * (3.37097) + PC * (-0.7689) + FA * (0.7921) + GGBFS * (-1.92834) + SF * (-0.94927) + MK * (0.74246) + fa * (-1.29281) + ca * (-0.07434) + SP * (2.96141) + (0.80617) \quad (7g)$$

$$F_7 = W * (1.41093) + PC * (0.79675) + FA * (-0.83135) + GGBFS * (-0.01966) + SF * (0.75519) + MK * (-0.12985) + fa * (-1.82513) + ca * (1.55293) + SP * (-3.19842) + (-0.03275) \quad (7h)$$

$$\text{Splitting tensile strength} = \left(\left(\frac{2}{1 + e^{-2F}} - 1 \right) - (-2.86875) \right) / (0.5625) \quad (8)$$

$$F = (-1.12888) * \left(\frac{2}{1 + e^{-2F_1}} - 1 \right) + (-3.52545) * \left(\frac{2}{1 + e^{-2F_2}} - 1 \right) + (2.57908) * \left(\frac{2}{1 + e^{-2F_3}} - 1 \right) + (2.95337) * \left(\frac{2}{1 + e^{-2F_4}} - 1 \right) + (-1.98466) * \left(\frac{2}{1 + e^{-2F_5}} - 1 \right) + (-0.26075) * \left(\frac{2}{1 + e^{-2F_6}} - 1 \right) + (-1.27431) \quad (8a)$$

$$F_1 = W * (-0.70982) + PC * (2.00671) + FA * (0.64704) + GGBFS * (0.60116) + SF * (-2.93023) + MK * (0.43749) + fa * (-0.16462) + ca * (-2.77485) + SP * (0.09002) + (-2.37463) \quad (8b)$$

$$F_2 = W * (0.88551) + PC * (-0.47324) + FA * (-0.02841) + GGBFS * (0.36274) + SF * (0.49704) + MK * (-0.0291) + fa * (-2.57072) + fa * (-0.7928) + SP * (-1.74538) + (-0.6406) \quad (8c)$$

$$F_3 = W * (-2.33969) + PC * (-1.02781) + FA * (0.48571) + GGBFS * (-0.81244) + SF * (-0.1712) + MK * (1.27039) + fa * (2.78359) + ca * (2.23939) + SP * (-2.34195) + (0.83204) \quad (8d)$$

$$F_4 = W * (-3.29905) + PC * (-1.13472) + FA * (1.11609) + GGBFS * (0.06507) + SF * (1.0142) + MK * (0.03298) + fa * (2.88405) + ca * (-1.3451) + SP * (-1.96819) + (-0.54146) \quad (8e)$$

$$F_5 = W * (-0.90972) + PC * (-0.77817) + FA * (-0.76403) + GGBFS * (-0.65163) + SF * (-1.50003) + MK * (1.39417) + fa * (-0.9897) + ca * (0.77508) + SP * (-3.14042) + (1.10477) \quad (8f)$$

$$F_6 = W * (2.61914) + PC * (0.73251) + FA * (3.19466) + GGBFS * (-5.00886) + SF * (-0.07085) + MK * (-4.85482) + fa * (1.49833) + ca * (-2.33908) + SP * (-0.4502) + (-0.05073) \quad (8g)$$

$$\text{Free shrinkage} = \left(\left(\frac{2}{1 + e^{-2F}} - 1 \right) - (-3.21759) \right) / (0.0077253) \quad (9)$$

$$F = (1.93623) * \left(\frac{2}{1 + e^{-2F_1}} - 1 \right) + (-2.19978) * \left(\frac{2}{1 + e^{-2F_2}} - 1 \right) + (-3.24227) * \left(\frac{2}{1 + e^{-2F_3}} - 1 \right) + (-4.02652) * \left(\frac{2}{1 + e^{-2F_4}} - 1 \right) + (-0.71931) * \left(\frac{2}{1 + e^{-2F_5}} - 1 \right) + (-1.0762) * \left(\frac{2}{1 + e^{-2F_6}} - 1 \right) + (5.05812) * \left(\frac{2}{1 + e^{-2F_7}} - 1 \right) + (0.12531) \quad (9a)$$

$$F_1 = W * (2.4907) + PC * (2.5323) + FA * (1.61004) + GGBFS * (-2.0282) + SF * (-2.58576) + MK * (-1.29273) + fa * (0.57837) + ca * (-0.9388) + SP * (3.93628) + (-1.91042) \quad (9b)$$

$$F_2 = W * (-2.44278) + PC * (-1.1142) + FA * (0.24315) + GGBFS * (1.01695) + SF * (2.72447) + MK * (-1.17853) + fa * (0.57219) + ca * (0.07794) + SP * (-1.68142) + (0.7375) \quad (9c)$$

$$F_3 = W * (-0.26165) + PC * (1.57631) + FA * (0.55484) + GGBFS * (-0.43364) + SF * (-1.73653) + MK * (0.42228) + fa * (-0.00557) + ca * (0.0169) + SP * (1.319) + (-1.27186) \quad (9d)$$

$$F_4 = W * (0.02498) + PC * (1.46142) + FA * (1.8859) + GGBFS * (-1.1203) + SF * (-1.94866) + MK * (-0.32486) + fa * (3.59402) + ca * (0.32167) + SP * (2.15025) + (-1.10119) \quad (9e)$$

$$F_5 = W * (-0.75883) + PC * (1.26926) + FA * (1.30814) + GGBFS * (-0.86391) + SF * (-3.64678) + MK * (-1.18449) + fa * (0.43538) + ca * (0.03336) + SP * (-0.06639) + (-0.11654) \quad (9f)$$

$$F_6 = W * (-0.59996) + PC * (0.24026) + FA * (-0.52223) + GGBFS * (0.19444) + SF * (-0.55282) + MK * (2.25819) + fa * (1.89896) + ca * (-0.05322) + SP * (3.26087) + (0.00368) \quad (9g)$$

$$F_7 = W * (2.10311) + PC * (1.44704) + FA * (-0.52018) + GGBFS * (0.24318) + SF * (-1.02259) + MK * (-0.11024) + fa * (-3.33054) + ca * (-0.62145) + SP * (0.89485) + (-0.74186) \quad (9h)$$

$$\text{Chloride ion permeability} = \left(\left(\frac{2}{1 + e^{-2F}} - 1 \right) - (-1.010071) \right) / (0.00092497) \quad (10)$$

$$F = (0.49684) * \left(\frac{2}{1 + e^{-2F_1}} - 1 \right) + (-1.08142) * \left(\frac{2}{1 + e^{-2F_2}} - 1 \right) + (0.97277) * \left(\frac{2}{1 + e^{-2F_3}} - 1 \right) + (0.43872) * \left(\frac{2}{1 + e^{-2F_4}} - 1 \right) + (0.56086) * \left(\frac{2}{1 + e^{-2F_5}} - 1 \right) + (-1.04852) * \left(\frac{2}{1 + e^{-2F_6}} - 1 \right) + (0.74297) \quad (10a)$$

$$F_1 = W * (0.40435) + PC * (-0.16973) + FA * (-0.59903) + GGBFS * (1.05356) + SF * (-0.93581) + MK * (-1.19492) + fa * (-1.6266) + ca * (-0.33016) + SP * (-2.19895) + (-0.16686) \quad (10b)$$

$$F_2 = W * (0.05302) + PC * (-4.48869) + FA * (1.35206) + GGBFS * (-1.30912) + SF * (0.09971) + MK * (-1.32372) + fa * (-0.37164) + ca * (-0.66348) + SP * (4.98716) + (3.45962) \quad (10c)$$

$$F_3 = W * (0.05496) + PC * (0.79362) + FA * (-2.63393) + GGBFS * (-0.45591) + SF * (-1.99848) + MK * (1.63061) + fa * (0.34324) + ca * (1.81082) + SP * (2.30743) + (1.69541) \quad (10d)$$

$$F_4 = W * (0.92895) + PC * (1.66151) + FA * (0.28848) + GGBFS * (-1.19385) + SF * (-0.03356) + MK * (-0.64324) + fa * (-0.94024) + ca * (-0.7336) + SP * (1.75524) + (-1.03164) \quad (10e)$$

$$F_5 = W * (0.74101) + PC * (0.19014) + FA * (2.66853) + GGBFS * (0.54844) + SF * (-0.53539) + MK * (-0.14516) + fa * (0.40195) + ca * (-1.34356) + SP * (0.12941) + (-2.00847) \quad (10f)$$

$$F_6 = W * (-0.59513) + PC * (0.73576) + FA * (-2.16755) + GGBFS * (0.41839) + SF * (-1.61618) + MK * (0.43008) + fa * (0.59048) + ca * (1.13528) + SP * (2.04026) + (0.96422) \quad (10g)$$

$$\text{Electrical resistivity} = \left(\left(\frac{2}{1 + e^{-2F}} - 1 \right) - (-1.9018) \right) / (0.08144796) \quad (11)$$

$$F = (-2.01989) * \left(\frac{2}{1 + e^{-2F_1}} - 1 \right) + (-6.98883) * \left(\frac{2}{1 + e^{-2F_2}} - 1 \right) + (1.06572) * \left(\frac{2}{1 + e^{-2F_3}} - 1 \right) + \\ (0.25955) * \left(\frac{2}{1 + e^{-2F_4}} - 1 \right) + (1.34665) * \left(\frac{2}{1 + e^{-2F_5}} - 1 \right) + (-5.66499) * \left(\frac{2}{1 + e^{-2F_6}} - 1 \right) + \\ (0.59031) \quad (11a)$$

$$F_1 = W * (1.34261) + PC * (0.58653) + FA * (0.24986) + \\ GGBFS * (-1.05547) + SF * (-1.32864) + MK * (-0.19919) + \\ fa * (0.71706) + ca * (-2.01356) + SP * (0.97126) + (-0.53653) \quad (11b)$$

$$F_2 = W * (-0.85781) + PC * (-1.95571) + FA * (0.3391) + \\ GGBFS * (-0.28436) + SF * (-2.46161) + MK * (-1.22249) + \\ fa * (0.99851) + ca * (-1.6093) + SP * (2.56063) + (1.67863) \quad (11c)$$

$$F_3 = W * (1.4907) + PC * (3.61819) + FA * (-2.27478) + \\ GGBFS * (-3.36836) + SF * (0.99833) + MK * (1.45253) + \\ fa * (-2.27927) + ca * (-3.6071) + SP * (-5.83251) + (-0.0867) \quad (11d)$$

$$F_4 = W * (-2.22438) + PC * (-0.14192) + FA * (0.2758) + \\ GGBFS * (0.71656) + SF * (2.33341) + MK * (0.04538) + \\ fa * (-1.35635) + ca * (0.95893) + SP * (-8.07068) + (-1.58936) \quad (11e)$$

$$F_5 = W * (9.45066) + PC * (-3.45534) + FA * (-1.57158) + \\ GGBFS * (1.44186) + SF * (-3.12812) + MK * (-1.81672) + \\ fa * (-7.31484) + ca * (2.30209) + SP * (6.36616) + (0.95859) \quad (11f)$$

$$F_6 = W * (4.0527) + PC * (-0.2226) + FA * (0.30576) + \\ GGBFS * (-0.20307) + SF * (0.03338) + MK * (-0.2349) + \\ fa * (-3.45256) + ca * (4.0152) + SP * (-0.36492) + (-1.67333) \quad (11g)$$

$$\text{Water absorption} = \left(\left(\frac{2}{1 + e^{-2F}} - 1 \right) - (-1.35757) \right) / (0.29145077) \quad (12)$$

$$F = (0.71680) * \left(\frac{2}{1 + e^{-2F_1}} - 1 \right) + (-2.98604) * \left(\frac{2}{1 + e^{-2F_2}} - 1 \right) + (1.74168) * \left(\frac{2}{1 + e^{-2F_3}} - 1 \right) + (4.57933) * \left(\frac{2}{1 + e^{-2F_4}} - 1 \right) + (-0.45318) * \left(\frac{2}{1 + e^{-2F_5}} - 1 \right) + (4.29936) * \left(\frac{2}{1 + e^{-2F_6}} - 1 \right) + (2.85809) \quad (12a)$$

$$F_1 = W * (-2.12814) + PC * (-6.23725) + FA * (6.25143) + GGBFS * (-5.13967) + SF * (-2.61285) + MK * (0.38646) + fa * (-3.12488) + ca * (-3.52086) + SP * (-0.55292) + (4.98446) \quad (12b)$$

$$F_2 = W * (1.39355) + PC * (-7.08376) + FA * (2.87437) + GGBFS * (-4.29887) + SF * (0.21300) + MK * (0.11226) + fa * (-2.91032) + ca * (-2.27404) + SP * (1.03774) + (6.51375) \quad (12c)$$

$$F_3 = W * (2.71155) + PC * (1.91036) + FA * (-1.27762) + GGBFS * (1.05689) + SF * (-0.29384) + MK * (-1.82992) + fa * (-4.96565) + ca * (-2.16233) + SP * (0.26134) + (-1.17564) \quad (12d)$$

$$F_4 = W * (-1.12519) + PC * (1.83097) + FA * (0.51477) + GGBFS * (-1.96356) + SF * (-1.58012) + MK * (0.66283) + fa * (4.41166) + ca * (-1.82318) + SP * (-2.66013) + (0.64615) \quad (12e)$$

$$F_5 = W * (-0.95470) + PC * (-1.13849) + FA * (-3.15625) + GGBFS * (5.37221) + SF * (2.86869) + MK * (-7.10751) + fa * (-0.41366) + ca * (1.22955) + SP * (-2.90477) + (-0.74898) \quad (12f)$$

$$F_6 = W * (-4.46766) + PC * (-1.65750) + FA * (0.52155) + GGBFS * (2.8647) + SF * (2.05562) + MK * (-0.51137) + fa * (1.43472) + ca * (-0.33075) + SP * (2.97083) + (0.11659) \quad (12g)$$

$$\text{Water sorptivity} = \left(\left(\frac{2}{1 + e^{-2F}} - 1 \right) - (-1.636363) \right) / (27.272727) \quad (13)$$

$$F = (4.44465) * \left(\frac{2}{1 + e^{-2F_1}} - 1 \right) + (-3.32057) * \left(\frac{2}{1 + e^{-2F_2}} - 1 \right) + (0.65329) * \left(\frac{2}{1 + e^{-2F_3}} - 1 \right) + (-3.07629) * \left(\frac{2}{1 + e^{-2F_4}} - 1 \right) + (-1.0535) * \left(\frac{2}{1 + e^{-2F_5}} - 1 \right) + (-1.72264) * \left(\frac{2}{1 + e^{-2F_6}} - 1 \right) + (0.96723) * \left(\frac{2}{1 + e^{-2F_7}} - 1 \right) + (0.60902) \quad (13a)$$

$$F_1 = W * (1.11367) + PC * (0.4671) + FA * (-0.25024) + GGBFS * (-1.10565) + SF * (-0.32343) + MK * (-0.55676) + fa * (-1.65363) + ca * (1.43378) + SP * (1.56187) + (0.01935) \quad (13b)$$

$$F_2 = W * (-1.57026) + PC * (-0.36932) + FA * (-0.62932) + GGBFS * (-0.97371) + SF * (0.30567) + MK * (2.41396) + fa * (0.51075) + ca * (-0.42825) + SP * (-0.04358) + (1.70878) \quad (13c)$$

$$F_3 = W * (-0.96527) + PC * (2.27043) + FA * (-0.22115) + GGBFS * (-1.29368) + SF * (0.41893) + MK * (3.37737) + fa * (-0.54013) + ca * (1.42774) + SP * (-5.957) + (-1.40838) \quad (13d)$$

$$F_4 = W * (-1.71604) + PC * (1.30274) + FA * (0.35625) + GGBFS * (-0.69518) + SF * (-0.87434) + MK * (-1.1307) + fa * (1.13323) + ca * (-1.80262) + SP * (2.62282) + (0.05027) \quad (13e)$$

$$F_5 = W * (-0.94055) + PC * (0.13789) + FA * (-1.93885) + GGBFS * (2.36276) + SF * (0.21093) + MK * (-0.72067) + fa * (1.41079) + ca * (1.16103) + SP * (-0.08948) + (0.05753) \quad (13f)$$

$$F_6 = W * (-0.89075) + PC * (-0.46944) + FA * (-0.72164) + GGBFS * (1.41946) + SF * (0.05194) + MK * (1.13967) + fa * (-0.77347) + ca * (-0.15121) + SP * (-2.39654) + (-0.00511) \quad (13g)$$

$$F_7 = W * (-1.63675) + PC * (1.38894) + FA * (-4.14399) + GGBFS * (6.75254) + SF * (-0.4962) + MK * (-2.33558) + fa * (0.36757) + ca * (3.58558) + SP * (-0.90088) + (-1.57587) \quad (13h)$$

$$\text{Water permeability} = \left(\left(\frac{2}{1 + e^{-2F}} - 1 \right) - (-1.1347826) \right) / (0.0782608) \quad (14)$$

$$F = (0.26081) * \left(\frac{2}{1 + e^{-2F_1}} - 1 \right) + (-1.58615) * \left(\frac{2}{1 + e^{-2F_2}} - 1 \right) + (0.86184) * \left(\frac{2}{1 + e^{-2F_3}} - 1 \right) + (3.82859) * \left(\frac{2}{1 + e^{-2F_4}} - 1 \right) + (1.56745) * \left(\frac{2}{1 + e^{-2F_5}} - 1 \right) + (2.71288) * \left(\frac{2}{1 + e^{-2F_6}} - 1 \right) + (-0.37966) \quad (14a)$$

$$F_1 = W * (3.02003) + PC * (-0.20676) + FA * (4.48144) + GGBFS * (-1.80723) + SF * (-0.73607) + MK * (2.62703) + fa * (1.27411) + ca * (-2.80099) + SP * (0.58837) + (-2.84348) \quad (14b)$$

$$F_2 = W * (2.51247) + PC * (-2.5267) + FA * (0.2524) + GGBFS * (0.59727) + SF * (-2.04226) + MK * (0.41915) + fa * (-4.3337) + ca * (1.40562) + SP * (-1.26689) + (0.98266) \quad (14c)$$

$$F_3 = W * (-1.49817) + PC * (-0.23692) + FA * (0.85072) + GGBFS * (0.20874) + SF * (-2.57101) + MK * (0.07111) + fa * (-0.74696) + ca * (1.22971) + SP * (-2.52094) + (0.29597) \quad (14d)$$

$$F_4 = W * (0.09734) + PC * (-0.12437) + FA * (-0.89494) + GGBFS * (-0.20973) + SF * (0.91519) + MK * (0.05243) + fa * (-0.32689) + ca * (-1.0063) + SP * (0.15095) + (0.21391) \quad (14e)$$

$$F_5 = W * (-1.92645) + PC * (-1.58328) + FA * (1.99959) + GGBFS * (1.13426) + SF * (-1.14585) + MK * (-2.73619) + fa * (1.73997) + ca * (-0.61173) + SP * (-0.24318) + (0.2996) \quad (14f)$$

$$F_6 = W * (1.18814) + PC * (0.86849) + FA * (-0.00662) + GGBFS * (0.50741) + SF * (-2.34482) + MK * (0.44454) + fa * (-2.88889) + ca * (0.14693) + SP * (-0.83147) + (-0.99999) \quad (14g)$$

APPENDIX B

GEP based explicit mathematical formulations for the properties of SCCs

$$T_{50} \text{ Slump flow time} = F_1 + F_2 + F_3 + F_4 + F_5 + F_6 + F_7 \quad (1)$$

$$F_1 = \text{Arctan}((((ca * ca) * MK) + (GGBFS + FA)) * SF) + \text{Arctan}(ca) \quad (1a)$$

$$F_2 = (\text{Arctan}(\text{Arctan}(MK) * PC)) + (\text{Arctan}((GGBFS * ca)/(SP + FA))) \quad (1b)$$

$$F_3 = \text{Arctan}(\text{Arctan}((FA + ((85.264) - fa)) + ((9.23386 - PC) * (-70.288)))) \quad (1c)$$

$$F_4 = \text{Arctan}((GGBFS/((-10.8399) + MK) + (GGBFS - SF))) \quad (1d)$$

$$F_5 = \text{Arctan}((((ca^2) * FA) + ((GGBFS * fa) + (ca * MK))) + 2.08599) \quad (1e)$$

$$F_6 = (\text{Arctan}(((SP - (FA + 6.910584)) - (SF * MK)) - ((SP * GGBFS) - SF))) \quad (1f)$$

$$F_7 = \text{Arctan}(((fa - ca) - (9.8285 - (SF - 5.01147))) + PC) \quad (1h)$$

$$V - \text{funnel flow time} = F_1 + F_2 + F_3 + F_4 + F_5 + F_6 \quad (2)$$

$$F_1 = e^{((2 * SF)/((MK - SP) + 3.7225) - FA)} \quad (2b)$$

$$F_2 = (((MK - 7.13519)/((363.259)/(SP - SF))) + 2.87735) \quad (2c)$$

$$F_3 = ((((-10.6525) * (SP + SF)) - ca)/((-1.951325 * SP) - SP) + (W + MK)) \quad (2d)$$

$$F_4 = \text{Log}((PC + (PC - ((2 * MK) + (MK + SF)) + (9.97619 + W)))) \quad (2e)$$

$$F_5 = (((fa + ((GGBFS - W) * W))/((SP^2) * ca)) + SP) \quad (2f)$$

$$F_6 = \text{Log}((((W^2) + (PC * MK)) + SF) + (FA * (MK * GGBFS))) - 8.504 \quad (2g)$$

$$L - \text{box } H_2/H_1 \text{ ratio} = F_1 * F_2 * F_3 * F_4 * F_5 * F_6 \quad (3)$$

$$F_1 = [-8.572/(-17.1442 + ca)] \quad (3a)$$

$$F_2 = ((-5.56 + (((W - SF) + (-8.128 * MK))/((-8.128 * PC) + fa))) - 5.56) \quad (3b)$$

$$F_3 = (ca + (GGBFS/(((MK - 6.5874) * SP) + FA))) * 4.8566 \quad (3c)$$

$$F_4 = (((7.63324/(GGBFS - ((FA + SP)/7.47736))) - 7.63324) + W) \quad (3d)$$

$$F_5 = ((1.45404/W)/(((fa - 9.84037) * fa) + ((SF * MK) * 9.84037))) \quad (3e)$$

$$F_6 = ((fa - (14.8738/((3.85666 - SP) - FA))) - 9.925) \quad (3f)$$

$$\text{Initial setting time} = F_1 + F_2 + F_3 + F_4 + F_5 + F_6 + F_7 + F_8 \quad (4)$$

$$F_1 = ((FA * \text{Cos}(\text{Log}((GGBFS + ca)))) + \text{Log}((ca + (9.5 * fa)))) \quad (4a)$$

$$F_2 = \sqrt{((((\text{Cos}(SP) * PC) - ((FA - fa) + (GGBFS + W))) * 3.83929))} \quad (4b)$$

$$F_3 = (FA + ((\sqrt{2 * (MK * 9.45334)} + PC) - W)) \quad (4c)$$

$$F_4 = (MK/\text{Sin}((((SP + MK)^4) * (ca + FA)) * \text{Log}((fa + SP)))) \quad (4d)$$

$$F_5 = ((\sqrt{((fa * MK) + GGBFS)}) - (FA + SP)) / SP \quad (4e)$$

$$F_6 = ((\text{Sin}(ca) * ((FA - (MK + SF)) + (0.28119 * GGBFS)))/1.78473) \quad (4f)$$

$$F_7 = ((GGBFS/\text{Log}((PC + ((9.33831 + SP) * (-9.90265 + SF)))))) * SP \quad (4g)$$

$$F_8 = (\text{Sin}((\text{Cos}((\text{Log}(ca) * (ca - sp))) * SP)) * MK) \quad (4h)$$

$$\text{Final setting time} = F_1 + F_2 + F_3 + F_4 + F_5 + F_6 + F_7 \quad (5)$$

$$F_1 = (\text{Sin}((7.29364 + \text{SP})^3) * ((6.45343 - \text{PC}) + (7.29364 * \text{SP}))) * \sqrt{\text{ca}} \quad (5a)$$

$$F_2 = (\text{Sin}((7.29364 + \text{SP})^3) * ((-6.45376 - \text{PC}) + (7.29364 * \text{SP}))) * \sqrt{\text{ca}} \quad (5b)$$

$$F_3 = (\text{Sin}(W) * (((-9.68484 * \text{SF}) + \text{FA}) + ((\text{FA} - \text{SF}) + (\text{SP} * \text{GGBFS})))) \quad (5c)$$

$$F_4 = ((\sqrt{((\text{SF} + (\sqrt{(\text{MK} * (\text{PC} + \text{FA}))))))} + \text{FA}) - \text{SF}) \quad (5d)$$

$$F_5 = (\text{FA} * (\text{FA} / (((\text{SF} - \text{SP}) * \text{GGBFS}) + ((\text{fa} - \text{FA}) - \text{SF})))) \quad (5e)$$

$$F_6 = (\sqrt{((\text{SF} * (2 * \text{MK})))} + \text{PC}) \quad (5f)$$

$$F_7 = (\text{GGBFS} - (\sqrt{(\text{Log}((\text{PC})^3))} * (\sqrt{((\text{ca} + \text{fa}))} / \text{SP}))) \quad (5g)$$

$$\text{Compressive strength} = F_1 + F_2 + F_3 + F_4 \quad (6)$$

$$F_1 = \sqrt{((((((\text{GGBFS} + \text{MK}) - (\text{fa} - \text{ca})) + \sqrt{(\text{FA})}) + ((\text{PC} - \text{SP}) - (W - \text{GGBFS})))))) \quad (6a)$$

$$F_2 = \sqrt{((((((\text{GGBFS} - \text{SP}) + (4.37277 + \text{PC})) + \sqrt{(\text{FA})}) + ((\text{ca} - W) - (\text{MK} + \text{fa})))))) \quad (6b)$$

$$F_3 = (5.95169 + ((((-3.08789 * \text{MK}) + \text{PC}) * 0.04559) + (\text{SP} - \sqrt{\text{SP}}))) \quad (6c)$$

$$F_4 = \sqrt{(((W + (\text{SF} - ((W * \text{MK}) / 3.992))) + \sqrt{\text{FA}})) \quad (6d)$$

$$\text{Velocity through concrete} = F_1 + F_2 + F_3 + F_4 + F_5 + F_6 + F_7 + F_8 \quad (7)$$

$$F_1 = \sqrt{(((SP * (\sqrt{MK * FA} + (\sqrt{MK} + SP))) * SP))} \quad (7a)$$

$$F_2 = (ca + \text{Cos}((((SP - W) + FA) * 4.30316) - ca))) + \sqrt{FA} \quad (7b)$$

$$F_3 = (MK / (MK - (\text{Cos}((\text{Log}(ca) + 0.0159)) + SF))) \quad (7c)$$

$$F_4 = (\text{Cos}(((\text{Log}((fa - W)) + ((GGBFS - 1.23352) + 6.036)) * W)) * MK) \quad (7d)$$

$$F_5 = \text{Log}((0.46317 - (((e^{SF} * (-0.256 * FA)) * (GGBFS * FA)) - GGBFS))) + SP \quad (7e)$$

$$F_6 = ((2 * SP) - ((W - ((FA - PC) - 8.6859)) / SP)) \quad (7f)$$

$$F_7 = (\text{Cos}((W * (\text{Log}(fa - W) + ((GGBFS + SF) + 6.589)))) * MK) \quad (7g)$$

$$F_8 = (ca + ((ca - (SF - fa)) + (ca + (fa + SP)))) \quad (7h)$$

$$\text{Splitting tensile strength} = F_1 + F_2 + F_3 + F_4 + F_5 \quad (8)$$

$$F_1 = ((ca * (SP / (FA + W))) / (W - 97.71916)) + (GGBFS - MK) + (ca - (SF - 4.95187)) \quad (8a)$$

$$F_2 = e^{\sqrt[4]{ca - (7.40948 + SF)}} + (fa - GGBFS) + MK \quad (8b)$$

$$F_3 = ((SP * \sqrt{(4.2) / (fa - 8.42724)} - fa) - ca) \quad (8c)$$

$$F_4 = (SF - ((MK + (((PC / 8.08176) * 8.08176) / (8.08176 - GGBFS))) / PC)) \quad (8d)$$

$$F_5 = [e^{fa / [(PC - 9.91138) + (PC + GGBFS)]}] / (MK - 5.51798) \quad (8e)$$

$$\text{Free shrinkage} = F_1 + F_2 + F_3 + F_4 + F_5 + F_6 \quad (9)$$

$$F_1 = (\text{PC} + (\text{GGBFS}/(((-6.92065 - \text{SP})/7.29489) * \text{MK}) + \text{W})) \quad (9a)$$

$$F_2 = ((-6.92065 + \text{SP}) - \sqrt{((\text{FA} + (\text{MK} * \text{SF})) + \text{MK}))}) \quad (9b)$$

$$F_3 = (\text{SF} + \text{fa}) + ((\text{SP} - 3.20514) * 9.335) + \text{GGBFS} \quad (9c)$$

$$F_4 = \sqrt{((\text{PC} - (\text{FA} - (2 * \text{MK}))) + ((\text{PC} + \text{MK}) + (-9.30151 - \text{SF})))} \quad (9d)$$

$$F_5 = (\text{FA} + (((\text{PC} - ((\text{FA} * 0.970673) + \text{FA})) - \text{FA})/\text{W})) \quad (9e)$$

$$F_6 = (((((\text{PC} + \text{FA}) - \text{GGBFS})/(\text{fa} - \text{SF})) * (9.65 + \text{SF})) - \text{ca}) + ((-2.35 * (-2.352753\text{SP})) - 9.033)) \quad (9f)$$

$$\text{Chloride ion permeability} = F_1 + F_2 + F_3 + F_4 + F_5 \quad (10)$$

$$F_1 = ((\text{ca}/(\text{GGBFS} - (\text{MK} - \text{SP}))) + (\text{W} * \text{Sin}((2 * \text{PC})))) \quad \dots\dots\dots(10a)$$

$$F_2 = (((\text{Cos}(\text{MK}) * \text{MK}) - \text{MK}) - (((\text{MK} + \text{SF}) + \text{MK}) - (\text{fa} - \text{ca}))) \quad (10b)$$

$$F_3 = (\text{SP} - (((\text{FA} * ((21059.54) + (\text{SF} * \text{W})))^{(1/3)} + \text{SF}))) + \text{GGBFS} \quad (10c)$$

$$F_4 = (\text{FA} + (\text{MK} * (((((\text{MK} * 6.69363) * \text{SF}) * (2 * \text{ca}))^{(1/3)})^{(1/3)}))) \quad (10d)$$

$$F_5 = ((\text{MK} - ((-9.16449 * ((\text{PC} + 1.6643) - \text{GGBFS})) - \text{MK}))/\text{SP}) + \text{W} \quad (10e)$$

$$\text{Electrical resistivity} = F_1 + F_2 + F_3 + F_4 + F_5 \quad (11)$$

$$F_1 = (\text{SP}) + \text{Arctan}((((\text{GGBFS}/\text{W}) * (8.09588 - \text{SP})) + (5.52438)) - \sqrt{6.81012 + \text{SP}}) \quad (11a)$$

$$F_2 = \sqrt{\text{MK} + \sqrt{\text{FA}}} \quad (11b)$$

$$F_3 = (((\text{GGBFS} * (\text{MK} - \text{PC})) - \text{ca})/(((\text{FA} - \text{fa}) * 8.09588) + \text{ca})) \quad (11c)$$

$$F_4 = \text{Arctan}(\text{FA}) + \text{GGBFS} + \sqrt{\text{MK} + \text{SP}} + (\sqrt{\text{SF}} - \text{GGBFS}) \quad (11d)$$

$$F_5 = \text{Arctan}(((\sqrt{2 * \text{ca}} - ((\text{PC} * 2.73291) * \text{MK})) + ((1.12069 - \text{SF}) * (\text{fa} * \text{FA})))) \quad (11e)$$

$$\text{Water absorption} = F_1 + F_2 + F_3 + F_4 + F_5 + F_6 \quad (12)$$

$$F_1 = (4.93972 / (\text{SP} + ((\text{MK} * \text{fa})^{\text{SF}}) / (\text{MK} - 1.67682)) * \text{GGBFS})) \quad (12a)$$

$$F_2 = (((((\text{SF} - \text{W}) * (-9.2265)) / \text{W}) / ((\text{MK} - \text{SF}) - (\text{W} - \text{FA}))) + (-3.57049)) \quad (12b)$$

$$F_3 = ((3.19158 / \text{SP}) - e^{((e^{\text{FA}} * (-5.035)) / (\text{SF} + \text{SP}))}) + (-7.15023) \quad (12c)$$

$$F_4 = (\text{ca} / (((\text{SF} * 3.87573) * \text{SF}) + \text{ca}) - (e^{(\text{MK})} * (\text{PC} + 3.87573)))) \quad (12d)$$

$$F_5 = \text{Log}((\text{Log}((0.02929 / (e^{(\text{FA})} + \text{fa}))) - (\text{MK} - \text{fa}))) \quad (12e)$$

$$F_6 = \text{Log}(((\text{SP} + (((\text{GGBFS} + \text{W}) + (\text{FA} + \text{GGBFS})) / (-0.7153 * \text{SP}))) + \text{fa})) \quad (12f)$$

$$\text{Water sorptivity} = F_1 * F_2 * F_3 * F_4 * F_5 * F_6 * F_7 \quad (13)$$

$$F_1 = (((((\text{PC} - \text{MK}) * (\text{FA} * \text{GGBFS})) - ((\text{fa} * \text{W}) * \text{W})) + \text{ca}) + \text{ca}) * (0.001638) \quad (13a)$$

$$F_2 = ((\text{fa} - (\text{FA} + \text{SP})) - (((\text{MK} + \text{SF}) + 1.47638) + \text{SP})) \quad (13b)$$

$$F_3 = (\text{fa} + (\text{GGBFS} + (((\text{W} + 7.63778) + (\text{FA} - \text{SF})) + ((\text{W} - 0.89609) + \text{FA})))) \quad (13c)$$

$$F_4 = ((\text{fa} - (((\text{SP} - \text{W}) / -6.41397) * e^{(\text{MK} / -3.2491)}))^{-6.41397}) \quad (13d)$$

$$F_5 = ((\text{FA} / (((-9.69537 * \text{GGBFS}) - (\text{SF} + \text{W})) + ((\text{SP} + \text{MK}) * \text{FA}))) + 8.03088) \quad (13e)$$

$$F_6 = ((\text{GGBFS} + \text{Log}(((\text{SF} * \text{FA}) - (-0.4 / \text{ca})) + (\text{ca} * \text{GGBFS})))) - \text{fa} \quad (13f)$$

$$F_7 = (\text{fa} + (\text{PC} / ((0.655 + e^{(\text{FA})}) + (-0.367 * \text{MK}) + \text{SF}))) \quad (13g)$$

$$\text{Water permeability} = F_1 + F_2 + F_3 + F_4 + F_5 + F_6 + F_7 \quad (14)$$

$$F_1 = \text{Sin}((0.060844 - ((W + PC) - (-2.79944 - ca)) + ((ca + 2.79944) - SP))) \quad (14a)$$

$$F_2 = \text{Sin}((\text{Cos}((-2.79162 + W) * fa)) * ((GGBFS + 2.79162) + PC)) \quad (14b)$$

$$F_3 = \text{Cos}\left[\sqrt{\left(\left(e^{\text{Sin}((0.42+SP)-PC)} + fa\right) * MK\right)}\right] \quad (14c)$$

$$F_4 = ((9.44564/(FA + (\sqrt{(\sqrt{W})}) + (MK - SF)))) + (-6.01675)) \quad (14d)$$

$$F_5 = \text{Cos}((MK * (((-2.84 * ca)/SP) + (-3.22)) - 2.84)) \quad (14e)$$

$$F_6 = (((SP/((-3.37271/SP) + (MK + 3.37271))) - SP) + \sqrt{W}) \quad (14f)$$

$$F_7 = \text{Log}((((SF - W) - GGBFS) + (SP * PC)) + \text{Sin}((GGBFS * PC))) - MK) \quad (14g)$$

CIRRICULAM VITAE

PERSONAL INFORMATION

Surname, Name: ÖZBAY, Erdoğan

Nationality: Turkish (TC)

Date and Place of Birth: 2 October 1973, Gaziantep

Marital Status: Married

Phone: +90 505 317 52 96

Fax: +90 348 814 26 69

E-mail: ozbay@gantep.edu.tr

EDUCATION

Degree	Institution	Year of Graduation
MS	Department of Civil Engineering University of Gaziantep	2002
BS	Department of Civil Engineering University of Gaziantep	1996
High School	Gaziantep Science High School	1991

WORKING EXPERIENCE

Year	Place	Enrollment
1999-	Kilis Vocational High School in Higher Education	Instructor
1996-1999	Gaziantep Levent Construction Firm	Site Engineer

FOREIGN LANGUAGES

Turkish (Native Language), English

PUBLICATIONS

1. **Erdoğan ÖZBAY**, Mehmet GESOĞLU, Erhan GÜNEYİSİ, (2007). Empirical modeling of fresh and hardened properties of self-compacting concretes by genetic programming. *Journal of Construction and Building Materials*, (Article in press)
2. Mehmet GESOĞLU, **Erdoğan ÖZBAY**, (2007). Effects of mineral admixtures on fresh and hardened properties of self-compacting concretes: binary, ternary and quaternary systems. *Journal of Materials and Structures*, (Article in press)
3. Murat PALA, **Erdoğan ÖZBAY**, Ahmet ÖZTAŞ, M. İshak YÜCE (2007). Appraisal of long-term effects of fly ash and silica fume on compressive strength of concrete by neural networks. *Journal of Construction and Building Materials*, 21(2), 384-394.
4. Ahmet ÖZTAŞ, Murat PALA, **Erdoğan ÖZBAY**, Erdoğan KANCA, Naci ÇAĞLAR, M.Asghar BHATTI (2006). Predicting the compressive strength and slump of high strength concrete using neural network. *Journal of Construction and Building Materials*, 20(9), 769-775.
5. Ahmet ÖZTAŞ, **Erdoğan ÖZBAY**, Asım YEGİNOBALI (2004). Current Status of Total Quality Management Implementation in the Turkish Cement Industry. *Journal of Total Quality Management*, 15(7), 985-999.
6. Nevzat ULUÖZ, Hakan ÖZBEBEK, **Erdoğan ÖZBAY**, Mehmet GESOĞLU, Erhan GÜNEYİSİ (2006). Uçucu kül içeren betonların basınçlı su geçirimsizliği ve maliyet parametrelerinin Taguchi deney tasarımı yöntemi ile optimizasyonu, 75, 68-74.
7. **Erdoğan ÖZBAY**, M.Asghar BHATTI, Ahmet ÖZTAŞ, Adil BAYKASOĞLU (2007). Cost Optimization of High Strength Concretes by Soft Computing Techniques. *Advances in Cement Based Materials and Applications in Civil Infrastructure (ACBM-ACI)*, Lahore Pakistan (Accepted for publication)
8. Ahmet ÖZTAŞ, Adil BAYKASOĞLU, **Erdoğan ÖZBAY** (2007). Prediction of Permeation Characteristics of High Strength Concretes by Neural Networks.

Advances in Cement Based Materials and Applications in Civil Infrastructure (ACBM-ACI), Lahore Pakistan (Accepted for publication)

9. **Erdoğan ÖZBAY**, Adil BAYKASOĞLU, Ahmet ÖZTAŞ, Hakan ÖZBEBEK (2006). An Experimental Comparison of Optimum Mix Proportions of High Strength Concrete Proposed by Taguchi Method and Genetic Algorithm. Proceedings of 5th International Symposium on Intelligent Manufacturing Systems, May 29-31, pp. 1062-1070.

10. Ahmet ÖZTAŞ, **Erdoğan ÖZBAY** (2005). Türk İnşaat Sektörünün Toplam Kalite Yönetimi Açısından Değerlendirilmesi. 3. Yapı işletmesi kongresi, Eylül 2005, İzmir.

11. **Erdoğan ÖZBAY**, Ahmet ÖZTAŞ (2005). Güneydoğu Anadolu Bölgesinde Konut Üretimi Yapan Firmalarda Üretim Planlama Metodolojisinin Uygulanabilirliği. 3. Yapı işletmesi kongresi, Eylül 2005, İzmir.

12. Ahmet ÖZTAŞ, **Erdoğan ÖZBAY**, Murat PALA. (2002) “4708 Sayılı Yapı Denetim Yasasının Uygulanabilirliği Üzerine Bir Araştırma”, GAP VI. Mühendislik Kongresi, Şanlıurfa.

13. Ahmet ÖZTAŞ, **Erdoğan ÖZBAY** (2002). “Türk İnşaat Sektörünün Toplam Kalite Yönetimi Açısından Değerlendirilmesi”, İnşaat Sektöründe Yönetim Sorunları Sempozyumu, Mimar Sinan Üniversitesi, Mayıs 2002, İstanbul.

RESEARCH PROJECTS

1. Erdoğan ÖZBAY (Araştırmacı) “Yüksek Mukavemetli Betonların Sezgisel Yöntemler Yardımı ile Çok Amaçlı Tasarım ve Üretim Optimizasyonu” TUBİTAK 105M025 nolu proje (Proje yöneticisi: Yrd.Doç.Dr. Ahmet ÖZTAŞ).

2. Erdoğan ÖZBAY (Araştırmacı) “Dayanım ve Dayanıklılık Bakımından Yüksek Performanslı Betonların Tasarım, Üretim ve Maliyet Optimizasyonu” Gaziantep Üniversitesi Araştırma Fonu MF0703 nolu proje (Proje yöneticisi: Yrd.Doç.Dr. Mehmet Gesoğlu).

HOBBIES

Visiting his friends and neighbors